REPORT DOCUMENTATION PAGE

Form Approved OMB No. 0704-0188

1. AGENCY USE ONLY (Leave blank)	2. REPORT DATE	3. REPORT TYPE AND DATES COVERED
	19 May 1997	Conference Proceedings

4. TITLE AND SUBTITLE

Proceedings for the International Workshop on the Monitoring of Aircraft Structures

5. FUNDING NUMBERS

F6170896W0071

6. AUTHOR(S)

Conference Committee

7. PERFORMING ORGANIZATION NAME(S) AND ADDRESS(ES)

Physical-Technical Institute Scientific
G. Mavlyanova, 2B, PTI of AS
Tashkent 700084
Uzbekistan

8. PERFORMING ORGANIZATION REPORT NUMBER

N/A

9. SPONSORING/MONITORING AGENCY NAME(S) AND ADDRESS(ES)

EOARD
PSC 802 BOX 14
FPO 09499-0200

10. SPONSORING/MONITORING AGENCY REPORT NUMBER

CSP 96-1002

11. SUPPLEMENTARY NOTES

12a. DISTRIBUTION/AVAILABILITY STATEMENT

Approved for public release; distribution is unlimited.

12b. DISTRIBUTION CODE

A

13. ABSTRACT (Maximum 200 words)

The Final Proceedings for International Workshop on the Monitoring of Aircraft Structures, 3 September 1996 - 5 September 1996

The Topics covered include: use of undestroyed testing and heterogeneous semiconductor structures to estimate airframe components fatigue, aircraft strength and service life, aircraft's operating conditions too fit their specification

14. SUBJECT TERMS

Guidance, High Power Generation

15. NUMBER OF PAGES

268

16. PRICE CODE

N/A

17. SECURITY CLASSIFICATION OF REPORT	18. SECURITY CLASSIFICATION OF THIS PAGE	19. SECURITY CLASSIFICATION OF ABSTRACT	20. LIMITATION OF ABSTRACT
UNCLASSIFIED	UNCLASSIFIED	UNCLASSIFIED	UL

PHYSICAL - TECHNICAL INSTITUTE, SCIENTIFIC ASSOCIATION
"PHYSICS - SUN" ACADEMY OF SCIENCES OF UZBEKISTAN

SIBERIAN STATE AERONAUTICAL RESEARCH INSTITUTE

THE FERGHANA STATE UNIVERSITY

THE NATIONAL AIR COMPANY "UZBEKISTON AIRWAYS"

PROCEEDINGS
FOR THE INTERNATIONAL WORKSHOP ON THE MONITORING OF AIRCRAFT STRUCTURES

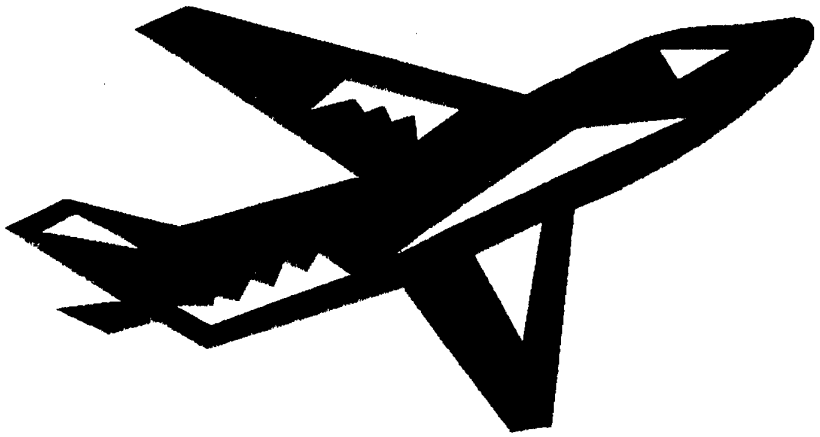

September 18, 19, 20, 1996

Ferghana - Yordan

U Z B E K I S T A N

Tashkent- Novosibirsk - Ferghana 1996

UDK 629.735.33.15.4 + 629.735.33.017.1

PROCEEDINGS FOR THE INTERNATIONAL WORKSHOP ON THE MONITORING OF AIRCRAFT STRUCTURES

The theme of this Workshop was fundamental and applied research in the area of Aircraft Strength and Service Life including Fatigue Strength, Reliability and Serviability of Structural components and units of aircraft by using the undestroyed methods of control.

Topics include : Use of undestroyed testing and heterogeneous semiconductor structure to estimate airframe components fatigue; Arcraft strength and service life; Aircraft's operation conditions too fit their specification; Aircraft's operation conditions with a large amount of flight time and dissimilar damages; Tribodiagnostic analys; Using the new materials in aviation.

We wish to thank the United States Air Force European Office of Aerospace Research and Development for its contribution to the success of this Workshop.

PARTICIPANTS

of the International Workshop on the Monitoring of Aircraft Structure

September 18, 19, 20 1996, Fergana
UZBEKISTAN

Tashkent

Prof. Shamirzaev S.Kh.	-	Physical-Technical Institute of Uzbek AS
Prof. Saidov M.S.	-	Physical-Technical Institute of Uzbek AS
Prof. Mirsagatov Sh.A.	-	Physical-Technical Institute of Uzbek AS
Ing. Vainerman G.I.	-	Physical-Technical Institute of Uzbek AS
Ing. Smirnov V.V.	-	Physical-Technical Institute of Uzbek AS
Prof. Khamrakulov I.V.	-	Uzbekistan Airways Company
Dr. Shishmarev V.A.	-	Plant № 243 of Civil Aviation, Uzbekistan Airway
Dr. Shuppe K.E.	-	Tashkent Aircraft Production Corporation named after V.P.Chcalov
Ing.Usmonov B.Sh.	-	State Aviation Institute

London (UK)

Dr. Sellers J.J	-	EOARD AFOSR USA

Zhukovsky (Russia)

Prof. Raicher V.L.	-	Aerohydrodynamic Institute
Prof. Kut'inov V.E.	-	Aerohydrodynamic Institute
Prof. Stuchalkin Yu.	-	Aerohydrodynamic Institute
Dr. Shcherban' K.S.	-	Aerohydrodynamic Institute

Novosibirsk (Russia)

Prof. Serioznov A.N.	-	Siberian Aeronautical Institute, SibRIA
Prof. Pykov D.F.	-	Siberian Aeronautical Institute, SibRIA
Prof. Maksimenko V.N.	-	Siberian Aeronautical Institute, SibRIA
Dr. Ryabinov M.I.	-	Siberian Aeronautical Institute, SibRIA

Moscow

Prof. Nozhnitsky Y. A.	-	Central Institute of AviationMotors (CIAM)
Dr. Kuevda V.K.	-	Central Institute of AviationMotors (CIAM)
Dr. Kadjarduzov P.	-	Central Institute of AviationMotors (CIAM)
Ing. Bobkova T.	-	Yakovlev Design Burean
Prof. Kogan Yu.	-	Sukhoi Design Burean
Prof. Kirin Yu.	-	State Research Institute of Civil Aviation
Dr. Daskovsky I.M.	-	State Research Institute of Civil Aviation

Dr. Troenkin D.A. - State Research Institute of Civil Aviation

Rostov on Don (Russia)

Dr. Bakirov A.A. - Institute of Physics, State University

Krymsk (Russia)

Dr. Sviridov V.M. - State Technical Colledg

Fergana

Prof. Karabaev M.K. - State University
Prof. Abdullaev E. - State University
Prof. Mćrzamakhmudov T. - State University
Prof. Rasulev R. - State University
Prof. Uyldashev N. - State University
Dr. Mirzakulov A - State University
Dr. Olimov Kh. - State University
Dr. Anarkulov K. - State University
Dr. Ubaidullaev M.I. - State University
Dr. Azimov T.A. - State University
Dr. Otadjanov S.M. - State University
Dr. Naimanbaev R. - State University
Dr. Khudoiberdiev A. - State University
Dr. Sagatov E.S. - State University
Dr. Akhmedov M.A. - State University
Ing. Rakhimov N. - State University
Ing. Jumaboev J. - State University
Ing Muiddinov A. - State University

CONTENTS

STRUCTURAL MODELS FOR FATIGUE DAMAGE OF HETEROGENEOUS SEMICONDUCTOR MATERIAL

Shamirzaev, S.Kh.
Physical Technical Institute Uzbek Academy of Sciences, Tashkent,
LeClair, S.R.
Wright Laboratory Wright Patterson AFB, Dayton, Ohio

INTRODUCTION

The fatigue damage of construction materials is governed by parameters of the strain placed on them. These parameters be estimated by means of sensors for accumulated fatigue damage (SAFD) [1,1a,2,3].Sensitive elements of these sensors are rigidly established on construction members, e.g. airplane fuselage. An irreversible reaction ($\Delta R[d]$) of sensitive element to the superimposed cyclic deformation must considerably exceed the reaction ($\Delta R[T]$) to the attendant thermocyclic process. Sensitive elements of this sort are briefly outlined in [2,3]. The sensitive elements are small weight (no more than 5g) and have either 3D or film geometry. They are produced either by a method of powder metallurgy (cold pressing with the subsequent agglomeration in a quartz ampoule) or by thermal vacuum evaporation of the charge onto the polyamide support. The charge consists of a finely-dispersed semiconductor (or semimetall) mixture (SM) with carbonyl iron. The films had variable volume contents of initial components. On loading irreversible random (cycle) deformation, changes occur both the effective electric resistance - R_{eff} of sensitive element and its microstructure , so as microstructure of the construction material.

The problem on the development of SAFDs is to find a correlation between $R_{eff}[d]$ of SM-film and change in microstructures [3]. The structure models of the construction materials are given in [4,5]. The correlation between R_{eff} of semiconductor mixtures (SMs) and volume contents of initial components and form as well as effective electron masses of its granules are given in [1,6,11]. The model of fatigue damage of SM-films for regular loading were first given in [2,3]. This paper is aimed at developing a structural models of fatigue damage of SM-films for irreversible random deformation.

This work shows that with an electron subsystem of granulated material of initial components of the mixture and their bulk composition selected in a certain way, the electron subsystem of the SM - film to be obtained (acquires) two unique features. The first is that the irreversible change of electric resistance (ΔR) of SM-film on the imposed deformation considerable exceeds R changes connected with accompanying , e.g. thermocyclic processes. The second feature is that for all kinds of imposed deformation (extension-compression; bending variations with different coefficients of asymmetry; various spectra of imposed deformation at which the resistance R_n of SM-film is recorded in equal time intervals) the following recurrent relation

$$R_{n+1}[\sigma] = Q_n[\sigma] * R_n[\sigma] = B_n * R_n[\sigma] + (1 - B_n) * M_n , \qquad (1)$$

is valid.

Here: R_n is the electric resistance of SM-film measured under the same state of the environment; **n** is the ordinal number of measurement (**n** = 1,2,3, ..., g); g is the maximum number of the measurement performed; Q_n is the loading operator

transferring the SE resistance from R_n-th state to R_{n+1} -th state ; σ is a complicated parameter to characterize the type of imposed deformation ; B_n and M_n depend on K_g of previous values of the SM-film resistance to be measured (K_g=1,2,3,...), i.e.

$$B_n = F_1 (R_n , R_{n-1} , \dots , R_{n-Kg}) ;$$
$$M_n = F_2 (R_n , R_{n-1} , \dots , R_{n-Kg}) ; \qquad (2)$$

where F_1 and F_2 are functions connected with formulas of linear regression. Their explicit form is given in the paper; K_g assumes integral values ($K_g < g$) and is equal to size of enclosures of the "time series", compose of experimental data of the type:

$$R_1 , R_2 , \dots , R_{n-1} , R_n , R_{n+1} , \dots , R_g \qquad (3)$$

In the work the heterogeneous material of SM-film is modeled by network of randomly connected electric resistances (impedances of various grains or their clusters).

Two models are discussed. The first is an illustrative model to elucidate high sensitivity (reaction) of efficient resistance R_n of SM-film to imposed deformation.

Two main situation are considered here. (A) A great set of electrically-passive single modules corresponding to an equilibrated Winstone bridge may always be found in the network of random resistances to be modeled ; (B) The network of random resistance to be modeled has a huge set of electrically-active modules with VA characteristics either of N-type or S-type.

The second model is intimately connected with the first model and disclosed the physical content of the coefficients B_n and $(1 - B_n)^* M_n$ entering into (1).

CONSTRUCTION MODEL OF SE FOR SIMPLE MODES OF DEFORMATION

Figure 1 shows R_{eff} versus the number, N, of loading cycles. This is typical of the SM-films for simple modes of deformation. Under irreversible random deformation, R_{eff} - N dependence became more intricate. A correlation between these situations is discussed below.

For the most part of elements both deformation potential and lattice distortions could not significantly affect the mass of free electrons M_0, i.e. $0.5 < M_{eff}/M_o < 2$ for Al,Cu, Zn ,.... .On the other hand Bi, Sb and their solutions as well as for La and some another elements $M_{eff} / M_o < 0.2$ (or $M_{eff}/M_o > 5$). Some compositions as well as condition ($M_{eff} << M_0$ (or $M_{eff} >> M_0$) provided high sensitivity of films to deformation [1,6,11]. For typical SE of SAFD a number of elements, measured by X-ray fluorescence spectrometer, are given in Tables 1,2

Table 1 shows the fluorescence spectrum line elicited from analyze of initial mixtures. Table 2 shows the fluorescence spectrum line elicited from analyze of the semiconductor film mixtures. There are exist series elements lines added to Table 1 .

A. THE ELECTRIC NON - ACTIVE MODULES . It has been known [8] that resistance, R_{eff}, of SE is simulated by lattice at the corners of which randomly located resistances - R_i (i = 1,2,3,..., M ; M - total number of grains [or clusters] of SMs). R_i is the resistance of the grains of the SMs randomly connected with neighboring grains. In that model lattice one may find a simple module in Fig.2 Model lattice consists of L modules, of this kind , each having index - k, (k = 1,2,...., L).

Table 1

λ 10^{-11}cm	929	942	1144	1314	1334	1392	1418	1432
I Imp/sec	108	111	18699	1548	294	921	450	830
Corresponding element	Cd 930.66 KB2	Sb 940.71 KA1	Bi 1143.86 LA1	Bi 1316.10 L1	Nb 1331.52 KB1,3	Cu 1392.22 KB1,3	Mo 1418.60 KA1	Re 1432.90 LA1
λ 10^{-11}cm	1490	1540	2284	2408	2568	2776	3077	3031
I Imp/sec	733	1573	163	28	79.5	41.8	162	306
Corresponding element	Nb KA1	Cu 1540.56 KA	V 2284.40 KB1,3	La 2410.50 LB3	Ba 2568.21 LB1	Ba 2775.95 LA1	Te 3076.80 LB1	Sc 3030.9 KA

Table 2

λ 10^{-11}cm	764	784	792	812	828	876	940
I Imp/sec	4504	3267	2992	2523	1878	3842	7094
Corresponding element	Th 765.21 LB1	Sr 782.92 KB1,3	Th 792.57 LB4	Bi 813.11 LG1	Y 828.84 KA	Sr 875.26 KA	Bi 938.55 LB3
λ 10^{-11}cm	956	968	976	1104	1140	1156	1312
I Imp/sec	8572	4569	2507	874	10254	6257	886
Corresponding element	Bi 955.18 LB2,15	Th 967.88 LA2	Bi 976.90 LB4	Se 1104.77 KA	Ir 1140.85 LB3	Bi 1155.36 LA2	Pt 1313.04 LA1

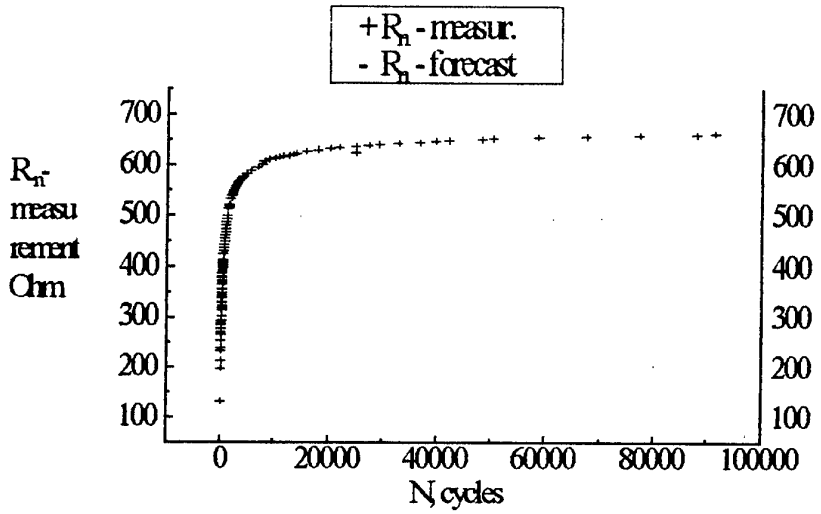

Fig 1a. HS-CFM's R_{eff} versus the number N cycles. Simple mode of loading (alternating [bending] strain}.

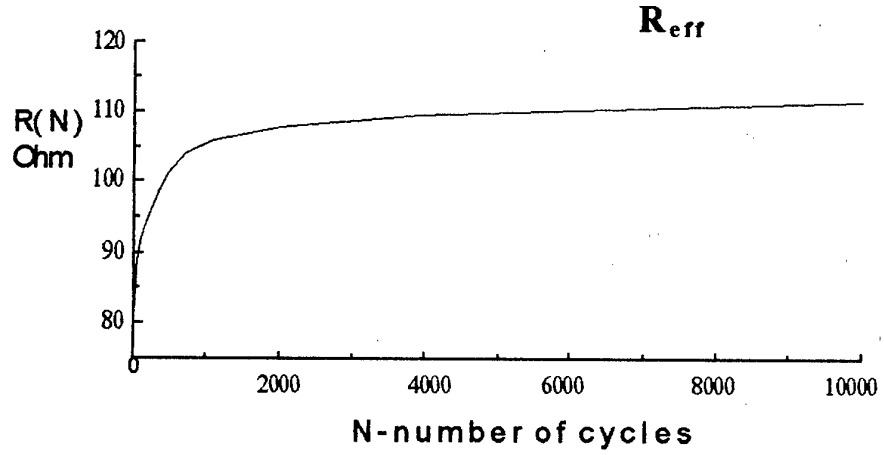

Fig. 1b. . Simple mode of loading (alternating [compressive-extension]strain])

At the equilibrium state the effective resistance R [a-b]= R_{eff} (measured from **a** to **b** points) of such module is independent of the quantity of resistance R_5 = R[c-d], intervening between the **c** and **d** points (Fig.2). The electric balance is disturbed under loading cycle (irreversible) of deformation. So, R[a-b] varies according to quantity of R[c-d]. It is the simplest model of high sensitivity of SM- films.

$$R(\mathbf{a\text{-}b}) = R_{eff} = R_\alpha * (1 + R_5 / R_\beta) / (1 + R_5 / R_\gamma)$$

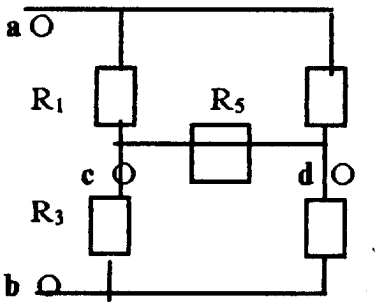

Here

$$R_\alpha = [R_1 * R_2 / (R_1 + R_2) + R_3 * R_4 / (R_3 + R_4)],$$

$$R_\beta = [R_1 * R_3 / (R_1 + R_3) + R_2 * R_4 / (R_2 + R_4)],$$

$$R_\gamma = [(R_1 + R_2) * (R_3 + R_4) + (R_1 + R_2 + R_3 + R_4)],$$

Fig.2 $R_{eff} = R(\mathbf{a\text{-}b})$ - resistivity of modules is measured by use **a** and **b** points. For equilibrium situation electric potential in **c** and **d** points are equal; so R(a-b) become independent from value of resistivity R_5.

To gain a greater insight into why the R_{eff} - N dependence has the form given in Fig.1 assume that for every module (Fig. 2)

$$\Delta R_k(\sigma, N) = \begin{cases} G(\sigma, m) * N & \text{if } N \le N_k \\ G(\sigma, m) * N_k & \text{if } N \ge N_k \end{cases} \qquad (4)$$

takes place; N_k vary in quantity. A scale factor - $G(\sigma,m)$ is the same for each module of the SM- film and depend on the amplitude - σ and degree of asymmetry - m of the superimposed regular cyclic deformation.

Each module (Fig.2) will be able to contribute to the ΔR_{eff} accordance with statistic g(k,) [6]:

$$\Delta R(\sigma, N) = \sum_{k=1}^{L} [\, g(k,) * \Delta R_k(\sigma, N)\,]; \quad \sum_{k=1}^{L} g(k,) = 1. \qquad (5)$$

$\Delta R_k(\sigma,m;\ N)$ - variation of resistance of a k-th module depend on the amplitude - σ and degree of asymmetry - m of the superimposed regular cyclic deformation. N is a number of cycles. For the sake of convenience, assume that $\Delta R_{max} = M(\sigma, m)$ and

$$Z_k = G(\sigma,m) * N_k / M(\sigma,m) \quad , (k = 1,2,3,..., L). \qquad (6)$$

Z_k and g(k,) can be found from experimental data, Fig. 1, and formula (5). Proceed as follows:

$$\Delta R(N) = G * N * \sum_{k=1}^{L} g(k) = G * N, \qquad 0 \le N \le N_1$$

$$\Delta R(N) = G * N_1 * g(1) + G * N * \{1 - g(1)\} \qquad N_1 \le N \le N_2$$

$$\Delta R(N) = G^*N_1^*g(1) + G^*N_2^*g(2) + G^*N^*\{1-g(1)-g(2)\}; \qquad N_2 \le N \le N_3$$

.....

$$\Delta R(N) = G^*\sum_{k=1}^{L} [N_k^*g(k)] \qquad N_L \le N \qquad (7)$$

Notice that $N_1 < N_2 < N_3 <.....< N_l$ and N vary in each of interval of $[N_k, N_{k+1}]$. Let us take a derivative of ΔR (N) with respect to N in each of (7) equalities. Then each subsequent equality can be subtracted from the preceding one. As a result one find all quantities of g(k, σ), N_k, as well as $G(\sigma,m)$ and $M(\sigma.m)$. Figure 3 presents the state of SE - film after both various number of cycles and value of the superimposed deformation.

Information entropy S

$$S = \sum_{\kappa=1}^{L} [\, g(k,)^*Ln\ g(k,)\,]. \qquad (8)$$

is a measure of the amount of disorder (different states) in MS-films. This model admits control of the structure mutations in SM - films after N cycles of a superimposed regular deformation. Nonelastic deformations of granules accounts for irreversible change of effective resistance R_{eff} of the SM-films [2,3]. Fig. 3a - 3c show the regular decrease of probability g(k) for arise a modules having a big value Z_k (see (6)). The increase of entropy S (see (8)) SM-film is presented on Fig. 3e. For nonregular deformation there is other situation (see Fig. 3d)

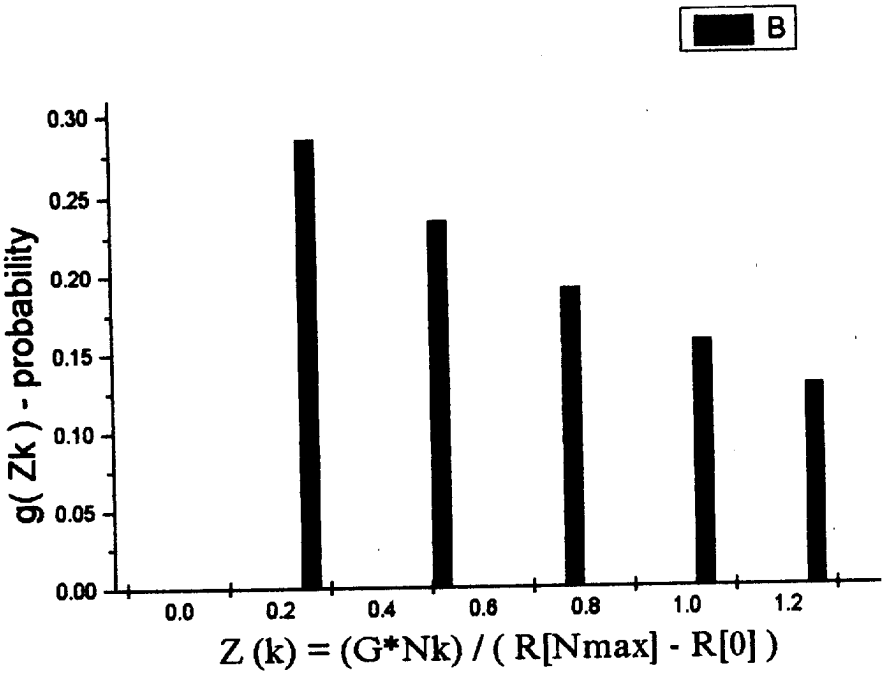

Fig. 3 a. The state of SM-film after be loaded 250 cycles of regular deformation : (σ_{eff} = 17 Kg/mm^2); σ_a = 7.42 Kg/mm^2 ; σ_m = 12.04 Kg/mm^2

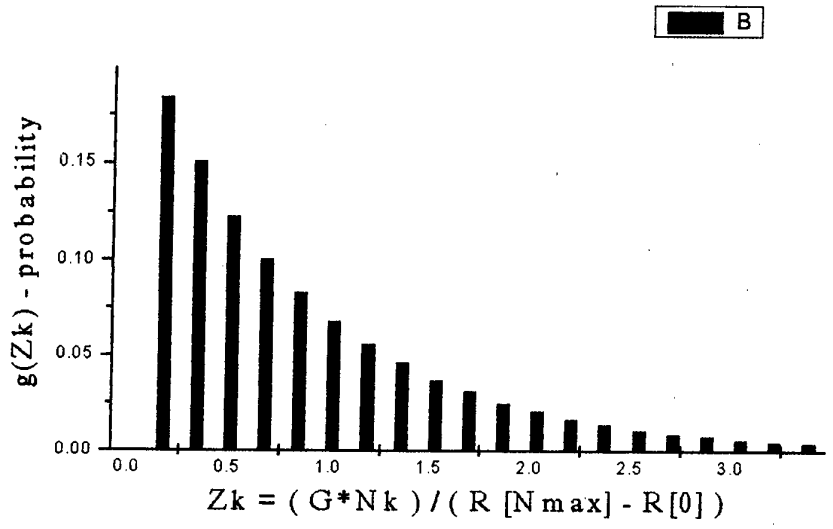

Fig. 3 b. The state of SM-film after be loaded 1000 cycles of regular deformation: (σ_{eff} = 17 Kg/mm²); σ_a = 7.42 Kg/mm² ; σ_m = 12.04 Kg/mm²

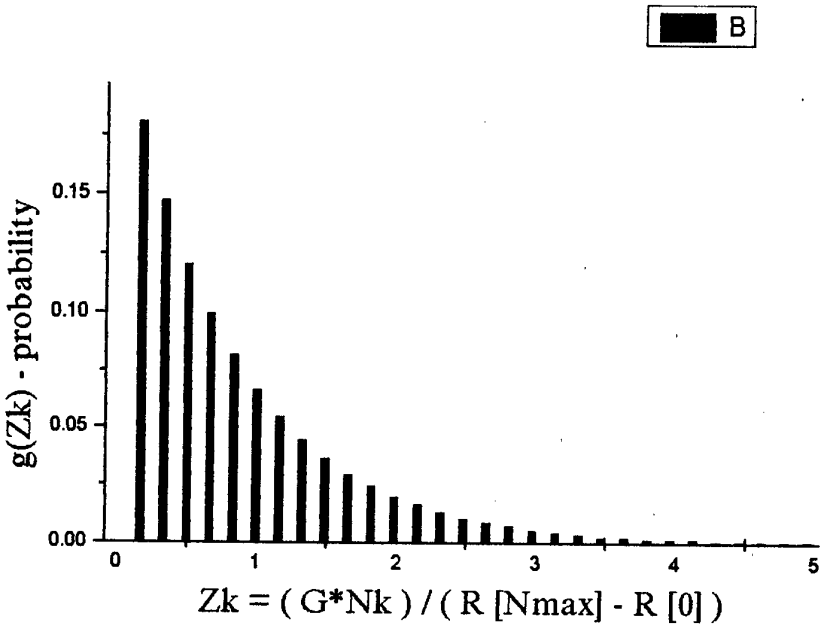

Fig. 3 c. The state of SM-film after be loaded 1500 cycles of regular deformation : (σ_{eff} = 17 Kg/mm²); σ_a = 7.42 Kg/mm² ; σ_m = 12.04 Kg/mm²

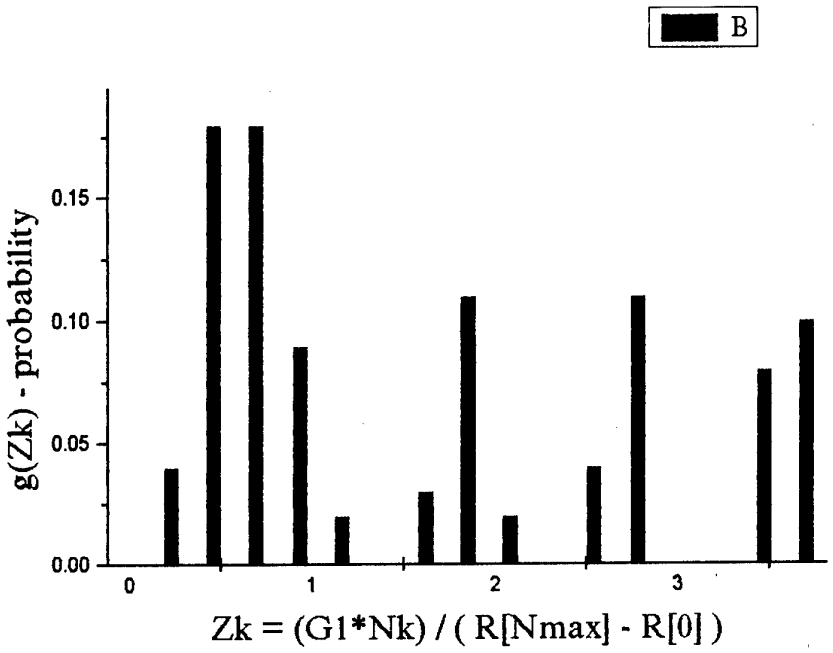

Fig. 3 d. The state of SM-film after be loaded 800 cycles of arbitrary deformation (σ_{eff} = 20.02 Kg/mm²)

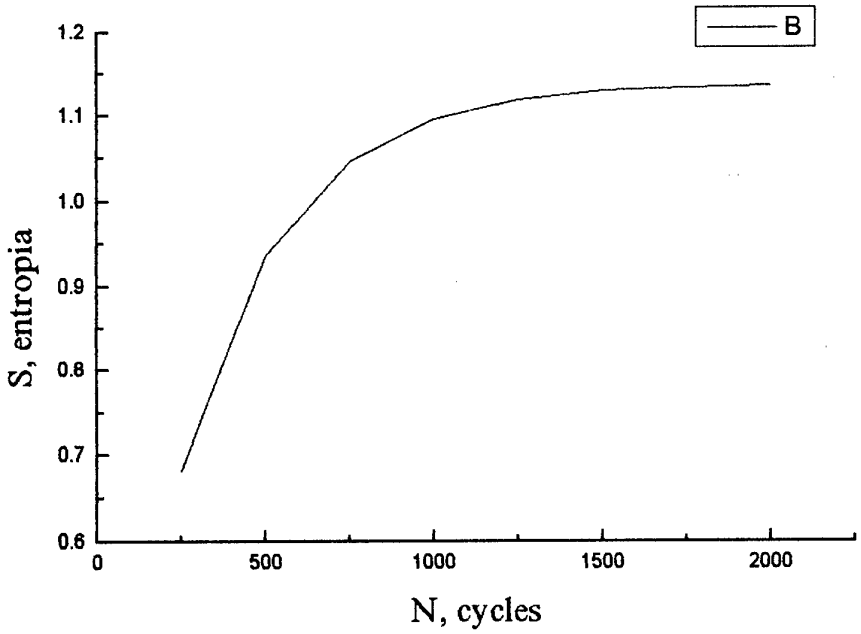

Fig. 3e . The increase of entropy (S) versus (N) regular cycles.

Б. THE ELECTRIC ACTIVE MODULES. In this model some granules (or active clusters) have the negative surfaces resistivity be conditioned by both inverse electron layers and intergranules surfaces electron states. So some modules (Fig. 2) can have negative efficient resistivity . Electron current be flying through these modules are dictated by both **principle of least ohmic (Joule) loss** and granules configuration of the SM.

TIME SERIES (SURVIVAL DATA)

Films obtained by evaporation of Bi_2Te_3 - Sb_2Te_3 onto poliamide substrates were studied. The films had variable volume contents of initial components. As mentioned above for Bi, Sb and their solution $M_{eff}/M_o < 0.2$ takes place. So they might be used for creating SE for SAFD. When superimposing deformation , the film state changes. There are two ways to describe it [1]:

(a) to derive physical and mathematical models of the system reaction; to find factors governing the behavior of the parameter to be measured;

(b) based on the experimental data, to derive a 'time series' (survival data) consisting of g terms. Analyzing the series, establish its *phase dimension* and carry out an adaptive prediction of the parameters are composing a numerical value of the (n+1)th term of the 'time series'. Then, based on (n+1) terms of series, predict a numerical value of the (n+2)th term of the series, and so on. A complicated semiconductor film system is being monitored.

Method (a) is appropriate for simple 1-D model films. Method (b) is preferable for multidimensional real film, such as semiconductor mixture films. The time series consisted of effective resistances $R_{eff}[n]$ of the films measured in an equal number (n) of cycles of a superimposed deformation :

$$\begin{aligned} R(N):\ R(N_o) = R_o;\ R(N_o+n) &= R(N_1) = R_1; \\ R(N_o+2*n) &= R(N_2) = R_2;... \\ &..... \\ R(N_o+i*n) &= R(Ni) = Ri\ ;\ ...\ . \end{aligned} \qquad (9)$$

$i = 1,2,.....$; N_o - initial number of cycles of a superimposed deformation.

As we have mentioned in [3] for simple modes one have

$$R(N_o),R(N_1),...,R(N_i),R(N_{i+1}),..., \qquad (10)$$

and the relationship

$$R(N_{i+1}) = B[\sigma]*R(N_i) + (1 - B[\sigma]) * M[\sigma\ ]\ , \qquad (11)$$

or the more convenient form :

$$R_{i+1} = Q_j\ R_j = B*R_i + (1 - B) * M \qquad (12)$$

$$R_{i+1} = Q[n;m,B,M] * R_i = B[m, \sigma\ ]*R_i + (1-B[m, \sigma])*M[m, \sigma]\ . \qquad (13)$$

takes place, there $B[\sigma] = B$; $M[\sigma] = M$ are constants. They depend on the amplitude - σ and degree of asymmetry (m) of the superimposed regular cyclic deformation. Q [n,m,B,M] is the loading operator . Two - fold application of operator Q leads one to

$$R_{i+2} = Q[n;m,B,M] * R_{i+1} = Q[n;m,B,M] * Q[n;m,B,M] * R_i =$$

$$= Q^2 [n;m,B,M] * R_i = B^2 * R_i + (1 - B^2) * M. \quad (14)$$

So if sequence (10) have l-terms, then relation

$$R_l = Q^l * R_o = B^l * R_o + (1 - B^l) * M . \quad (15)$$

takes place.

Both, the growth number of superimposed cycles as well as random deformation have a result an "agitation" of electronic compositions of SM-film. Such "agitation" accompanies with loss of the energy deformation and leads to irreversible change of the previous electronic configuration. So for SM-films the new factor appears - "history" of a sequence electronic compositions. In other words the SM-films have new factor - historical (or phase) dimension. A fracture dynamic of SM-films requires the sequence measurements of R_n (**n** - is the number of a measurement) .

For simple and complicated modes Fig.4 and Fig. 5 show the R_{n+1} dependence on previous h - terms of "time series" (10). h - is the phase dimension of time series. h = 1 for simple modes. In others causes h >1. For a complex modes there are exist $Q_j [\sigma_j ; m_j]$ operators. $Q_j \equiv Q_j [\sigma_j ; m_j]$ are the loading operators, and j is a complicated symbol (j = 1,2,3,...) describing both various amplitudes (σ_j) and asymmetry degrees (m_j) of loads .

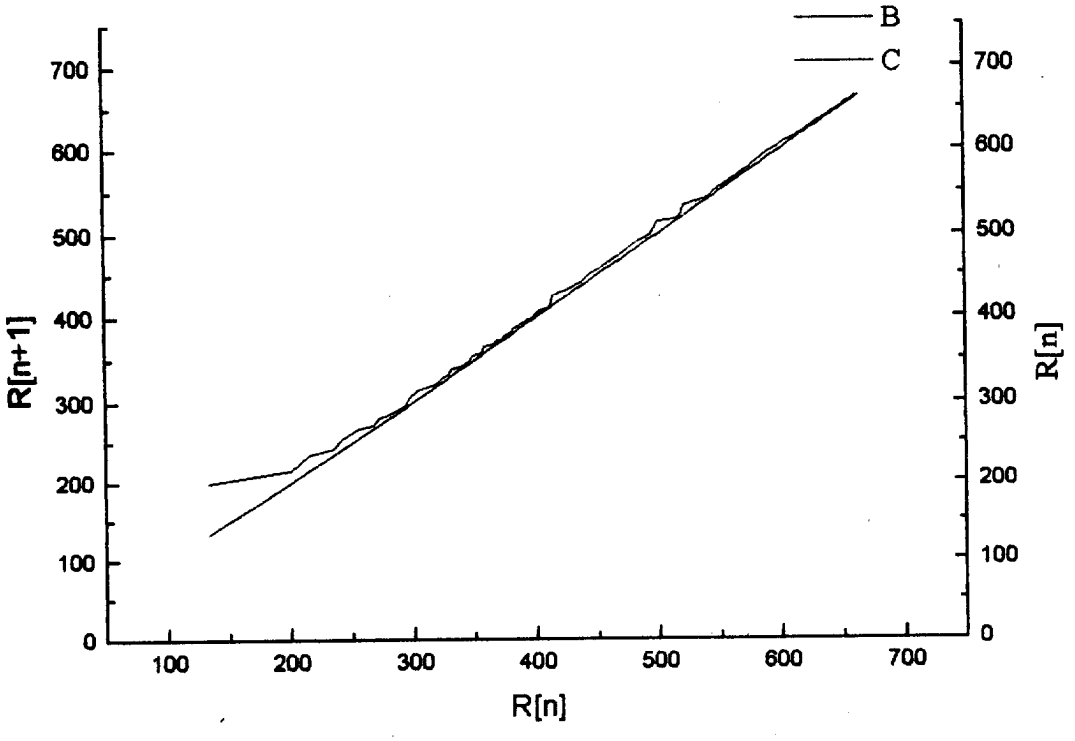

Fig. 4 The R_{n+1} versus R_n for a simple mode of loading ($\sigma_\pm = \pm$ 25 kg/mm^2)

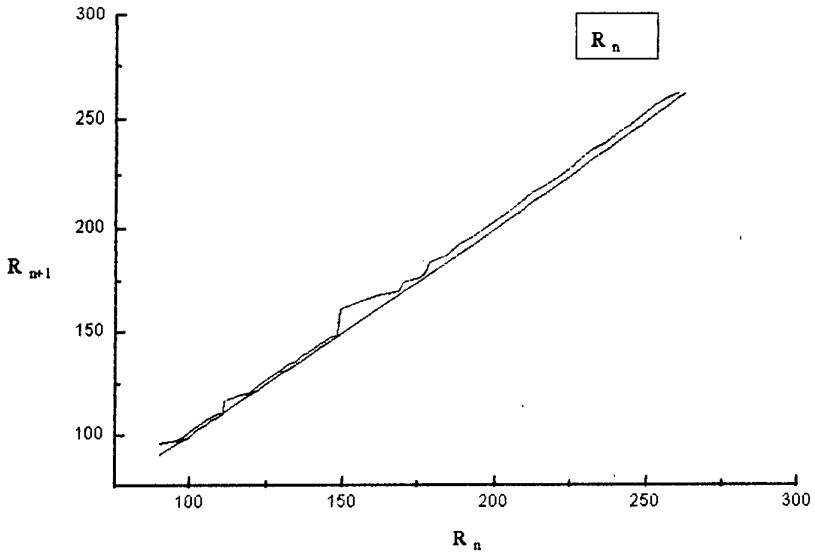

Fig. 5 The R_{n+1} versus of R_n ; n - number of measurement . Complex mode of loading (alternating [bending] strain}. N = 300; 400; 300 for $\sigma_{\pm} = \pm 15$ kg/mm^2 ;$\sigma_{\pm} = \pm 20$ kg/mm^2 ;$\sigma_{\pm} = \pm 25$ kg/mm^2, respective.

THE COMMUTATION of Qi and Qj OPERATORS. For complicated modes we have to study the condition of commutation of Q_i and Q_j operators. Let us assume at first Q_j and next Q_i are used to R_0 :

$$Q_i * Q_j * R_o = Q_i * \{ B_j * R_o + [1 - B_j] * M_j \} = B_i*B_j*R_o + [1 - B_i*B_j]*M_{i,j} , \qquad (16)$$

where $M_{i,j}$ is a limiting value of complex loading operator Q_{ij}

$$M_{i,j} = \frac{B_i*[1 - B_j]*M_j + [1 - B_i]*M_i}{[1 - B_i*B_j]} . \qquad (17)$$

An inverse sequence Q_i and Q_j leads to

$$Q_j * Q_i * R_o = Q_j * \{ B_i * R_o + [1 - B_i] * M_i \} = B_j*B_i*R_o + [1 - B_j*B_i]*M_{j,i} \qquad (18)$$

where Mj,i is a limited value of operator Qj,i = Qj*Qi :

$$M_{j,i} = \frac{B_j*[1 - B_i]*M_i + [1 - B_j]*M_j}{[1 - B_j*B_i]} . \qquad (19)$$

From (17) and (19) one find conditions of commutation of operators Q_i and Q_j :

$$1)\ B_i = 1 ;\quad 2)\ B_j = 1 ;\quad 3)\ M_i = M_j. \qquad (20)$$

First and second conditions corresponds to the situation of $Q_i = 1$ or $Q_j = 1$. In accordance to the third condition, limited value of Q_i and Q_j are equal

Now we will deal with the sequence of $\{Q_i * Q_j\}^r$. O_j- operating u - times, then Q_i -operating v - times and this combination operating r times. At first we obtain

$$Q_i^v*(Q_j^u*R_o) = B_i^v * (Q_j^u*R_o) + (1 - B_i^v)*M_i =$$

$$= B_i^v*\{B_j^u*R_o + (1 - B_j^u)*M_j\} + (1-B_j^v)*M_j =$$

$$= B_i^v*B_j^u*R_o + B_i^v*(1-B_j^u)*M_j + (1-B_i^v)*M_i . \qquad (21)$$

Applying complex operator $Q_{i,j}$ to (21) we obtain

$$Q_{u,v} * R_o = B_{u,v} * R_o + (1 - B_{u,v}) * M_{u,v} \qquad (22)$$

where $B_{u,v} = B_i^v*B_j^u$, and $M_{u,v}$

$$M_{u,v} = \frac{B_i^v*(1-B_j^u)*M_j + (1-B_i^v)*M_i}{1 - B_{u,v}} \qquad (23)$$

We make use of the operator $Q_{i,j}$ r times :

$$Q_{u,v}^r * R_o = B_{u,v}^r * R_o + \{ 1 - B_{u,v}^r\} * M_{u,v}. \qquad (24)$$

For u = const and v tending toward infinity, we have :

$$\lim_{v \to \infty} M_{u,v} = M_i , \quad M_i \neq 1. \qquad (25)$$

Otherwise, for v = const and u ----> oo , we have

$$\lim_{u \to \infty} M_{u,v} = B_i^v * M_j + (1-B_i^v)*M_i . \qquad (26)$$

The results of an arbitrary sequence of operators - Q acting on the SE film may be predicted in this way.

The nature of migration of the defects, shaping the effective resistance , R_{eff}, in film, is unaffected by the initial value of R_0 . The migrations of the defects are consistent with linear nature of the loading operators Q. So, we can circumvent the difficulties connected with the need to investigate the nature of process of defect migration. This suggests the use of the black box concept.There are input signals (irreversible deformations) and output reactions (ΔR_{eff}). Linearity of loading operator - Q allows ones to calculate a reaction of SM-film resistance on spectrum of random deformation. As an example, we consider such situation when both Q_{n1} and Q_{n2} occurs with the p_1 and p_2 ($p_2 = 1 - p_1$) probability. For the weighted mean of effective resistance -$\langle R_{eff} \rangle$ we have

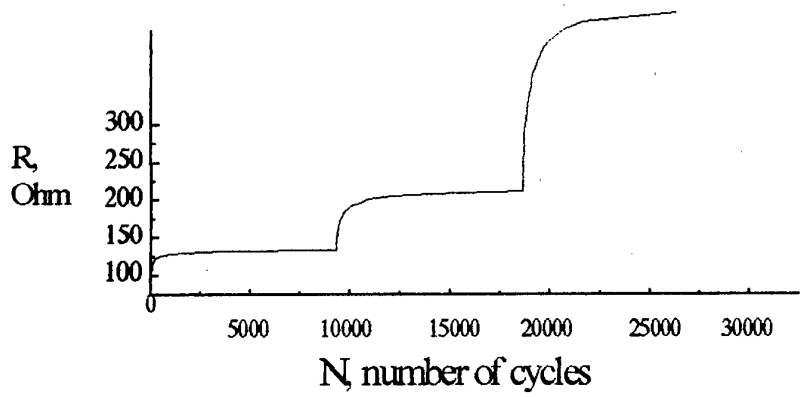

Fig. 6. Complicated mode of loading.

$$<R_{eff}> = p_1*Q_{n1}*R_o + p_2*Q_{n2}*R_o = <B> * R_o + (1 - <B>) * << M >> , \qquad (27)$$

Here

$$<B> = p_1*B_{n1} + p_2*B_{n2}$$

$$<< M >> = \{ p_1 * (1 - B_{n1})*M_{n1} + p_2* (1 - B_{n2})*M_{n2} \} / \{ 1 - < B > \},$$

take place.

For operators Q_i occurring with probability p_i ($i = 1, 2, 3, ..., K$), the formulas

$$< B >= \sum_{i=1}^{K} (p_i * B_{ni}) \quad ,$$

and

$$<< M >>= \{\sum [p_i *(1 - B_{ni}) * M_{ni}]\} / \{1 - < B >\}$$ take place.

In a similar manner it is easy to receive formula for $<R_{eff}>$ associated with the Markoff process .

MODEL OF STIMULUS ELEMENTS.

In this model the imposed deformation and one of the modules (either electrically active or electrically passive) are considered to be a stimulus element . The sensitive element of SAFD contains a set of such stimulus elements. The active subset C of the set S forms variable electric resistance R_n of SM-film to imposed deformation.

The subset C of the set S contains only active stimulus elements. Resistance R_n of SM-film is an additive function determined on the set S. It is established that for SM-film of SAFD at any ordinal number n of measurement there are always two nonintersecting subsets (A_n and B_n) of set S having the following property. All the stimulus elements of subset A_n become active, while all the stimulus elements of subset B_n, on the contrary, become passive.

The conception reported permits adaptive prediction of the numerical value of the electric resistance of the SM-film of SAFD from K_g of their earlier measured values.

This conception is applied to SM-film of SAFD, on which the whole load of the TU-154B wing was imposed. Electric resistance $R(A_n|A_n)$ of the subset A_n is shown as a function of the number of the airplane landings (n).

STIMULUS ELEMENTS. SM-films have an intricate electrical potential relief. So there are many couples of points possessing the same electrical potential. The certain regions of SM-film containing couples mentioned above are active. They form the irreversible changes R_{eff} of SM-film (Fig.2).

An enormal array of different electronic compositions are generated in single SM-film installed on the operating aviation design. One can fix irreversible changes of electronic compositions having taken sequence measurements of SM-films the electric resistance at equal number of superimposed deformation intervals [1].)

In [12] it was found, that the variations of R_{eff} correspond to N_{sum} - number acoustic emission originated in aviation design material (Fig.7). In this paper the superimposed deformation and allied SM-film's microstructure are the stimulus element (*SE*) of set S.

The response of SM-film (for example, irreversible change of its electrical resistance $R = R(S|C)$) depends on separate SEs, making set S. The part of SEs can be subject of the experimental control, and an other part can be constant or casually changed. The active subset C of SEs of set S forms variability of effective resistance HS-CFM at superimposing of chaotic deformation.

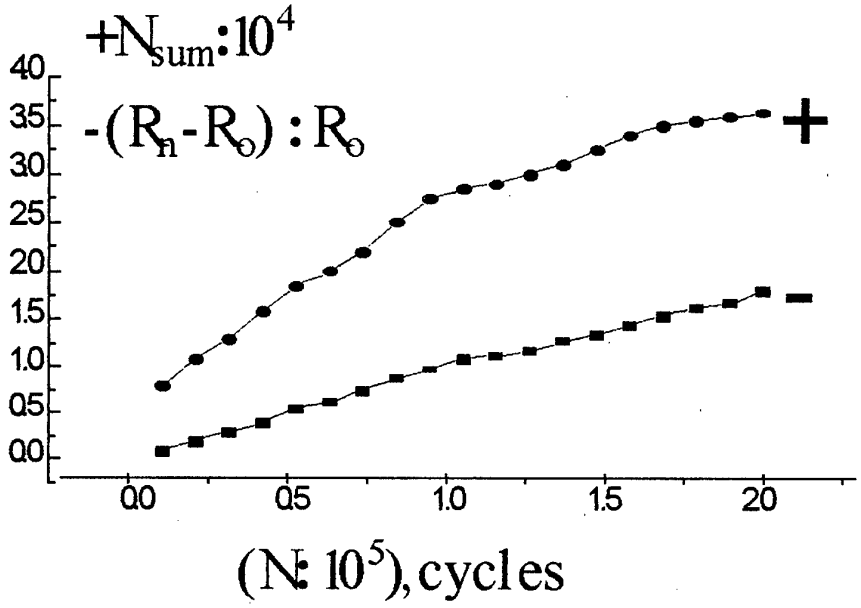

Fig. 7 HS-CFM resistance $[(R_n - R_o)/R_o]$ and total acoustic emission N_{sum} of the D-16T specimen versus number of cycles N of the superimposed deformation corresponding to a 25 kg/ mm^2 load. The asymmetry coefficient is unity (m =1). The HS-CFMs as well as D-16T specimens are sensitive to cracking.

UNCROSSING SUBSETS A and B. In general, *SEs* change of a subset C results in the irreversible change R - response of HS-CFM on superimposed deformation. R - function, determined on the set S and satisfying with additivity condition. For example, R=R(S|S) - resistance of HS-CFM, in which all stimulus elements of set S - are active: the crossing of subset C and set S gives the set S [$C \cap S = S$]. R(S|0) - resistance of HS-CFM in which active SE is not present. R(A|(A$\cap$C)) and R(B|(B$\cap$C)) - resistance are associated with two uncrossing subsets A and B (crossing $A \cap B = 0$) of the set S. In general both R(A|(A$\cap$C)) and R(B|(B$\cap$C)) may be positive as well as negative.

Using the experimental data we find , that after each damage process all stimulus elements of a subset A become active, and all stimulus elements of a subset B on the contrary become non active. This situation is discussed just below.

Let X - time to be the time in cycles of loading : X = 0, 1, 2, ... , and this value is not proportional to chronological time. Let Y - time to be chronological time measured in hours, days, etc., so Y = 1, 2, 3, ... in corresponding units of time. If loading cycles duration varies at random as it occurs, for example, at the aircraft flights, it is desirable to be able to convert damages accumulation in X - time in to the average number of damages accumulation in Y - time and inversely. It can be done with the help of "time-transmission" function Y = G(X) [7].

Let us, **n** is a number of superimposed deformation, **n** - may be a number of cycles, or **n** - may be a number of minutes (seconds) and so on. Before **n+1** deformation is superimposed we have the next situation:

* S - is a set of all SEs;
* C - is a subset of active SEs from set S (before **n + 1**);
* A - is a subset containing both active as well as non active SEs from set S;
* B - is another subset, containing both active as well as non active SEs from set S;
* subset A and subset B are uncrossing;
* A$\cap$C - is a subset of active SEs from subset A;
* B$\cap$C - is a subset of active SEs from subset B;
* R_n= R(S|C) - electrical resistance of HS-CFM after **n** superimposed deformation;
* r_n = R(S|C)/ R(S|S) = R(A|(A$\cap$ C)) / R(A|A) = R(B|(B$\cap$ C))/ R(B|B).

After **n+ 1** superimposed deformation subset C changes and we have the next situation:

* S - is a set of all SEs;
* (C + dC) - is a subset of active SEs from set S;
* $A_n \cap (C + dC) = A_n$ - all SEs of subset A_n become active (index **n** in subset A indicated on to previous measurement);
* $B_n \cap (C+dC) = 0$ - all SEs of subset B_n become non active;
* R_{n+1} = R(S|(C+dC)) - electrical resistance of HS-CFM after **n+1** superimposed deformation;
* r_{n+1} = R(S|(C+dC)) / R(S|S)

After (**n+1**) superimposed deformation the resistivity of SM-film changes:

$$R(S|(C+dC)) - R(S|C) = [R(A|A) - R(A|(A \cap C))] - R(B|(B \cap C)), \quad (28)$$

or

$$r_{n+1} = r_n * (1 - [R(A|A)+R(B|B)]/R(S|S)) + R(A|A)/ R(S|S). \quad (29)$$

Finally, one can receive

$$R_{n+1} = B_n * R_n + (1 - B_n) *\cdot M_n = Q_n^i * R_n = Q * R_n \quad (30)$$

where,

$$B_n = (R(S|S) - R(A|A) - R(B|B)) / R(S|S), \quad (31)$$

$$M_n = R(S|S) * (R(A|A) / [R(A|A) + R(B|B)]), \quad (32)$$

$Q_n^i = Q$ - is the loading operator transforming R_n to R_{n+1}, and i is a complicated symbol describing amplitude and degree of load asymmetry. The k-fold application of the simple loading operator Q_n^i transforms the resistance R_n (i) into R_{n+k}(i) :

$$R_{n+k}(i) = B_n^k * R_n(i) + (1 - B_n^k)*M_n \quad (33)$$

Formulae (30) and (33) correspond to (13) and (15) accordingly. Formulae (31) and (32) are indicating the physical meanings of parameters B_n and M_n from (1) and (30).

Figure 6 shows the dependence of R_n (N) for complicated modes of loading. We select R(S|S) being the same for all HS-CFM researched. R(A|A), and R(B|B) might be changed with number (n) growth. B_n and M_n are associated with couple subsets **A** and **B**. It turns out, that for regular cyclic loadings B_n as well as M_n are constants .For chaotic loadings M_n and B_n features are discussed below.

BI_2TE_3 - SB_2TE_3 FILMS FOR SAFD.

Films obtained by evaporated of Bi_2Te_3 - Sb_2Te_3 onto poliamide substrates were studied. The films had variable volume contents of initial components. As mentioned above for **Bi, Sb** and their solutions $M_{eff} / M_o < 0.2$ takes place. So they might be used for CFDG creating. Some compositions provided high sensitivity to deformation [1].

The characteristics (B_n and M_n) of coupled subsets **A** and **B** as well as complex dynamics of their change with growth of number of superimposed deformation cycles were determined. HS-CFM resistances R_n = **R(S|C)** are measured through equidistant "time" intervals τ :

$$\{ R(T_n) \} \rightarrow R[T_0]; R[T_1]; R[T_2] ; .... R[T_n]; ...; R[T_g] ; \quad T_{n+1} = T_n + \tau. \quad (34)$$

Where n is the number of measurement, g- is the maximum number of measured resistance R(S|C). This experimental data array is considered as a "time series". By using the Grassbereger and Procaccia [8] procedure, efficient phase dimensionalities K_g is calculated. K_g is integer and, in general, depends on the magnitude of the chosen interval (τ).

Taking into account the numerical value of K_g , formulas (1) for R_n, and using formulas of regression, we can find the $n*\tau$ depends of parameters B_n and M_n.

$$Bn = \frac{(\sum_{i=1}^{Kg} Rn-i)*(\sum_{i=1}^{Kg} Rn+1-i) - Kg*\sum_{i=1}^{Kg}(Rn-i*Rn+1-i))}{(\sum_{i=1}^{Kg} Rn-i)^2 - Kg*\sum_{i=1}^{Kg}(Rn-i)^2} \quad ; \qquad (35)$$

$$Mn = \frac{\sum_{i=1}^{Kg} Rn+1-i - Bn*\sum_{i=1}^{Kg} Rn-i}{Kg*(1-Bn)}; \qquad n > K_g > 2. \qquad (36)$$

The relationships

$B_n = B_{n-1} = B_{n-2} = ... = B_{n-Kg+1}$; and $M_n = M_{n-1} = M_{n-2} = ... = M_{n-Kg+1}$ (37)

take place. As a result R_{n+1} can be forecasted from previous values of R_n (34) (See Fig.1,6; Table 2).

The **Bi_2Te_3 - Sb_2Te_3** HS-CFMs were placed on to D-16T aluminum specimens and Tu-154B plane wing. Figure 3 shows the resistance R_n and total acoustic emission (A.E.-N_{sum}) from D-16T specimens versus the number of superimposed cycles [1,6]. This shows that the HS-CFMs as well as D-16T specimens are sensitive to cracking.

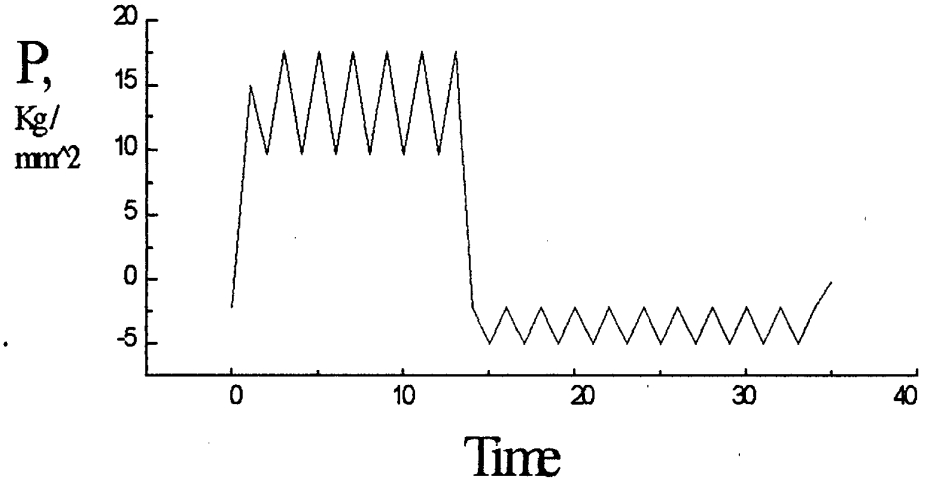

Figure 8. Typical loading spectrum of Tu-154B wing.

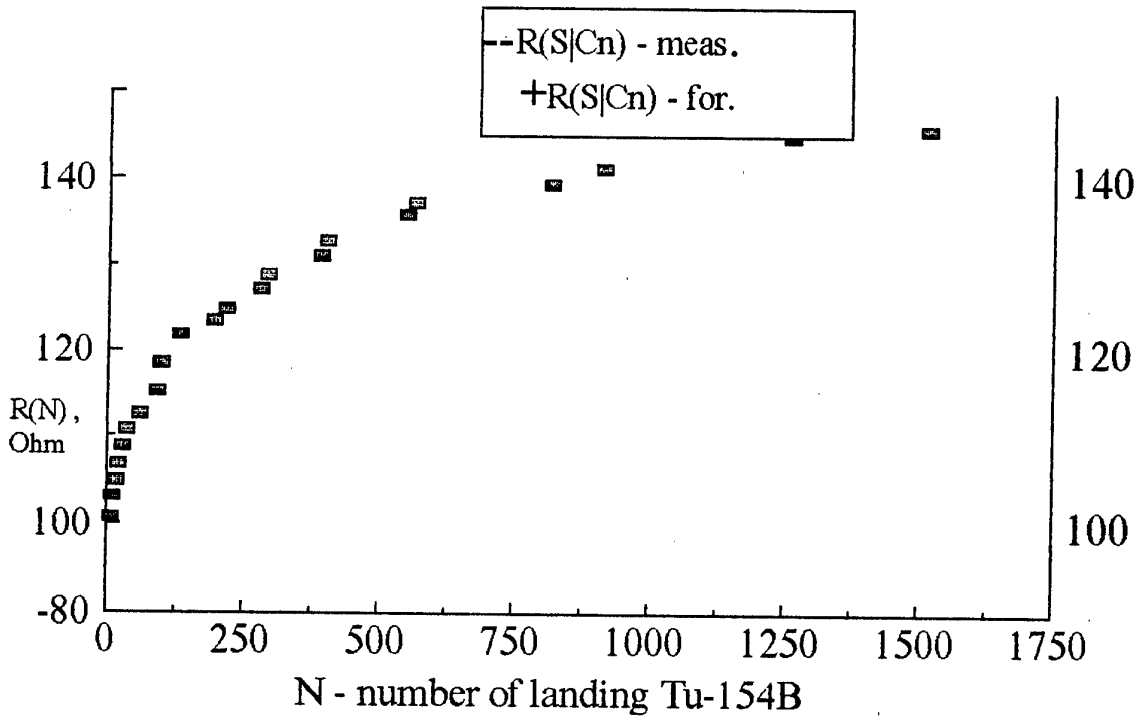

Figure 9. HS-CFMs R(S|Cn) changes for TU-154B wing loading spectra.

Table 3 shows the dependence of $(1 - B_n)*M_n = R(A_n|A_n)$ (FIG. 10) for complicated modes of Tu-154B loading (Fig 8).

Figure 9 and Table 3 show the dependence of R_n for complicated modes of loading (See Fig.8). There are experimental data (-) and forecasting data (+) calculated by using the formulae (1) ,-(4,5). Applicability of formulas (1) for a load of Tu-154 plane wing is obvious.

According to the output SAFD parameters (predictors) as well as to the calibration data it is easy and reliably (with 95% trustworthy boundary) to determine N_{sum} of AE impulses (Fig. 7), generating in the constructions elements under the control, when the operation spectra of loading are over laid on it.

SM-films allow to determine the efficient number of AE impulses ($N_{sum.\ eff}$ - effective) corresponding to special deformation (m=0) loading on the construction, that is equal to operation (including random) loading spectra.

CONCLUSION.

As mentioned above the Bi_2Te_3 - Sb_2Te_3 films as well as D-16T specimens are sensitive to cracking [1,12]. Changes of their microstructures have some common features and are fixed by continuous measurements of both the changes of the films resistivity R and summary number of acoustic impulses (N_{sum})of D-16 Aluminum. Conclusions regarding proportionality R and
N_{sum} under sufficiently extensive spectrum of deformation are made.

It is necessary to put through the next items for adaptive forecasting of fatigue damage of aviation designs with HS-CFMs help :

1. The HS-CFMs must be rigidly placed onto different elements of the aviation designs. All selected HS-CFMs have to have the same R(S|S) . The part of HS-CFMs with their resistivity R_n previously measured (See "times serious") must be calibrated. The aim of calibration is to estimate (B_n , M_n) parameters in equations (1) for simple cycles of loading with different coefficients (m) of asymmetry as well as different amplitudes and number of loading cycles. The loading of m=0 cycles and conversion of complicated block (See fig. 8) cycles to m=0 cycles. So calibrating data can be created.
2. Equidistant "time" interval (τ) must be selected.
3. From " time series" one can calculate K_g , using Grassberger Procassia [8] procedure.From formulae (35) and (36) one can calculate B_n and M_n for real situations. Then using (30) one can forecast R_{n+1} for every SM-films , installed on designs.

Then using the calibrating data one can adaptively forecast the fatigue damage of aviation designs.

Table 3

n - number of measurement	N - number of landing Tu-154	R_{n+1} - measured resistance; Ohm	R_{n+1}-forecasted resistance;Ohm K_g= 3	$(1-B_n)*M_n$ = $R(A_n\|A_n)$:Ohm K_g =3
1	0	97.3		
2	2	99.2		
3	4	101.2	100.7	60.1
4	7	103.1	103.1	2.0
5	10	104.9	104.9	7.1
6	17	106.8	106.8	1.9
7	20	108.8	108.8	- 3.8
8	28	110.7	110.7	2.0
9	36	112.5	112.5	7.5
10	59	115.4	115.2	-27.4
11	90	118.3	118.5	-21.4
12	98	122.1	121.9	-14.7
13	132	123.0	123.5	40.2
14	195	126.0	124.9	44.4
15	217	126.9	127.2	23.4
16	279	129.7	128.8	29.1
17	294	130.7	131.0	18.5
18	391	133.6	132.7	17.5
19	402	135.5	135.8	-11.5
20	550	137.4	137.2	31.5
21	566	139.3	139.3	1.9
22	817	141.2	141.2	1.9
23	914	145.1	144.8	-70.7
24	1262	145.1	145.7	62.6
25	1516			

We wish to thank the SibNIA (Novosibirsk, Russia), GosNII GA, TsAGI ,Ilushin Const. Bur, (Moscow, Russia), US Air Force EOARD (London, UK) ,and the Fund of Fundamentals

Research of Uzbek Academy of Science (Tashkent, Uzbekistan) for their contribution to the success of this paper.

References :

1. Shamirzaev S., Khamrakulov I.V. and Sviridov V.M. Effective interface density of electron states in semiconductor mixture films. 1994// Int.J.Electronics,London,Special ussue. ;
   1a). Orlov S.G. The calibration method of fatigue damage gages..// Problemi Prochnosti .- 1981, No.10, p. 42-47.
2. Shamirzaev S., Sviridov V., Khamrakulov I.l., Conductance of heterogeneous media under superposition of irreversible random deformation.1992//PreprintNo.172-92,PTI,Tashkent,pp.1-23.
3. Shamirzaev S., et all. Deformation coefficient of Bi_2Te_3 - Sb_2Te_3 films.// Izvestiya Academii Nauk Uzbekistana. No 1, 1990
4. Gochfeld D., Sadakov O., Plasticity and crawlibility of construction elements under repeatedly loadings.1984//Moskov, "Mashinostroenie", pp.11-26.
5. Bothvina L., Damage kinetics of construction materials, 1989// Moscov, "Nauka".
6. Azimov S., Shamirzaev S., et.al., Efficient dielectric permeability of selected coverings, 1985// Geliotechnica.,pp. 31-35.
7. Bogdanoff J., Kozin F., Probabilistic Models of Cumulative Damage,1985//John Wiley&Sons .Inc.
8. Dubrov V.E., Levinstein M.E., Shur M.S. // Soviet JETP - 1976. v- 70, no.5 - p.2014.
9. Kunce Kh. I.. Methods of Physical measurements . / Moscow, Mir,1989,p.214 (59-62).
10. Grassberger P., Procassia I., 1983// Physica, 9D, 189-208.
11. S. Shamirzaev Adaptive forecasting of fatigue damage of aviation designs with help HS-CF // PROCEEDINGS FOR THE ADPC SYMPOSIUM , Dayton(Fairborn), Ohio, USA , AUGUST 8-9,1996, pp. 344 - 354.
12. V.M. Sviridov , A.N. Seriouznov , D.A. Troenkin, S.Kh. Shamirzaev. $(Bi\text{-}Sb)_{2+x}Te_{3-x}$ heterogeneous films effective resistance under superimposing irreversible cyclic deformation., 1994// Uzbek Physic Journal, No.2,pp. 21-24.

MONITORING PRINCIPLES, MEANS AND METHODS FOR AIRFRAME INDIVIDUAL LOADING

V.L.Raikher
TsAGI, Zhukovsky

The degradation processes in airframe structures will be accumulate in different copies of the same type of the structure at different rates. One of the main reasons is the difference in the individual environment for every specimen. Therefore, if we want to organize the optimal service procedure we must establish individual values of intervals for "interference actions", for example, inspections or overhauls. The main physical reason for many service airframe failures is fatigue. If we want to monitor the fatigue damage accumulation we must define the individual loading influence for every airframe copy.

The most information of structural durability including data about crack growth rates comes from the full-scale tests. Although the present-day test systems make it possible to load the structure according to high simulation accuracy standards and to achieve a close similarity to real loading, special attention must be paid to property loading of Structure Significant Items (SSI's), i.e. structure critical areas. But it is very well known that good adequacy level of test conditions to the real flight loads cannot be achieved now for a big lot of all SSI's. Therefore a single "exit" is a reliable one: we must establish FOR EVERY CRITICAL POINT (Structure Significant Item) the equivalent, the "exchange" value between real and test loading.

But two main questions are arised:

- what do we name as "real loading"?
- what are the means of comparency for real and test loading?

The first question is difficult because every single copy of the same structure lives under its own "loading field" connected with its own, individual service conditions. However, the answer is simple: let us come to an agreement (this agreement is a wide spread point of view and it is used as a domestic approach), that the "real loading" is a MEAN loading of many "individual loadings", one of which (the "worst") may be greater (in fatigue sense) up to 1.5 times or more than the mean value. The corresponding reliability factor $\eta = 1.5$ is standardized, and all full-scale fatigue test result must be devided by this factor.

The second question is more difficult because the answer must be based on the physics of the fatigue cumulation process. To our regret understanding in this field is very far from excellence. But there are many physical and phenomenological fatigue and crack growth models; there is a big lot of fatigue test results for different structure fragments, elements; there is much engineering experience in aviation and in other fields of technology. All this "environment" gives the assurance that a simple and wide used calculation method based on the Linear Hypothesis of Fatigue Cumulation is an acceptable method for comparing of two different but similar "loading patterns" (one has to remember that tests loading is made according to high simulation accuracy standards!). This method contains of following successive steps (Figure 1):

1. For every critical point the loading parameter X must be "designed" or chosen which is "responsible" for fatigue cumulation in this critical point. This parameter depends on external loading and structure characteristics and may be very simple (for example, the tensile nominal stress in the area where the stress concentrator exists; the tangent stress on the selvage of a hole, etc.) or complex as a linear (it is better) or nonlinear function of stress components.
2. The well-known "rain-flow" or any analogy method, for example, the so called "method of complete cycles", should be applied in order to modify the loading time

history of the parameter X to the scope of cycles (or half-cycles) each having any mean and amplitude value.

3. Special formulae should be applies in order to modify every initial cycle to an equivalent positive pulsing (the minimum value is zero) cycle. Two parameters: æ and b must be existed in the formulae; they are dependent on material and their values are near $\tilde{æ} = 0.5$ and $\tilde{b} = 0.2$ for aluminum alloys.
4. The "threshold" parameter X_0 may be taken into account in order to exclude the "noise" and eliminate very small loads which are not important for fatigue damage cumulation. A conservative value of $\tilde{X}_0=0$ is usually applied.
5. An exponent form Wohler curve of fatigue resistance is usually in order to obtain the fatigue value induced to the structure critical point by pulsing cycle having maximum value of X_{max}. Therefore this one-cycle fatigue value $A\xi_i$ will be calculate as $A\xi_i = X^m_{maxi}$, where A and m are parameters of the Wohler curve. The usually used value of $m = 4$ is practically applied to aluminum alloy structures.
6. Linear addition procedure of fatigue values for all cycles which were acting during the chosen time interval, for example, during one typical (mean) flight, should be made this summa $\xi_{flight} = \sum_i X^m_{max\ i}$ is accepted as a fatigue resistance value which was "spent" during one typical flight.

The same algorithm of calculation may be applied to the test loading, for example, to one repeating block of cycles having different mean and amplitude values (the "test flight"). The fatigue resistance value $\xi_{test} = \sum_j X^m_{max\ j}$ which was "spent" during one "test flight" and the equivalent value $E_q = \xi_{test} / \xi_{flight}$ may be derived.

This simple procedure is a generally accepted one and its effective practical applications to many types of airframes is well known.

And now we can put a question: if we want to compare different (but similar, of course) loadings of the critical point during two different real flights, what a procedure may be recommended? The answer is obvious. The "only" difficulty is about the means by help of which the responsible parameters X for a lot of critical points can be "on line" measures and the values of ξ_{flight} can be derived.

A simple "input" such as the nominal three-component plane stress-strain state of the SSI area (in wing panel, for example) may be used. The information about this "load field" may be obtained from strain gauges installed in the zone as it can be realized by the On Board Fatigue Life Counter (FALC - System) [1, 2]. The most simple FALC parameter Y is calculated as a linear function of stress-strain components. The parameter Y may be much different from the abovementioned parameter X which is of "true" responsibility. For example, it is known that parameter X is an essentially non-linear function of stress-strain components if the loaded hole in the riveted joint as an SSI is considered. But it is possible to use a simple Y-parameter instead of much more complicated X-parameter if a special TUNING PROCEDURE is applied.

Let us consider the calculation algorithm parameters æ, b, m and the "threshold" parameter to be "free parameters" while being applied to the Y-parameter (they are "cycled" in Figure 1). Their values must be specially chosen to result the minimum difference from "ideal" X-parameter (which includes $\tilde{æ}$, $\tilde{b}$, $\tilde{m}$ and usually zero "threshold" parameter) influence on the fatigue cumulation. The "free parameters" choosing procedure is the tuning one. The tuning criterion may be taken as the relationship $\hat{\xi} = \xi_x / \xi_y$ of the "ideal" fatigue damage ξ_x to the damage ξ_y calculated on the Y-parameter basis. If this relationship (or its logarithm as at the Figure 2) is near the constant value for EVERY OF MANY VERY DIFFERENT FLIGHTS the Y-parameter of the FAC|LC- System may be accepted instead of X-parameter as a measure of flight loading difference and therefore as a fatigue loads monitoring parameter. The

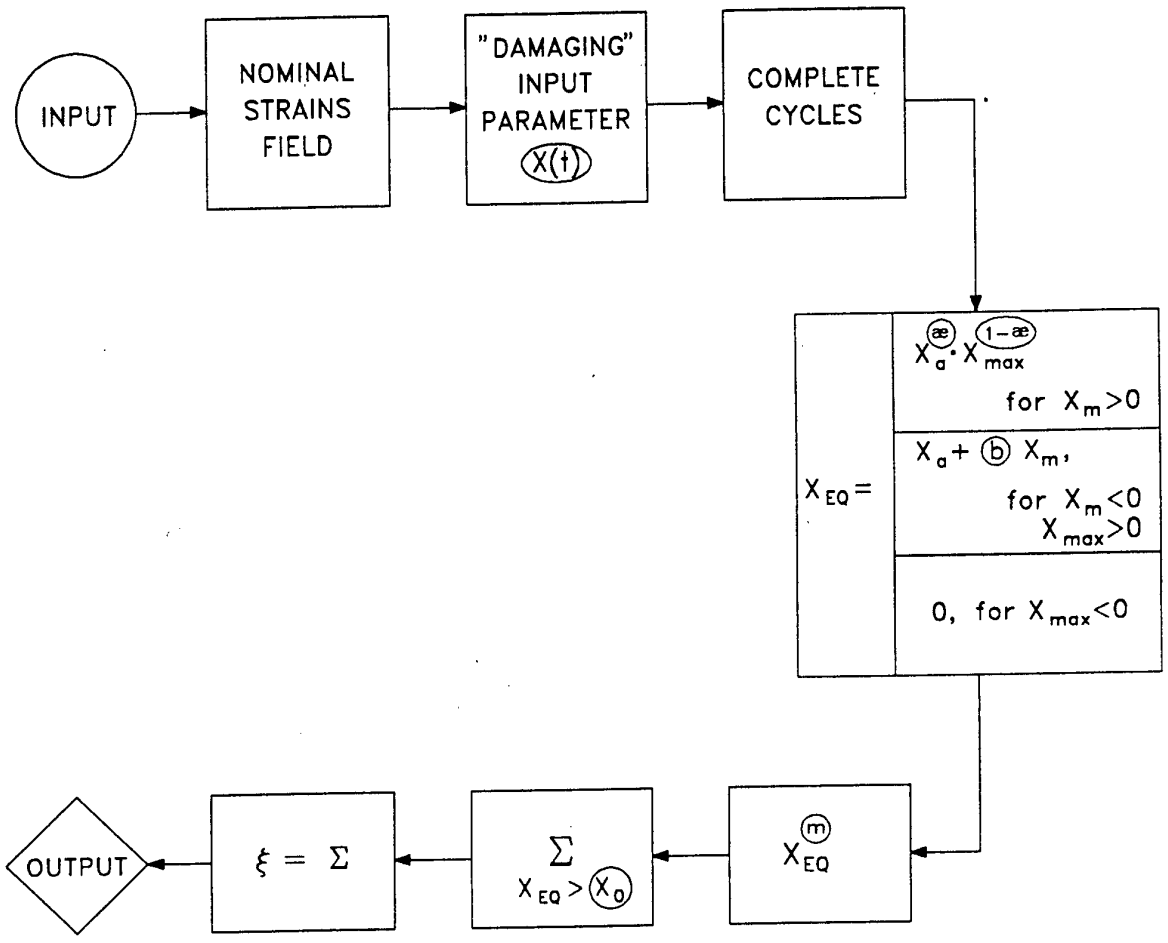

Fig. 1 Calculation Algorithm

CALCULATED FATIGUE DAMAGE ξ
FALC - SYSTEM TUNING PRINCIPLES

SSI

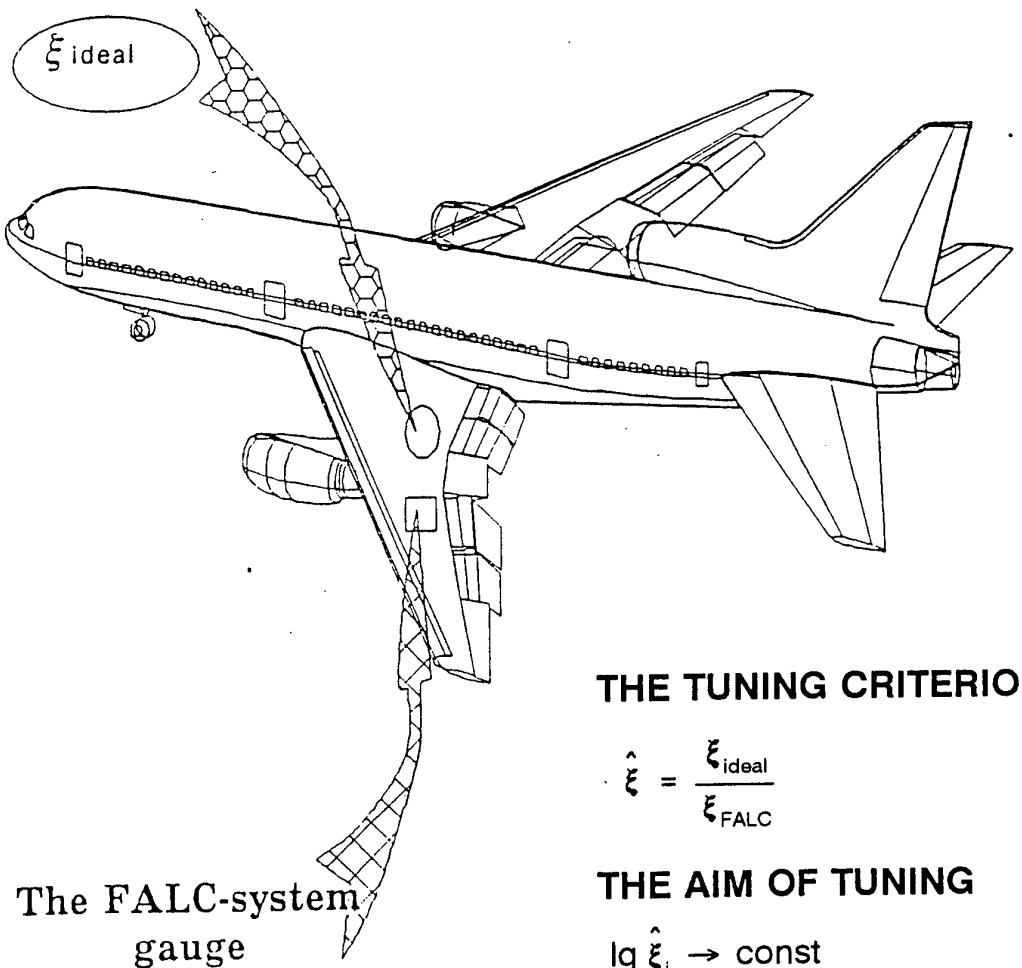

The FALC-system gauge

ξ FALC

THE TUNING CRITERION

$$\hat{\xi} = \frac{\xi_{ideal}}{\xi_{FALC}}$$

THE AIM OF TUNING

$\lg \hat{\xi}_i \rightarrow$ const

for every flight

THE QUALITY OF TUNING

$$\sigma_{lg\hat{\xi}} = \sqrt{\frac{1}{n-1}\sum_{k}^{n} (lg\hat{\xi}_k - lg\hat{\xi}_{mean})^2} \rightarrow min$$

THE "IDEAL" TUNING

$\sigma_{lg\hat{\xi}} = 0$ for $lg\ \hat{\xi}_i$ = const

Fig. 2

quality of tuning is characterized by the value of σ - the root-mean-square (RMS) of the $\log \hat{\xi}$ value; the closer it is to zero, the better the Y-parameter is chosen and tuned.

The efficiency of tuning by changing the "free parameters" can generally be illustrated by the example in Figure 3. Let six different load sequences marked in Figure 3 with the number 1, 1A, 2, 2A, 3 and 3A be the models of six different "flights". Some specimen were tested and different fatigue mean endurances were obtained. Let the "ideal" fatigue damage for each loading sequence be the value $\xi_{ideal} = \xi_x$ that is the inverse value of the fatigue endurance measured by number of "flights". The damage values were calculated on the basis of Y-parameter tuning process by changing only two main parameters: m and æ ; the rest ones were kept as $b = \tilde{b}$ and $\tilde{Y} = 0$. The values $m = 5$ and $æ = 0.5$ give the minimum of σ , i.e. maximum of tuning quality. This tuning case did not give an excellent result, the RMS is far from zero. But the value of σ (for $\log \xi$, remember) is TWICE less than the RMS for the case, than no calculation algorithm is used and every "flight" is considered as the same "life unit" independently of the difference in loading. Such a difference between the RMS values can give the moderate but essentially decrease (about 20% in the life margins needed for the airframes' life maintenance schedule definition.

Much more efficiency can be achieved with the FALC-System in the practical case when the structure has many SSI's, Investigations have shown that 100 - 200 SSI's can be served by only 16 - 32 strain gauges with acceptable accuracy. Such results may be achieved by two special procedures;

- optimum strain gauges (SG) installation, and
- multicriterial optimization of tuning.

The method of OPTIMIZED SG INSTALLATION is based on comparison of Stress-Strain States (SSS) in the SSI zones for different types of load distributions for main static limit conditions for two cases: direct SSS calculation in each SSI zone and "indirect" calculation in zones where strain gauges may be installed. The root-mean-square difference (RMSD) between direct and indirect data for all considered static load distributions is used as a basis further calculations. Optimal SG installation will be realized when the RMSD maximum (for all SSI's) from the RMSD minimum (for all possible SG installations) is minimized.

As a methodical example (see Figure 4, where RMSD is marked as S), a wing panel with four SSI's (zones 20, 24, 30, and 36) is considered. The calculations were based on Finite Elements Method (FEM). In the first table of Figure 4 we can see the RMSD maximums and minimums for every SSI zone. It is very interesting that the RMSD (for many considered static load distributions, remember) of the SSS values extrapolated to the i-th zone from the measurements in the same i-th zone is not the minimum one. The best extrapolation relates to the zone which is located far enough from the i-th zone. The reason for this effect is the influence of discrete loads caused by the rivets. The practical conclusion is the following: the nearest ti the SSI strain gauge may be not the best installation. The second table in Fig.4 shows that only two SG installations are enough to serve all four SSI's with the highest accuracy. Even with the installation of just one strain gauge the accuracy will be approximately the same.

The following TUNING PROCEDURE is necessary the case when many SSI's are served by optimally installed several SG's:

- each strain gauge must be turned separately by choosing the necessary values of "free parameters" to minimize the maximum of $\sigma_{\log \hat{\xi}}$ values for all considered SSI's;
- for each SSI its Serving SG shall be established ; it corresponds to minimum $\sigma_{\log \hat{\xi}}$ for all tuned SG's.

A methodical example (see Figure 5) is considered for the case of three SSI's and one SG (rosette). The "true" three components loading history for each SSI was imitated by center of gravity load factor data for 20 different flights of three types of airplanes. Some clipping actions (the deleting of negative values of load factor) with these loading histories have been fulfilled: the clipping only the first "component" (the loading history imitation for the first SSI), the same procedure only for the second "component" (the loading history imitation for second SSI) and the clipping for all "components" (the loading history imitation for the third SSI). The "ideal" fatigue damage was calculated for every SSI based on this information and typical values (see earlier) of algorithm parameters. The initial "non-clipped" loading history was used as the "three-component rosette measurements"; the difference between SSI'a loading histories and the "rosette measurements" became very significant , The FALC fatigue damage was calculated on the basis of the Y-parameter as a linear function of "rosette measurements" with three factors α_1, α_2, and α_3 considered as additional tuning parameters. Some results of a turning are shown for every SSI in term of $Q = \sigma_{\log\hat{\xi}}$ in Figure 5. The first row of the table is related to No-FALC case where RMS valued are very large. The second row is the No-Tuning case where all "free parameters" have typical values. The Complex Tuning Row of table shows that accuracy may be increased more than ten times (!) against the No-FALC case and approximately twice or more against the No-Tuning case.

Thus, it is seen that the "computational nature" of the FALC-type on-board system has a great advantage because of their relatively simple "tunability" to many possible practical situations. For the purpose of turning, data available at different stages of design, manufacture and operation may be used. During the early stages of analysis, FEM models of airframes and models of environment and operation conditions may be widely used. A full-scale fatigue test of airframe employing the loading at many different "flight-blocks" (similar to TWIST program) produces more complete and correct information useful for tuning. A special flight test program comprising different flight missions which covered an entire area of possible variations of the considered aircraft type loading, may be implemented for most precise tuning.

And from such point of view one shall answer a question: what are the advantages of "physical nature" means of loading monitoring such as bonded special gauges (sensors) which change their electric resistance or any other properties during the cyclic deformation jointly with the structure in its operation. The main advantage is big and very useful: such sensors are simple and inexpensive, they are "autonomic", i.e. independent of the airframe and the aircraft. Such properties give us the opportunity to install a great number of sensors to serve each SSI by several gauges; the only problem is to have time for "putting questions" to many gauges. But this beautiful situation will be realized only if the main property is existed: the measured value of the sensor "output" is connected (for correlated) in a known manner with the fatigue accumulation process. This correlation should be not only in the case of simple cyclic loading but in the general (and much more practical) case of real complicated loading. At the worst it would be acceptable to simulate the wrong but wide used and "familiar" Linear Hypothesis.

To a big regret even the now-a-days situation in this direction is far from well-being. No one of many different types of proposed means can be considered as an expectable one. The main shortcoming of all these objects is the same: the "physical remaking" of alternating loads (strains) process to any measured "output" is strongly "sewed up" into the material of the sensor, and only the one way - the "Trials and Mistakes Method" - is usually can be used. Some hopes on "material properties tuning" are arised in connection with the investigations being provided during several last years by scientists of Uzbek Academy of Science [3]. But these interesting results before their practical using ought to be applied and checked during long-time and expensive fatigue

	"FLIGHT" LOADING	N, "FLIGHTS"	$\xi = 1/N_{ideal}$
1	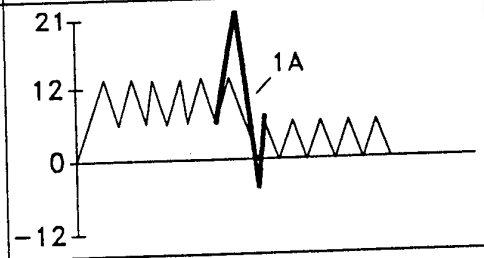	38070	$2.63\ 10^{-5}$
1A		117999	$8.47\ 10^{-6}$
2	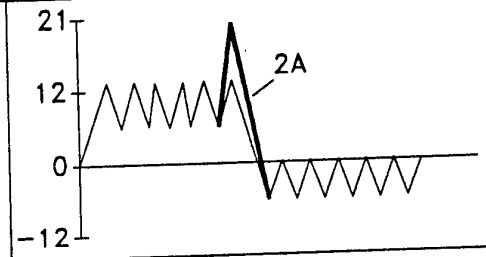	18810	$5.32\ 10^{-5}$
2A		29740	$3.36\ 10^{-5}$
3	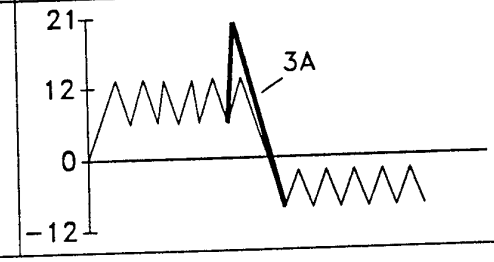	10200	$9.80\ 10^{-5}$
3A		13680	$7.31\ 10^{-5}$

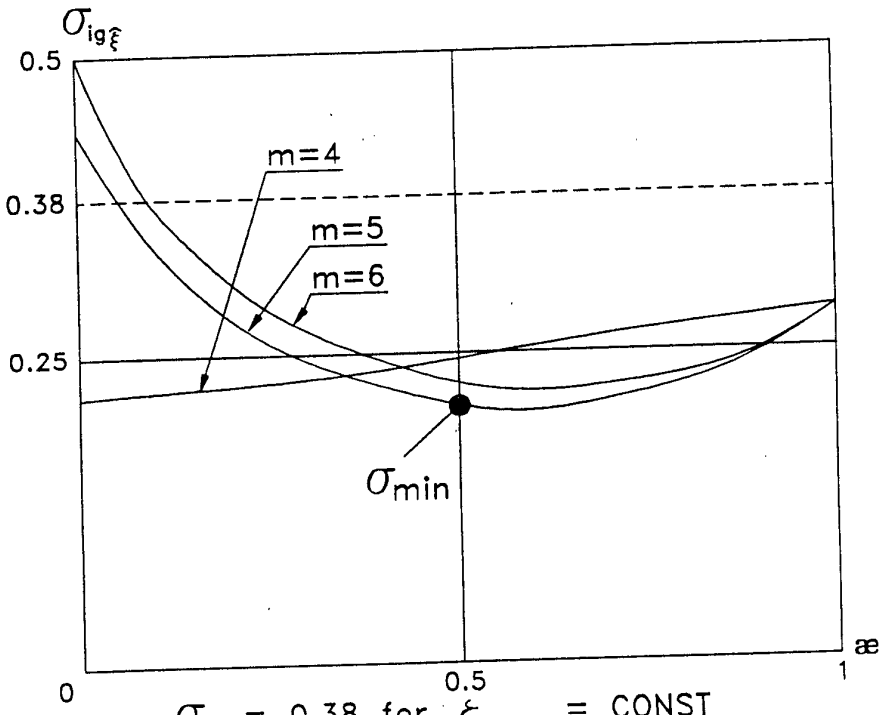

$\sigma_{ig\xi} = 0.38$ for ξ_{FALC} = CONST

$\sigma_{ig\xi} = 0.21$ for ξ_{FALC} $\begin{cases} m = 5 \\ æ = 0.5 \end{cases}$

JE-A901-D004

Fig. 3. Efficiency of Tuning Parameters

SG Optimum Installation

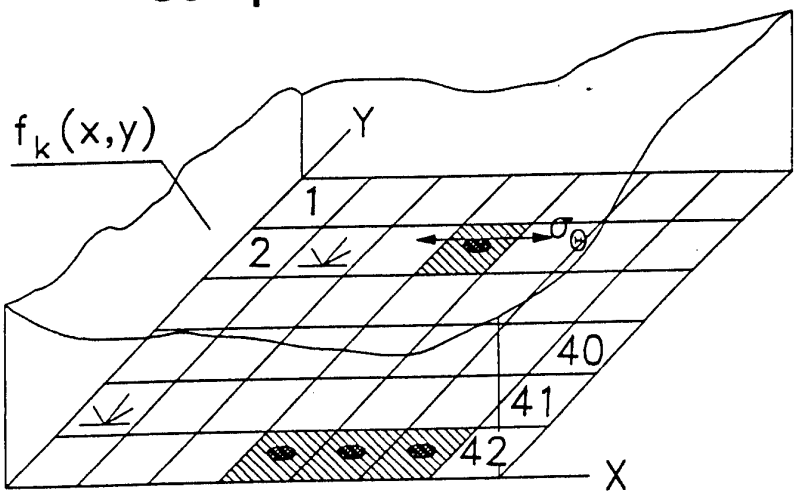

$$\tilde{\sigma}_\theta^{kij} = C_1^{ij}\sigma_x^{kij} + C_2^{ij}\sigma_y^{kij} + C_3^{ij}\tau_{xy}^{kij}$$

k - loading type number (m)
i - SSI number (N)
j - zone number (M)
r - SG number (n)

$$S_{ij} = \sqrt{\frac{1}{m-1}\sum_{k=1}^{m}\left(\frac{\tilde{\sigma}_\theta^{kij} - \sigma_\theta^{kj}}{\sigma_\theta^{kj}\underset{k}{\text{mean}}}\right)^2}$$

S_{ij} ZONE NO.	20	24	30	36
min	0.023	0.007	0.038	0.015
max	0.086	0.113	0.098	0.180
s_{ij}	0.064	0.113	0.085	0.068

$$S_{ij} \rightarrow C_M^n \rightarrow S_{ir}$$

$$\delta_n = \min_i \max_r \min S_{ir}$$

n	1	2	3	4
δ_n	0.124	0.099	0.099	0.099

Fig. 4

FALC - SYSTEM TUNING PRINCIPLES. THE "MORE SSIs - LESS SGs" CASE.

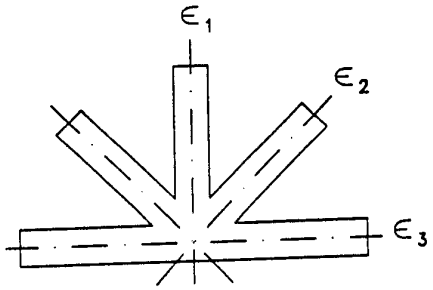

k - loading type (flight) number (m = 20) .
i - SSI number (N = 3)
r - SG number (n = 1)

$$X = \alpha_1\epsilon_1 + \alpha_2\epsilon_2 + \alpha_3\epsilon_3 \quad \text{for} \quad |\alpha_1| + |\alpha_2| + |\alpha_3| = 1$$

JE-A901-D006

THE QUALITY OF TUNING

$$\Delta = \min_{T.P.} \max_{i} \sigma^{(i)}_{lgz}$$

	Q_1,%	Q_2,%	Q_3,%	Tuning Parameters					
				α_1	α_2	α_3	m	æ	b
No FALC	35.1	31.8	36.0						
No Tuning	8.8	4.9	9.6	0.20	0.47	0.33	4.000	0.5	0.2
No α_i - Tuning	4.0	4.4	4.4	0.20	0.47	0.33	5.285	0.277	0.2
Complex Tuning	2.1	2.6	2.6	0.18	0.52	0.30	4.046	0.424	0.2
SG1 Tuning	1.3	4.0	1.6	0.18	0.52	0.30	4.339	0.293	1.0
SG2 Tuning	4.2	0.4	4.9	0.20	0.50	0.30	3.919	0.507	1.0
SG3 Tuning	1.6	4.7	1.4	0.18	0.52	0.30	4.432	0.293	1.0

Fig. 5

tests. The existing situation in our countries does not give any optimism in providing necessary tests in the expectable time interval.

The general conclusion is the following:

The idea of fatigue loads monitoring is so obvious and attractive that there are a lot of proposals about different means and methods concerning this subject. But in the same time the general world experience shows that the real application of this "simple" idea is practically near to zero level. There are two reasons of that situation: a "commercial" and a technical ones.

1. The first of them is the following: nobody has clear filling or an answer to the question who will take profits from the monitoring application. Therefore nobody has an enthusiasm to invest money to work out, produce and apply the monitoring systems.
2. The second reason is the problem of monitoring results reliability level; it must be enough for application in the very important field of service safety. It is evident that concerning safety problems the advantage now lies among the calculating systems based on remaking the information about usual and measurable loading parameters such as loads, moments, load factors, strain, stress etc. The "tunability" of such systems gives an opportunity to accommodate themselves to very wide scope of different contradictory requirements which are inherent to the serious engineering problems. As regards to the "physical nature" means of fatigue loading monitoring their future is depended entirely on possibility and optimization of necessary fatigue tests providing.

REFERENCES

1. P.Miodushevsky and B.Podboronov (1991) FALC - On Board Fatigue Life Counter (Fatigue Meter) Proc. of International Conference on Aircraft Damage Assessment and Repair, 26-28 August 1991, Melbourne, Australia.
2. V.Raikher, P.Miodushevsky, Yu. Svirsky, I.Teeme, R.Statnicov (1993) Procedures and Analyses providing Accumulated Fatigue Computation Assessment for On-board Fatigue Life Counter (FALC). Proc. of the 5-th Australian Aeronautical Conference, 13-15 September 1993, Melbourne, Australia.
3. S.Kh.Shamirzaev, V.M.Sviridov, I.V.Khamrakulov (1992) The conductivity of heterogeneous materials at being superimposed a random irreversible deformation.Preprint № 172-92-ФТПТ, PhTI of AS Uzbekistan, Tashkent, 1992.

INTEGRATED AUTOMATIZATION AND INSTRUMENTATION SYSTEM FOR STATIC AND LIFE TESTING OF FULL-SCALE MODERN MANEUVERABLE AIRCRAFT STRUCTURES

A.N.Serioznov
SibNIA, Novosibirsk

1. Aims and purposes of static and life testing of modern maneuverable aircraft structures

The main aims of laboratory static life testing of modern aircraft structures are:

- experimental substantiation of static and fatigue strength characteristics of a structure with the view point of compliance with the strength requirements and the life specified in the performance requirements;
- establishing of structure zones witn nonsatisfactory static and fatigue strength characteristics;
- refinement of calculation methods.

The main purposes of the static and life testing are:

a) Program loading of structure.

The static test program consists of a set of loading for units and an airframe as a whole which correspond to the cases stipulated in the strength requirements. The program includes a proper program determining a loading sequence with indication of the applied load values expressed in fractions of the calculated load, and a test task, determining the procedure for each loading with load distribution for units, etc. To determine the static strength margins, the destructive testing of the unit or its part is carried out for a number of loadings.

Note: The residual strength testing of the structure can be methodically considered as the static testing with some particularities.

Programs for the life testing of modern maneuverable aircraft structures are cyclograms of load combinations with a given distribution on the structure. These are the cyclogram of combined block multistep loading with using the "typical flight" conception and the cyclogram with quasi-random levels and load sequence in "flight" with using the "flight by flight" conception.

In connection with the above-said the static and life test rigs must include computer-aided control systems (CACS) for loading process and system providing the CACS operation: for measurement by channel of forces, displacement, excessive air pressure; protection from unforeseen overloads; aircraft attitude stabilization.

b) Measurement of stress-strain state (SSS).

For experimental verification of designs and correspondence of the rig loading to the results of flight-strength experiment as well as for control of the loading process, the test rigs must be equipped with information measuring system (IMS) providing the measurements of:

- stresses (strains) in structures with the help of some thousands of gauges;
- displacements of the structure under the static loading to determine its stiffness characteristics;
- integral its stress-strain state characteristics of the realized program loading.

c) Control of the structural integrity and damage processes.

The test rigs must include control systems providing fixation of:

- onset of the damage initiation and extension;
- onset of a fracture process or non-elastic strain arising in structure unforeseen by the test program, with issue of the commands for CACS to stop loading and/or to remove a load;
- onset of a fracture process or non-elastic strain appearance foreseen by the test program, with issue of commands for CACS to fix a load value and a zone (element) of the structure responsible for the fracture process;
- sequence of the fracture zones (elements).

Figures 1 and 2 show block-diagrams of the rigs for static and life tests of the modern maneuverable aircraft structure which contain the above-mentioned systems.

2. Computer-aided loading control system.

The system is intended for control of the technological equipment for the purpose of synchronous reproduction of the mechanical loads acting on the structure in accordance with a given program. The system consists of a high-level computer, software and hardware for the loading control (Fig.3).

Performed tasks:

- preparation of the initial data for the strength tests;
- control by the synchronous reproduction of the technological loads is performed both in dialog and automatic regimes. In the automatic regime the loads are reproduced in accordance with a sequence given by the test program;
- possibility of the program scaling both in time and loads;
- control and processing of the emergency situations provide actions for damage prevention of the test structure.

Realized function:

a) Control function:

- generation of the programs for each channel;
- local ajustment for local channel;
- control of actuators and information-measuring system;
- autometic "bumpless" channel switching;
- recovery from the emergency situations;
- trasition to any prodram area.

b) Information functions:

- load measurement at any moment;
- control of the load reproduction;
- analysis and registration of the emergency gauge actuation and blockages;
- full protocolling of the test process;
- test software.

As a matter of experience in the testing of such structures as Su-27, CACS must have the *following main technical characteristics*:

- number of loading channels, not less than....60
- load reproduction frequency at CACS output ....to 10Hz;
- number of input/output signals 256/250;
- normalizing converter .....$\pm$10V

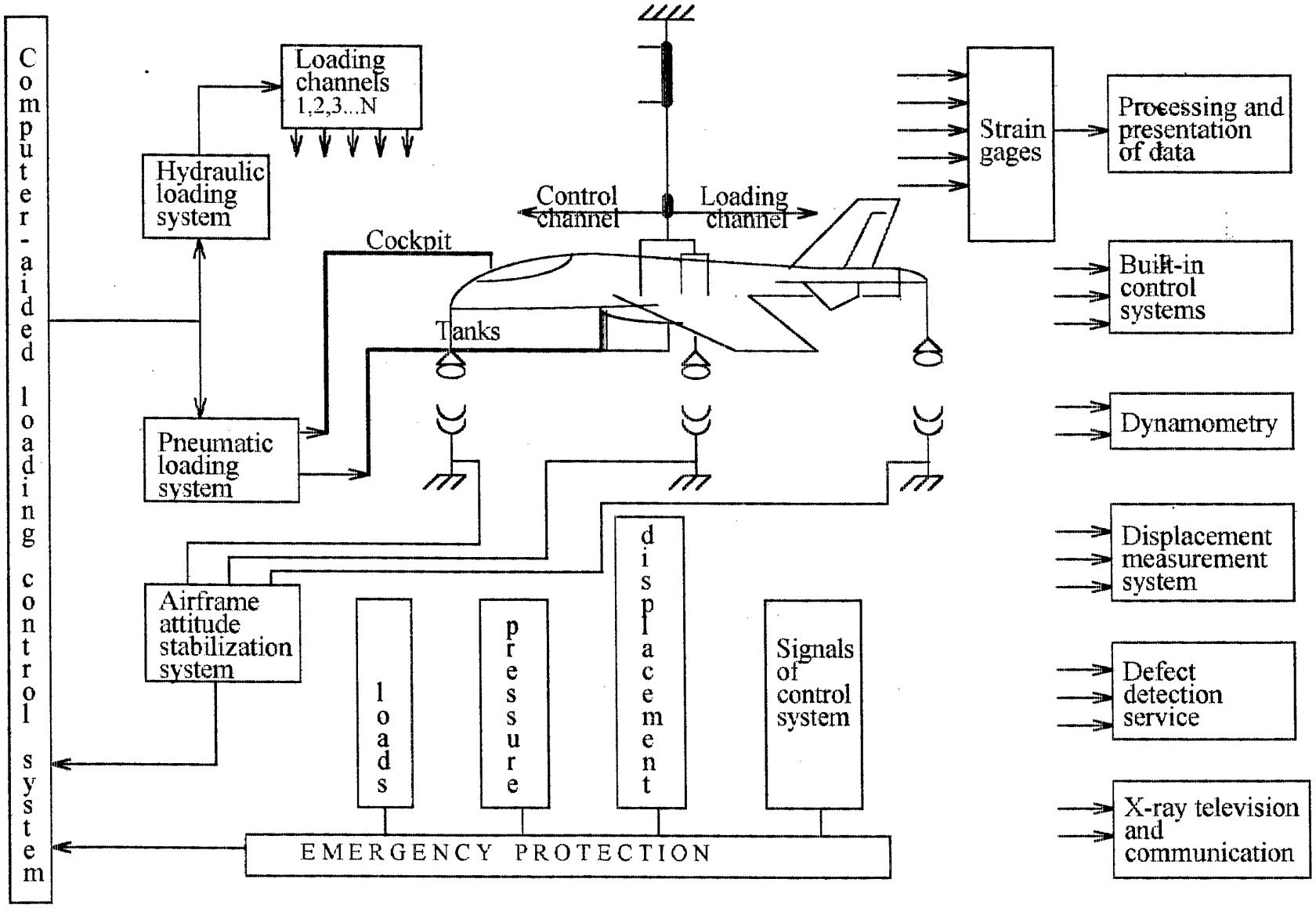

Fig.1.Block-diagram of the airframe static test rig.

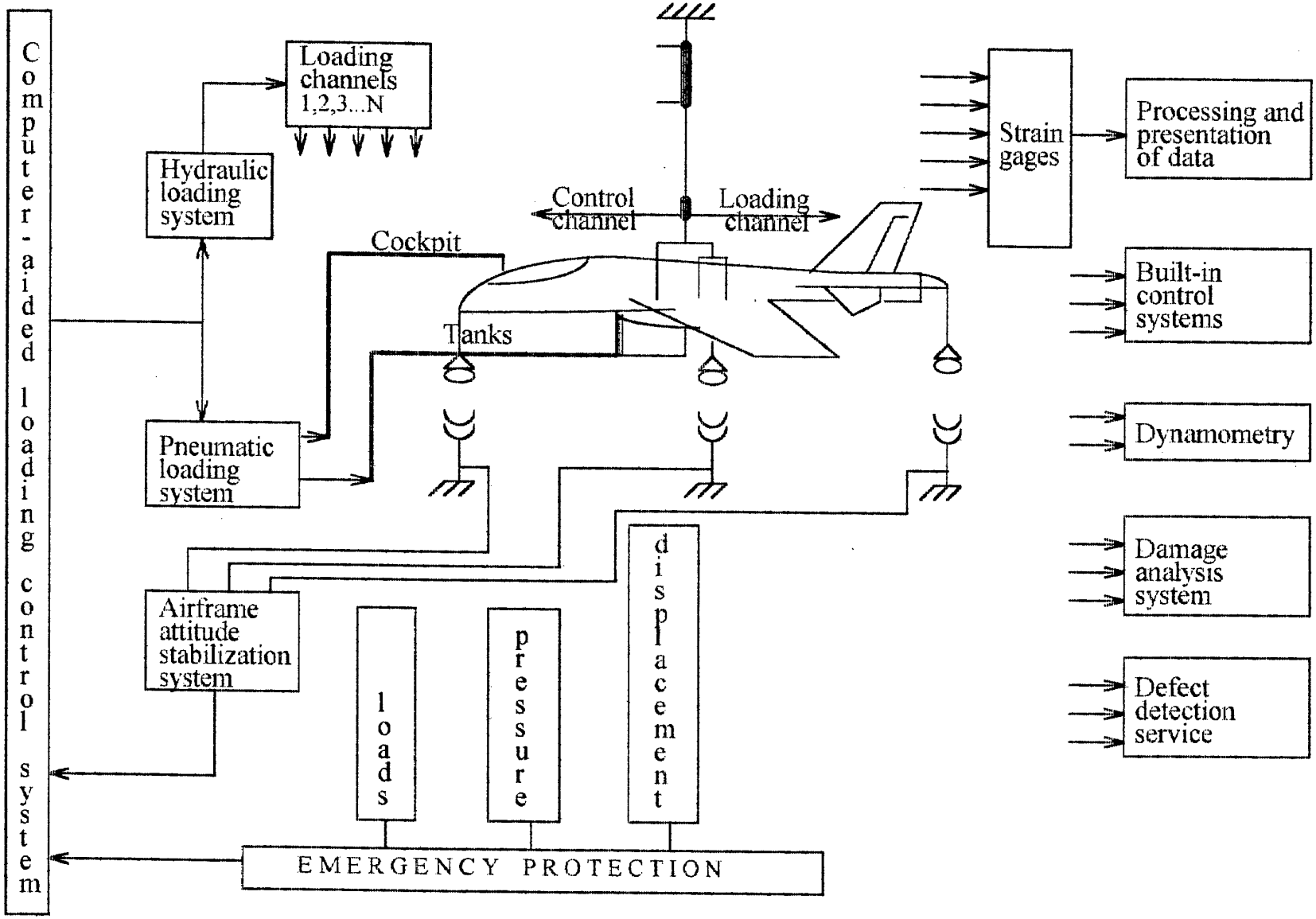

Fig.2.Block-diagram of the airframe life test rig.

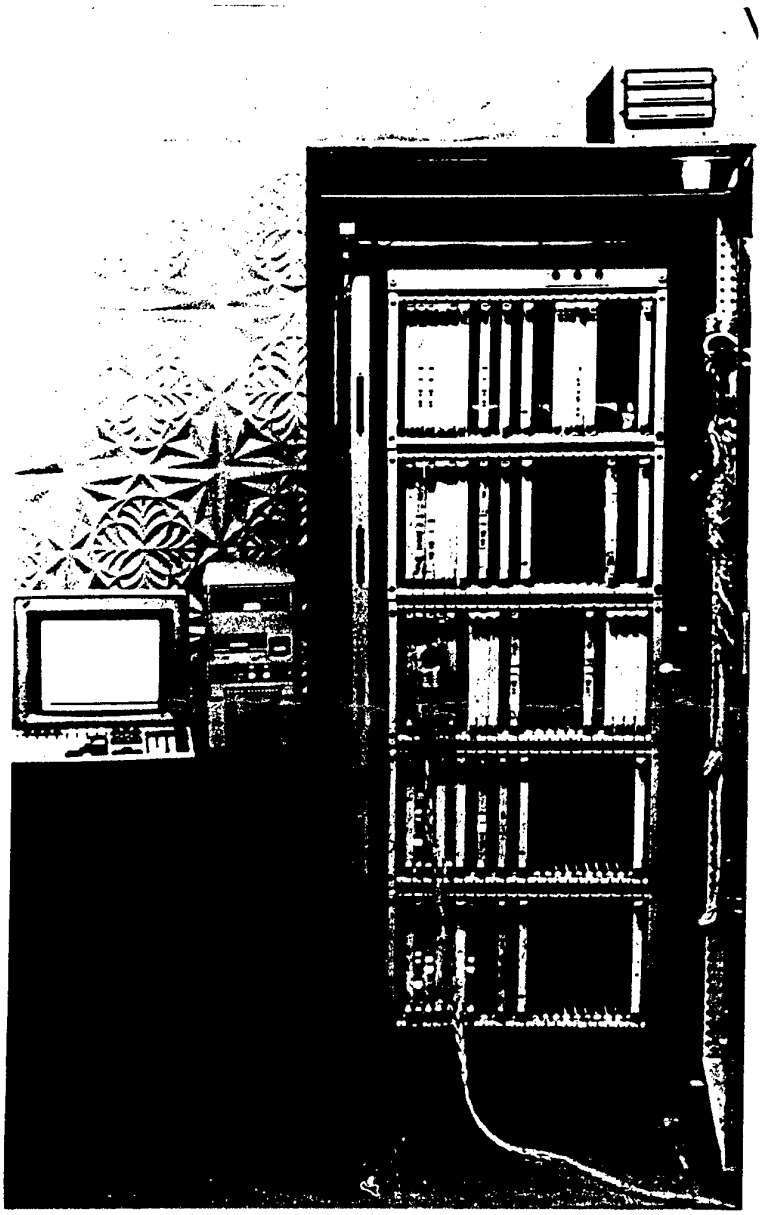

Fig.3. Hardware and software for CACS of loading and high-level computer.

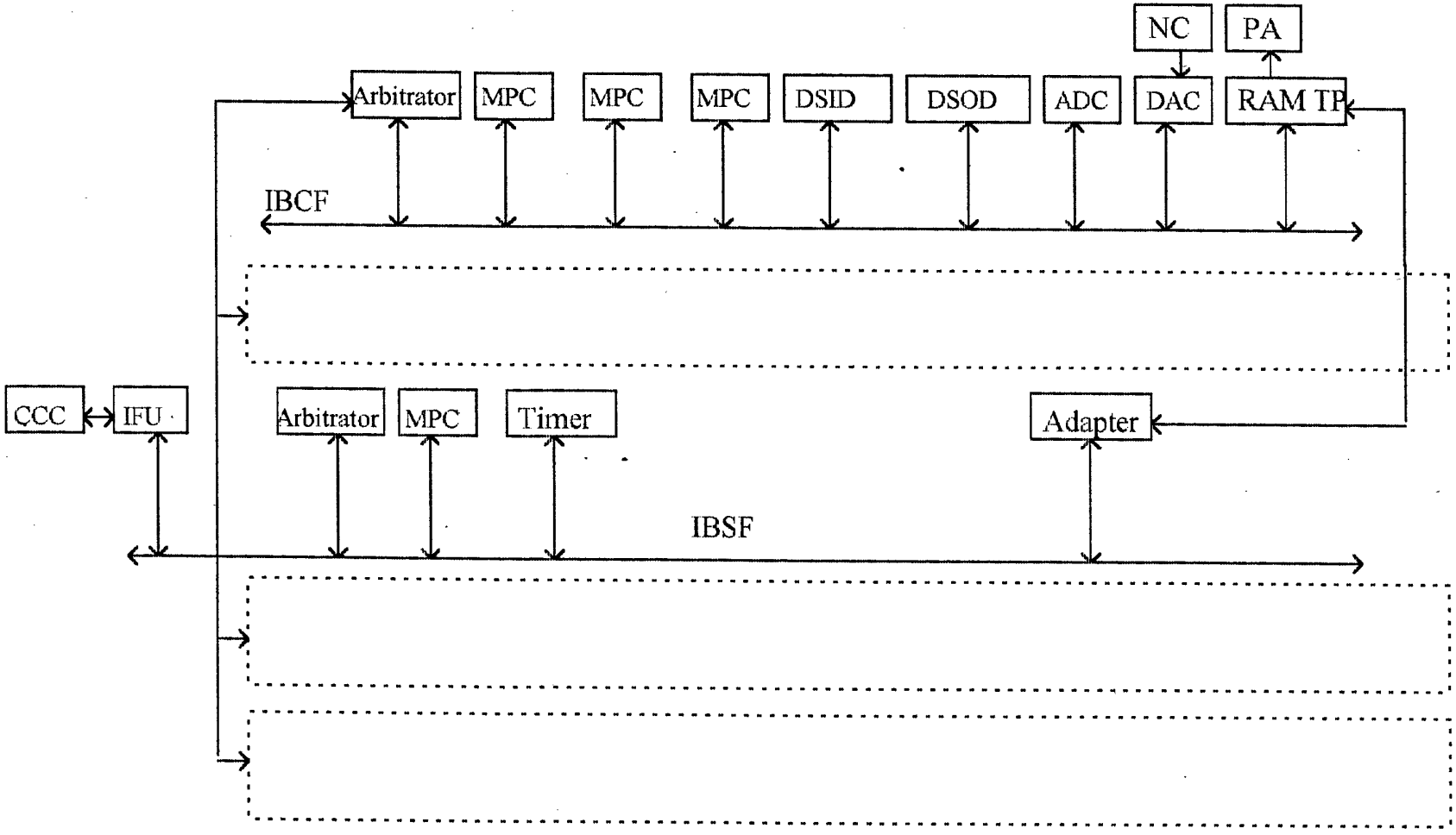

Fig.4. Block-diagram of CACS.

A block-diagram of the computer-aided loading control system is presented in Fig.4.

Composition and purpose of CACS elements:

- *CCC* (controlling computer complex) - personal computer of IBM series for generation, processing and storing of the data base, loading of the test program, carrying out of the tests, display of the experiment course, storing of the results;
- *IFU* (interface unit) - for connection of the personal computer with LCC (loading control complex);
- *Arbitrator* - for connection of the internal bus of the central frame (IB CF) with the peripheral frames and for arbitration of the active devices' access to the bus of own frame;
- *MPC* (microprocessor controller) - for providing of program generation, realization of the digital PID-controller, reception and processing of the input information;
- *Timer* - for providing of the synchronization between the active devices being in composition of the LCC;
- *DSID* (discrete signal input device) - for information reception from the emergency and position transducers;
- *DSOD* (discrete signal output device) - for issue of the discrete control signals to the hydraulic and other equipment:
- *ADC* (analog-digital converter) - for reception of the analog signals from the strain-gage - normalizing transducer track for the following processing in the digital PID - controller;
- *DAC* (digital-analog-converter) - for issue of the analog control signal to the hydraulic or other equipment through PA (power amplier);
- *RAM TP* (random-access memory, two-port) - for storage of the program, functioning of the processors and information interchange between the frames.

The computer-aided loading control systems for the static and life tests differ by specialized software, connections with other systems.

3. Force control System.

The force control system (FCS) suggests presense of two measuring channels in each loading channel and is intended for qualitative reproduction of the loads applied to the structure.

FCS consists of software and hardware interactiong with computer-aided loading control system and allowing to perform control and emergency functions during testing.

FCS allows to compare indications of two measuring systems constantly or at the control points of the program. In the case when a difference between them is more than a given level, FCS supplies the emergency signal to CACS. A block-diagram of the force control system is illustrated in Fig.5.

4. Dynamometric system.

The system is intended for measurement, processing and transfer of the information about loads applied to the test object in the strength experiment to the computer-aided loading control system.

The system must measure the following types of loads:

- static (tension or compression);
- repeated static (alternating or constant sign).

The system is built on the module principle. The normalizing transducer of the force gage is in the gage itself. The system provides address, serial single/multiple poll of the measuring channels.

It is descriable to design the aircraft loading system (especially for the life tests) in such manner that maximum number of loading channels operate in the alternating regime, tracing, for example, the air and ground regimes on different program areas. Such loading reduces the number of channels, man-hours for mounting, adjustment and starting of the test rig. The gage for measurement of the alternating forces screws directly on the hydraulic power cylinder rod (Fig.6).

SibNIA manufactures the force gages with two measuring srain-gage bridges, which, using FCS (see p.3), provide the trouble-free operation of the loading system. To reduce the influence of external industrial noise on the measurement accuracy the impulsive power supply is used for strain-gage bridges.

A force measurement error musnt'n exceed 0.4÷0.5% of the dynamometer scale, therefore to obtain a sufficient accuracy of the load reproduction for all channels a variety of the dynamometers of different ratings from ±100N to ±500kN is necessary.

5. Airframe attitude stabilization system

The system is intended for the attitude stabilization of the airframe in pitch and roll during tests.

At SibNIA, contactless ultrasonic stabilization systems based on measurement of the ulurasonic signal transmitter-receiver transit time are used in the tests of the modern maneuverable aircraft. Transmitters are placed on the wing and fuselage as far as possible from the airframe center of mass, receivers - on a stationary rigid rigit base, for example, on the load-carrying floor of the static test room. The transmitters and recesvers may be placed in the reverse order. With fixed distances from the gages to the center of mass, the angular displacements are determined by the linear displacements between the transmitters and receivers.

A signal of deviation from the normal aircraft attitude is transmitted to the computer- aided loading conrol system. Thus, stabilization system is a two-channel measuring system for displacement control. A block-diagram of the airframe attitude stabilization system is show in Fig.7.

6.Strain-gaging system

The measuring information system (MIS) for investigation of the stress-strain state in a test structure is intended for acquisition, processing, presentation and storage of the measuring information from the strain-gages mounted on the structure.

At SibNIA, the wire and foil temperature-compensated gages of own design and manufacture with a base of 2±20 mm are applied for measurement of the stress-strain state in the structure. The foil gages may be performed before in the form of a strain-rosette on a single platform. The structure is prepared with strain-gages generally using cold-setting adhesives.

In the thermal strength tests, for example of the Su-27 canopies, the high-temperature strain-gages with standing a temperature to 400^{0}C are used. For this purpose a resistance strain-gage and microthermocouple combined into a single gage were developed and used.

MIS must provide operation with strain-gages of different nominal resistances including the bridge-connected gages.

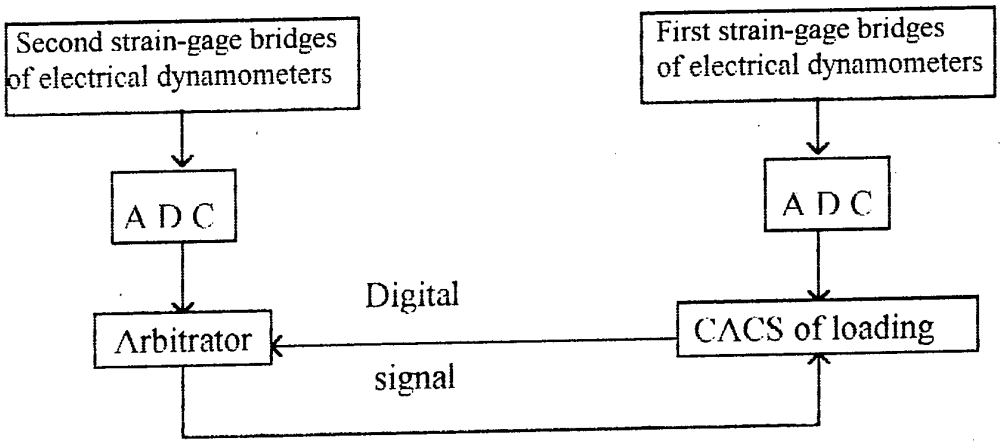

Fig.5. Block-diagram of the force control system.

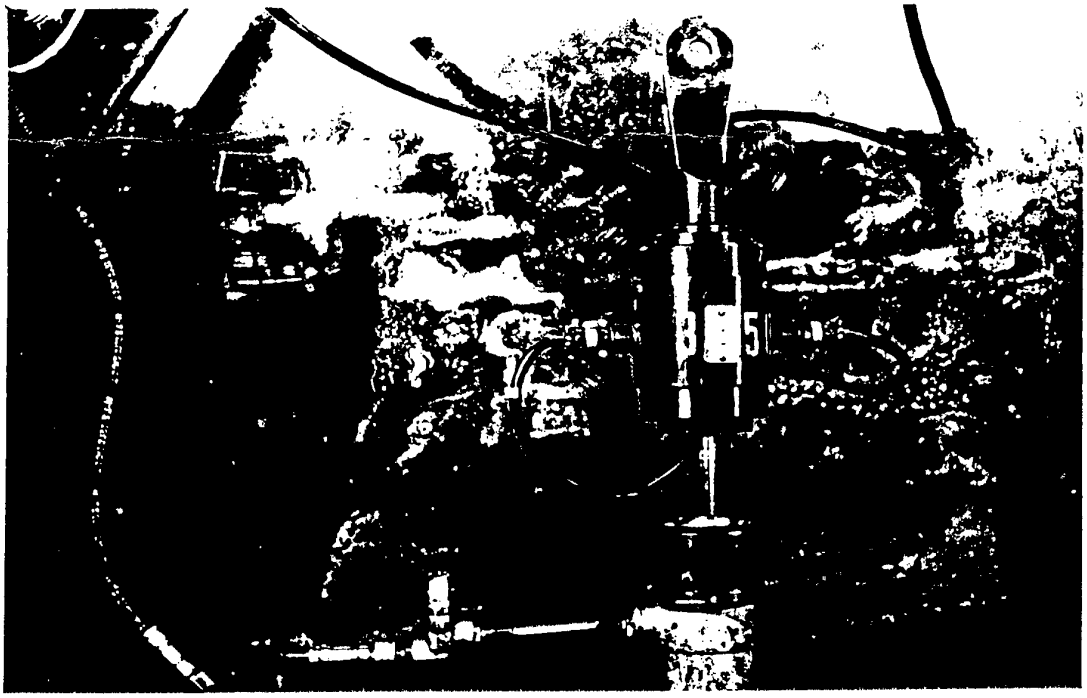

Fig. 6. Dynamometer on the hydraulic power cylinder rod.

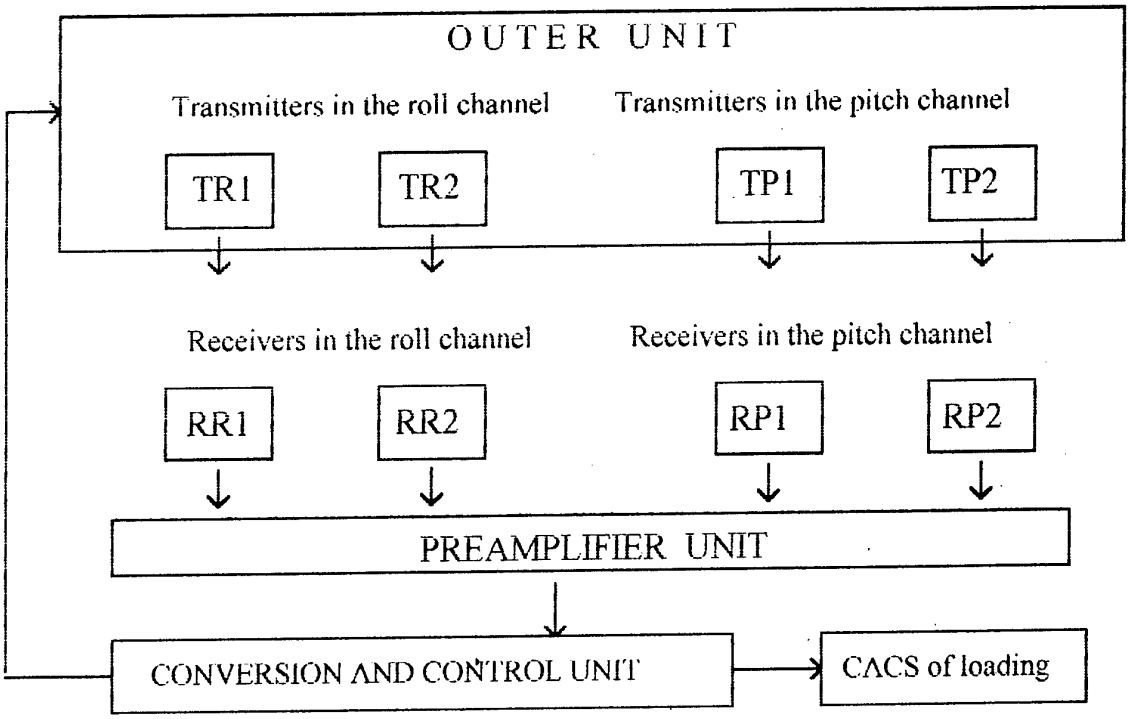

Fig.7.Block-diagram of the airframe atitude stabilization system.

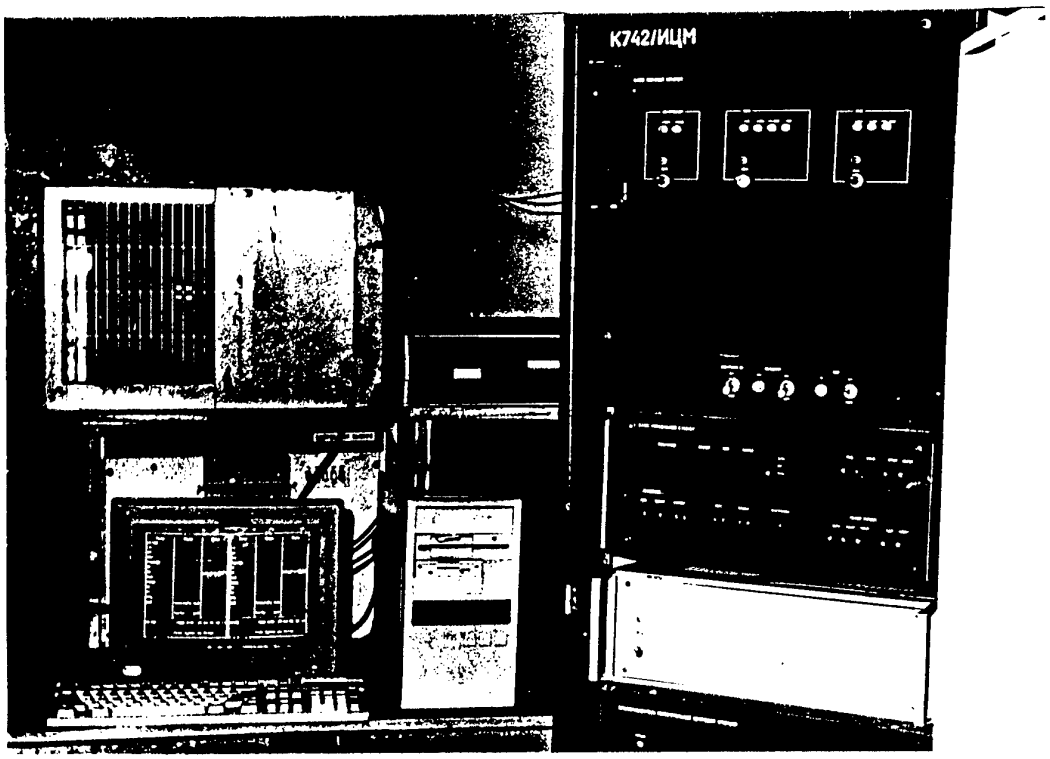

Fig.8. K742 MIS connected to the computer.

A number of the strain-gages in the static and life tests of modern maneuverable aircraft reaches of 3.000÷5.000 in consequence of which a problem of sufficiently rapid information reading at any of the loading program regimes arises. A set of standard 1000-channel K742 MISs (Fig.8) with a channel speed of 1.000 ms is used at SibNIA. To reduce the influence of external industrial noise on the measurement accuracy, the strain-gages are connected with MIS by means of optical fibers after switching. Besides, a program of sorting out of the measuring information spikes is also provided, for that in esch regimes a vector of readings is taken and ranked, the extreme values are rejected, and a mean or median value is selected from remained ones.

MIS is connected by an interface with the computer-aided loading control system which going into certain regime of the measuring experiment program gives the reding signal for MIS. A block-diagram of the strain-gaging system is illustrated inFig.9.

Presentation of the life test results, obtained using modern programs with some thousands of the strain-gages and quasi-random loading cyclogram (see p.1) having some thousands of levels, in usual form is unreasonable due to its non-informativity. Therefore, the following methjdical approaches are used.

In the first case, the integral characteristic within a considered cyclogram interval - a stress equivalent by fatigue damage as well as maximum and minimum stresses within the interval - is determined for each measurement point of the structure.

In the second case, a so-called matrix of effect of a load vector (q) in the channels on a stress vector (σ) at the structure points is determined:

$$(\sigma) = [A](q)$$

Determining experimentally the matrix of effect, the stresses can be sub sequently calculated for any possible load population, including hypothetical. The main complexity of the matrix determination is optimal plannig of the calibration experiment.

Note, that the latter approach can be extended to the static tests except cases of nonlinear structure deformations.

7. Fatigue damage control system

The system is intended for integral estimatiom of the structure loading accuracy for each loading program or block equivalent by fatigue damage to a certain number of the flight/flight hours. During perfrmationg the loading program it must take continuous measurements of all extreme values of generalized external and/or internal forces (bending and twisting moments, shearing forces and/or their certain combinations) as well as SSS components (and/or combinations) in the structure with calculation of the integral stress-strain state characteristic - equivalent of the realized program with respect to a given and/or to operational stress-strain state of one flight/hour.

The system sets high requirements to the speed of the used MIS, therefore at SibNIA K742 MIS is applied for it with restriction of a number of the measuring channels to some tens during operation with external forces and to units during operation with internal force factors.

Furthermore, special requirements are established to the calibration of the internal force factors for maneuverable aircraft structure as a redundant structure.

The fatigue damage control system is connected through an interface with the computer-aided loading control system which issues the reading signal approaching to the

extreme load value. A block-diagram of the fatigue damage control system is presented in Fig.10.

8. System for measurement of displacements and stiffness characteristics in structure

The system is intended for measurement of the eladtic structure displacements at the static loading and determination of the struature stiffness characteristics in application to aeroelastic and aerodynamic problems.

At SibNIA a computer-aided ultrasonic (to 100 channels) contactless system (Fig.11) using the same principles as the airframe attitude stabilization system (see p.5) is applied.

The system consists of the displacement measuring system proper and the information processing block with its software. It provides determination of the stiffness characteristics both by the traditional method (beam calculation scheme) and determing the matrix of effect (see p.6) of the loads in loading channels on the displacements of the structure points.

9. System for control of structural integrity and damage propagation processes

Life testing:

At SibNIA traditional and advanced structural integrity control methods are used in the life tests. The traditional methods are methods of built-in control: foil and optical - fiber crack gages giving the signal about gage failure through MIS into the computer that an operator or CACS decide to continue or stop tests (Fig.12).

One of the most advanced methods of nondestructive structural integrity control in the life tests is an acoustic emmision method. The physical base of this method is an phenomenon of acoustical wave radiation by material during dynamical processes of its restructure, for example, plastic deformation, nucleation and growth of fatigue crack. The 16-channel AE complex at SibNIA is shown in Fig.13. It includes:

- 16-channel data acquisition system;
- interface card for IBM PC/AT computer;
- set of piezogages, preamplifiers, cables;
- AE signal simulator;
- software.

Main technical characteristics of 16-channel acoustical-emission complex:

- number of measuring channels.....8, 16 ;(with possibility of increasing to 32);
- operational bandwidth, MHz.....(0.01...0.7);
- noise level at preamplifier input, μV.....5;
- preamplifier gain factor, dB.....40;
- dynamic range of processed sighals, dB 80;
- AE signal detection thresholds set in program, dB.....(0...60);
- supply voltage.....220±22V with frequency 50Hz;
- sizes, mm .....(420x320x180);
- weght of measuring unit, kg, max.....5.

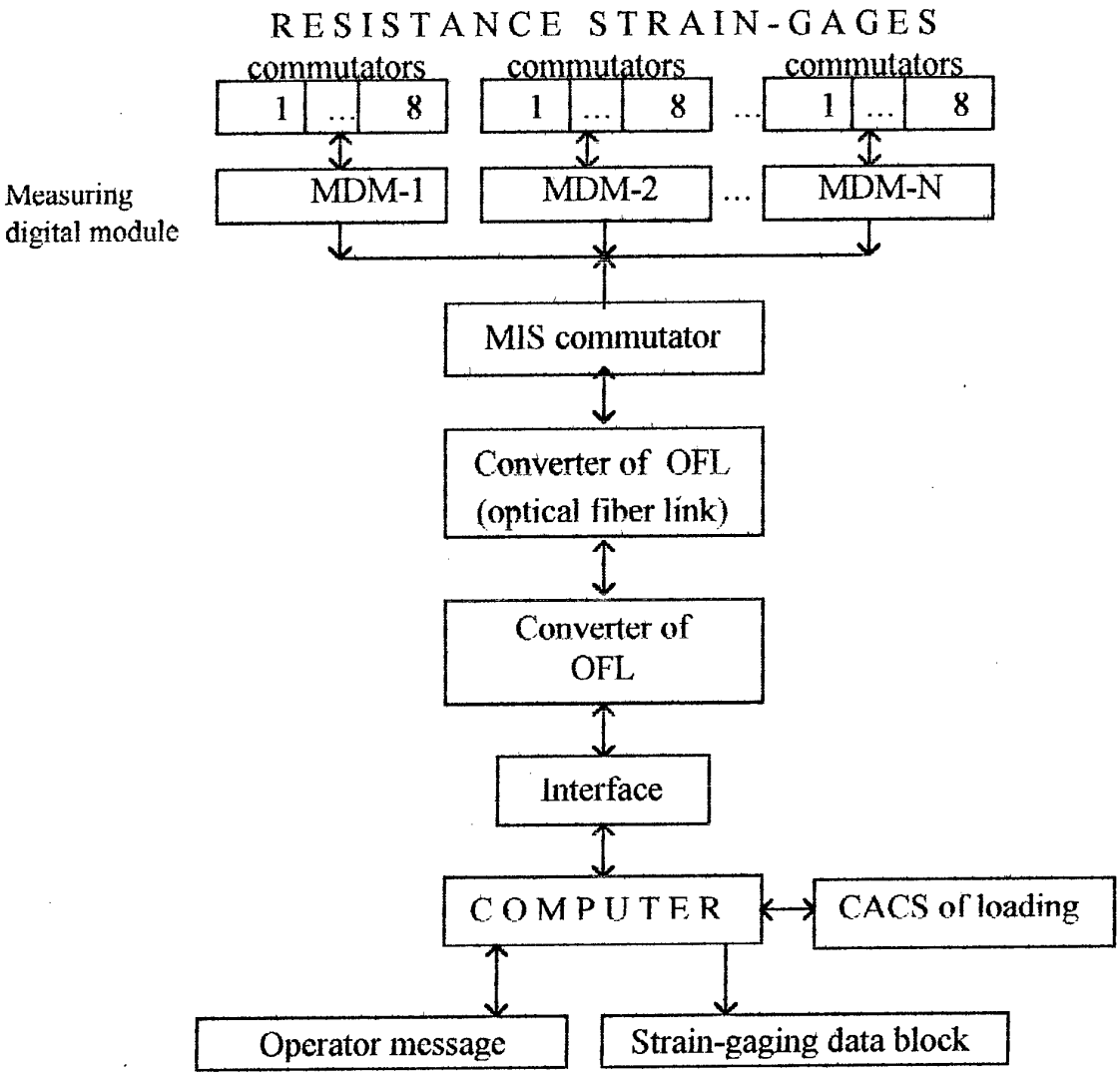

Fig.9. Block-diagram of the strain-gaging system.

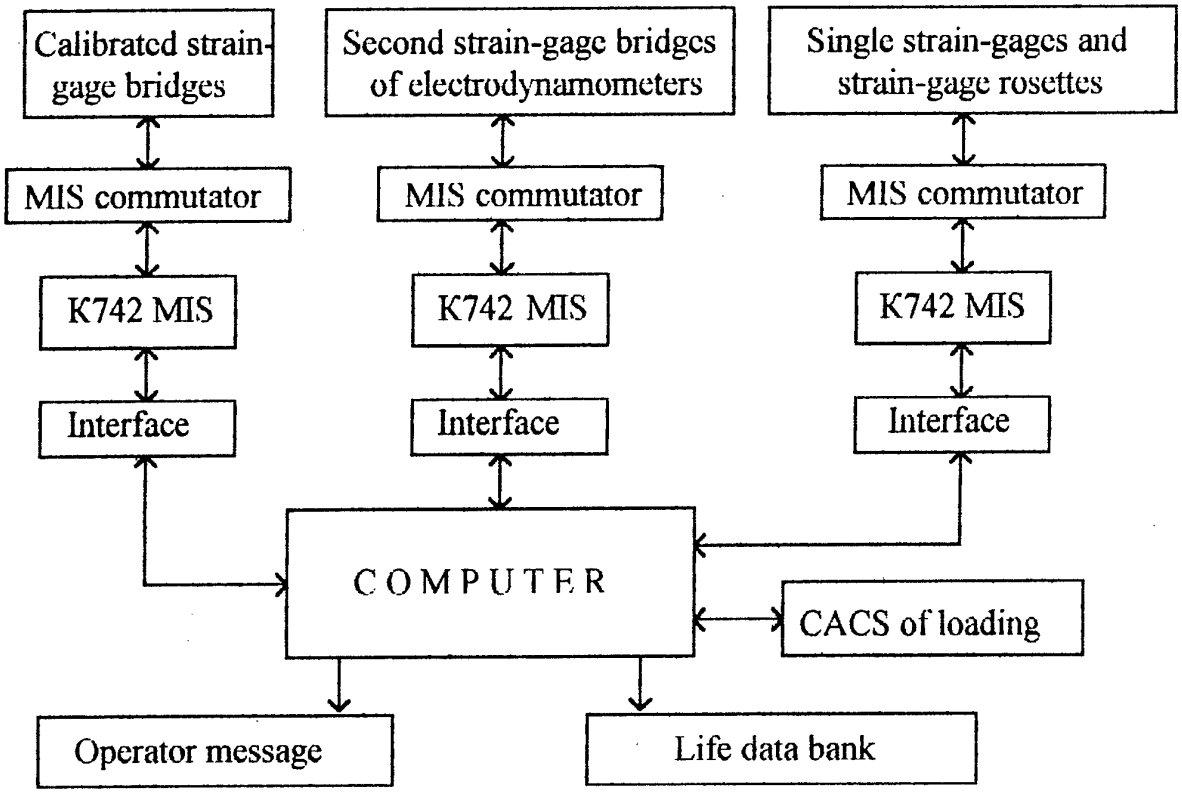

Fig. 10. Block-diagram of the fatique damage control system.

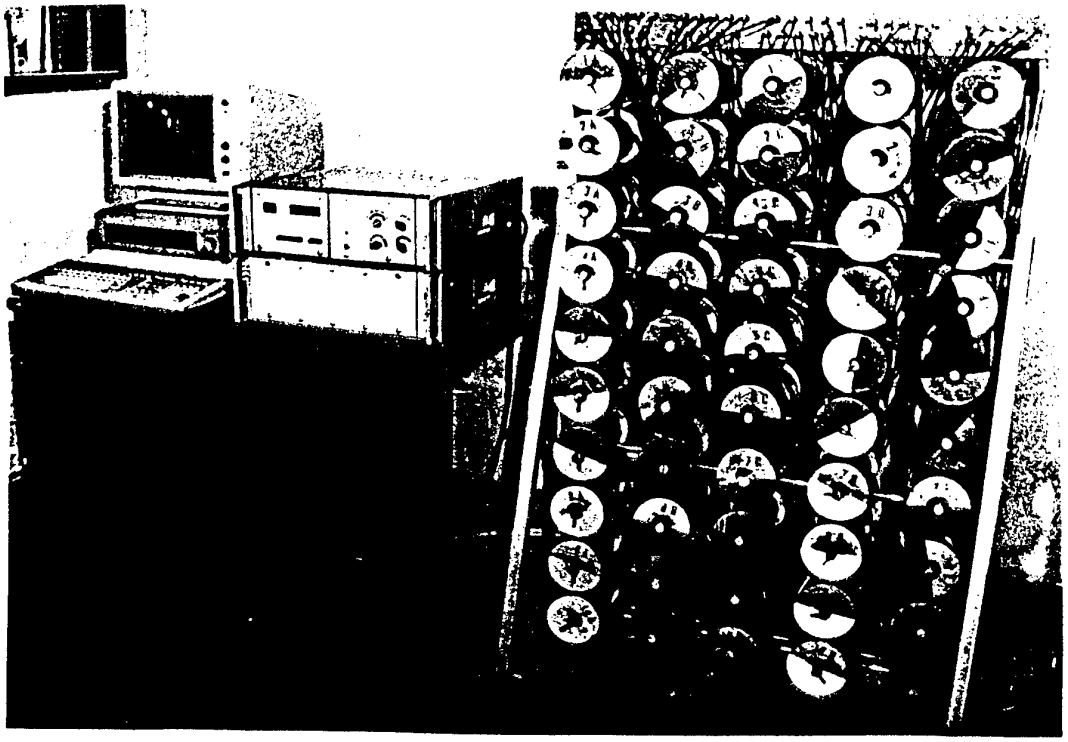

Fig. 11. 100-Channel computer-aided ultrasonic system for measuring of the airframe stiffness characteristics.

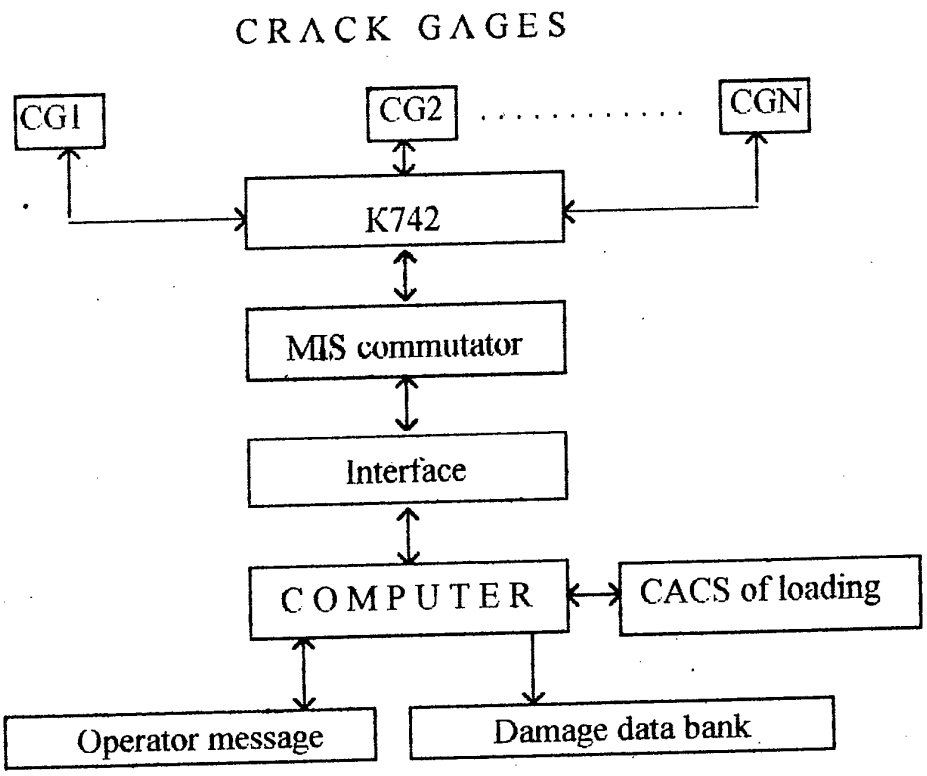

Fig. 12. Block-diagram of the crack registration system.

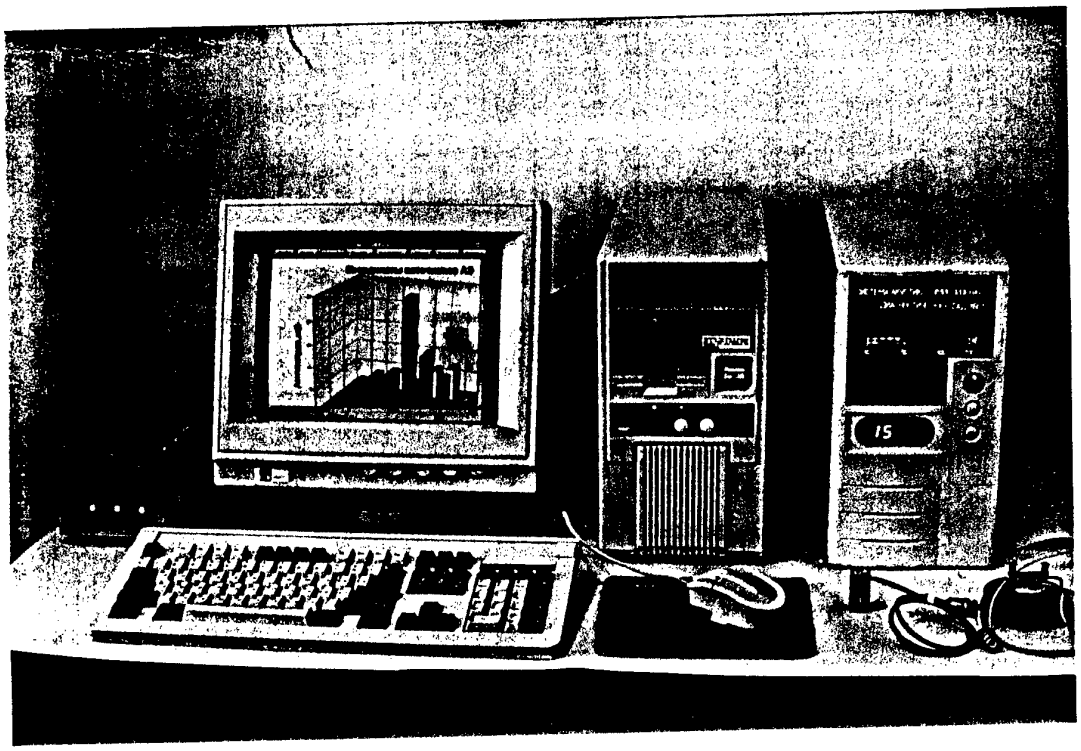

Fig. 13. Acousto-emission diagnostic complex.

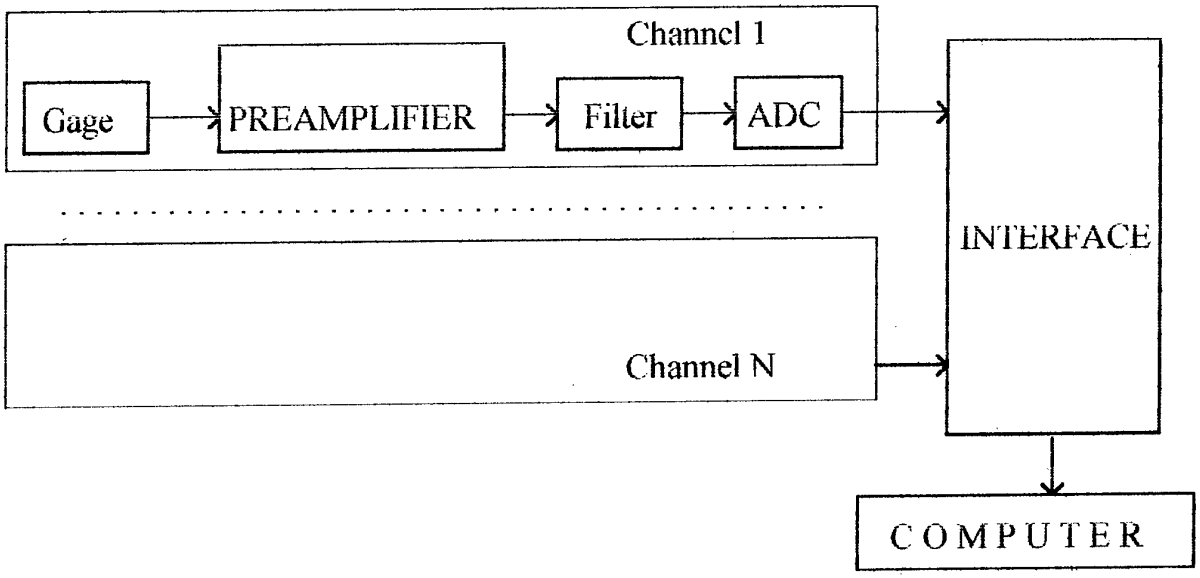

Fig.14.Block-ddiagram acousto-emission diagnostic complex.

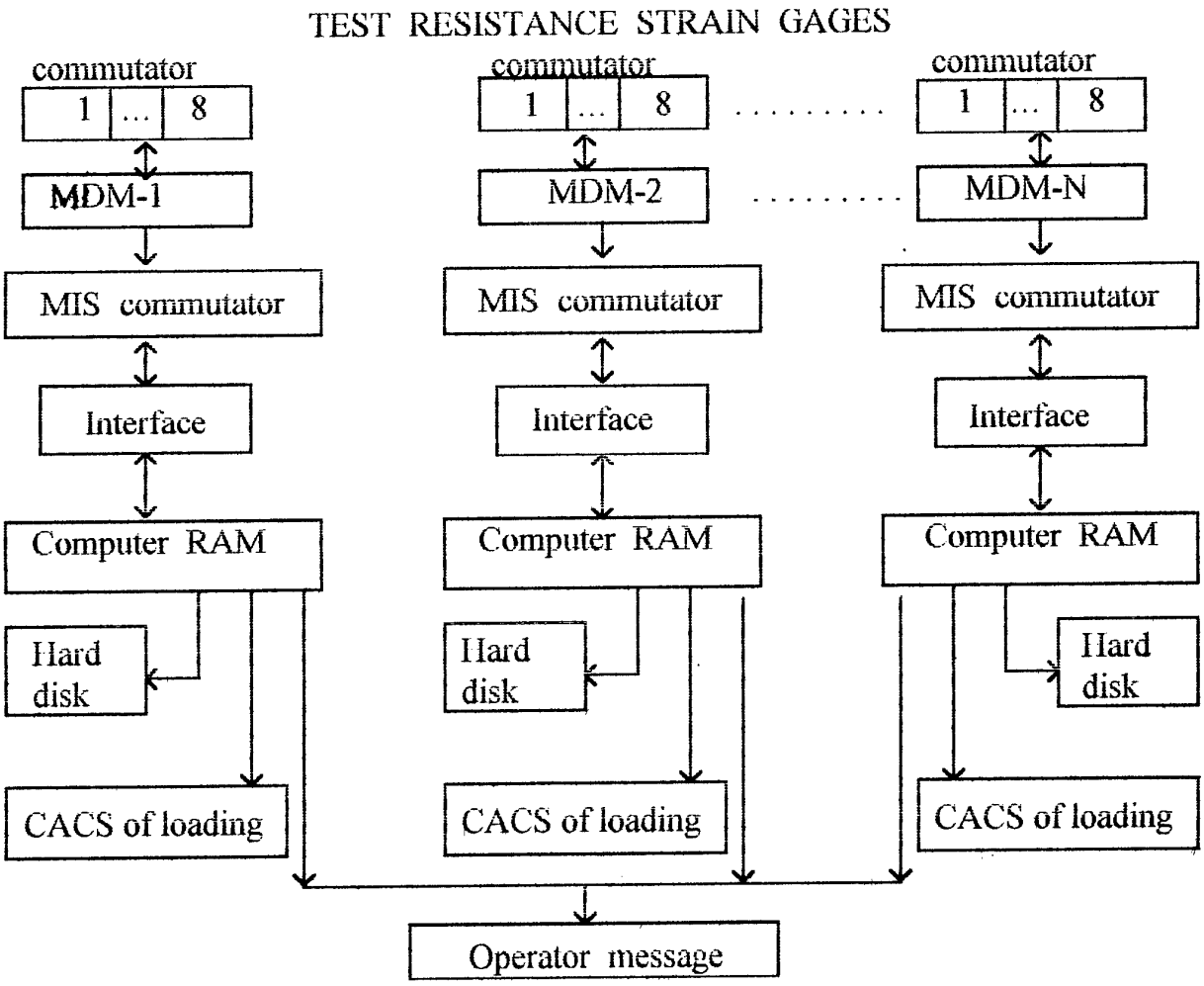

Fig.15. Block-diagram the high-speed strain-gaging system.

This complex allowed to detect the initiation of the fatigue fractures of a number of difficulty accessible zone of the Su-27 airframe during the life tests.

A block-diagram of the complex is given in Fig.14.

Should be noted that one of MIS function is to control the integrity of the test structure by means of periodical comparisons of the strain-gaging results for the same load at different structure lifes.

Static testind:

During the static tests it is necessary striotly to control the processes of plastic strain initiation, onset of a spontaneous fatigue crack propagation and static fracture of load-carrying elements.

A block-diagram of such control system using the high-speed strain-gaging of the structure in the loading process is shown in Fig.15.

In view of a high speed of the fracture processes a limited number of MIS channels is used; in the case of necessity some MISs and computers connected with the CACS of loading are used "non-effectively". The usual statistical processing on the information and processing for determination of the stress values aren't performed in the process of the experiment. Operation is carried out in codes, using the computer direct access memory. In the tests with the foreseen structure fracture, the information with filling of RAM is dumped on hard disk.

Conclusions

In the paper a complex of the automatization and measuring means for conducting of the full-scale static and life tests in considered. Using this complex, SibNIA has successfully carried out and is carrying out the tests of modern maneuverable aircraft of various types and modifications.

TOWARDS INCREASING THE SCIENTIFIC AND TECHNICAL LEVEL OF EVALUATION AND PREDICTION OF CIVIL AIRCRAFT LIFE CONSUMPTION

A.P.Zubarev, V.P.Lapaev, Yu.S.Obodovsky, D.F.Rykov
SibNIA Novosibirsk

1. Design Stage

In designing the airplane for Civil Aviation, an Important problem is the prognostication of the airplane loading under supposed field conditions. These conditions include a set of simultaneous variable factors affected and airplane loading and its failure probability. Such factors are: the aerodrome
surface irregularity (roughness), the air roughness (turbulence), the flight and taxing velocities, the airplane weight, the duration of the current mode of motion. within this trend, the most advanced problem in SibNIA is the prognostication of the airplane loading for the ground motion mode.

So, the surface roughness for the native aerodromes have been studied in Institute in 30 years. The methodology for measuring and estimating the spectral density of the surface roughness is developed. The spectral efficient system that measures and monitores the roughness is made. The contiguous profile measurement along the runway or taxway (length 3000-5000m) is executed in 20-30 min.

The significant statistics on the roughness spectral density along the runway and the taxway is collected upon almost 400 native aerodromes. In the recent years, the roughness analysis is made in the 20 formulation the reciprocal amplitude and phase roughness characteristics along several longitudinal section of the way were estimated.

All above characteristics are very specific for every aerodrome: the differences between each other are very large.

Basing on the flight and strength test for several airplane types and for several aerodromes, the statistical distributions for the following quantities are found in the ground motion modes: the velocity, the typical routes, and the taxing time.

Additionally, the experimental methodology is developed on the same data; it provides calculating the dynamic responses of the airplane (as a nonlinear system), and its loading.

The features of the methodology are:

1) The transfer function of the system is represented as a product of two functions, linear and nonlinear:

$$T(i\omega, \sigma_x) = T_0(i\omega) \cdot B(\sigma_x) \qquad (1)$$

where
$T_0(i\omega)$ is the transfer function of a linearized dynamic system for small perturbations: the masses and stiffnesses assumed to be prescribed; T_0 is found in calculations or it is aken from the experiment;
$B(\sigma_x)$ *is* the r.m.s. behaviour function of the nonlinear dynamic system; it is nonlinear characteristic of the system in a prescribed range of σ_x; it is found experimentally;
$\sigma(_x)$ is the r.m.s. aerodrome roughness within the specified frequency range.

2)The transfer functions of the system and the spectral densities of the loads are separated into the symmetric and nonsymmetric oscillation modes as for independent events:

$$T(i,\omega) = T_0^c(i\omega) \cdot T_0^H(i,\omega)$$
$$S_y(\omega) = S_y^c(\omega) + S_y^H(\omega) \qquad (2)$$

This approach provides the separate determination of the symmetric and nonsymmetric loading characteristics (i.e. the repeatability, the spectral densities, and the moments).

Such a separation is caused by the essentially different behaviour of the changes in intensity for the symmetric and nonsymmetric loading in consequence of the changes in the airplane velocity. In Fig. 1 the normalized spectral densities are shown for the loading P_y in the right undercarrige leg of the airplane IL-86 at two motion velocities. At the velocity V=11.3 m/sec, the share of the nonsymmetric modes (about 2.7 Hz) is essential; whereas at V=23 m/sec, the symmetric modes are prevailed.

To estimate the nonsymmetric loading, the 2D characteristics of the aerodrome roughness are to be found.

When the loading is estimated at the design stage, the basic problem is to find the nonlinear characteristic of the system, the function B (σ_x.).

At present, this function is fitted by means of a prototype; its characteristics $B(\sigma_x)$ are found experimentally from the flight and strength test. After that, the airplane loading is calculated for any aerodrome; the calculation is based on the statistics for: the external exposures, the velocities. and the motion routes. That sort of analysis was made in Institute when the airplane Tupolev Tu-204 was designed; the results are included in appraisal study for this aircraft.

The new research trend grounded in Institute: the methodology is developed for estimating the axial loading components in the undercarridge shock damper, and its damping abilities; these characteristics in both the linear and in the nonlinear formulation can found at design stage and under field conditions. The methology is based on the statistical analysis of the axial loading components in the undecarriage damper subjected to a external random stationary exposure in the laboratory or in the flight experiment.

The following numerical and spectral characteristics of the axial components of a force P in the damper can be obtained within the methodology: the air pressure Q_b, the hydraulic resistance Q_r,, the alternating component of the friction force Q_T, the function $\bar{\gamma}$ of the hydraulic resistance

$$(\bar{\gamma}^2 = \frac{\gamma_1^2 + \gamma_2^2}{2}).$$

The following innovations are developed in Institute: the laboratory stand for the chock-damper testing (all rights are reserved by the inventor's certificate), the testing methodology, the methology of data processing and their presentation; furthermore, the experimental model of the stand was created; the damper for a light airplane was tested.

The flight tests of the airplane shock-dampers for airplanes Tupolev Tu-134 and the IL-86, as well as the laboratory tests of the damper for a light airplane show that the hydraulic resistance variables $\bar{\gamma}$ are related to the displacement h of the damper stock trough a statistical relation $\bar{\gamma}D_h$ = const (where D is dispersion); such a relation is typical for the airplane dampers, see Fig. 2. In Fig. 3, The ratio D_p / D_h is shown as a function of

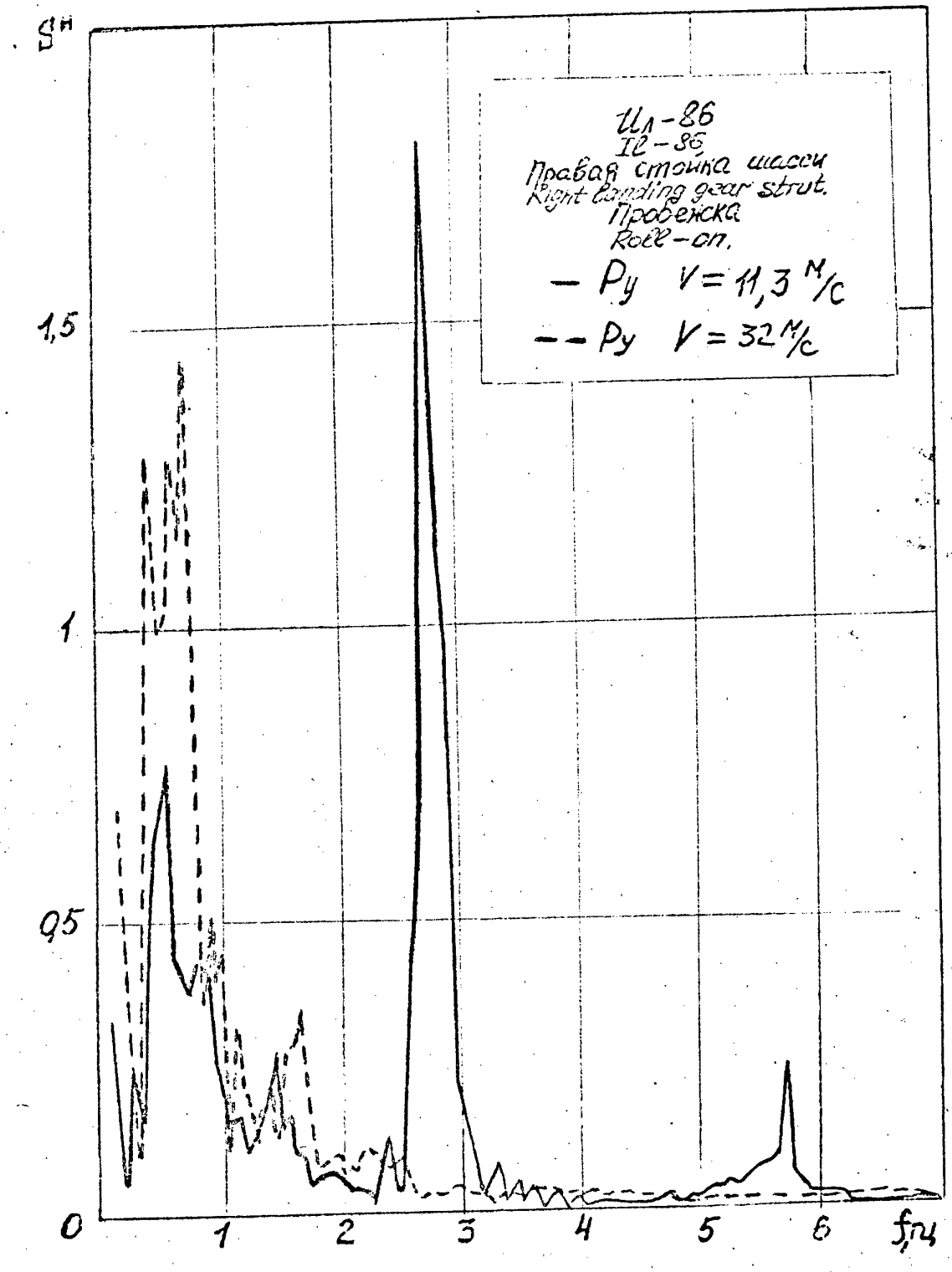
Sн
Ил-86
Il-86
Правая стойка шасси
Right landing gear strut.
Пробежка
Roll-on.
— Py V = 11,3 м/с
-- Py V = 32 м/с
1,5
1
0,5
0
1
2
3
4
5
6
f,Гц

Fig. 1

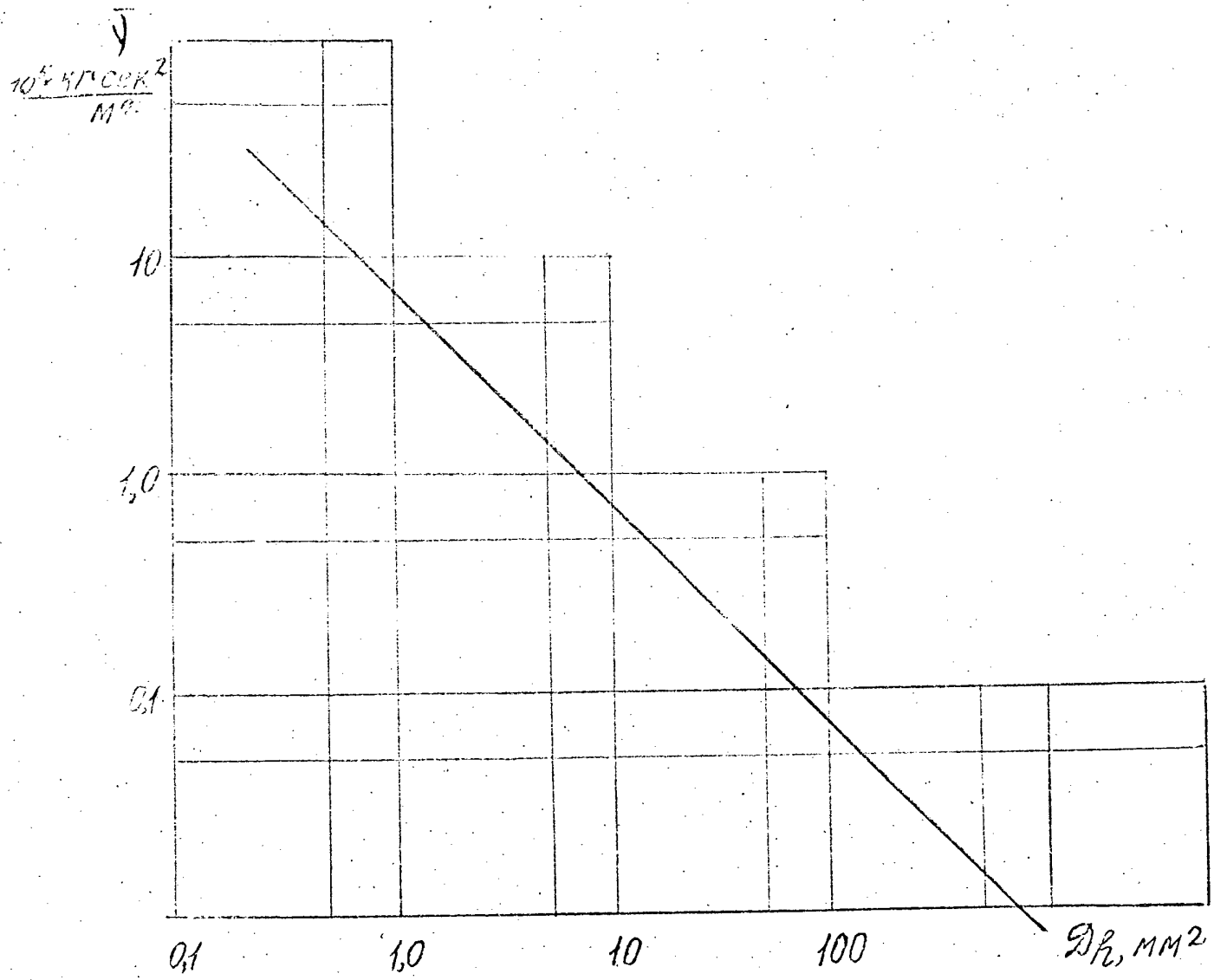
$\bar{\gamma}$
$10^{-5} \frac{кГ \cdot сек^2}{м^4}$
10
1,0
0,1
0,1
1,0
10
100
ΔR, мм²

Fig. 2

Fig. 2

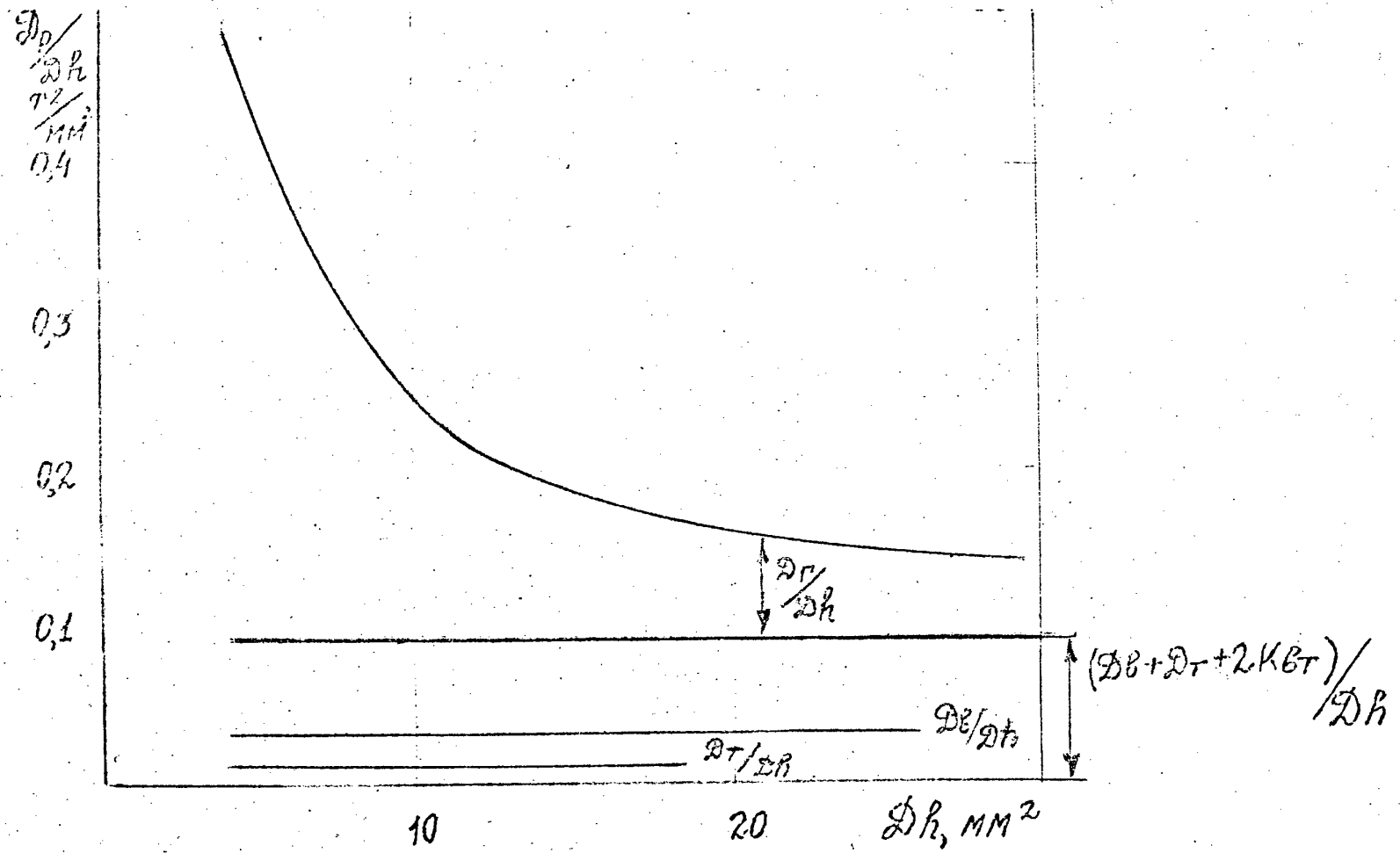

Fig. 3

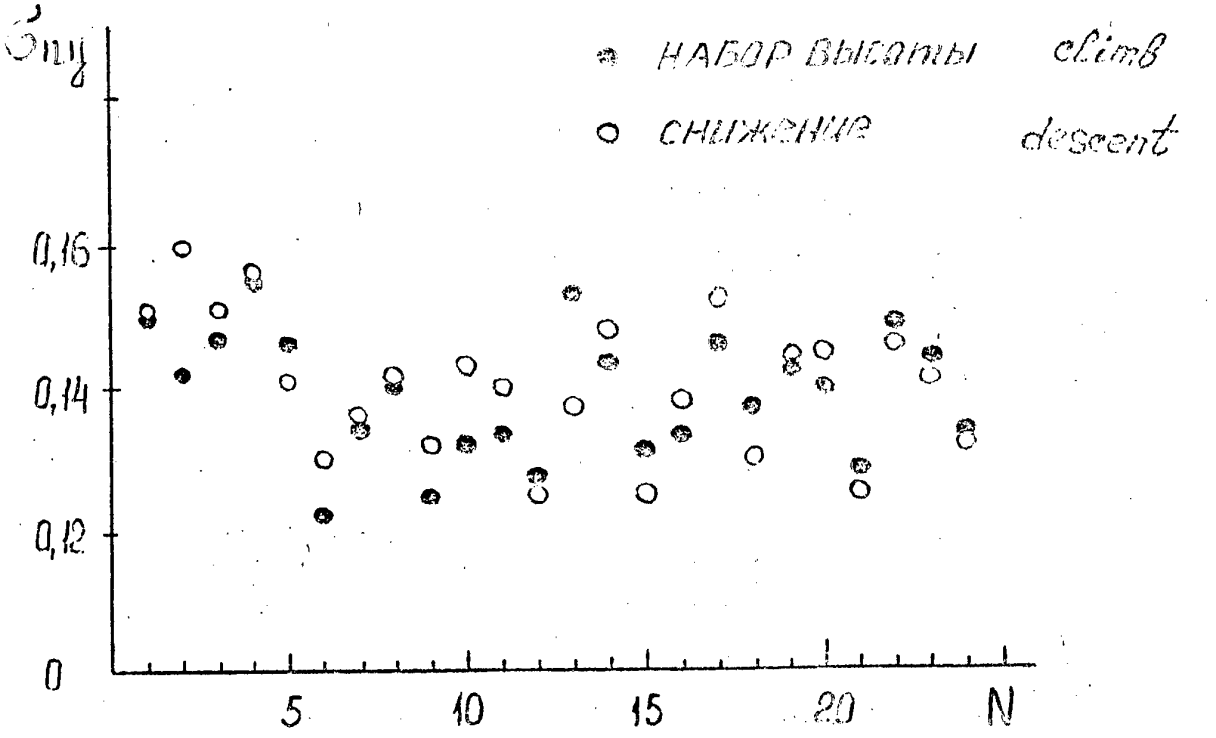
$\delta_{пд}$
НАБОР ВЫСОТЫ climb
СНИЖЕНИЕ descent
0,16
0,14
0,12
0
5
10
15
20
N

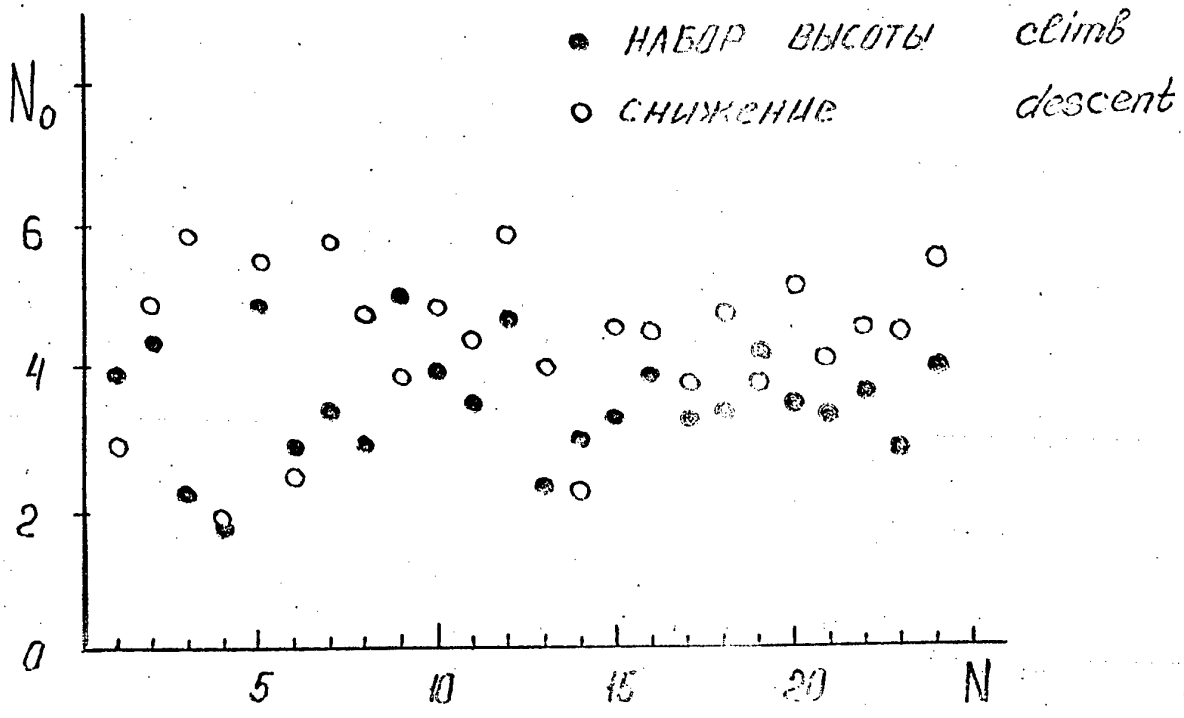
N_0
НАБОР ВЫСОТЫ climb
СНИЖЕНИЕ descent
6
4
2
0
5
10
15
20
N

Fig. 4

the compression degree in the damper D_h; the share of each component into the total load P is also shown.

In accordance with the practical requests on calculating the dynamic response and on the airplane loading , the new linearization methodology for the hydraulic resistance variables is proposed; the nonlinear "quadratic" formulation is changed to the linear one, $\bar{\gamma}_n (h^2) \rightarrow \gamma (h)$

The following connection is found:

$$\bar{\gamma} = \gamma_H \sqrt{3}\, \sigma\, h \qquad (3)$$

As a result, the linear system with a variable parameters is obtained; their behaviour is known. Both resulting transfer functions and the numerical loading properties are in a good conformity with experimental data.

The practical introduction of the methodology (to determine the damping abilities for the manufactured dampers) provides the loading calculations, the fitting and the optimization of these properties under the relevant criteria at the design stage.

2. Operational Stage

The following problems were studied in Institute during 30 years: the determination of the loading and the lifetime derating (the damage accumulation) for the airplanes in field conditions; these problems include:

- The statistical analysis on the external exposures (the aerodrome and air roughness) and on the velocities of the airplane motion;
- The determination and the investigation of the dynamic response of the airplane under various combinations of the external exposures, the airplane parameters, and its motion modes;
- The probability analysis on the field conditions under the criterion whether the airplane is a member of 1-th aviation subdivision or not;
- Designing the estimation methods for the loading and the failure probability as well as methods of referring these properties to the field conditions;
- The determination and the investigation of the loading and the damage accumulation for airplanes in different subdivision of Civil Aviation.

Within all these trends, the extensive investigations were made in Institute for several airplane types; as a result, the following facts are stated:

- The parameters of the typical flight and the airplane loading are essentially different in the different detachments of Civil Aviation;
- The failure probability in the different detachments can differs up to 1.5 times as compared with the mean value all over the whole fleet;
- The failure probability and the parameters of the typical flight can be considered as equal when the operating age is over 1.500 hours;
- The separated estimation of the lifetime derating and the residual lifetime is advisable.

The separated estimation model of the loading and the failure probability for civil airplanes is proposed basing on the above statements; the model includes, as a probable factors, the specific field conditions for the airplanes in 1-th Civil Aviation subdivision (or for the particular airplane) under external exposures, i.e. the air and aerodrome roughness.

A few words about the air roughness (turbulence)

In the flight, the failure are occurred mainly in the ascent and in the decent modes in the near-aerodrome zone; the air roughness spectra, like the aerodrome roughness, are very specific for every aerodrome: these spectra are essentially different in the intensity and in the spectral density pattern.

In Fig. 4 the q-loading parameters in the airplane C.G. in the ascent and in the descent modes are shown for 24 aerodromes depending on the air roughness intensity σ_{ny} and on the spectral density pattern N_0 only; the sample size is 500-2000 flights. There is the essential difference in parameters.

To make the loading analysis for any airplane type (including the design stage) in the ascent and in the descent modes, the spectral density of the air roughness in the near-aerodrome zone should be found. To find them, it is convenient to use the statistics on the q-loading in the airplane C.A., since the body of stored information is very large and provides the reliable estimations. For this purpose, the new methodology is developed; the spectral density of a vertical gust basing on the flight and strength experiment can be found; within the methodology, the intensity and the spectral density pattern are related to the q-loading parameters in the airplane C.G. In Fig. 5, the normalized spectral density approach for the gusts in 4 turbulence zones is shown; these graphs are obtained in the flight and strength experiment for the airplane IL-86. It is clear that the spectral density pattern in the zones (K = 2.1... 2.5) are different. The introduction of this method into manufacturing and its future development provide obtaining the turbulence properties in the near-aerodrome zones basing on the q-loading statistics.

The estimation of the technical status of the airplane structure within the fleet is also studied in Institute; it is shown that the intensity of failure in the airplane structure in different detachments of Civil Aviation is in a good correlation with the estimated one, see Fig. 6.

Introducing the above of the airplane lifetime provides the high reliable estimations of lifetime departing and the residual lifetime of the airplane structure.

At the recent years, the new trend is developed in Institute ; it upgrades the reliability and the life time of the civil airplanes; it is based on the combined multi-disciplinary investigations and on the tune adjusting of the aerodynamic structures.

As a dimensions and the weight of the airplane are increased, large localized masses (2 or 3 engines hanged on pylones with essential stagger) are placed under the wing: thus the frequency of the higher elastic modes in the structure becomes more lower. Upon this fact, the share of the elastic modes into the loading and into the failure probability of a structure is increased; the strained state becomes more combines as well as the interaction between the loading components. Thus, further improvement of the lifetime support for the up-to-date and future airplanes in Civil Aviation should be based on the multi-disciplinary combined organization of both investigation and the adjustment of the structure strength properties. First and foremost, it concerns the investigation of the working loading and further its implementation as some equivalent loading programs for the in-situ laboratory lifetime test of the product since:

- The life time test program should confirmed the reliable working loading al over the whole variety of the real field conditions;
- The multi-component loading of an operational airplane is studied insufficiently; the requests on the data representation are not present;
- As the rule, the real multi-component operating loading is included not in full measure in the available methodologies and programs for the laboratory tests: the testing stands are not realize it;
- The data convergency on the failures occurred in use and in laboratory is insufficient.

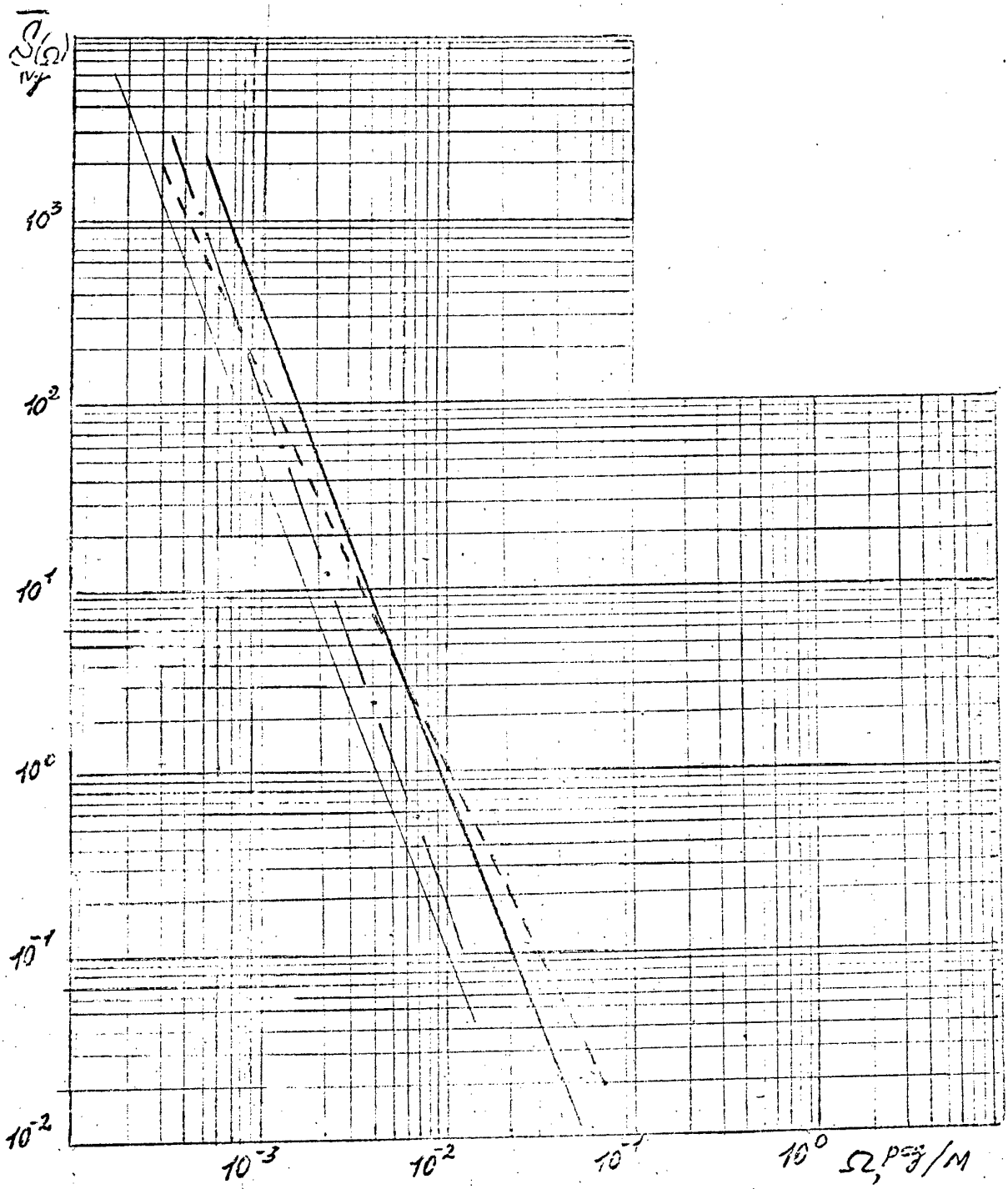
$\overline{S(\Omega)}$
10^{3}
10^{2}
10^{1}
10^{0}
10^{-1}
10^{-2}
10^{-3}
10^{-2}
10^{-1}
10^{0}
Ω, рад/м

Fig. 5

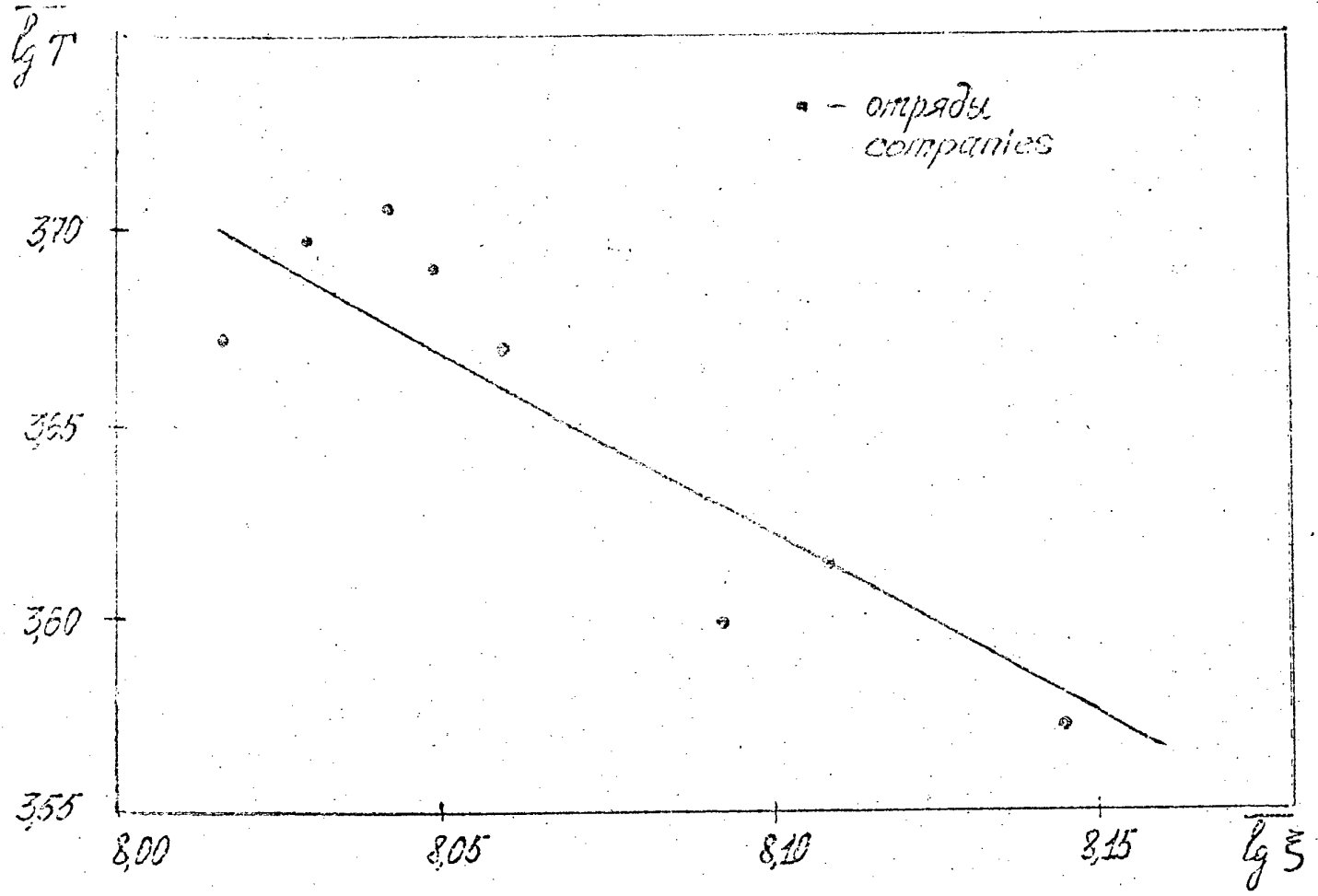

Fig. 6 Влияние условий эксплуатации в различных отрядах ГА на долговечность панели.
Influence of operational conditions of different companies on a panel life.

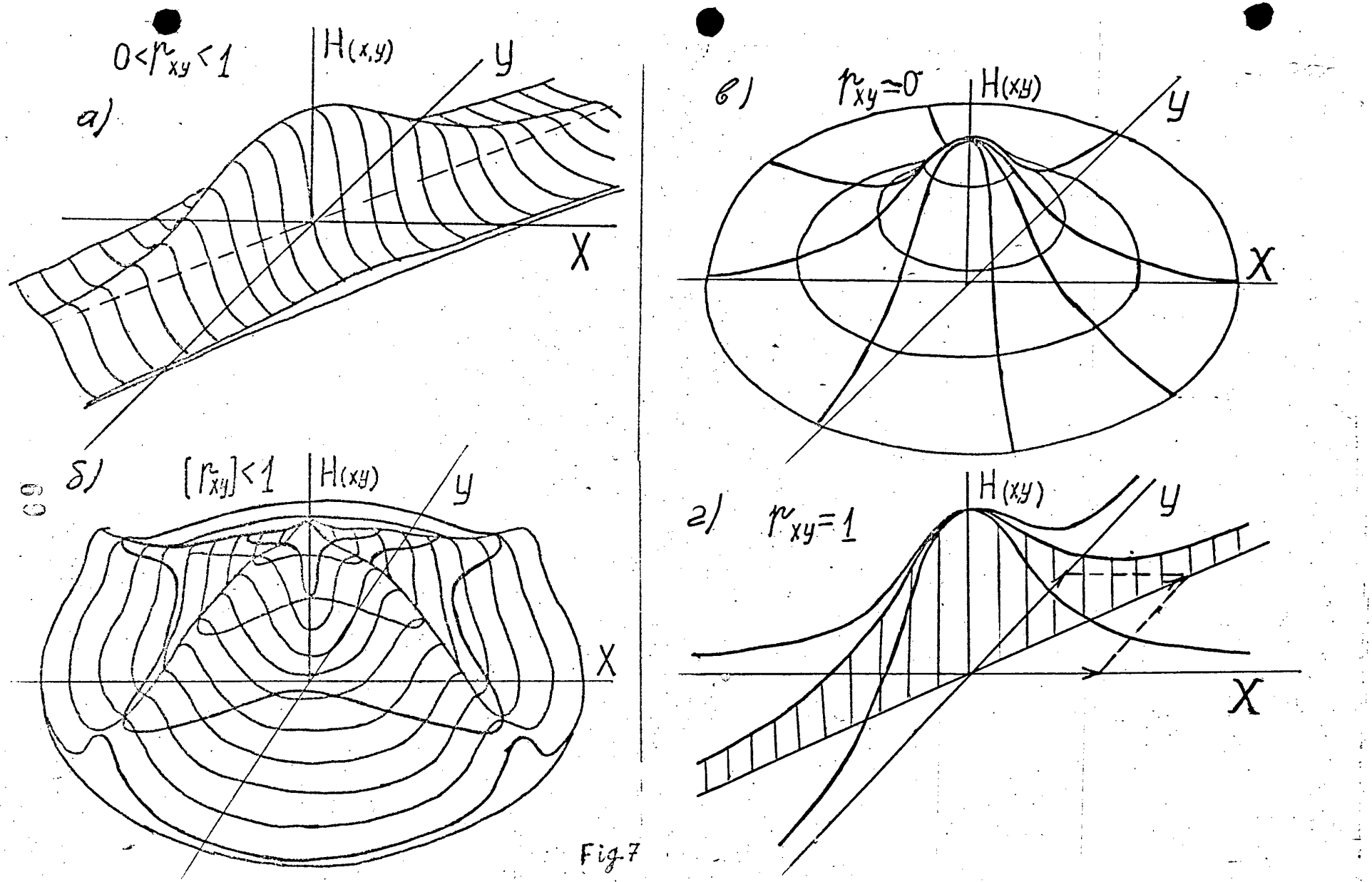

Fig.7

The investigations on the 2D loading units of an large airplane with 4 engines hanged in pylones under the wing show that 3 types of 2D loading are mainly occurred; these types are distinguished in the internal structural interdependence of the loading components.

In Fig. 7 the following repeatability dependencies are shown: in Fig.7a, the *2D* repeatability for x - and ψ - components of the process $\{x, \psi\}$ with a high enough positive correlation and a simple internal interdependance pattern; in Fig.7б the 2D repeatability with a complex internal interdependence pattern and with a more lower correlation degree ($|\Gamma_в| > |\Gamma_а|$); in Fig. 7в, the 2D repeatability of the non-correlated process $\{x, \psi\}$; and finally in Fig.7г, the repeatability of the loadings x andψ realized in the laboratory test.

In the current methodology of the lifetime definition is based mainly on the loading representation of type Fig. 7a, than the approach methods in the interpretation for the multi-dimensional loading of the type of Fig.7б,7в should be improved. The examples of that type are, e.g. , the alternating components of the bending and the twisting in the wing zone between the engine nacelles and the fuselage, the loads P_x, P_y, P_z acted on the airplane undercarriage , the alternating components of the bending moments in the fuselage taken in vertical and horizontal planes, etc.

The realization of the multi-dimensional loading in a structure during the laboratory test requires the newest methodologies and the highly automated stands.

Further, the methodology of the service life definition requires a hard work in an insufficiently studied sphere, an investigation on the distribution and the numerical characteristics of the lifetime for materials, for the members, the units and the whole product under the multi-component loading under exposure of any factors.

Within this new trend, the long-term investigation program is developed in Institute; it includes 5 scientific sections. The airplane loading and the external exposures in the 2D formulation are studied; some results obtained are:

- The methodology and data processing program are developed; the interdependence properties for the 2D stationary and tentative $H(x,\psi)$ and tentative $N(Y/\bar{X}_i)$ load repeatability can be found;
- The numerical, spectral, reciprocal spectral, and correlation characteristics of the 2D loading in the undercarriage, in the wing, and in the fuselage of the airplane IL-86 are obtained from the experimental data;
- The technique for calculation the 2D and the tentative repeatability of the load peaks from numerical characteristics of the 2D process with the particular internal interdependence patterns.

As the program is implemented, the following factors should increase: the weight efficiency, the reliability in finding the strength, the lifetime the survivability of the airplane, as well as the economical efficiency and the flight safety.

COMPOSITE MATERIALS IN AIRCRAFT STRUCTURES

V.F.Kut'inov
TsAGI, Zhukovsky, Russia.

1. SURVEYING THE USE OF COMPOSITES IN AIRFRAMES

The composite materials are regarded to be promising from the viewpoints of both extending the aircraft capabilities and improving the economy figures. Therefore aircraft companies conduct comprehensive projects for utilising the composites.

The international and Russian data available, see Fig.1, clearly demonstrate permanent growth in aviation composite materials utilisation. According to forecast in the technical literature, the amount of composites in passenger-carrying airplane airframes will by year 2000 be as large as 15 -20% (referred to the weight of all materials used), and in military airplanes, 35%.

As to aircraft industry of the Commonwealth of Independent States, all major design bureaus have mastered these materials. Let us practical examples of the use of composite materials in domestic airplanes.

In TU-204 passenger-carrying airplane (Fig.2) the amount of composites is 9% of the weight of all materials used; the plan is to increase this parameter to 15% by introducing composites in structures of vertical and horizontal stabilisers.

In AN-70 transport (Fig.3) the weight of composites is 25% amongst all materials used. Large-size structures of vertical and horizontal stabilisers are completely manufactured out of composite; sandwich panels are with tubular cores.

A mass-produced MIG-29 fighter (Fig.4) has 7% fraction of composites (by weight); in future fighters the weight fraction of composites in lifting surfaces, wing high lift devices, and body components will be as high as 30%.

Composite materials were also used in Buran orbiter: payload bay doors have been manufactured out of a carbon/carbon material (Fig.5).

2. LAYUP AND CHARACTERISTICS

Widespread aviation composite materials are the polymer matrix composites; used as a filler in them are glass, organic and/or graphite fibers. Figure 6 demonstrates usual combinations components for the fibrous composites utilized in aviation.

Levels of specific strengths and stiffnesses of composites are mainly defined by properties of the fibers. The diagram compares specific strengths and stiffnesses of unidirectional composites with epoxy matrices and various reinforcing fibers.

Glass-reinforced plastic have high allowable stresses and low stiffness. Organoplastics can carry high tensile stresses but have a relatively low Young's modulus and low compressive strength. Carbon fiber reinforced plastics are now the main structural materials for load-bearing components of structures. Various fillers can be combined in a material system, forming a hybrid material.

Mechanical properties of a matrix are determinants for a shear load capability, buckling behaviour, and maximum use temperatures; fatigue and impact resistance depends on a matrix.

Currently, efforts are untaken to develop composites based on thermoplastics. The latter yield at elevated temperatures and harden at room temperature. As compared with thermoset composites, the thermoplastic-based systems have a number of advantages:

- ease of use,
- simpler repair, the potential for reuse,
- almost no limitations on prepreg storage duration,
- insignificant sensitivity to moisture,
- high fracture toughness, damage tolerance, see Fig.6.

Most widely the aircraft companies manufacture the composite structures from prefabricated prepregs, i.e. indirectional layers impregnated with a matrix material. The prepregs are built-up in compliance with prescribed pattern, thereafter united in a final material by polymerizing the stack (Fig.7). The resulting material has certain average stiffnesses and strengths, which can be controlled by varying the composition parameters such as the total number, layup angles/sequence, and thicknesses of the layers.

The average properties of composites are predicted by analysis based on anisotropic multiplayered plate theories. Used as unitial data characteristics of undirectional orthotropic ply that are listen in a table in Fig.7. The ply characteristics are evaluated experimentally.

3. DESIGN OF COMPOSITE STRUCTURES

A traditional task during design of primary structure to prescribed load is to specify structural parameters such as to attain a minimum mass under constraints. In the case of composite structures the set of design parameters is extended by adding parameters of the stack, - the directions and amounts of undirectional layers. The increase in the total number of design parameters; more details in the analytical model; extra limitations associated with manufacture and use of composite structures; these factors result in a very cumbersome design process. The problem can be simplified by dividing the design procedure into stages as presented in Fig.8.

First stage: a multidisciplinary aero/strength/dynamic design of beam/plate models in order to preliminary specify parameters of minimum-weight structure under requirements for strength, aeroelastic behaviour, controllability, fatigue life, etc.

Second stage: a coarse finite-element model is used to formulate reasonable structural concept and to improve parameters including the "microstructure" of materials.

Third stage: individual structures, assemblies and joints are optimized.

Fourth stage: a structural analysis is carried out using the final FE model of high dimension; all requirements are checked out.

At TsAGI, methods for the first and second stages are implemented in ARGON complex; its schematic may be seen in Fig.9.

Proceeding from the initial data represented in this Figure, the problem conducts the multidisciplinary aero/strength/dynamic design of a continuum-mechanics model. Airloads are evaluated with due accout for aeroelasticity; the extreme load conditions are revealed; the fiber orientation angles and thicknesses are chosen; aeroelastic behaviour is evaluated.

At the second stage , a finite-element model is formed; a reasonable structural concept is outlined; fiber orientation angles and thicknesses are refined. Figures 10 and 11 illustrate the use of ARGON in application to design of vertical stabilizer of a high-technology aircraft.

At stage 1 (Fig.10) the analytical model is as simple as a sandwich panel with a rigid core. Weight and stiffness requirements are complied with by establishing a reasonable composition of primary layers. At the stage 2 (Fig.11) the finite-element model is used to form a reasonable structural concept, a stack composition, and thicknesses for each structural unit.

VALUE OF COMPOSITE MATERIALS IN AIRFRAME

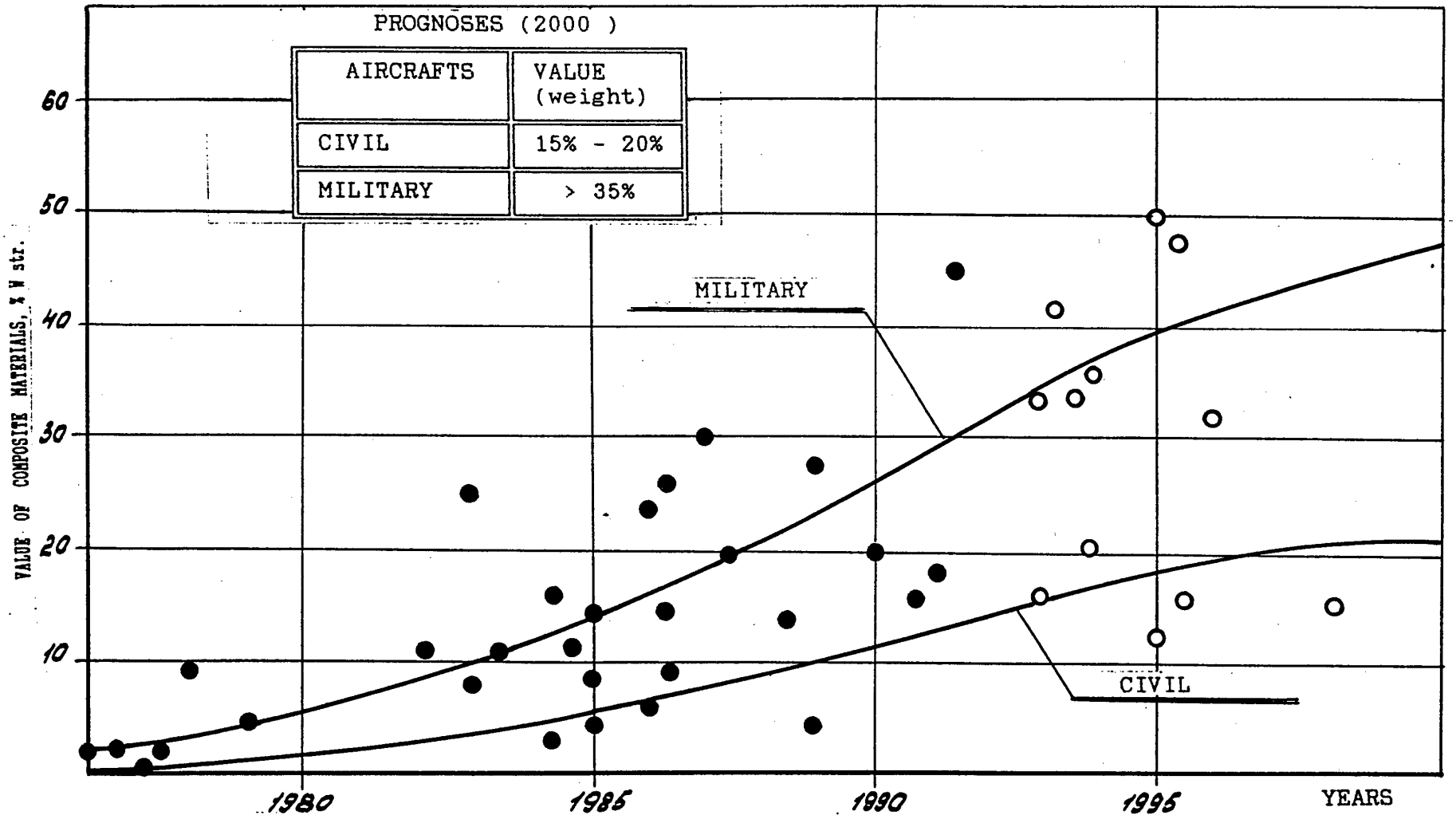

COMPOSITES IN PASSEUGER AIRKRAFT TU-204.

VALUE COMPOSITES 14 % (WEIGHT)

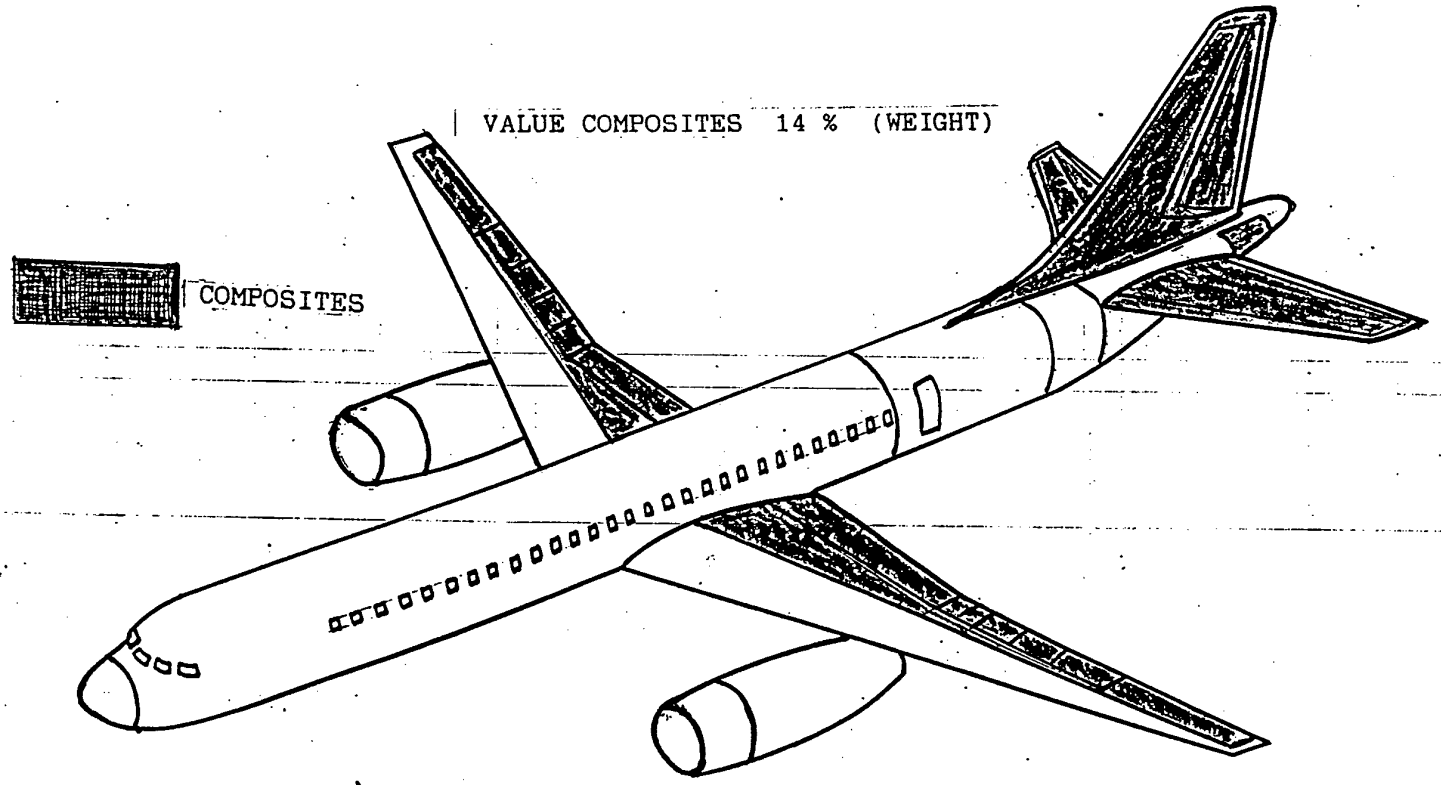

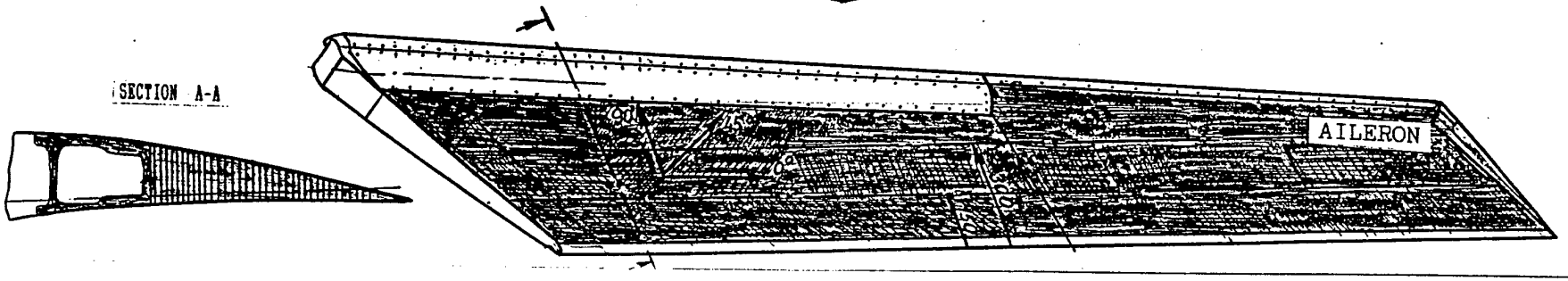

COMPOSITES IN MIG-29 FIGHTER.

VALUE OF COMPOSITES 14% (WEIGHT)

COMPOSITE FOREWING OF LONG-RANGE FIGHTER

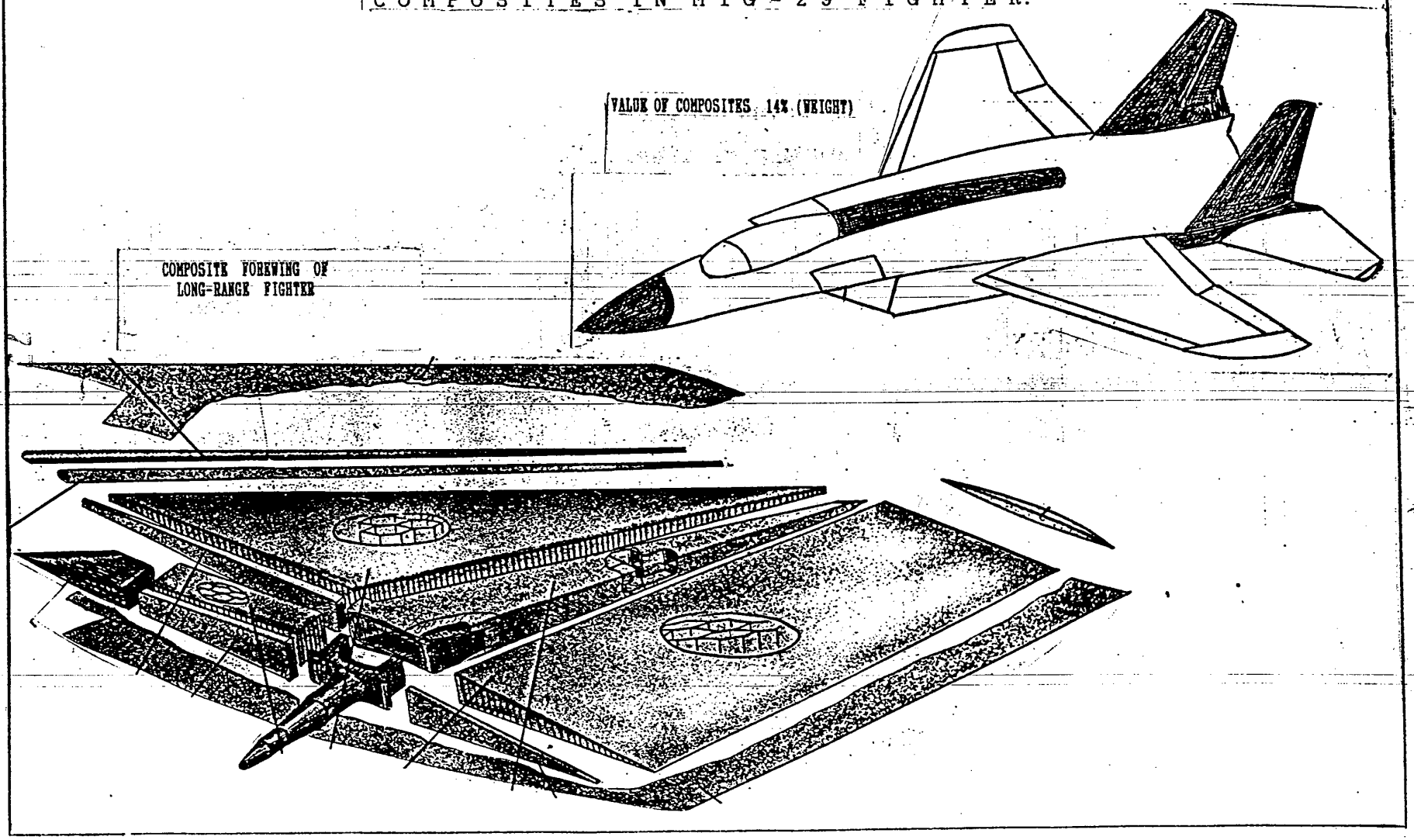

COMPOSITES IN TRANSPORT AIRCRAFT AN-70

VALUE OF COMPOSITES 25% (weight)

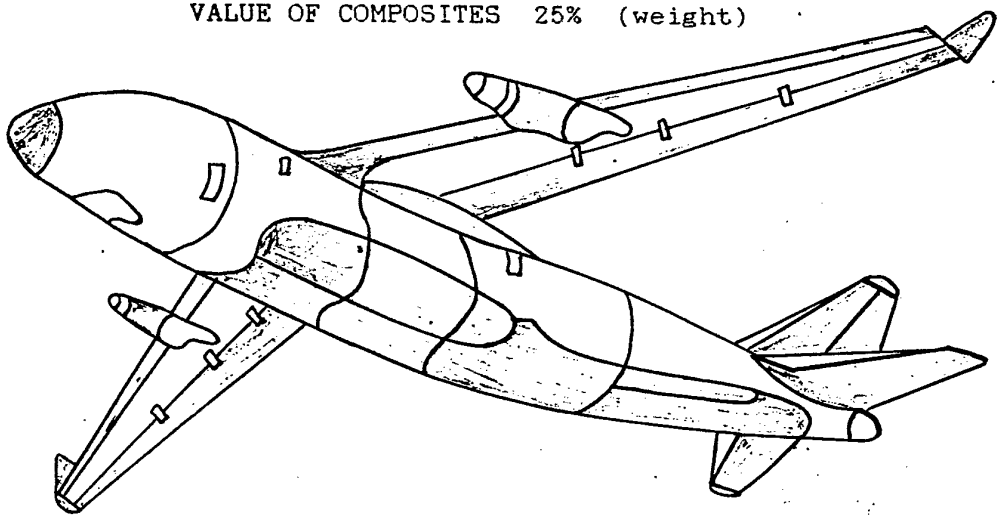

- COMPOSITES

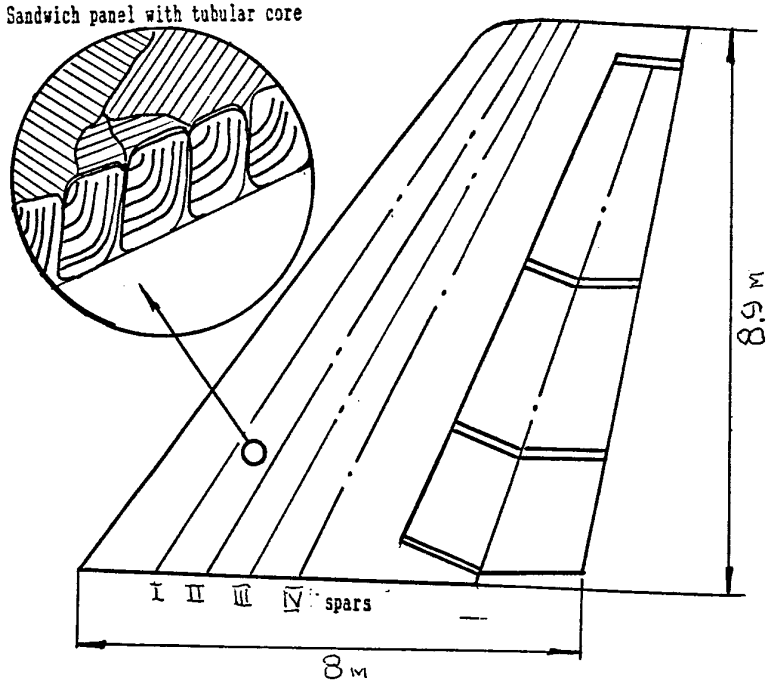

COMPOSITES IN VEHICLE " BURAN "

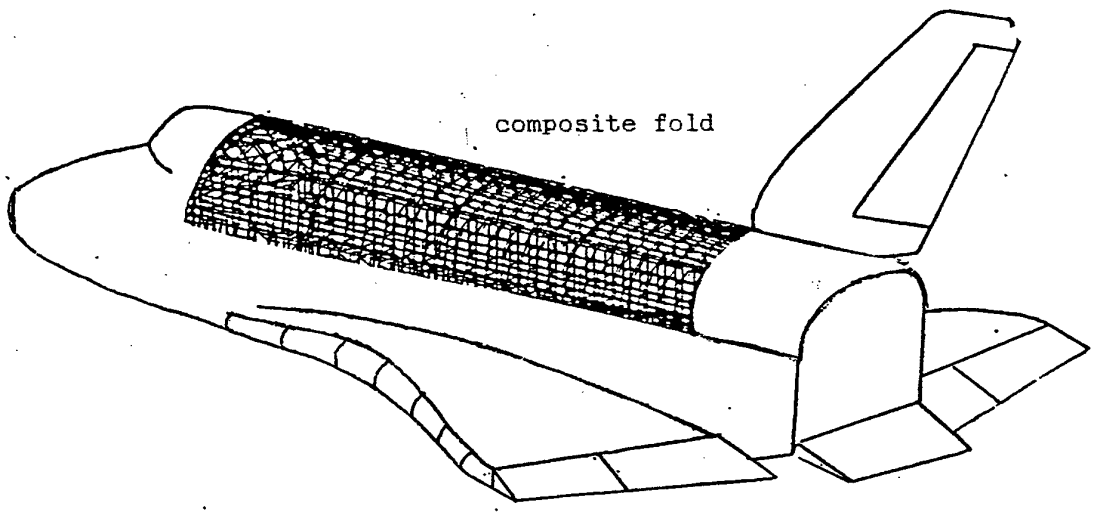

61

FIER COMPOSITES WITH RESIN MATRICE

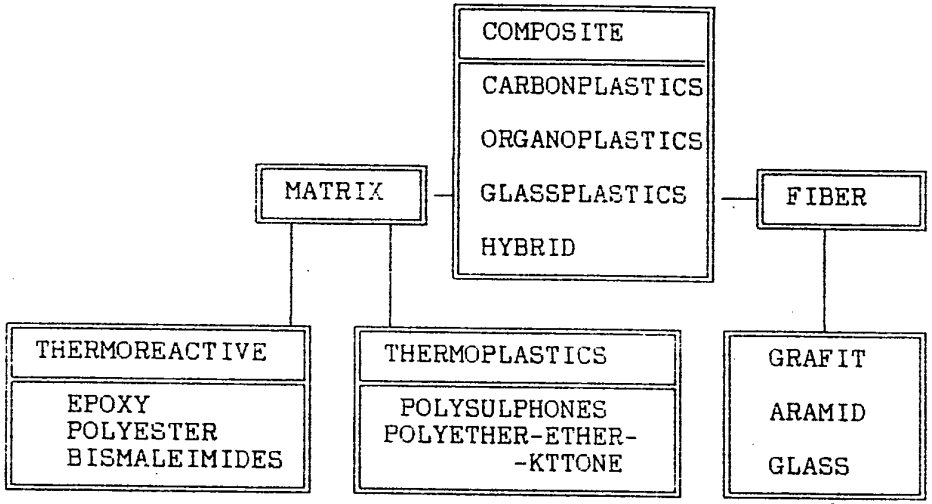

ADVANTAGES OF THERMOPLASTICS MATRIX COMPOSITES

1. MORE TECHNOLOGICAL.
2. MAY BE REPAIRED, MAY BE USED FOR REPATED MANUFACTURING.
3. THERE IS PRACTICALLY UNLIMITED PERIOD OF CEEPING PREPREGS.
4. MORE RESISTANT TO HUMIDITY ACNION.
5. CHARACTERISTICS OF VISCOCITY OF DESTROYING AND DAMAGE TOLERANCE ARE BETTER

UNIT CHARACTERISTICS COMPARISON

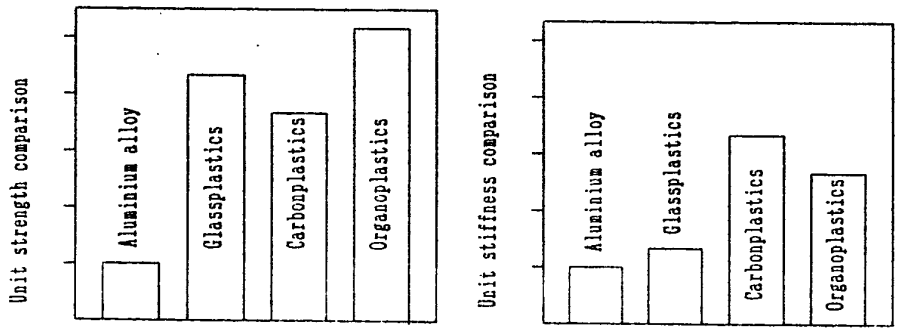

RELATIONSHIP BETWEEN RESIDUAL STRENGS OF COMPRESSED CARBONPLASTICS WITH VARIOUS MATRCES AND UNIT ENERGY OF IMPACT..

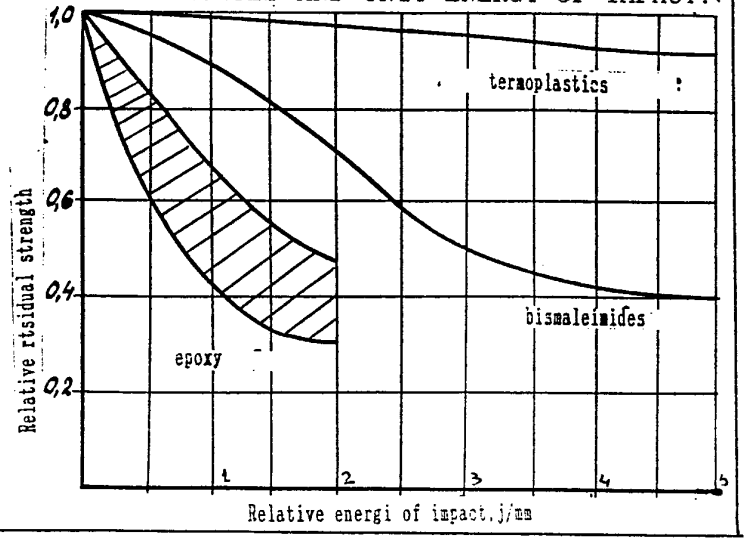

INTERNAL STRUCTURE AND PROPERTIES OF FIBER POLYMER COMPOSITES

INTERNAL STRUCTURE OF FIBER COMPOSITES

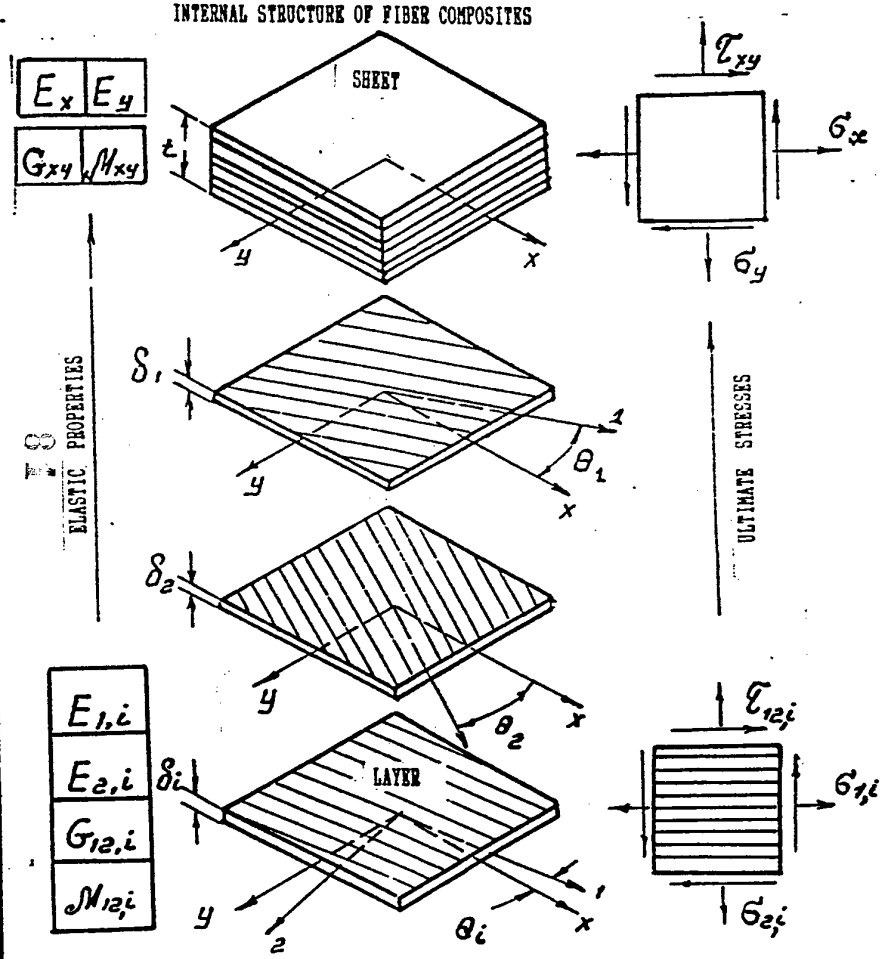

TYPICAL PROPERTIES OF UNIDIRECTIONAL COMPOSITES.

NN	PROPERTIES		MATERIAL DESIGNATION	CARBONPLASTICS EPOXY .V=60%	ORGANOPLASTICS EPOXY.V=60%	GLASSPLASTICS EPOXY.V=45%
1	JOUNG MODULL	ALONG	E1 kg/mm2	13000	8000	4000
2		ACROSS	E2 kg/mm2	700	600	300
3	SHEAR MODULE		G12 kg/mm2	600	200	400
4	POISSON RATIO			0.28	0.34	0.25
5	ULTIMATE STRESS (TENSION)	ALONG	kg/mm2	110	140	110
6		ACROSS	kg/mm2	2	1	3
7	ULTIMATE STRESS (COMPRESSION)	ALONG	kg/mm2	70	20	60
8		ACROSS	kg/mm2	13	5	12
9	ULTIMATE STRESS (SHEAR)		kg/mm2	6	3	7

- UNIDIRECTIONAL LAYER PROPERTIES ARE DETERMINED EXPERIMENTALLY,
- AVERAGED PROPERTIES OF A LAMINATEW ARE DETERMINED NUMERICALLY BY TECHNIQUES BASED ON THEORY OF LAYERED ANISOTROPIC PLATES.

MAIN STAGES IN DESIGNING THE COMPOSITES AIRFRAMES

ARGON

I STAGE	
Aim	Determination of thicknesses and lamination parametres
Model	Continuum mechanics : roads, beams, plates
Design variables	Thicknesses, ply angles
Constraints	Strength, displacements, aeroelastic behaviour, min/max thickness

II STAGE	
Aim	Upgrading the thickness distribution and structural concept
Model	Coarse, discrete, finite-element
Design variables	Thiknesses, ply angles, structural concepts
Constraints	Strength, stiffness, etc.

COMPOSITE

III STAGE	
Aim	Optimization of joints and individual components
Model	Roads, beams, plates. Finite Element Model
Design variables	Microstructure of material Structural concept
Constraints	Strength, stiffness. Mass

MARS

IV STAGE	
Aim	Structural analysis
Model	Detailed discrete model
Design variables	-
Require-ments	Check for all constraints and restrictions

Data flow in ARGON during aero/strength/dynamic designing of the composite lifting surfaces

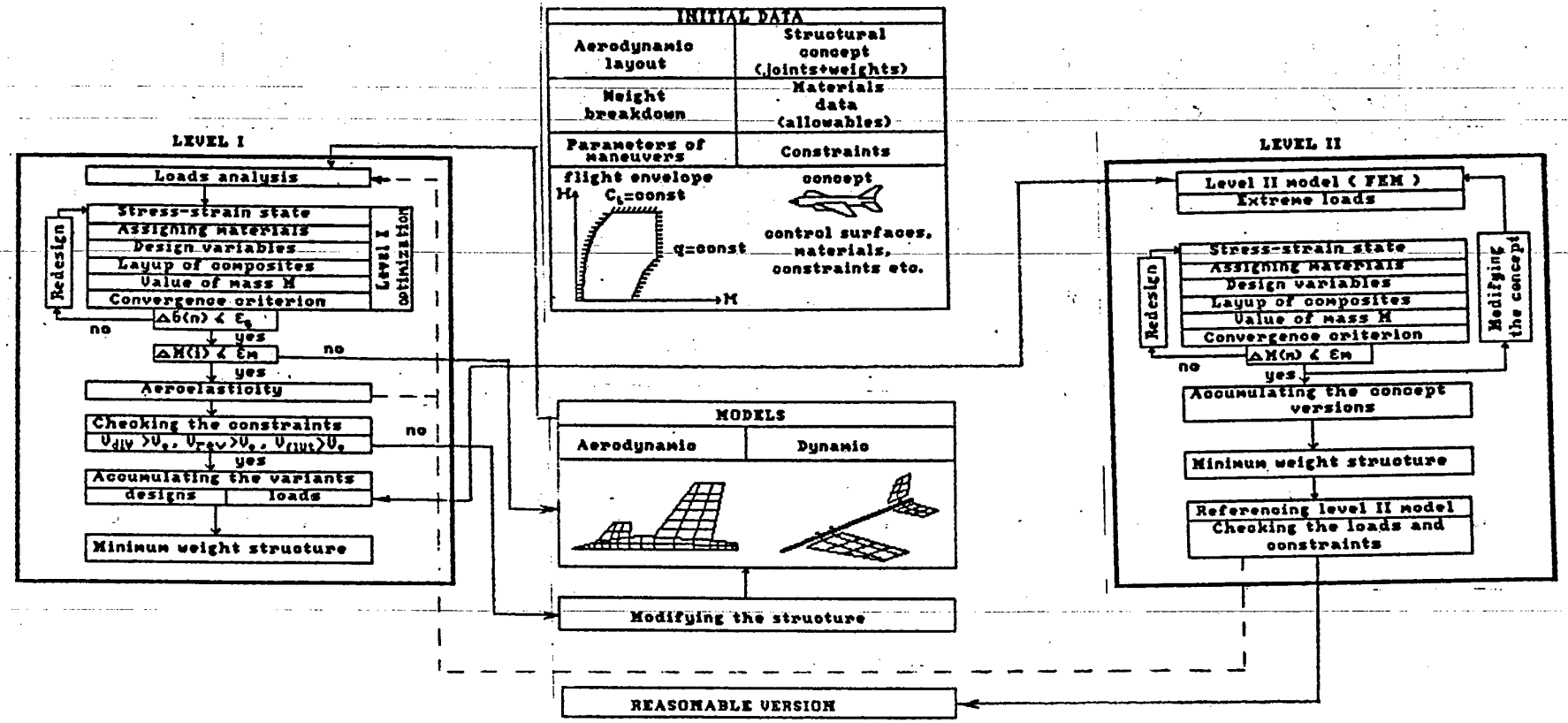

VERTICAL FIN OF A HIGH-PERFORMANCE AIRCRAFT

Level I model

A–A

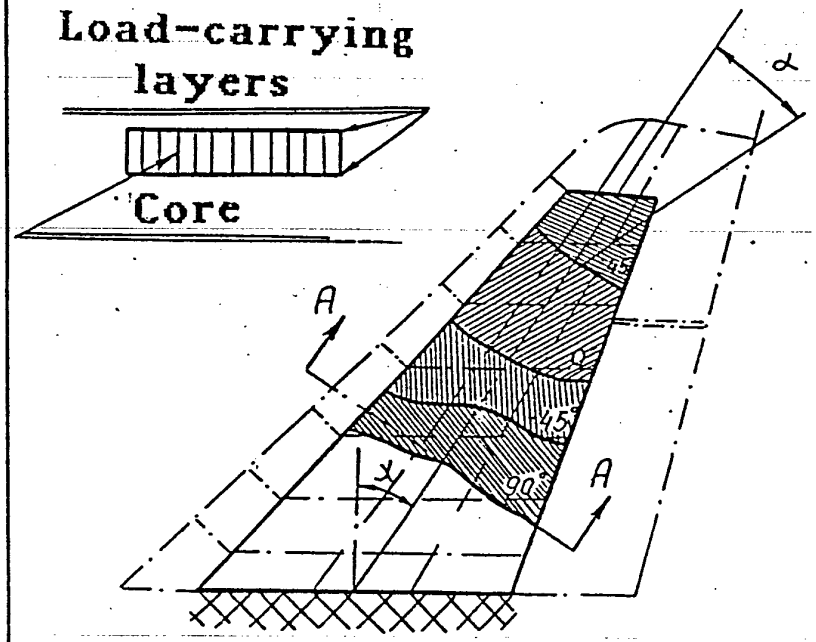

Mass M and fin tip rotation angle $\varphi_к$ vs. laminate principal axis angle α

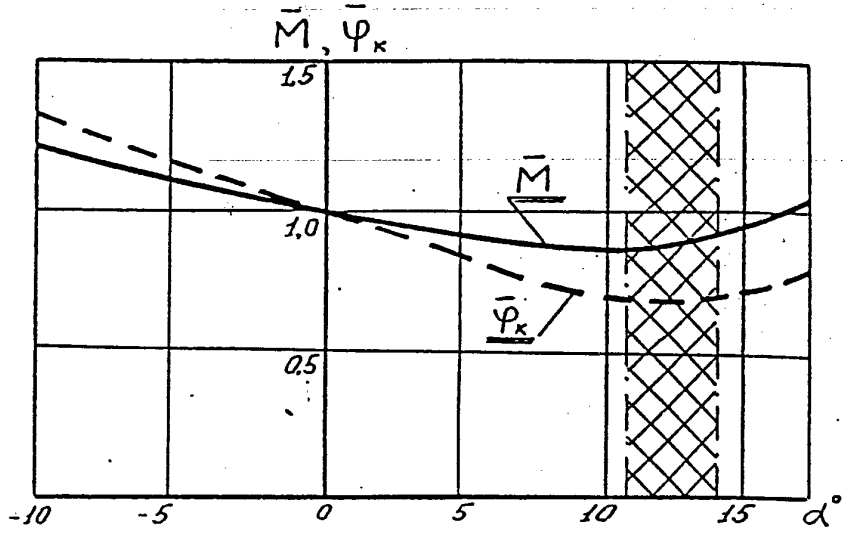

$$\bar{M} = \frac{M}{M_{\alpha=0}} \qquad \bar{\varphi}_к = \frac{\varphi_к}{\varphi_{к,\alpha=0}}$$

VERTICAL FIN OF A HIGH-PERFORMANCE AIRCRAFT

Level II model

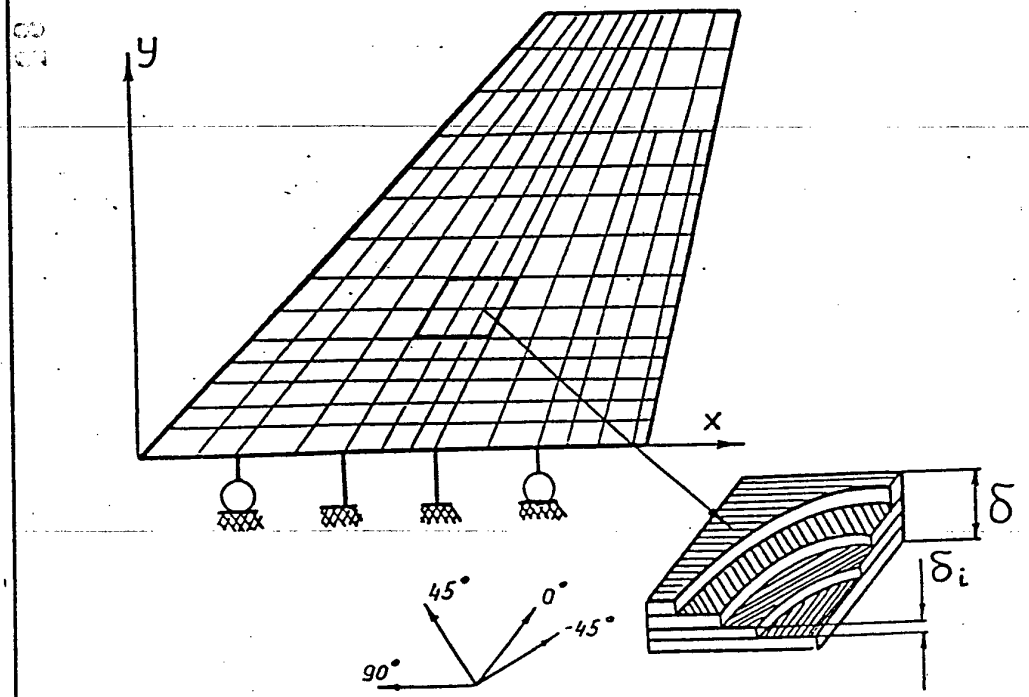

Spanwise distribution of thickness

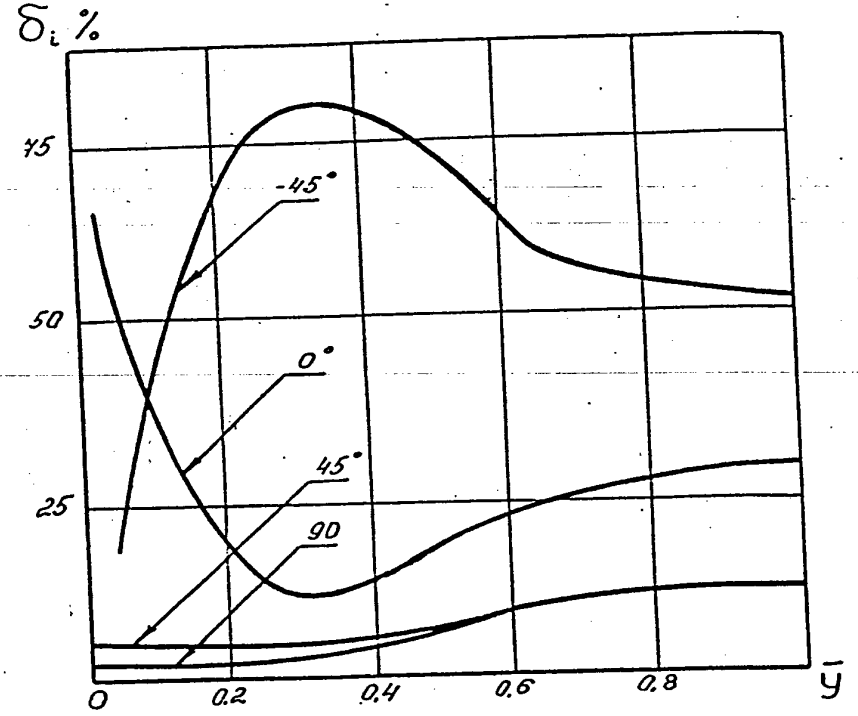

$$\bar{\delta}_i = \frac{\delta_i}{\delta}$$

COMPOSITE

PACKAGE OF INTERRELATED PROGRAMS FOR ANALYZING THE COMPOSITE STRUCTURES

PURPOSE

Automation of Strength Analysis at Stage of Designing Separate Composite Structures

LANGUAGE

FORTRAN-77

AUTHORS

Mishulin I.B., Andrienko V.M., Zamula G.N.,
Sukhobokova G.P.,Ierusalimsky K.M.

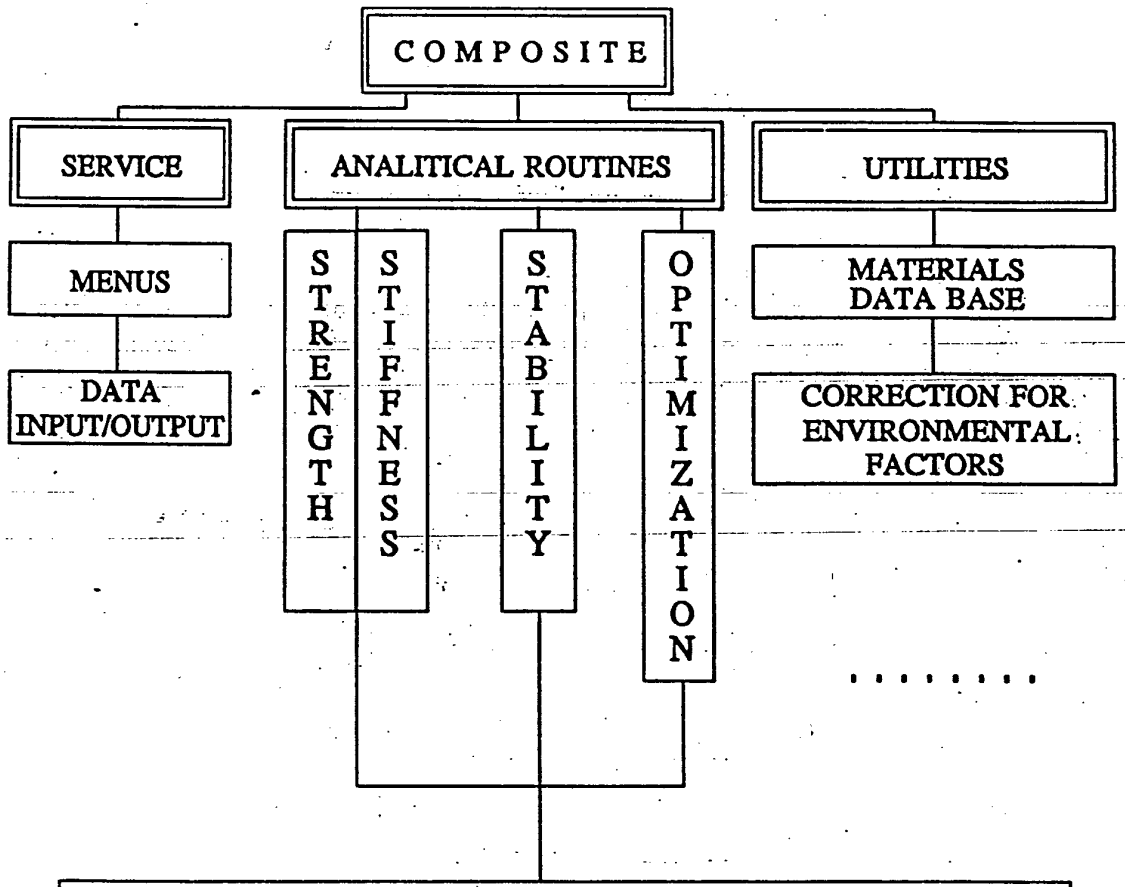

Structural components: uni/bi-axially stiffened and unstiffened, flat/cylindrical, sandwich/solid panels; simple torsion-boxes
Homogeneous and diverse fibres
Three-components membrane loading

Interaction through multilevel menus

C O M P O S I T E

PACKAGE OF INTERRELATED PROGRAMS FOR ANALYZING THE COMPOSITE STRUCTURES

CALCULATION OF STRENGTH PARAMETERS

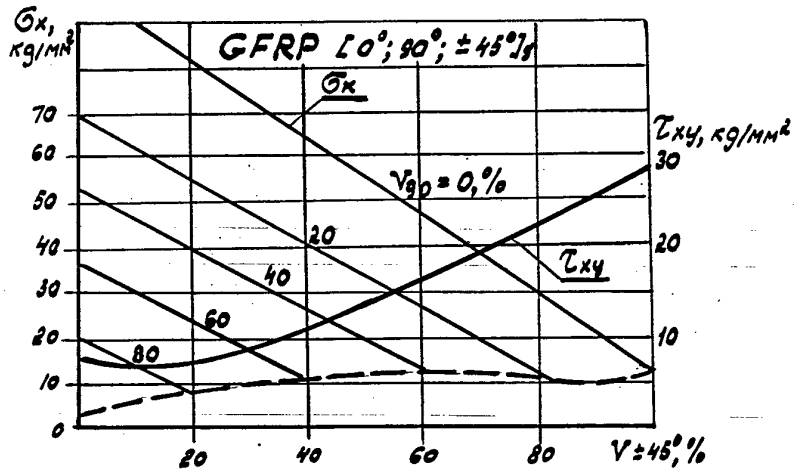

CALCULATION OF ELASTIC PARAMETERS

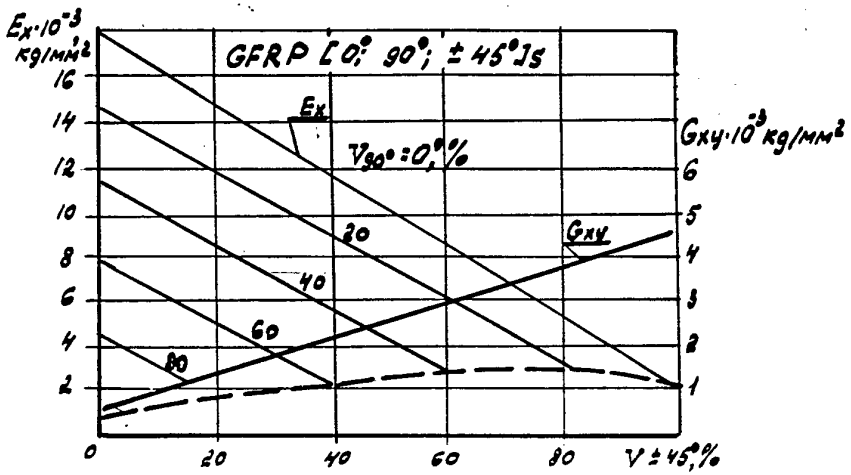

ANALYSIS OF STRUCTURAL MEMBERS

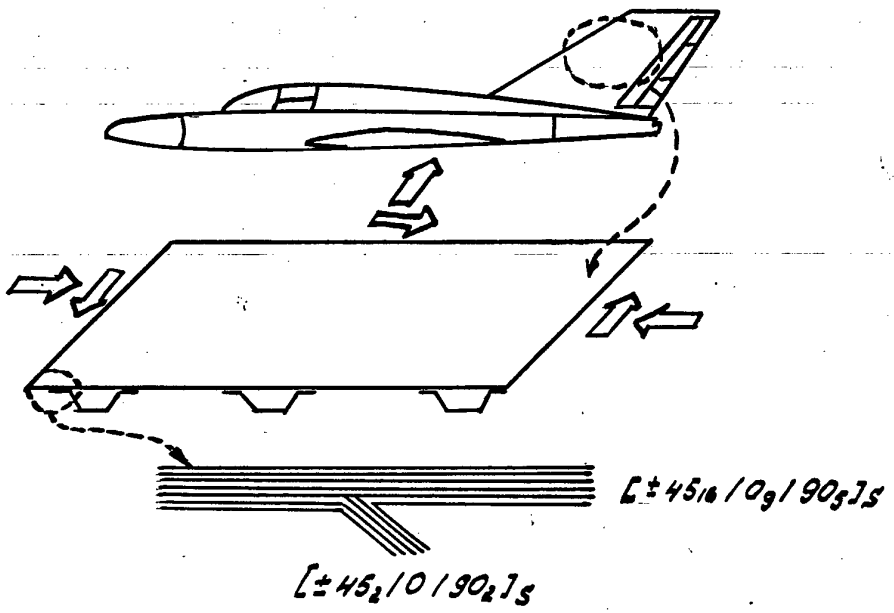

COMPOSITE is a convenient means for designers to use at their working stations.

OPTIMAL DESIGNING OF COMPOSITE

PANEL / SHELLS

Problem formulation

Initial data	Objective function	Constraints
Load: Pcompr Geometry: R, L	Min weight: G min	Stress: $\sigma_i <= \sigma_b$; $\sigma_i <= \sigma$ crit Manufacture: (t_i / t_{lam}) = integer

Design variables
Detailed geometry skin, web, str, fr, ..

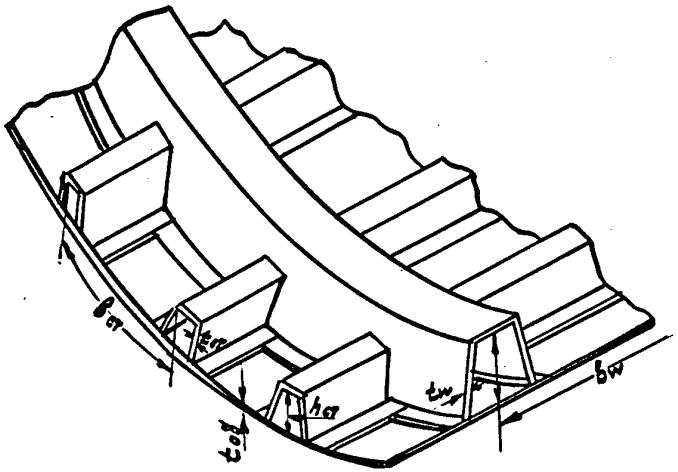

Type of material

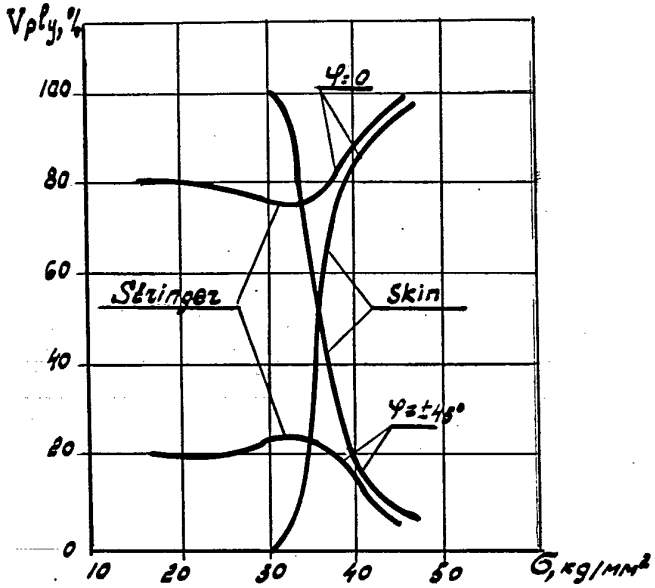

Parameters of panel member

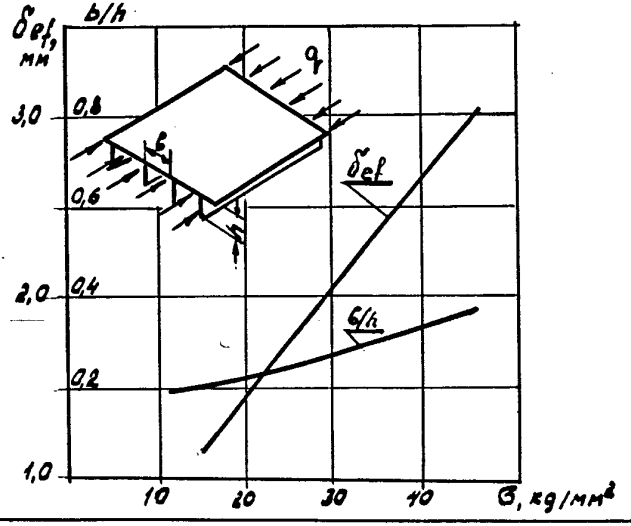

FACTORS REDUCING STRENGTH OF COMPOSITES.

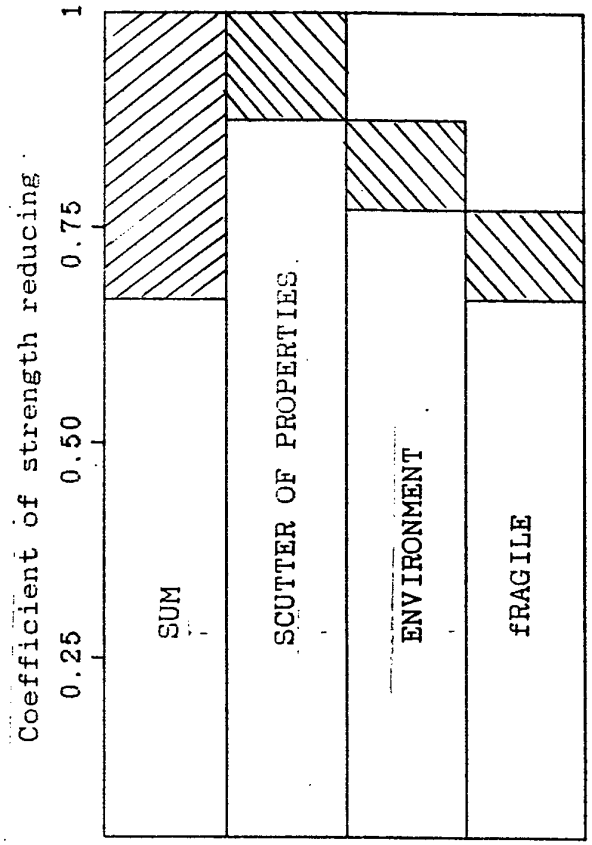

SCUTTER OF PROPERTIES.

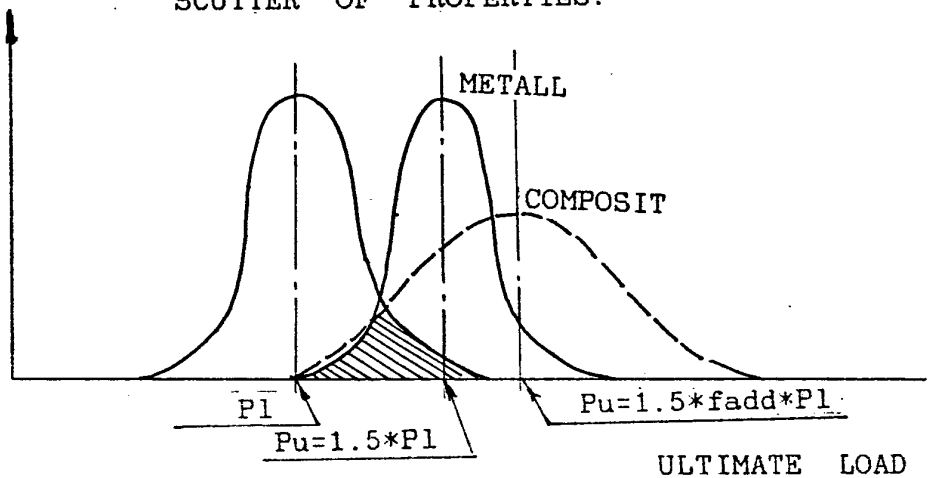

γ_N	Coefficient of variatia in realisation N

N	3	4	5	10	20
h_N	1.50	1.44	1.4	1.2	1.1

$$\gamma = \gamma_N (1 + h_N)$$

Pu=1.5*fadd*Pl

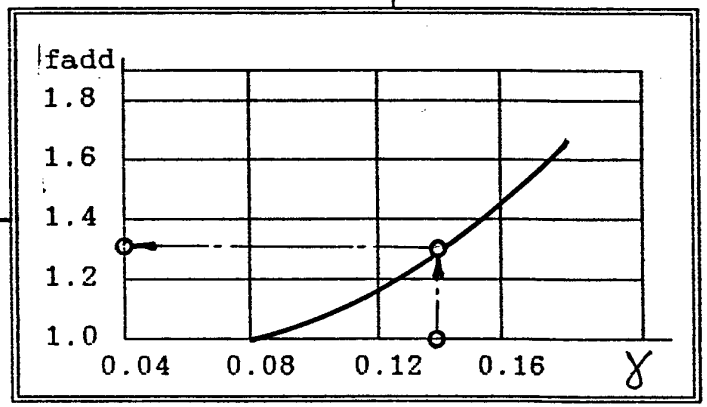

ENVIRONMENT INFLUENCE ON CARBONPLASTIC STRENGTH.

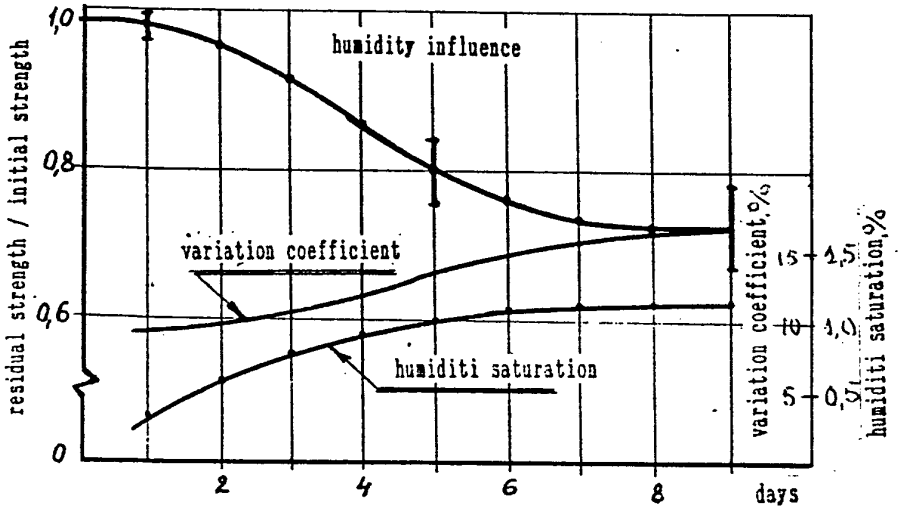

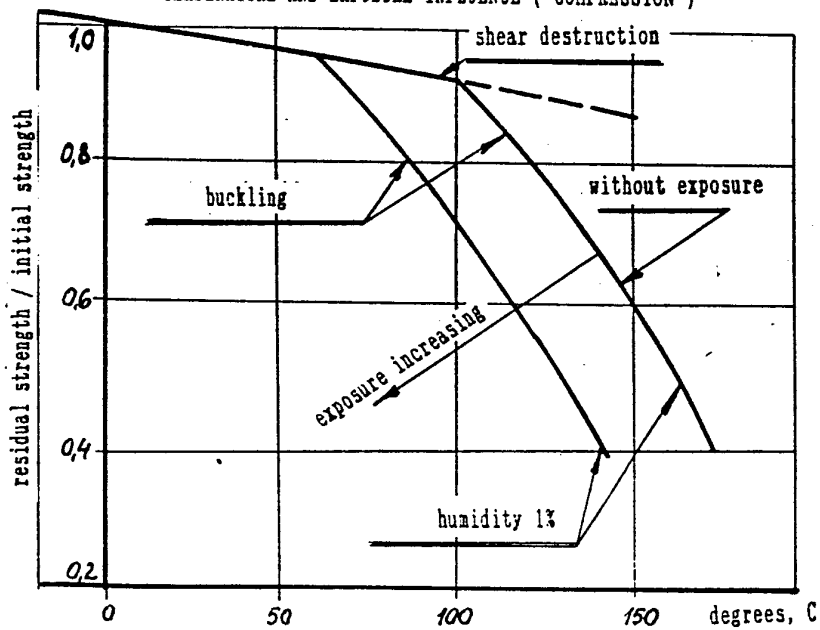

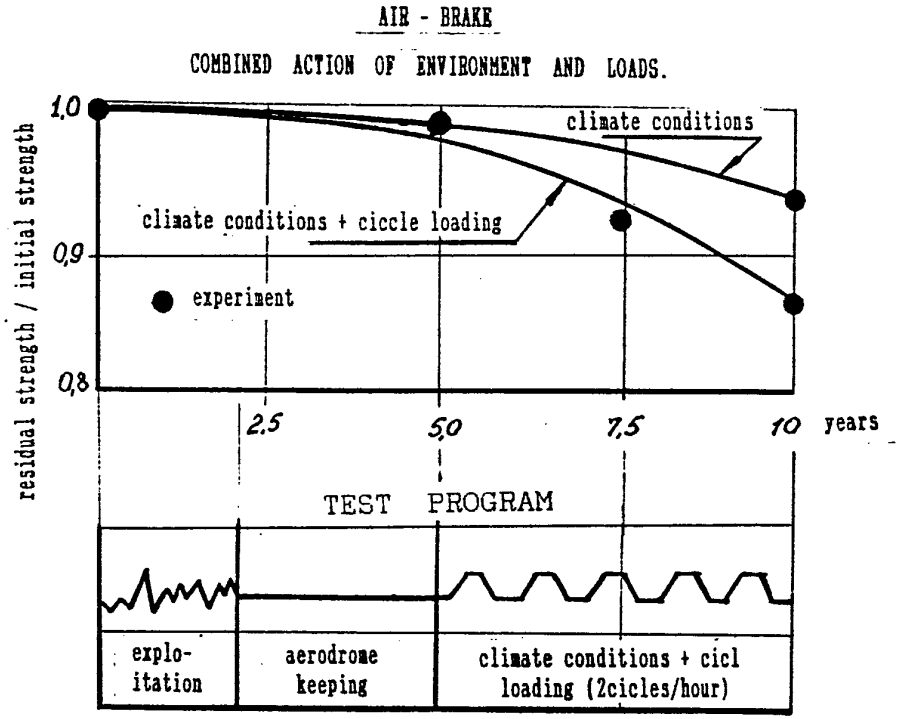

Ken < 1 - correction because of environment influence on design stress choice

Established on a basis of:
- analysis of exploitation experience,
- experiments.

The stage 3 (i.e. an individual treatment and optimization of structural elements) is implemented in the TsAGI-developed COMPOSITE program package. Figure 12 demonstrates major parts of the package. The next Figures represent some applications of the COMPOSITE complex:

- computation of strengths and stiffness characteristics, evaluation of load-carrying capability and stability of panels (Fig.13) and
- optimization of ccc panels and shells to withstand the general loads shown (Fig.14).

4. FEATURES OF MEETING THE STATIC AND FATIGUE STRENGTH REQUIREMENTS FOR COMPOSITE STRUCTURES

When designing the composite structures, account should be taken of additional factors that weaken the structure. The main factors are as follows (Fig.15):

- scatter in mechanical properties, more notable than that metals,
- brittleness and the related sensitivity to stress concentration and impacts,
- sensitivity of structural characteristics to environmental attack and length of service.

The influence of these factors should be allowed for at design stage; with this, the conventional system of measures for meeting the static and fatigue strength requirements that was developed for metallic structures.

4.1. Notable scatter of mechanical properties

The more significant scatter in strengths of structures made out of composites is taken into account by introducing an additional factor to multiply the ultimate load (Fig.15).

For each value of failure probability there exists a direct relation of the strength variance to the additional factor (Fig.15). The variance is determined by experiment; corrections for the sampling amount is introduced.

4.2. The influence of environmental conditions

The presence of moisture results in notable moisture absorption - and degradation of breaking stresses of a material. Figure 16 demonstrates the results of testing the carbon fiber reinforced plastics after attaining a moisture content level 1%; allowable stresses drop by 10-15%, and the characteristics become unstable.

Elevated temperatures and long-term influence of the moist air cause a further degradation.

Simultaneous action of environment and cyclic loads can produce a more severe reduction of strength characteristics. A plot in Fig.16 represents the results of a static test of spoilers on a transport airplane. Residual strength of the unit after simultaneous application of the adverse environment and cyclic loads is 87%, whereas the environmental factors do reduce down to 92%.

Designers should allow for environmental attack by introducing a degradation coefficient K_os to be applied to the allowables; this coefficient is to be defined based on:

1) operational experience survey and
2) special tests.

4.3. Brittle fracture

Figure 17 compares in-service behaviour of metal composite elements. As to the metal structures, a damage (such as scratch, indentation) detectable by eye does not almost degrade the load-bearing capability, while provoking initiation of fatigue cracks. After a crack reaches a critical length, the structure fails.

Damage in a composite structure appears mainly due to accidental mechanical impact that can occur at any time during operational use. In this case the strength characteristics fall suddenly. As a rule, usual variable in-service loads develop a damage extremely slowly.

A composite-structure failure mode depend on an impact energy level (Fig.17). High and medium energy impacts damage a surface; such areas can be detected visually and repaired. The most hard danger is associated with low-level impacts; indications are difficult to reveal visually, and nondestructive inspection methods should be imployed.

Investigations show (see Fig.17) that a low-energy impact can drastically degrade a component strength, and a compression load carrying capability reduces more notably than a tensile load limit.

The sensitivity to impacts poses a number of extra requirements on designers:

- the composite structure should be desired as a fail-safe concept, i.e., it must maintain a desired strength after a standardized damage occurs;
- the influence of the standardized damage must be allowed for when specifying the allowable stresses - by introducing a coefficient $K_{des} \leq 1$.
- operators should establish a systematic pre-flight visual inspection and periodic nondestructive inspections;
- new typical processes for repairing the damaged structures in field conditions should be developed.

5. CERTIFICATION OF AIRCRAFT COMPOSITE STRUCTURES

The exiting approach to airframe certification has been made perfect; it assumes structural analyses and theoretical evaluations of the strength properties, to be validated by certification ?.

The diagram in Fig.18 represents the amounts of certification works for the composite structures; the shaded cells indicate additions caused by the replacement of metals by composites. In comparison with the metallic structure, the composite structure must be shown to be capable of meeting the static and fatigue strength requirements after introduction of standardized damage in the most severe environments; complementary efforts are undertaken to substantiate:

- fail-safe operation capability;
- damage tolerance;
- inspectability, and
- repairability,

The analytical estimation of the strength includes:

- a theoretical computation of stresses and strains by means of state-of-the-art methods; currently, finite element methods are widely employed;
- the use of data available in handbooks and from the experience of designing and operating similar structures.

FRAGILE DESTROYING.

BEHAVIOR EXPLOITATION MODEL OF METAL AND COMPOSITE

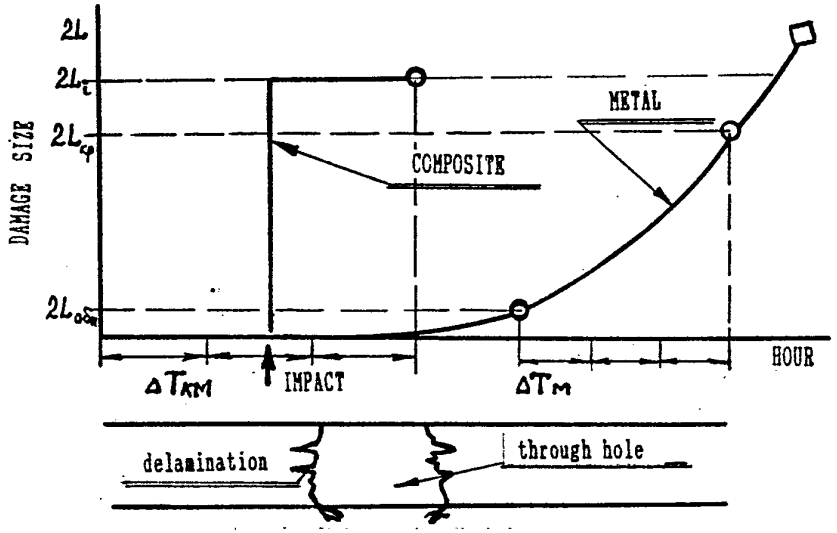

a) HIGH - ENERGY IMPACT.

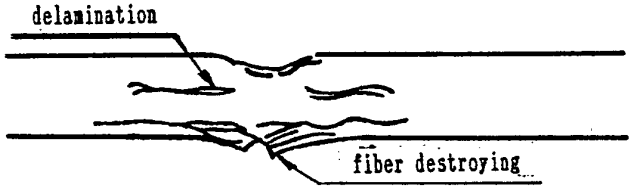

b) MODERATE - ENERGY IMPACT.

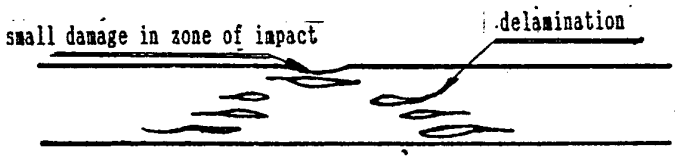

c) LOW - ENERGE IMPACT.

COMPRESSED PLATE STRENGTH DECREASE FOR IMPACT DAMAGE.

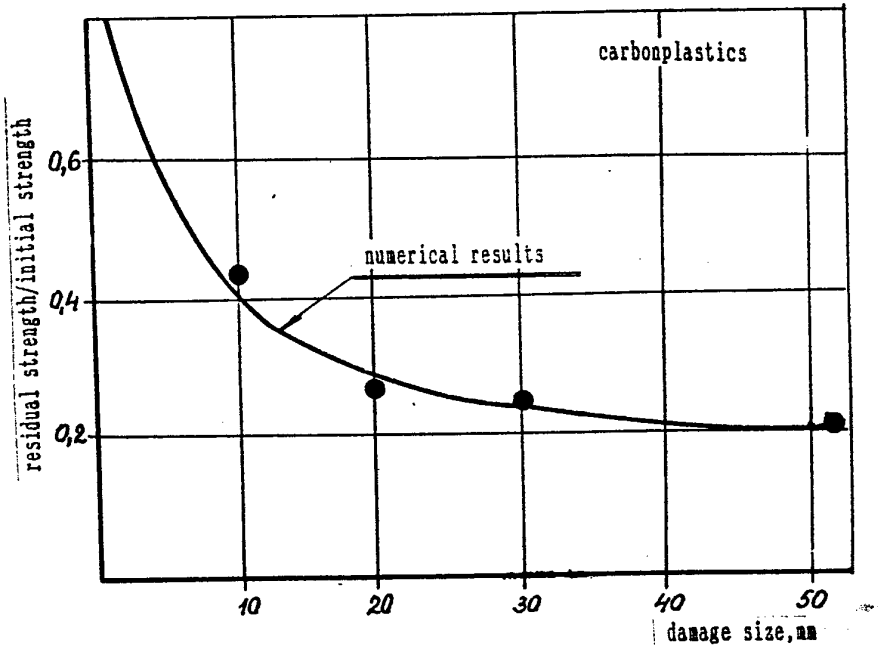

- DESIGN APPROACH - FAIL-SAVE STRUCTURE.
- CHOICE OF DESIGN STRESSES IN GIEW OF REGULATED DAMAGES (Kr.d <1).
- PROVISION WITH RELIABLE CONTRAL:
  a. VISUALLY DURING EXAMINATION BEFORE FLIGHT,
  b. INSTRUMTNTAL, NONDESTRUCTIVE DURING REGULATIVE EXAMINATION
- TYPICAL EXPLOITATION REPAIR TECHNOLOGIES DEVELOPMENT.

CERTIFICATION OF COMPOSITE AIRFRAME STRUCTURES

CERTIFICATION APPROACH
- THEORETICAL STRTNGTH ANALYSIS, -TESTS OF STRUCTURE SPECIMENS OF COMPLEXITY.

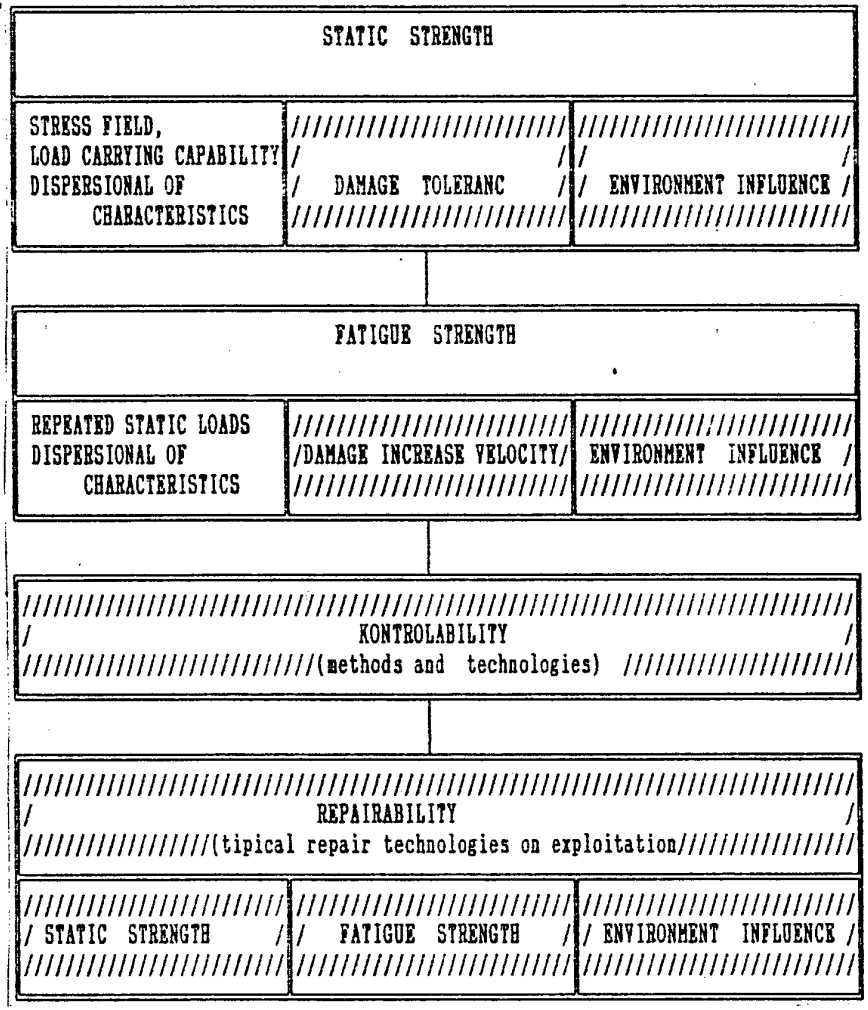

The estimates and validated by certification tests that envisage large amounts of testing for static and fatigue strength of various specimens. The range of specimens may be categorized in types (Fig.19) which differ in sizes, total numbers of specimens, and values of interest.

Elementary specimens are usually small-size and can easily be tested in prescribed environmental conditions. These testes supply mean values of characteristics and the scatters. Experimenters determine degrees of the influence of various service factors in various combinations; the worst conditions by strength degradation are outlined.

Some "fragments" being medium-size portions of a structure are used to evaluate technological concepts and/or to obtain the strength limits. Such specimens are too large to be used for evaluating the scatter., but the strength degradation under real environmental effects can well be estimated.

Units being important parts of an airframe can be very large. The experimentation usually involves one or two copies. The principal problem in this case is to evaluate the concepts and manufacturing processes by strength. For these tests two approaches are possible:

- the direct tests with simulation of service conditions and
- an "analysis and experiment" approach that envisage tests in conventional environment and a subsequent extrapolation of the data to the most severe conditions.

The entire airframe with composite parts are listed in compliance with the test amount requirements adopted for "all-metal" airframes. The full-size airframe is tested in normal environment and the results are corrected for in-service factors; here, reliance is made on analytical procedures and the data obtained from testing of specimens of other types.

The aim of the full-size tests is to comprehensively validate the airplanes put into service and to ensure their strength and long operational life.

6.DESIGN CONDITIONS FOR PASSENGER-CARRYING AIRPLANES

6.1. The influence of environmental conditions

As the passenger-carrying airplanes, the environment parameters are as defined in Fig.20. Extreme conditions are simulated during static tests and/or residual strength tests, whereas the long-term strength parameters are determined by exposing the airframe during the fatigue strength tests.

6.2. Fail-safe design requirements

The impact may be prescribed in terms of an impact energy or a damage area size - these values are interrelated. An in-service damage to a full-scale structure is modelled by a notch or a spherical indentation. The size of a design limit in-service damage is defined on the basis of a value at which the damage will be reliably (at a probability of not less than 90%) detected by the usual inspection technologies and inspector's skill.

An airplane operated within the fail-safe design principle must remain strong with in-service damage. The design limit conditions establish a relation between a standardized damage and the factor of safety. Figure 20 demonstrates fail-safe conditions; the abscissa axis represents ranges of the damages, and the other axis corresponds to the necessary strength margins which must be substantiated. Specific parameters of the standardized

damages depend on a number of aspects (a type of a structure , a material, skills. etc.) and should be established via statistical data and/or special tests for damage inspectability.

7. MEANS OF COMPLIANCE

To demonstrate the correspondence of real strength characteristics of a structure to the certification requirements, the means of compliance are developed. Let us cite some of these methods that were used for certifying the composite assemblies of TU-204 passenger-carrying transport.

7.1. Nondestructive inspection method validation

Using a certain nondestructive inspection technique (specifically, the ultrasound impedance method), the damage sizes are determined and compared with actual dimensions measured on a microsection of the damage area. The comparison makes it possible to estimate acceptability of the method and introduce the proper corrections (Fig.21).

7.2 Damage detectability

Boundaries of reliably detecting a damage by means of instrumented and visual inspection were outlined via detectability tests. The upper and lower surfaces of an aileron were damaged by impact with various energy levels, and the damage area sizes were measured. In so doing, the plot of characteristic length of a damage area versus the impact energy level have been generated, Fig.21; thereafter, boundaries of reliable detection by instruments and visual inspection were outlined.

7.3. Environmental effects

These arises the question of how to demonstrate fulfilling the static/fatigue strength requirements for the composite structure as of the finish of the design service life when properties degrade under environment effects and cyclic loading? One of approaches is to conduct the full-size structure test to a programme that ensures close simulation of critical environmental condition and loads. Such tests for an airframe as a whole are difficult to perform, but some, medium-size structural units may be studied in this way.

These positions may be illustrated by tests of a composite aileron for TU-204 transport. Combined static and fatigue strength tests (with simultaneous "application of environment and loads") were mounted to fulfil several objectives such as static and fatigue strength demonstration, repairability estimation, damage evolution rate, etc.

For these experiments a rig has been prepared, see Fig.22. The climatic chamber provides the desired environment by running the air with temperature and relative humidity prescribed. Loads are generated by hydraulic power cylinders and applies through the flexible wall of the chamber. The airplane has been designed to fly for 15-20 years, and real-time simulation of climate factors can not be carried out. Therefore accelerated tests were conducted: the rate of aging was increased by increasing the temperature and relative humidity. Figure 23 represents the programme of combined static and fatigue strength tests. The latter have been subdivided into three phases:

1. The as-delivered structure is impregnated with moisture to a concrete level, then loaded by flight load cycles to reach one design service life; residual strength is determined.

SPECIMEN TYPES FOR CERTIFICATION TEST.

N	TYPE	EXAMPLE /——— L ———/	L,M	NUMBER OF SPECIMENTS	PURPOSE	CORRESPONDENCE DETERMINATION METHOD
1	COUPON		UP TO 0,3	LARGE	STRENGTH CHRACTERISTIES; MEAN ONES, DISPERSION, INFLUENCE OF EXPLOITATION CONDITIONS (HUMIDITY, TEMPERATURE IMPACT DAMAGES ETS.)	TESTS IN CONDITIONS WHICH ARE CORRESPONDED TO EXPLOITATION ONES.
	STRUCTURAL DETAIL	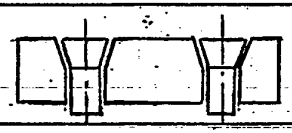	UP TO 1,0	LARGE		
3	SUB - COMPONENT	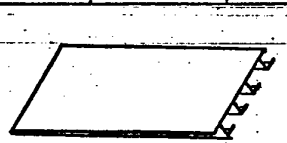	UP TO 3,0	MODERATE (5 - 10 pieces)	REAL STRENGTH AND FATIGUE CHARACTERISTIES. TECHNICAL SOLUTIONS CHECKING..	TESTS IN CONDITIONS WHICH ARE CORRESPONDED TO EXPLOITATION ONES. OR TEST IN NORMAL CONDITIONS WITH RECALCULATION TO EXPLOITATION ONES.
4	COMPONENT	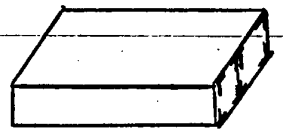	UP TO 10,0	1 - 2 pieces	TOTAL CHECK OF ALL TECHNICAL SOLUTIONS AND PROCESSES RELATED TO AIRFRAME CREATION.	
5	FULL SCALE AIRCRAFT	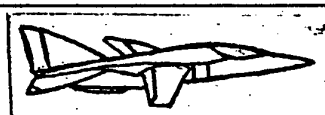	UP TO 30,0	1 piece		TEST IN NORMAL CONDITIONS WITH RECALCULATION TO EXPLOITATION ONES.

TEST FOR ALL SPECIMENT TYPES ARE OBLIGATORY

PART OF AIRPLANE FLIGHT MAINTENANCE CERTIFICATION.

ENVIRONMENT INFLUENCE.

PARAMETERS / AIRCRAFT	EXTREME PARAMETERS			DURATION OF EXPOSITION	
	Tmax,C	Tmin,C	Wmax,%.	T,C	F,%
TU - 204	80	- 60	1.0	35	70
B - 737	82	- 56	1.0	21	70
A - 310	70	- 50	1.2	20	80
	STATIC TEST			FETIGUE	

W - moisture content level
F - humidity in exposition

FAIL - SAFE DESIGN CONDITION.

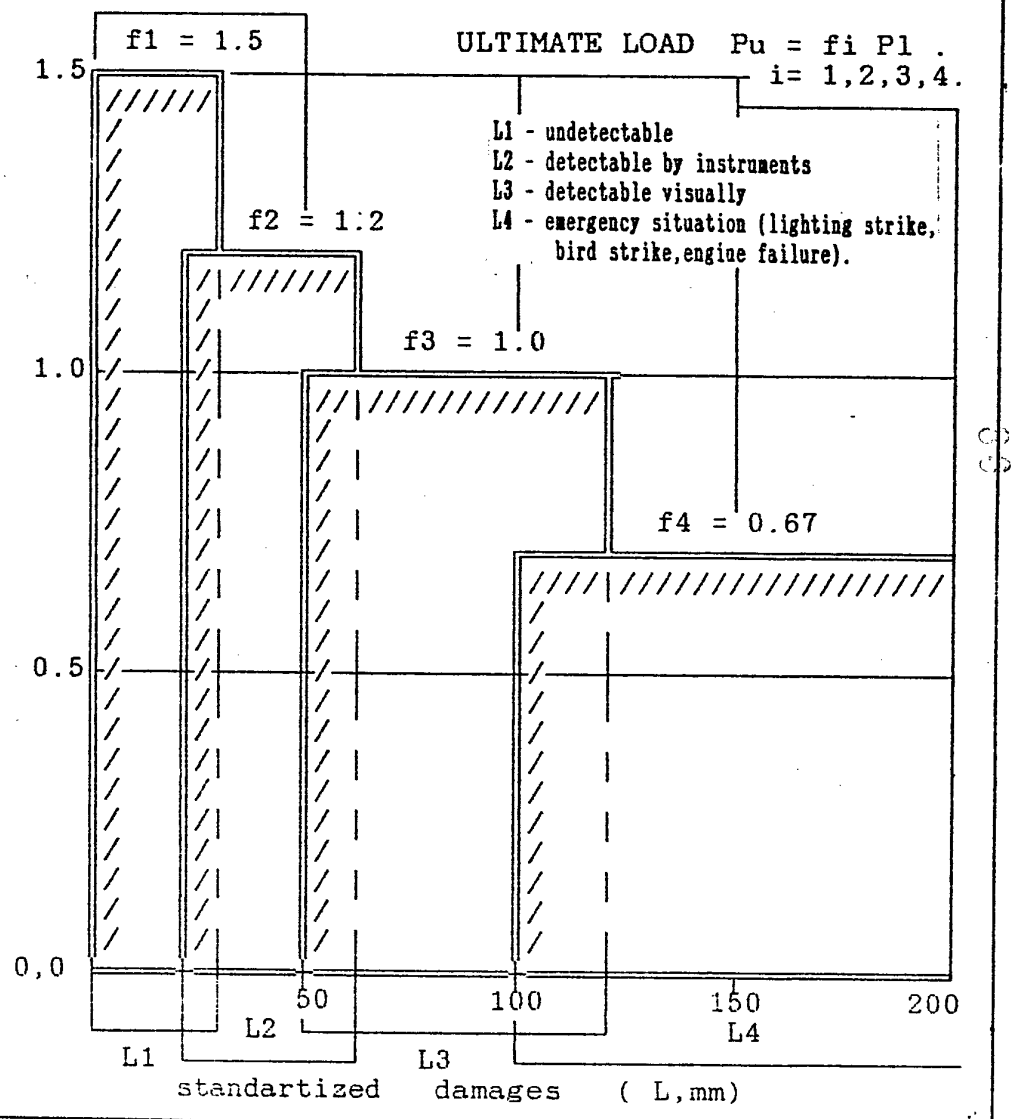

DAMAGE DETECTABILITY TEST.

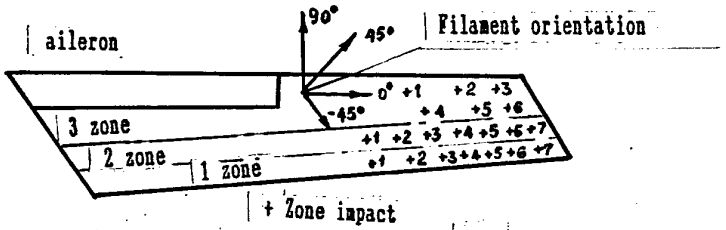

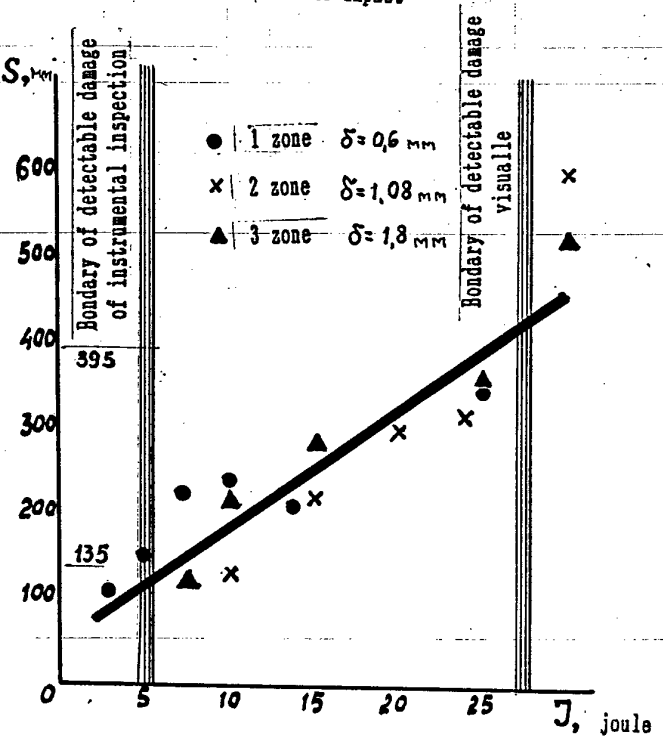

VERIFICATION OF ACUSTIK METHOD.

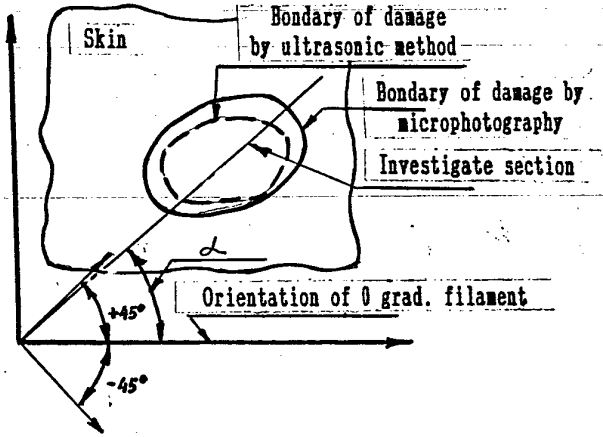

AILERON TEST STAND.

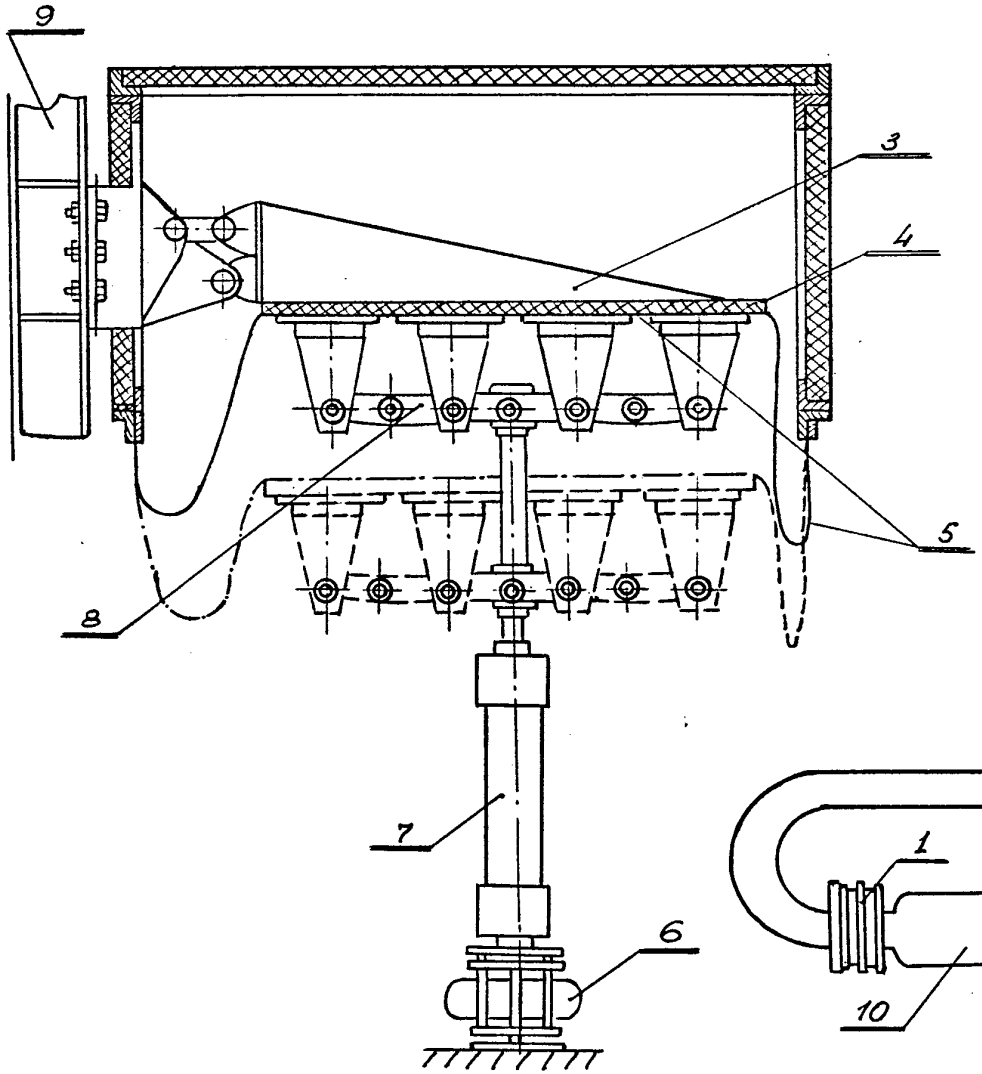

——— Membrane during loading.
– – – – – Membrane during moisture accumulation and inspection.

1. Fan.
2. Return duct.
3. Aileron.
4. Rubber washer.
5. Elastic membrane.
6. Load cell.
7. Hydraulic force exciter.
8. Levers.
9. Support.
10. Steam generator.

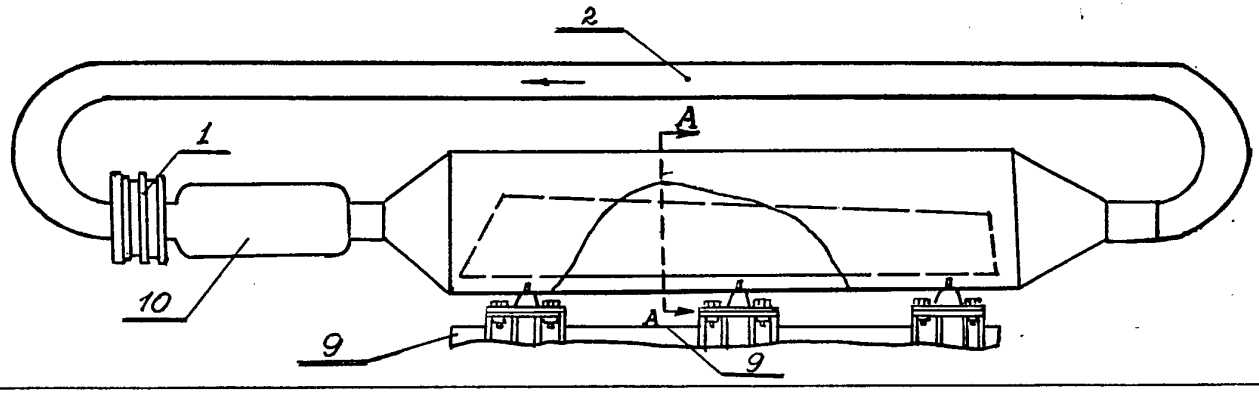

ENDURANCE TESTING PROGRAM.

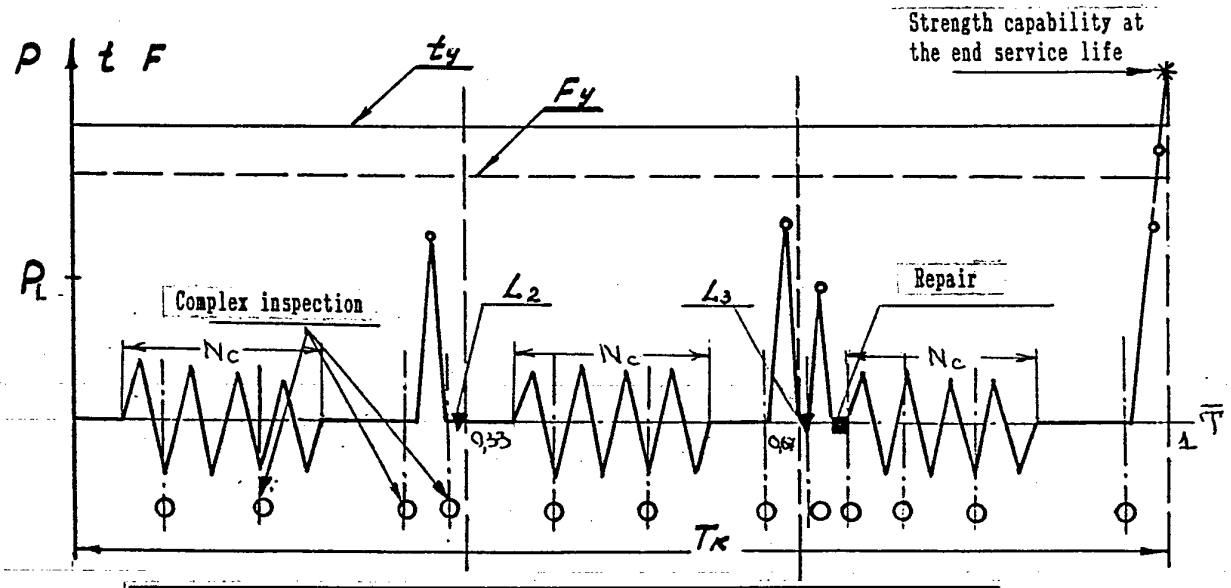

STAGE	1	2	3
DURATION	0,33 Tk	0,33 Tk	0,33 Tk
DAMAGE	L1	L2	1)L3 ,2)REPAIR
CYCLE NUMBER	Nc	Nc	Nc
STATIC LOAD	1.2 Pl	1.2 Pl	1)P1,2)1.2P1,3)1.5P1
TEMPERATURE	ty	ty	ty
HUMIDITY	Fy	Fy	Fy

Tk - cervice life.
Pl - limit loada.
Nc - cicling loading for one service life.
L1 - undetectable.
L2 - detectable by instruments.
L3 - detectable visually.

GROWTH RATE OF DAMAGES AND DEFECTS

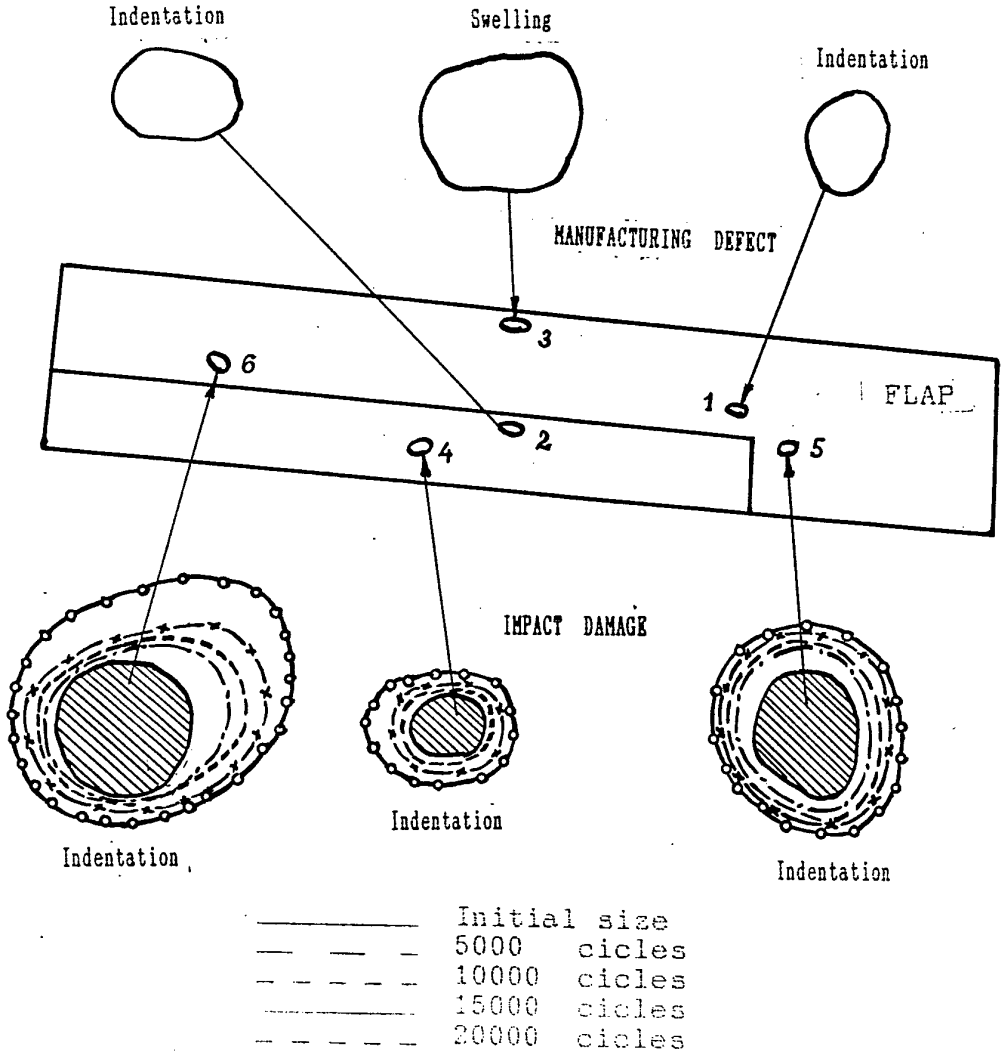

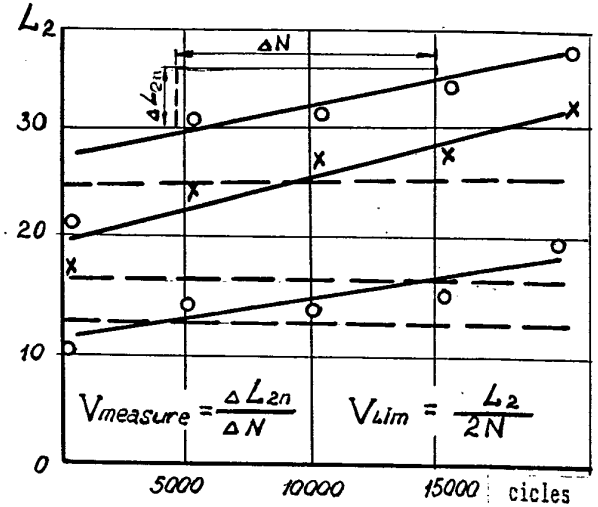

$$L_2 = 2\sqrt{\frac{1.4S}{\pi}}$$

N point	Type of damages	Damage growth rate, мм/с Measure	Limit
1	Indentation	0	40 E -4
2	Indentation	0	
3	Swelling	0	
4	Indentation	3.4 E -4	
5	Indentation	5.6 E -4	
6	Indentation	5.9 E -4	

V measure <= V limit

2. Standardized damage is introduced to simulate the in-service damage which can be revealed by nondestructive inspection techniques; flight load cycles are applied to reach one more design service life; residual strength is determined.
3. At the outset of the phase 3 the standardized damage is introduced which can be revealed visually; residual strength is determined; the aileron is repaired in accordance with a typical process; flight load cycles are applied to each one more design service life; finalizing, the load is increased to failure in order to evaluate the load-bearing capacity and strength margins.

7.4. Damage growth rate

This value is necessary to assess the inspection schedule and the structure life capability. The damage growth rate determination method is as follows: during the life evaluation the structure is systematically inspected with instruments to measure the visible sizes. These measurements are a basis for plotting the size variation versus the number of cycles; damage growth rate is computed. This method is illustrated in Fig.24.

Formation of continuous solid solutions with new chemical Compounds.

M. S. Saidov
Physical Technical Institute, Uzbek Academy of Sciences, Mavlanov St. 2 B, Tashkent, 700084, Uzbekistan.

Abstract

The brief review of experimental data on semiconductor continuous solid solutions with new chemical compounds is given. The Solubility in the multicomponent solution-melt is discussed. Conditions of the formation of the continuous substitutional solid solutions with covalent as well as metal bonds are substantiated. In the context of mutual solubility increase the following extended conception is suggested. In the multicomponent systems the formation of the continuous liquid or solid solutions is possible as a result of origination and dissolution of new chemical compounds, which are not shown on the traditional phase diagrams. The existence of many continuous solutions based on molecular elements, IV–IV, III–V, II–VI and I–VII type binary compounds is predicted. Four versions on the formation of the molecule of new chemical compounds in liquid - crystal · phase transition are considered. As an example the possibility of the synthesis of some continuous solid solutions based on the aluminum is discussed.

Introduction

There exist a great variety of solutions ranging from molecular ones to microemulsions with the size of particles of 100Å. One of the basic properties of the solution is the solubility, which expresses the concentration when phase is saturated by the component and phase transformation takes place. Because of the absence of the quantitative theory of the solubility in multicomponent systems to develop the advanced technologies some ideas on the formation of new concentrated solutions is needed. Progress in the growth of semiconductor layers by chemical vapor deposition and liquid phase epitaxy made it possible to obtain $(IV_2)_x$ $(III\text{-}V)_{1-x}$ type continuous solid solutions concerning Ge-GaAs, Ge-GaSb, Si-GaAs, Si-GaP and Ge-InP systems. On the basis of these data and considering IV_2 (Ge_2, Si_2) as a new chemical compound we have suggested the conception, according to which the formation of the continuous substitutional solid solution is a cause for origination of new chemical compounds not shown on the traditional phase diagrams [1].

In this paper the attempt is made to estimate qualitatively the solubility, suggest the condition of the fofmation of continuous solid solutions with new compounds, substantiate some ideas, concerning the structure of the liquid solutions, and extend the conception. The versions on the formation of compounds in low-temperature liquid phase crystallization of solid solutions as well as the existence of the concentrated solid solutions based on aluminum and compounds are discussed.

$(IV_2)_x(III–V)_{1-x}$ type continuous solid solutions.

A number of authors obtained solid solutions of molecular elements Ge_2 and Si_2, with some III–V type semiconductor compounds. In [2] from Ga solution-melt containing Zn continuous solid solutions of GaP and Si have been grown. We suppose that the formula of it should be $(Si_2)_x(GaP)_{1-x}$. In [3] by the method of coincident RF sputtering of GaAs and RF decomposition in Ar + SiH_4 medium on GaAs substrate at 530 – 600°C, 1 – 10 μ thick $Si_x(GaAs)_{1-x}$ epitaxial layer with Si concentration up to 55 at % were deposited. Long time annealing at 600 – 800°C has not changed the composition of the layers. The formula $Si_x(GaAs)_{1-x}$ is likely not be correct, since solubility of atomic Si in Ga and As sublattices of GaAs is less than 0,1 at %, and substituting GaAs molecule for one Si atom is hardly probable and forming only $(Si_2)_x(GaAs)_{1-x}$ is possible. The continuous solid solutions were obtained in Ge –GaAs and Ge – GaSb systems by diffusionless crystallization method [4] when 50mg drop of liquid solution was crystallized on the surface of copper cylinder rotating with rate of 8000 revs/min. However the formula of the solid solution was not suggested. J. E. Green et al. have grown from gaseous phase the solid solutions of $(Ge_2)_x(GaAs)_{1-x}$ [5] $(Ge_2)_x(GaSb)_{1-x}$ [6] in the range $0<x<1$. In [7,8], using a method of pyrolytic synthesis in $GeH_4 – Ga(CH_3)_3 – AsH_3 – H_2$ system $(Ge_2)_x(GaAs)_{1-x}$ epitaxial layers have been grown on GaAs (100) and Ge (100) substrates and their structures, optical and electric properties were studied.

Our results of growing variband layers of $(Ge_2)_x(GaAs)_{1-x}$ $(Si_2)_x(GaP)_{1-x}$ and $(Ge_2)_x(InP)_{1-x}$ solid solutions in the whole range of x by the method of liquid phase epitaxy were presented in [9]. Above mentioned complex semiconductors are the small part of possible cases of forming solid solutions on the basis of IV_2 and III–V materials.

Solubility and extended conception.

Using Boltzmann equation

$$\frac{C_i'}{C_i''} = \exp\left(-\frac{U_i' - U_i''}{kT}\right) \qquad (1)$$

dealing with (i+1) - component two - phase system in [10] we have suggested for the solubility of i - component the following formula

$$C_{Ni}' = \frac{C_{Ni}'' \exp(\Delta U_i')}{1 + \sum_i \left[\exp(\Delta U_i) - 1\right] C_{Ni}''} \qquad (2)$$

where C'_i, C'_{Ni}, U'_i and C''_i, C''_{Ni}, U''_i are volume concentration, mole fraction and mean potential energy of i - component in (') and ('') phases respectively, k - Boltzmann constant, T - absolute temperature

$$\Delta U_i = -\frac{1}{kT}\left[\left(U_i^{'} - U_j^{'}\right) - \left(U_i^{''} - U_j^{''}\right)\right] \tag{3}$$

index j concerns the solvent. Further considering each sublattice of the ABCD type compound as a separate solvent (phase) for the solubility of the i - chemical element in the compound in [11] we have suggested

$$C_{Ni}^{'} = C_{Ni}^{''} \sum_{j=A}^{D} \frac{\exp(\Delta U_{ij})}{1 + \sum_i \left[\exp(\Delta U_{ij}) - 1\right] C_{Ni}^{''}} \tag{4}$$

To predict qualitatively the behaviour of the component of solution V. K. Semenchenko [12] supposed that $U = \varphi \cdot m$. φ characterizes the phase and m called by him "generalized moment" defines the particles of dissolved component. For the ion $m=ez/r$, and molecule $m=e_d/r^3$, where e is charge on electron, z is valence of the ion e_d is the dipole moment of the molecule, r is radius of the ion or molecule. According to (3) and (4) the more $|m_1-m_j|$ the less solubility of the component 1 in the solvent j and the effect of i - component on solubility of the component 1 is determined by the sign and value of $m_{i\neq 1}-m_j$. However in the case of compounds with A_2 type non-polar molecules m becomes indefinite. Thus to estimate the solubility in such systems as A_2 - BC and AB - CD (A, B, C and D are chemical elements, AB and CD are compounds) with covalent or metal bonds we suggest to use together the differences of the sum of the valences and radii of the atoms of the molecules.

$$\Delta z = z_A + z_B - (z_C + z_D) \tag{5}$$

$$\Delta r = r_A + r_B - (r_C + r_D) \tag{6}$$

As the potential energy of the interactions of the molecules of the compounds in solution depends on the number of electrons participating in interactions of the molecules and the sizes of the latters ΔU_{ij} is determined by Δz and Δr. Therefore according to (3) the more $|\Delta z|$ and $|\Delta r|$ the less the solubility and the more $|\Delta z_{ij}|$ and $|\Delta r_{ij}|$ the more the effect of the additives on solubility of the component 1. But some difficulties arise with $|\Delta z|$ when the multiplicity of the bond in A_2 or BC is not known.

Taking into account the fact that the substitutional solid solutions of metal elements [13] and binary semiconductor compounds [14] are formed in the whole range of consentrations if their conponents have the same type of crystal lattice, chemical compounds and difference of interatomic distances not more then 15% as well as using (5) and (6) we suggest the following condition of the formation of the continuous solutions

$$\Delta z = 0, \qquad \Delta r = 2r_A - (r_B + r_C) < 0{,}2r_A\,. \tag{7}$$

On the table 1 are presented IV_2, IV–IV, III-V, II–VI and I–VII compounds, the sum of the radii of their elements and the values of Δr which satisfy (7) and

Table 1.: Values of $\Delta r = r_{IV} + r_{IV} - (r_B + r_C)$ Satisfying (7). B and C are III, II, I and V, VI, VII elements respectively.

IV_2, IV-IV		C_2	Si_2	Ge_2	Sn_2	GeC	SnC	SiGe	SiSn	GeSn
B-C	$\frac{r_{IV}+r_{IV}}{r_B+r_C}$	1.54	2.34	2.44	2.80	1.99	2.17	2.39	2.57	2.62
BN	1.58	-0.04	-	-	-	-	-	-	-	-
ALN	1.96	-	-	-	-	0.03	0.21	-	-	-
GaN	1.96	-	-	-	-	0.03	0.21	-	-	-
InN	2.14	-	0.20	-	-	-0.15	0.03	0.25	-	-
BP	1.98	-	-	-	-	-	0.19	-	-	-
AlP	2.36	-	-0.02	0.08	-	-	-0.19	0.03	0.21	0.26
GaP	2.36	-	-0.02	0.08	-	-	-0.19	0.03	0.21	0.26
InP	2.54	-	-0.20	0.10	-	-	-	-0.15	0.03	0.08
BAs	2.06	-	-	-	-	-0.07	0.11	-	-	-
AlAs	2.44	-	-0.10	0.00	-	-	-	-0.05	0.13	0.18
GaAs	2.44	-	-0.10	0.00	-	-	-	-0.05	0.13	0.18
InAs	2.60	-	-	-0.18	0.18	-	-	-0.23	-0.05	0.00
BSb	2.24	-	-0.10	0.20	-	-	-0.07	0.15	-	-
AlSb	2.62	-	-0.29	-0.18	0.18	-	-	-0.23	-0.05	0.00
GaSb	2.62	-	-0.28	-0.19	0.18	-	-	-0.23	-0.05	0.00
InSb	2.80	-	-	0.36	0.00	-	-	-	-0.23	-0.28
BeO	1.76	-0.22	-	-	-	-	-	-	-	-
ZnO	1.97	-	-	-	-	0.02	0.20	-	-	-
ZnS	2.35	-	-0.01	0.09	-	-	-0.18	0.04	0.22	0.27
ZnSe	2.45	-	-0.11	-0.01	-	-	-	-0.06	0.12	0.17
ZnTe	2.63	-	-0.29	-0.19	0.17	-	-	-0.24	-0,06	-0.01
CdS	2.52	-	-0.18	-0.08	0.28	-	-	-0.13	0,05	0.10
CdSe	2.62	-	-0.28	-0.18	0.18	-	-	-0.23	-0.05	0.00
CdTe	2.80	-	-	0.36	0.00	-	-	-	-0.23	-0.18
HgS	2.52	-	-0.18	-0.08	0.28	-	-	-0.13	0.05	0.10
HgSe	2.62	-	-0.28	-0.18	0.18	-	-	-0.23	-0.05	0.00
HgTe	2.80	-	-	-0.36	0.00	-	-	-	-0.23	-0.18
CuF	1.98	-	-	-		0.01	0.19	-	-	-
CuCl	2.33	-	0.01	0.11	-	-	-0.16	0.06	0.24	-
CuBr	2.45	-	-0.11	0.11	-	-	-0.28	-0.06	0.12	0.17
CuI	2.62	-	-0.28	-0.18	0.18	-	-	-0.23	-0.05	0.00
LiF	2.16	-	0.18	0.28	-	-0.17	0.01	0.23	-	-
LiCl	2.51	-	-0.17	-0.07	0.29	-	-	-0.12	0.06	0.11
LiBr	2.63	-	-	-0.19	0.17	-	-	-0.24	-0.06	-0.01
LiI	2.80	-	-	-	0.00	-	-	-	-0,23	-0.18
NaF	2.50	-	-0.16	-0.06	-	-	-	-0.11	0.07	0.12
NaCl	2.85	-	-	-	-0.05	-	-	-	-	-0,23
NaBr	2.97	-	-	-	-0.17	-	-	-	-	-0.33
NaI	3.14	-	-	-	-0.34	-	-	-	-	-

shows the possibility of the formation of the continuous solid solutions with new chemical compounds.

Consider the crystallization of substitutional solid solution of A with BC from liquid metal solvent S at the temperatures lower then the melting point of A and BC(B,C). The compound BC can also be dissociated in liquid phase. In forming the solid solution $(BC)_{1-x}(A_2)_x$ with $0<x<0,5$ (BC is solid solvent) A_2 substitutes BC and formation of $(A_2)_{1-x}(BC)_x$ takes place as a result of substitution of A_2 by BC which can also originate with crystallization.

A success of the experiments on growth of the solid solutions depends on the choice of all components A, BC (B, C) and S when the solubility of A and BC in S should be enough to provide the deposition rate required. In some cases to increase the solubility of A in S one should find the suitable additive to introduce into liquid solution. To this end one needs to carry out an additional experiment or use some new idea on the formation of solutions. It is not excluded that in introducing the additive D into S the solubility of A increases as a result of the formation of the compound AD the molecules of which substitute the pair of atoms (molecules) S_2 (2S) of the liquid solvent. So we suppose that there also exist substitutional and interstitial liquid solutions. To back up this idea we note such facts: 1. The solid and liquid substances are incompressible. 2. There is the short-range order in liquids. 3. The difference of binding energy of the elements in solid and liquid states is within 3-10%, since their heat of sublimation is 10-40 times as large as the heat of melting [15]. In this context we suggest the following extended conception. In the multicomponent systems the formation of the concentrated liquid or solid solutions is possible as a result of origination and dissolution of new chemical compounds, which are not shown on the traditional phase diagrams.

Versions on the formation of new compounds.

1. Initial phase the solution of *A* and *BC* in liquid (*L*) metal solvent *S* is at temperature close to melting (*L*) point of *A* $T_{L,A}<T_{L,BC}$. Atom (mole) fraction of $C^L_{N,S}>>C^L_{N,BC}$, $C^L_{N,A}$ and $C^L_{N,BC}>C^L_{N,A}$. In cooling to some reaction (r) temperature T_r when binding energy between *A* atoms $E_{AA} \geq 3/2kT_r$ the reaction $A+A \leftrightarrow A_2$ takes place. In further cooling to the crystallization (c) temperature $T_{c,BC}$ when liquid phase is saturated by the compound BC solid solution $(BC)_{1-x}(A_2)_x$ is deposited. (cooling version). If $C^L_{N,A}>>C^L_{N,BC}$ and liquid solution is cooled to $T_{c,A}$ when it is saturated by A $(A_2)_{1-x}(BC)_x$ crystals will be obtained.

2. Both Maxwell-Boltzmann and Gibbs distribution laws show that there are in the system considered above molecules A_2 with the life time τ. At saturating the liquid phase by *A* the consentration of A_2 increases. If the deposition time of A_2 from liquid phase-crystal boundry layer on the crystal $\tau_d<\tau$ $(BC)_{1-x}(A_2)_x$ solid solution is formed (statistical version). $(A_2)_{1-x}(BC)_x$ solid solution with $0<x<0,5$ (A_2 is solid solvent) is formed according to the versions described when compound BC is dissociated in the liquid phase.

3. All other things being equal an adsorbtion of molecule A_2 is more than that of atom A, since in forming the molecule A_2 the intensity of the field of A decreases.

In addition an adsorbtion is known to increase with a reduction in temperature. As the adsorbtion takes place to decrease the energy of surface it acts as the catalyst of the reaction $A+A \leftrightarrow A_2$ (fig.1.a), which leads to the formation of solid solution $(BC)_{1-x}(A_2)_x$ (fig.1c), (adsorbtion version). Similarly $(A_2)_{1-x}(BC)_x$ is formed when BC is dissociated in S (fig.1 b,d). In figures two-dimensional phases are described. 4. As a rule the solubility of the monoatomic A in the crystal BC and B and C in the crystal of A is less than 1 at % and dissolution deforms a lattice and induces the strain in it. In fig.2a the deposition of monoatomic layer of solid solution of BC saturated by A on BC substrate is presented. In fig. 2. the liquid phase is not swown. The pairing of A atoms in the previous layer decreases the lattice strain and causes an increase of concetration of A in the growing layer (fig.2c) and the formation of $(BC)_{1-x}(A_2)_x$ solid solution (fig. 2e). As the pairing of A atoms normalizes lattice parameter of BC crystal we call this pseudomorphism version. Siimilarly $(A_2)_{1-x}(BC)_x$ is formed when BC is dissociated in liquid phase (fig 2b,d,f). The formation of solid solutions according to the versions 2-4 can occur at the same time.

Possible aluminium concentrated solid solutions

Aluminium alloys are of special importance for flying vehicles and a lot of other applications. In order to predict some possible cases of the formation of aluminium continuous solid solutions with new chemical compounds, on the basis of above suggested conseption and the condition (7) we have considered phase diagrams of the aluminium and different binary systems [16] compared valencies metal and covalent radii of the majority of elements. On the table 2 are presented some of the possible new chemical compounds sum of the radii (upper numbers are metal and lower ones are covalent) of their components and values of Δr, which satisfy (7), and hence the formation of $(Al_2)_{1-x}(BC)_x$ solid solutions with $0<x<1$ can be expected. Note, that Ti, Mn, Fe, Co and Ni are not elements of II group, but in some cases they show divalence. There are CoSn, FeSn, and SiTi compounds on the phase diagrams of the binary systems Co-Sn, Fe-Sn and Si-Ti respectively. Sn, Bi and Pb seem to be the suitable liquid metal solvents.

References

1. M. S. Saidov, In proceedings of the 4th International Simposium on Advanced Materials, September 17-21, 1995, Islamabad, Pakistan, edited by A. Ul-Haq, F. Habibi, Nazeer Ahmad, A. A. Mazhar and A. Q. Khan, Dr. A. Q. Khan Research Laboratories, Kahuta, Pakistan, 1996, pp. 113-119.
2. E.E.Loebner, J.V.Hegyi, E.W.Poor, Met, of Elem. And Compound Semicond., Proc.Met.Soc.Conf., 1960, v.12,lntersei Publ.
3. A.J.Noreika and M.H.Frankombe, J.Appl.Phys. 1974, v.45, p.3690.
4. V.M.Glazov, A.V.Evdokimov, L.M.Pavlova, Doklady ANSSSR, 1977, vol.232, no.2, p.371.
5. A.Barnet, M.A.Ray, et al., Electr.Lett, 1982, v.18,p.891.
6. K.C.Cadien, A.H.Eltoukhy, J.E.Greene Appl.Phys.Lett.,1981, v.38, p.773.

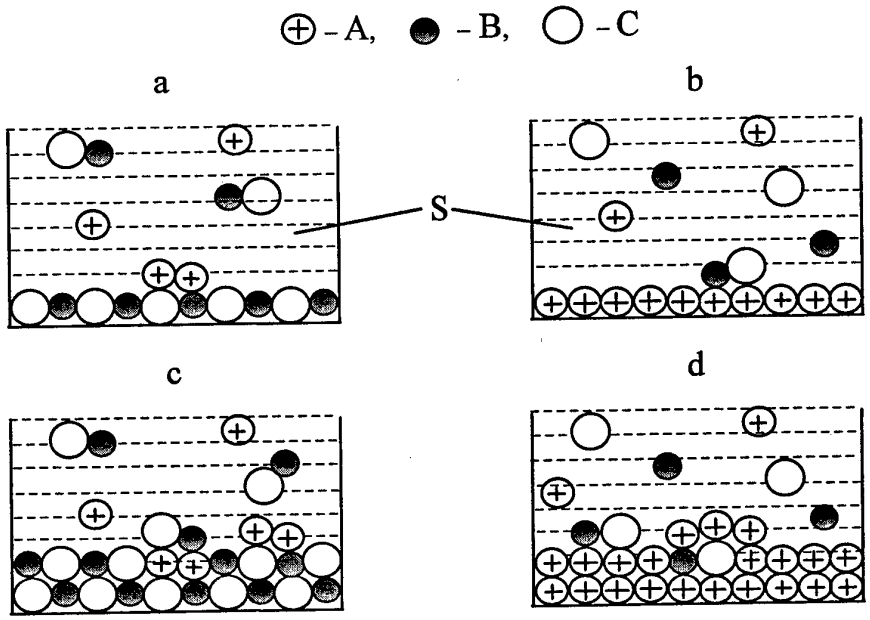

Fig.1. Pairing of A on the surface of BC crystal (a) B with C on A substrate (b) and formation of $(BC)_{1-x}(A_2)_x$ (c), $(A_2)_{1-x}(BC)_x$ (d) solid solutions.

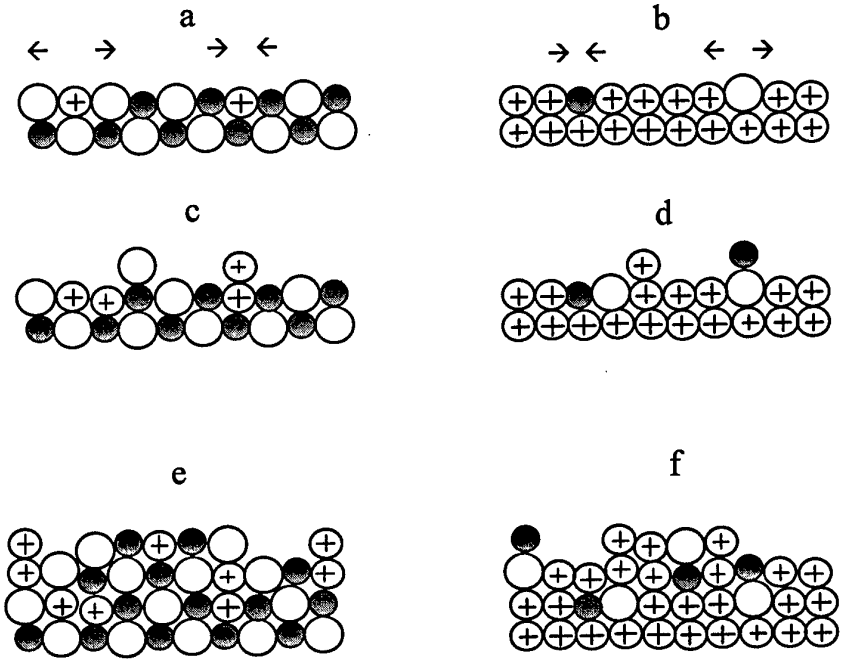

Fig.2. Dissolution of A in BC (a) B and C in A (b) pairing of A in BC (c) B with C in A (d) and formation of $(BC)_{1-x}(A_2)_x$ (e), $(A_2)_{1-x}(BC)_x$ (f) solid solutions.

Table 2.: Compounds forming $(Al_2)_{1-x}(BC)_x$ continuous solid solutions

$2r_{Al,m}$=2.86Å, $2r_{Al,c}$=2.52Å
indices: m–metal, c–covalent

BC type compound supposed	r_B+r_C, Å	Δr, Å	BC type compound supposed	r_B+r_C, Å	Δr, Å
CuSb	2.89 2.53	-0.03 -0.01	ZnPb	3.11 2.77	-0.25 -0.25
CuBi	3.10 2.63	-0.24 -0.11	CdSi	2.86 2.65	0.00 -0.13
BeGe	2.52 2.29	0.34 0.23	CdGe	2.91 2.70	-0.05 -0.18
BeSn	2.71 2.47	0.15 0.05	CdSn	3.10 2.88	-0.24 -0.36
BePb	2.87 2.53	-0.01 -0.01	HgSi	2.89 2.65	-0.03 -0.13
MgSi	2.94 2.57	-0.08 -0.05	HgGe	2.94 2.70	-0.08 -0.18
MgGe	2.99 2.62	-0.13 -0.10	TiSi	2.79 2.49	0.05 0.03
MgSn	3.18 2.80	-0.32 -0.28	TiGe	2.94 2.54	-0.08 -0.02
CaC	2.83 2.51	0.03 0.01	MnSn	2.89 2.57	-0.03 -0.05
ZnSi	2.71 2.48	0.15 0.04	FeSn	2.85 2.57	0.01 -0.05
ZnGe	2.76 2.53	0.10 -0.01	CoSn	2.84 2.56	0.02 -0.04
ZnSn	2.95 2.71	-0.09 -0.19	NiSn	2.82 2.55	0.04 -0.03

7. Zh. I. Alferov, M.Z.Zhingarev, et al., Fizika i Tekhnika Poluprovodnikov, 1982, v.16, pp.831-838.
8. Zh. I. Alferov, R.S.Vartanyan, et al., ibid, 1982, pp.887-890.
9. M.S. Saidov, A.S. Saidov, Proc. 6th Intern. Workshop on Phys.of Semiconductor Devices, New Delhi, India, Dec.2-6, 1991, p.227-234.
10. M. S. Saidov, phys. of metals and Phys. Metallurgy, 1964. V. 17. N5. pp. 795-797.
11. M. S. Saidov. Phys. chemistry 1964. V. 38. N11. p. 268.
12. V. K. Semenchenko, Physical theory of Solutions GITTL, Moscow, 1941.
13. Ya.S. Umanskii, B.N. Finkel'stein, et al., in Physical Metallurgy, Moskow, Metallurgizdat, 1955, pp.122-126.
14. L.I. Marina, A.Ya. Nashel'skii, L.I. Kolesnik, in Semiconductor Phosphides $A^{III}B^{V}$ and Solid Solutions on their basis, Moscow, Metallurgiya, 1974, pp.45-50.
15. Properties of Elements Part I, Physical properties Editor G. V. Samsonov, Moscow, Metallyrgy, 1976. p. 157-159.
16. Hansen , K. Anderko, Constitution of binary alloys, Moscow, 1962.

RESIDUAL STRENGTH PREDICTION OF COMPOSITE AIRCRAFT STRUCTURAL ELEMENTS WITH STRESS CONCENTRATIONS

V.N. Maksimenko

SibNIA, Novosibirsk

The general integral relations and the singular integral equations have been obtained for the plane elasticity theory problems of rectilinear anisotropic complex-form bodies with curvilinear cracks. The efficiency of relations proposed is shown by solving the strength problems of the plates of laminated composite fiber-reinforced materials with stress concentrators. The calculation technique is based on simulation of zones of damage by the fictitious cracks. The calculation results are compared with the experimental data.

Let an infinite anisotropic plate in the Cartesian system of coordinates xOy has a closed smooth curvilinear crack L that divides the plane into two regions: the internal domain D^+ and the external one D^-. The direction at which D^+ is to the left is assumed to be the positive path-tracing of the contour L. Let us make such analytical prolongation from D^- to D^+ that, in passing through the contour L, the stresses remain continuous and the displacements $G(z)=u+iv$ undergo the discontinuity $W(t)=G^+(t)-G^-(t)$.

The solutions of the problem on the action of concentrated dislocation with the Burgers vector $\overset{\mathrm{r}}{Q}=U+iV$ in the point τ of an infinite plate have the from

$$\Phi_\nu^*(z_\nu)=B_\nu(z_\nu-\tau_\nu)^{-1},\quad z_\nu=x+\mu_\nu y\quad(\nu=1,2) \tag{1}$$

$$\sum_{\nu=1}^{2}(\mu_\nu^{k-2}B_\nu-\overline{\mu}_\nu^{k-2}\overline{B}_\nu)=f_k(2\pi i)^{-1},\quad f_1=U,\ f_2=f_3=0,\ f_4=V.$$

From the latter relations it follows, in particular, that

$$a_0B_1-b_0\overline{B}_1+B_2=0, \tag{2}$$

$$a_0=(\mu_1-\overline{\mu}_2)(\mu_2-\overline{\mu}_2)^{-1},\quad b_0=(\overline{\mu}_1-\overline{\mu}_2)(\mu_2-\overline{\mu}_2)^{-1},$$

where μ_ν are the characteristic equation roots, a_{ij} are the strain coefficients from the Hooke law / 1 /.

Taking $\overset{r}{Q}(t)$ as the functions of the class H on L and using / 1 /, let find corresponding values of $B_\nu(t)$, then multiply $\Phi_\nu^*(z_\nu)$ by ds and integrate along L. This gives

$$\Phi_\nu(z_\nu)=\frac{1}{2\pi i}\int_L \frac{\omega_\nu(\tau)d\tau_\nu}{\tau_\nu - z_\nu}, \quad M_\nu(t)=\mu_\nu\cos\varphi-\sin\varphi, \qquad (3)$$

$$\omega_\nu(t)=-2\pi i B_\nu(t)/M_\nu(t), \quad d\tau_\nu=M_\nu(\tau)ds.$$

(the $\varphi(t)$ -angle between Ox and the external normal n to D^+ in the point $t\in L$).

From relation (2) it follows that

$$a(t)\omega_1(t)+b(t)\overline{\omega_1(t)}+\omega_2(t)=0, \qquad (4)$$

$$a(t)=a_0M_1(t)/M_2(t), \quad b(t)=b_0\overline{M_1(t)}/M_2(t).$$

Substituting (3) into relations / 1 /

$$(u,v)=2\,\mathrm{Re}\left\{\sum_{\nu=1}^{2}(p_\nu,q_\nu)\varphi_\nu(z_\nu)\right\}, \quad \Phi_\nu(z_\nu)=\frac{d\varphi_\nu}{dz_\nu},$$

$$p_1=a_{11}\mu_\nu^2+a_{12}-a_{16}\mu_\nu, \quad q_\nu=a_{12}\mu_\nu+a_{26}+a_{22}/\mu_\nu,$$

gives us that the unknown complex functions $\omega_\nu(t)$ are due to the displacement discontinuities $W(t)$ (a is the fixed point on L), i.e.

$$W(t)=\sum_{\nu=1}^{2}\{(p_\nu+iq_\nu)\int_a^t\omega_\nu(\tau)d\tau+(\overline{p}_\nu+i\overline{q}_\nu)\int_a^t\overline{\omega_\nu(\tau)d\tau_\nu}\}+const \qquad (5)$$

In this case the displacement singlevaluedness condition in tracing the contour L leads to the equality

$$\int_L\omega_1(\tau)d\tau_1=0. \qquad (6)$$

The functions $\Phi_\nu(z_\nu)$ (3) define such stressed state (both in D^+ and in D^-) that the main vector and moment of forces, applied to L from the left and from the right, are equal to zero. Hence, relations (3) can be used for the finite domain D^+ with an arbitrarily loaded boundary L. However, for the infinite domain D^-, expressions (3) should be added by some summands, since the load applied to L can be nonselfbalanced in the general case.

Let the anisotropic plate occupy the finite multi-valued domain D, restricted by the contour L that consists of simple closed curves L_0 , L_1, ... , L_k (L_0 embraces all the curves) and curvilinear sections L_{k+1}, ... , L_n. The origin of coordinates is considered to lie in D; the

main vector of external loads applied to L_j ($j=0,\ldots, k$) equal to zero (this always can be attained by introducing the known additions / 1 / into $\Phi_\nu(z_\nu)$); and the condition is fulfilled for that the main moment of external forces applied to $L' = \bigcup_{j=0}^{k} L_j$ is equal to zero and $X_n^{\pm}(t) + iY_n^{\pm}(t) = X_n(t) + iY_n(t), \quad t \in L'' = \bigcup_{j=k+1}^{n} L_j$, on the crack edges ($X_n(t), Y_n(t)$ are the projections of external forces on the axis x, y in the point $t \in L$). The path-tracing of the contours L_j ($j=0,\ldots, k$) is performed so that the domain D, occupied with a plate, be to the left; on L_j ($j=k+1,\ldots, n$) the tracing direction is arbitrary.

The value of $\Phi_\nu(z_\nu)$ is determined as

$$\Phi_\nu(z_\nu) = \frac{1}{2\pi i}\int_L \frac{\omega_\nu(\tau)d\tau_\nu}{\tau_\nu - z_\nu} + \sum_{j=1}^{k} \frac{b_{\nu j}}{(z_\nu - a_\nu^{(j)})^2}, \qquad (7)$$

$$b_{1j} = \int_{L_j} \left\{\bar{\tau}\omega_1(\tau)d\tau_1 - \tau\overline{\omega_1(\tau)}d\bar{\tau}_1\right\}, \quad b_{2j} = 0\,(j = 1,\ldots,k),$$

where $a^{(j)}$ are the arbitrary fixed points in the single-valued domains D_j, restricted by the curves L_j ($j=1,\ldots, k$).

Substitute the limiting values (6) into the boundary conditions / 2 /

$$a(t)\Phi_1^+(t_1) + b(t)\overline{\Phi_1^+(t_1)} + \Phi_2^+(t_2) = F^+(t), \quad t \in L',$$

$$a(t)\Phi_1^{\pm}(t_1) + b(t)\overline{\Phi_1^{\pm}(t_1)} + \Phi_2^{\pm}(t_2) = F^{\pm}(t), \quad t \in L'',$$

The expression $a(t)c_0 t_1^{-2} + b(t)\bar{c}_0 \bar{t}_1^{-2}$,where

$$c_0 = \mathrm{Re}\left\{\frac{1}{\pi i}\int_L \frac{\omega_1(\tau)d\tau_1}{\tau_1}\right\}$$

is added to the left-hand part of the obtained equalities. Then, to determine the unknown function $w_1(t)$, we'll derive the singular integral equations

$$\int_L \frac{\omega_1(\tau)d\tau_1}{\tau_1 - t_1} + \int_L \left\{K_1(t,\tau)\omega_1(\tau) + K_2(t,\tau)\overline{\omega_1(\tau)}\right\}ds + G(t) = f(t) \qquad (8)$$

$$G(t) = \pi i \sum_{j=0}^{k} \left\{\frac{\overline{a(t)}}{\overline{b(t)}} \frac{\bar{b}_{1j}}{(\bar{t}_1 - \bar{a}_1^{(j)})^2} + \frac{b_{1j}}{(t_1 - a_1^{(j)})^2}\right\},$$

where $a_1^{(0)} = 0$, the explicit expressions $K_p(t,\tau)$, $f(t)$, are presented in / 2 /.

It can be shown (in much the same way as in / 3 /) that if equation (8) has the solution, then it is unique and necessary, i.e. $c_0 = 0$. The index of singular integral equations (8) equals zero. The mentioned above and the third Noether theorem / 4 / result

in that a number of linear-independent solutions of the uniform singular integral equation associated with (8) is equal to zero. Thus, equation (8) with any right-hand part is solved and equivalent to the problem posed.

Since a number of additional conditions of the form (6), which must be satisfied by the unknown functions $w_1(t)$, coincide with a number of singular integral equations in the corresponding contours L_j ($j=k+1,\ldots, n$), then the value of $w_1(t)$ should be found in a class of functions which are infinite at the crack ends / 4 /.

By introducing the contour parametrization and using the known quadrature formulas for the singular integrals, we reduce solution of equations (8) with the additional conditions to that one of a system of linear algebraic equations with respect to the approximate values of the unknown functions $w_1(t)$ in the nodes / 5 /. Determining $w_1(t)$, with the help of potentials (7), find the stress distribution in the plate and calculate the normal and shears stress intensity factors in the crack tip.

The above-obtained singular integral equations can also be used for consideration of the piecewise smooth (curved or branching) sections and boundary curvilinear ones. In this case the piecewise smooth section is divided into smooth parts and considered as a system of smooth subsections with common nodes. A well-known simplified method of numerical solution of the singular integral equations (8) with the immovable peculiarities is also applied, that allows the study of behaviour of the unknown functions in the vicinity of the nodal points to be avoided / 2 /.

The solving system of the Fredholm integral equations for the plane problem in the elasticity theory of anisotropic body was, probably, obtained for the first time by D.I. Sherman / 3 /. In / 6,7 /, to solve the problem under consideration, use was made of relations by Sherman for the closed contours, and the mixed systems of singular integral equations on sections and regular ones on the closed contours of the body boundaries were obtained. The relations $\Phi_v(z_v)$ constructed in this paper allow identical formation of the system of the singular integral equations for the problem with the same analytical expressions of the integral equation kernels on the closed and open contours. This simplifies considerably the algorithm of numerical calculation of the singular integral equations. In addition, as is seen from numerical experiments, these algorithms are more stable and lead us to the purpose more quickly.

If the plate consists of $2k$ homogeneous orthotropic layers situated symmetrically respecting the middle plane xOy, then by using the efficient moduli of laminated composite materials, we reduce the problem of determination of the stress-strain plate

state to the above-formulated problem of the plane anisotropic elasticity theory. With the help of potentials $\Phi_v(z_v)$ (7), determine the average plate thickness stresses $< \sigma_{ij} >$ and, using them, the stresses in each layer $\sigma_{ij}^{(m)}$ *(m=1, ... ,k)* / 8 /.

Relations (6) turned out to be the efficient instrument for determining the stress-strain state in the vicinity of nodes of the intricate form sections in anisotropic and isotropic plates. For illustration, Fig 1 presents the results of numerical determination of the stress intensity coefficients of the break-off K_1 in the node of a crack coming from the contour of one of holes in a stretched plate of glass plastic, boroplastic, carbon plastic and metal alloy (E_1/E_2= *3; 10; 25; 1* respectively; the elastic characteristics of materials are given in / 2 /). The solid (dashed) lines correspond to the case when the main anisotropy direction corresponding to E_1 is perpendicular (parallel) to the load action direction. For the parameters under consideration, the stationary of the problem of determination of the stress intensity coefficients (with an accuracy to $\approx$1%) are found for a number of nodes on the contours of holes and cracks that is equal to $\approx$ 40. The calculation results for the isotropic material are obtained by the limiting transition in the medium anisotropy parameters at numerical solution and agree fairly well with the data available / 9 /.

For the methods of estimation of the static strength of a laminated composite plates with cuts-out, which are based on the linear facture mechanics, it is assumed that the "edge cracks' appear near the cut-out (a model of the damage zone) / 10,11 /. This approach provides rather accurate calculation estimates, however, as it was noted in / 10,11 /, the difficulty is in that it is not a simple matter to find the corresponding stress intensity coefficients. For this reason, researchers are often, without any substantions, compelled to use *K*- calibrations for the isotropic materials. Application of the finite element method for the case of small boundary cracks causes difficulties / 11 /. Potentials (7) allow such type problems to be effectively solved.

In / 10 /, the strength of rectangular specimens of carbon plastic with the layer packing $[\ 0°/90°/45°\ ]_{2S}$ and *a* - radius central hole, which were stretched by the forces σ applied to the upper and lower edges, was studied experimentally. The strength limit of the laminated composite materials σ_0 =581 Gpa, the elastic monolayer characteristics E_1 =138 GPa, E_2 =11 GPa, G_{12} =4 GPa, ν_1 =0.25.

To obtain the calculation estimate for the specimen strength, the damage zone is assumed to form with an increase in the load σ in the vicinity of the stress concentration point on the hole contour and to attain the characteristic critical size under the limiting

load $\sigma = \sigma_C$ (Fig. 2a). The damage notion is considered in the general sense, i.e. it is the fiber rapture, matrix cracking, interface fracture of the combination of all these factors. Let the damage zone be represented as the fictitious crack of the characteristic length d, that comes from the stress concentration point in the direction of the stress field gradient (Fig. 2b). For further consideration, two approaches are suggested. In the first approach, the crack edges are considered to be free and the dimension d to be independent of the hole from and size. The stress intensity coefficient in the dummy crack node is equal to $k_1 = \sigma\sqrt{\pi d}\, f(d/a, d/W)$, where f is the correction factor that takes into account the influence the hole, plate edge, material anisotropy. If f is found the limiting load equals $\sigma_c = k_c \left[\sqrt{\pi d} f\right]^{-1}$, where k_c is the viscosity of fracture of the laminated composite material. For $a \to 0$ and $W \gg d$ $f \to 1$ and according to the assumptions from / 7,11 /, we have $\sigma_0 = k_c\left[\sqrt{\pi d}\right]^{-1}$. Thus, $\sigma_0/\sigma_C = f(d/a, d/W)$. The calculation results with the potentials (7) show that the experimental data (2-3 values of σ_0/σ_C) are approximated best of all by the calculation curve for d = 1.9 mm / 7 /. This value is taken as the crack length that simulates the damage zone.

In the second approach, along the boundaries of the dummy crack, the adhesive force action $\sigma^* = \sigma_C$ is assumed till the crack opening determined by formula (5) exceeds the critical value of δ_C being the material characteristic (δ_C is the Leonov- Panasyuk-Dugdale model / 9 /, Fig. 2c). The fracture load σ_C is determined (according to the δ_C - model) by construction of the calculation diagrams $\sigma = \sigma(l)$ (Fig. 2d). The value of the parameter δ_C (analogously to the choice of d in the first approach) is chosen on the basis of 2-3 experimental data.

The Table presents the results of comparison of the values of σ_0/σ_C obtained by calculations with the help of the first and second approaches and also in the experiment / 10 / for different $\lambda = W/W_0$ (W_0 =70 mm, $2W$ is the specimen width) and radii of the hole a = 5; 10 mm. Here $\delta_{1,2}$ is the calculation error as compared to the experimental data. Coincidence is rather satisfactory for both hole sizes when $a/W < 0.5$. For $a/W > 0.5$, the calculation estimates σ_C are somewhat underestimated, probably because with a decrease in W, the damage zone is not restricted by the region that is close to the hole boundary. This is nonadequately taken into account in the models under consideration.

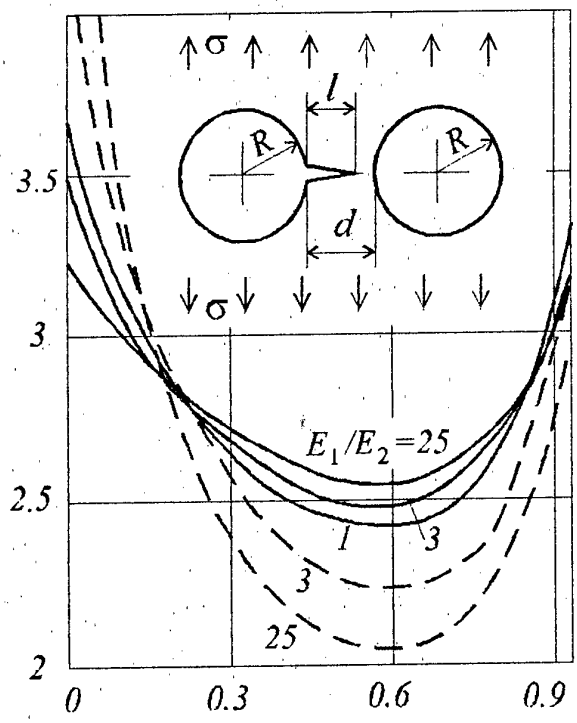

Fig. 1

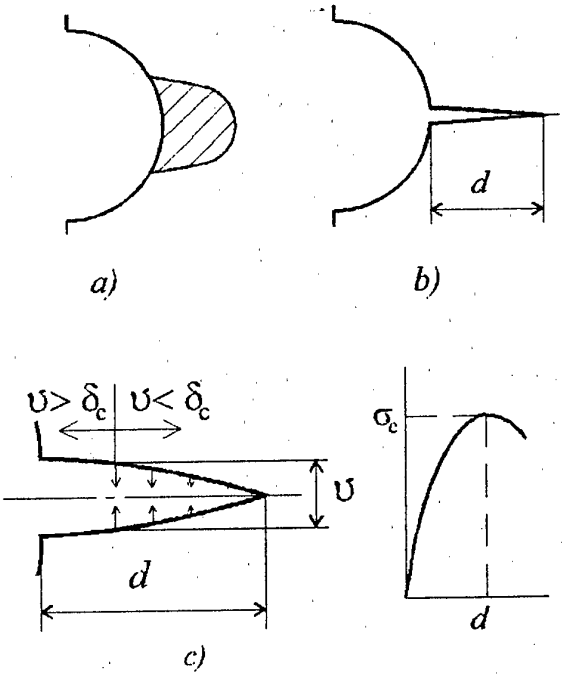

Fig. 2

Table

λ	experiment	calcul. 1	δ_1 (%)	calcul. 2	δ_2 (%)
			a =5 mm		
1	0.489	0.490	0.3	0.501	0.2
2/3	0.499	0.488	2.2	0.485	2.8
1/2	0.491	0.481	2.1	0.479	2.4
1/3	0.475	0.461	3.0	0.460	2.1
1/4	0.460	0.431	6.3	0.436	5.2
1/5	0.408	0.393	3.6	0.401	1.7
1/7	0.355	0.298	16.1	0.386	9.1
			a = 10 mm		
1	0.417	0.397	4.8	0.395	5.2
2/3	0.406	0.383	5.6	0.386	4.9
1/2	0.392	0.364	7.1	0.369	5.8
1/3	0.327	0.308	5.7	0.312	4.5
1/4	0.269	0.232	13.9	0.238	11.5

The proposed integral potentials and calculated models enables one with sufficient condidence to evaluate an ultimate strength of composite plates with stress concentrations. The approach given allow to obtain to with a high accuracy the strength values in a plate for different types of holes and boundary conditions. The simplicity and efficiency of the method proposed enables one to recommend it for practical use.

REFERENCES

1. Lekhnitsky S.G. Anisotropic plates. Gordon and Breack Science Publishers, New York, 1968. - 400p.
2. Maksimenko V.N. Stress concentration in the elements of aircrafts. Novosibirsk: Novosibirskii electrotekhn. institute, 1989, 68 h. (in Russian)
3. Sherman D.I. To the solution of the plane problem in the elasticity theory for anisotropic medium. // Appl. Math. and Mech. - 1942. - v.6, № 6. - p. 509-514. (in Russian).

4. Muskhelishvili N.I. Singular integral equations. Moscow, Fizmatgiz, 1968. - 511 p.
5. Belotserkovsky S.M., Lifanov I.K. Numerical methods in singular integral equations. Moscow, Nauka, 1986, 256 p.
6. Fil'shtinsky L.A. Boundary value problems in the elasticity theory for anisitropic half-plane with a hole or cut. // Izv. AN SSSR, MTT. - 1980. -№ 6. - p. 72-79.
7. Annin B.D., Maksimenko V.N. Fracture analysis of composite plates with holes. // Mech. Compos. Mater. - 1989, - № 2, p. 284-289.
8. Bert C.W. Calculation of plates. Composite materials, Ed. L.J. Broutman and R.H. Krock - v. 7. Structural Design and Analysis. Part 1. - Academic Press: New York, San Francisco, London, 1975.
9. Fracture mechanics and strength of materials. v. 1-4, ed. by V.V. Panasyuk, Kiev, Nauk. dumka, 1988, v. 2, 620 p.
10. Backlund J., Aronsson C.G. Tensile fracture of laminates with holes // J. Compos. Mater. - 1986. - v. 20, № 3, - p. 259-286.
11. Crews J.H. A survey of strength analysis methods for laminates with holes // J. Aero. Soc. India. - 1984, -v. 36, № 4. -p. 287-303.

RESIDUAL STRENGTH OF ISOTROPIC AND ANISOTROPIC BONDED-RIVETED PANELS.

V.N.Maksimenko, V.N.Pavshok

SibNIA, Novosibirsk

In recent time the wide use of adhesive and adhesive-mechanical joints in aircraft structures as well as the transition to aircraft designing based on the fail safe principle have led to necessity to develop efficient methods of solving the local strength problems for aircraft structures with crack-type defects and bonded (bonded-riveted) stiffeners.

The adhesive joints of structural elements acquire a particular actuality due to the increasing use of composite materials in different areas of engineering for which the usual mechanical attachments don't provide the required strength.

For most of structural elements a verification of the fail safe criterion must be carried out analytically. Frequently, this is the only economically possible approach. Well-developed and universal finite element method is not the most optimal in the problems with high stress gradients and variable boundaries. The integral equation method requiring discretization only of a domain boundary is more efficient for solution of such problems. Therefore, the development, on the basis of integral equations, of computational methods for stress-strain state (SSS) and residual strength (RS) of the bonded and bonded-riveted damaged aircraft structural elements made of metal alloys and composite materials is an actual problem.

To apply in practice the principles of fracture mechanics to aircraft component analyses it is necessary to solve a series of SSS and RS-determination problems for specific types of structural elements and variants of their connections.

1. We consider a problem of SSS-determination for an infinite anisotropic plate with a system of smooth curvilinear notches $L_j = \{t = t^{\,j}(\eta),\ |\eta|<1\},\ (j=1,k)$, which is reinforced along straight segments $\Gamma_s\ (s=1,m)$ by the bonded or bonded-riveted stiffeners - ribs or crack-stoppers (Fig. 1,a). The plate is loaded by stresses at infinity σ_x^{∞}, σ_y^{∞}, τ_{xy}^{∞}, self-balanced continuous forces $X_n^{\pm}(t)+iY_n^{\pm}(t)$ on the edges of the notches and concentrated forces on the ends of the stiffeners. It is assumed that the plate with thickness h is subjected to a generalized plane stress state, the ribs are deformed along their axis only, the adhesive layer operates in shear. The shear strain $\gamma_s(t)$ and shear stress

$\tau_s(t)$ are uniformly distributed on the width d_s of the contact area; the effect of the rivet (mechanical connection) with flexibility q_s is simulated by loading of the plate with constant tangential forces applied to a square area with side equal to the rivet diameter d (Fig. 1,b). We shall consider the summarized vector of the forces on each rivet $Q_i^s(t_i^s)=\tau_i^s(t_i^s)d^2$ $(i=1,N,\ s=1,m)$ and the contact forces $r(t)=\{r_s(t)=\tau^s(t)d_s,\ t\in\Gamma,\ s=1,m\}$, transferring from the ribs to the plate along the lines Γ_s as the body forces in the plate coinciding with its middle plane.

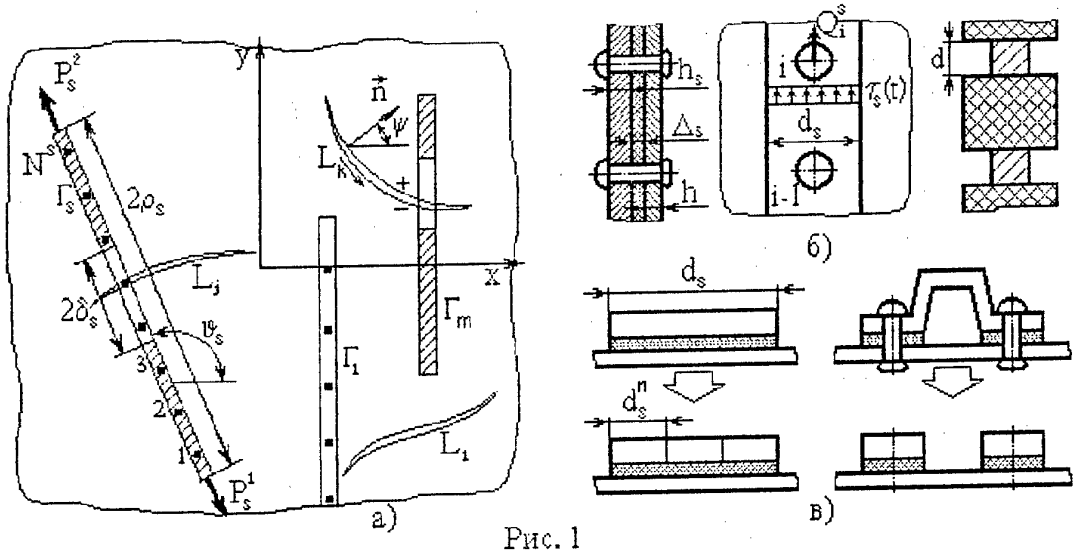

Рис. 1

The stresses and displacements in the anisotropic plate are expressed as two analytical functions $\Phi_\nu(z_\nu)$ $(\nu=1,2)$, satisfying the given system of external forces applied to the plate, boundary conditions on $\Gamma=\cup\Gamma_s$ and $L=\cup L_j$

$$\tau_n^- - \tau_n^+ = r(t)/h, \qquad \sigma_n^- = \sigma_n^+, \qquad u_n^- = u_n^+, \qquad v_n^- = v_n^+, \qquad t\in\Gamma, \tag{1}$$

$$a(t)\Phi_1^{\pm}(t_1)+b(t)\Phi_1^{\pm}(t_1)+\Phi_2^{\pm}(t_2)=F^{\pm}(t), \qquad t\in L, \tag{2}$$

as well as conditions of compatibility of the rib $w^s(t^s)$ and plate $w(t^s,\theta^s)$ displacements along the contact line Γ_s in the adhesive layer

$$w(t^s,\theta_s)-w_s(t^s)=\frac{\Delta_s}{G_s d_s}r_s(t^s), \qquad t^s\in\Gamma_s', \qquad s=\overline{1,m} \tag{3}$$

and attachment points t_i^s

$$w(t_i^s,\theta_s)-w_s(t_i^s)=q_s Q_i^s(t_i^s), \qquad t_i^s\in\Gamma_s'', \qquad i=\overline{1,N^s},$$
$$\Gamma_s''=\bigcup_{i=1}^{N^s}\{|t_i^s-t|\le d/2\}, \qquad \Gamma_s'=\Gamma_s\setminus\Gamma_s'', \qquad s=\overline{1,m}. \tag{4}$$

Here $\sigma_n^{\pm}$, $\tau_n^{\pm}$, $u^{\pm}$, $v^{\pm}$ - are the left-hand and right-hand limit values of the stresses and displacements on Γ; $a(t)$, $b(t)$ - are known complex functions; Δ_s, G_s - are thickness and shear modulus of the adhesive.

Modelling the cracks through dislocations continuously distributed along them and the bonded stiffeners through the contact forces $r(t)$ distributed along Γ using the solution of concentrated force action and the superposition principle we can present unknown Lehnitsky complex potentials in the form

$$\Phi_\nu(z_\nu)=\sum_{p=0}^{2}\Phi_{\nu p}(z_\nu),\qquad \Phi_{\nu 1}(z_\nu)=\frac{1}{2\pi i}\int_L\frac{\omega_\nu(\tau)d\tau_\nu}{\tau_\nu-z_\nu},\qquad \Phi_{\nu 2}(z_\nu)=\int_\Gamma\frac{A_\nu(\tau)r(\tau)ds}{z_\nu-\tau_\nu},\qquad (5)$$

$$\omega_2(t)=-a(t)\omega_1(t)-b(t)\overline{\omega_1(t)},\qquad z_\nu=x+\mu_\nu y,$$

where $\Phi_{\nu 1}(z_\nu)$ - are the solutions for continuous plate, μ_ν - are the roots of the characteristic equation $a_{11}\mu^4 - 2a_{16}\mu^3 + (2a_{12}+a_{66})\mu^2 - 2a_{26}\mu + a_{22} = 0$. The integral representations (5) built in such a manner automatically satisfy the boundary conditions (1).

Substituting (5) into the boundary conditions (2)-(4) and after some transformations the combined system of singular on L and regular (with logarithmic singularity) on Γ integral equations for determination of unknown functions $\omega_\nu(t)$, $r(t)$ is obtained:

$$H_s r_s(t)+\int_\Gamma k_1(t,\tau)r(t)ds+\int_L \mathrm{Re}\{k_2(t,\tau)\omega_1(\tau)\}ds+C_s^*=f_1(t),\qquad t\in\Gamma,$$

$$\int_\Gamma k_3(t,\tau)r(\tau)ds+\int_L\frac{\omega(\tau)ds}{\tau_1-t_1}+\int_L\{k_4(t,\tau)\omega_1(\tau)+k_5(t,\tau)\overline{\omega_1(\tau)}\}ds=f_2(t),\quad t\in L, \qquad (6)$$

$$H_s=\Delta_s(G_s d_s)^{-1},\qquad t\in\Gamma_s',\qquad\qquad H_s=q_s d^2 d_s^{-1},\qquad t\in\Gamma_s^*.$$

System of equations (6) combined with additional conditions of the rib balance and continuity of crack-tip displacements

$$\int_{\Gamma_s} r_s(t)ds=P_s^1-P_s^2,\qquad s=\overline{1,m},\qquad\qquad \int_{L_j}\omega_1(\tau)d\tau_1=0,\qquad j=\overline{1,k} \qquad (7)$$

gives the unique solution of the considered problem.

An algorithm is proposed for numerical realisation of the resolved system of integral equations that consists in employing the spline - collocation method for integrals over Γ and the mechanical quadratures method for integrals over L. In this case the integrals with logarithmic singularity are calculated in a closed form and the singularities of solution on the ends of the notches are extracted from it by a separate factor. The

problem is reduced to solution of linear algebraic equations relative to approximated values of unknown functions in the collocation nodes and Chebyshev nodes. Asymptotic formulas for evaluation of mode I and mode II stress intensity factors (SIF) $K_{1,2}$ in the crack tips are presented.

Validity and efficiency of the proposed models for the adhesive (adhesive-mechanical) joints and the computational method are illustrated by comparing with some known results obtained by using the integral equation method and FEM. Effects of the stiffener fracture, debonding of the adhesive, the rivet flexibility, the relative stiffness of the rib and adhesive layer, the anisotropy of the plate material, the mutual crack-stiffener-location as well as other factors on the SIF are investigated (see, for example, Figs. 2, 3). Computations have shown that employing the adhesive-mechanical joints doesn't give any marked advantage in view of the strength in comparison with the adhesive joint in well-designed structures without defects. However, in the presence of the faulty bonding or debonding-type damage of the adhesive layer the mechanical attachment delays or completely stops the defect grows.

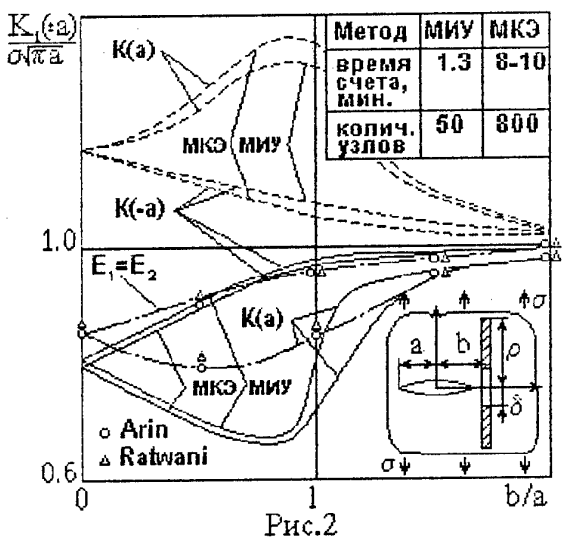

Рис.2

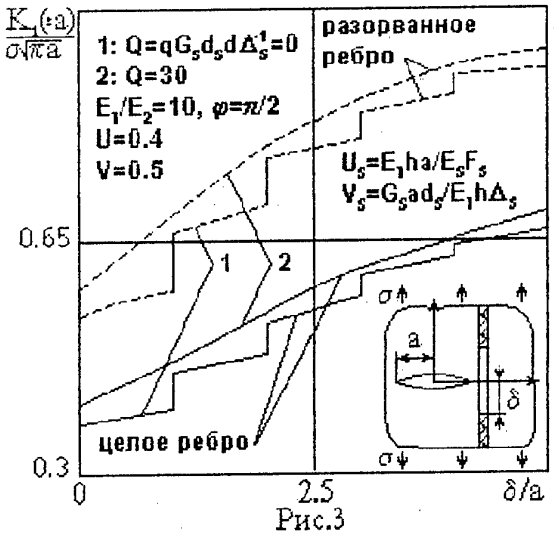

Рис.3

Solution of the problem is built in similar manner in the case of employing the modified integral representations automatically satisfying the boundary conditions on the half-plane boundary and contour of the elliptic hole; the case of the crack extension on the half plane or hole boundaries is considered.

Solution of the problem is generalized on the case of the multi-connected region restricted by contour L consisting of the simple closed curves L_0, $L_1,...,L_k$ and internal smooth non-intersecting notches $L_{k+1},...,L_n$. It is assumed that the contour L_0 covers all

other. The resolved system of integral equations with equal analytical expressions for kernels on closed and opened contours is written.

Using the obtained solutions for a number of problems as a basis, some improvements of the problem model are introduced, for example, methods for taking into account the excentricitet of the rib connection and the variable-in-thickness crack opening under an adhesively bonded patch. A method for taking into account the elasto-plastic deformation of the adhesive, mechanical attachment and stiffeners is developed. The problem is reduced to a system of non-linear integral equations. An efficient numerical algorithm for iterative solution of a system of integral equations was developed which requires re-estimation on each iteration not whole matrix but only its diagonal elements. The effects of various stiffness and geometrical parameters on SIF and maximum stiffener and adhesive strains are investigated for the case of elasto-plastic deformation of structural elements (Fig. 4). A method for introduction the stiffener width (Fig. 1,c) is proposed; different models of plate-to-stiffener force transmission (Fig. 5) are introduced that allows within the framework of the developed algorithm to evaluate efficiently the effect of the wide bonded and bonded-riveted patches including with multi-row riveted joints.

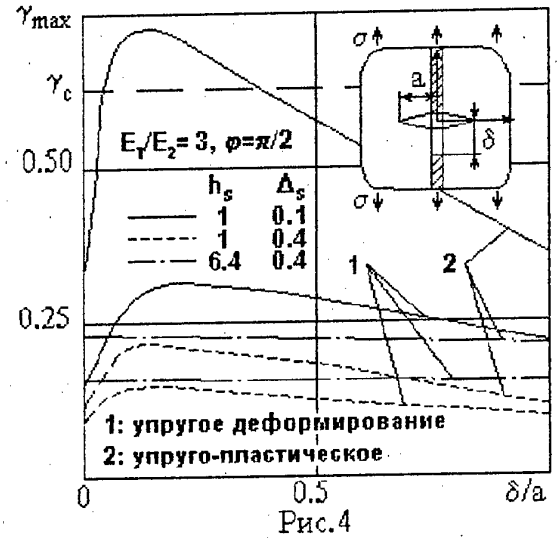

Рис.4

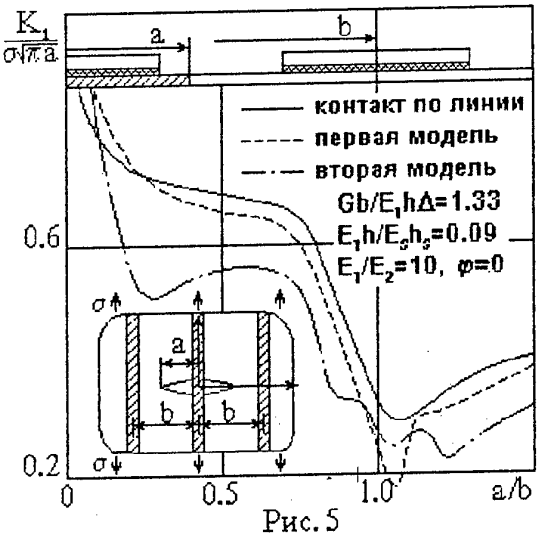

Рис. 5

2. Now we shall solve the problem of SSS-determination for a two-layer complex-form panel with cracks. We shall consider a plane structure consisting of two finite straight-linearly anisotropic plates; each of them presents the multi-connected region D^l restricted by contour consisting of the simple closed-non-intersecting curves $L_0^l, L_1^l, \ldots, L_k^l$ and the notches (cracks) $L_{k+1}^l, L_{k+2}^l, \ldots, L_n^l$ ($L^l = \cup L_j^l$), (Fig. 6). Along some region $D_0 \subset D=\{D^1 \cap D^2\}$ the plates are bonded by means of the adhesive layer of the thickness Δ with

the shear modulus G and mechanical connections (by rivets, bolts) at the points $z_m \subset D$ (m=1,N). The forces $X_n^l + iY_n^l$ applied to each contour L_j^l (j=1,n_l) are self-balanced and act in the middle plane of the plate l (l=1,2). The following simplifying assumptions are made: in the plates a generalized plane stress state is realized; the adhesive and rivets transmit the shearing forces only; the weakness of the plate due to setting of the rivets is ignored; the riveted joint is considered as the local elastic bond between the plates along the square region D_m (m=1,N) with side d and centre at the point τ_m; it is similar to adhesive bond but with different stiffness characteristic.

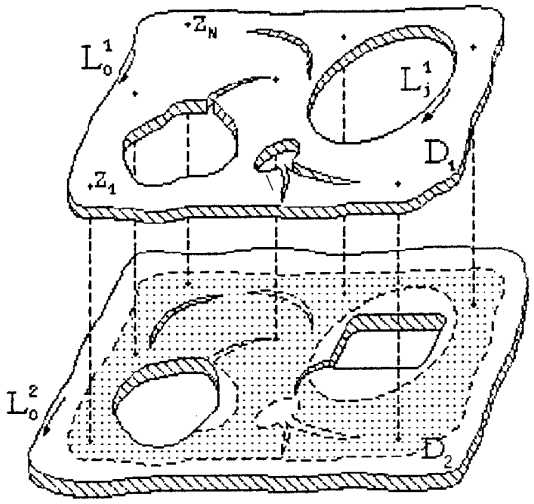

Рис. 6

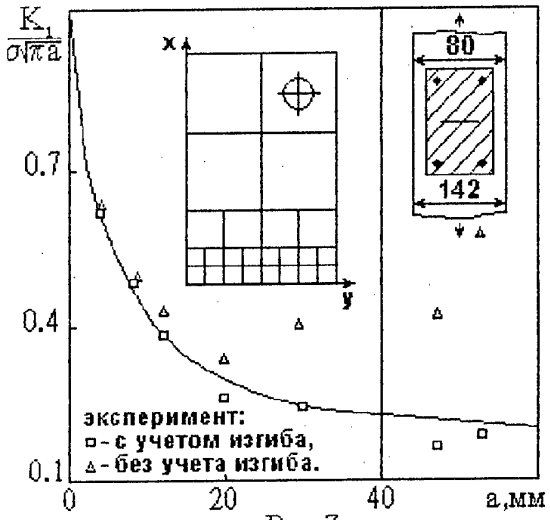

Рис.7

We shall write the conditions on L^l

$$a^l(t^l)[\Phi_1^l(t_1^l)]^+ + b^l(t^l)\overline{[\Phi_1^l(t_1^l)]^+} + [\Phi_2^l(t_2^l)]^+ = [F^l(t^l)]^+, \quad t \in L_j^l, \quad j = \overline{0,k_l}$$
$$a^l(t^l)[\Phi_1^l(t_1^l)]^- + b^l(t^l)\overline{[\Phi_1^l(t_1^l)]^-} + [\Phi_2^l(t_2^l)]^- = [F^l(t^l)]^-, \quad t \in L_j^l, \quad j = \overline{k_l+1,n_l} \qquad (8)$$

and compatibility conditions for displacements of the plates in region D

$$u^1(z) - u^2(z) = H_x(z)\tau_x(z), \qquad v^1(z) - v^2(z) = H_y(z)\tau_y(z),$$
$$H_{x,y}(z) = \Delta / G, \quad z \in D_0, \qquad H_{x,y}(z) = q_{x,y}d^2, \quad z \in D_m. \qquad (9)$$

Here $\tau_{x,y}(z)$ - are the tangential stresses in the adhesive layer, $q_{x,y}$ is the riveted joint flexibility. Similarly to p.1, using the solution for concentrated force and dislocation, the functions $\Phi_\nu^l(z_\nu^l)$ giving a solution of the problem (8)-(9) are fined in the form:

$$\Phi_\nu^l(z_\nu^l) = \sum_{p=0}^{2}\Phi_{\nu p}(z_\nu^l),$$
$$\Phi_{\nu 1}^l(z_\nu^l) = \frac{1}{2\pi i}\int_{L^l}\frac{\omega_\nu^l(t)dt_\nu}{t_\nu - z_\nu^l}, \qquad \Phi_{\nu 2}^l(z_\nu^l) = \iint_D \frac{A_{\nu x}^l(t)\tau_x(t) + A_{\nu y}^l(t)\tau_y(t)}{z_\nu^l - t_\nu}dxdy, \qquad (10)$$

where $\Phi_{v0}{}^{l}(z_v^l)$ is the solution for the continuous plate under external loading, $\omega_v^l(t^l)=\{\omega_{vj}{}^{l}(t^l),\ t^l \in L_j^l,\ j=0,n_l\}$ are the unknown complex functions on L^l.

Solution of the given problem is reduced to a system of integral equations, regular (in the region D_0) and singular (on L_j^l, $j=0,n_l$). To solve numerically the obtained system of integral equations the region D_0 is divided into square cells in which the unknown functions $\tau_{x,y}(z)$ are assumed constant and discrete analogues of the integrals over D are aken by using Gaussian quadrature formulas.

Similarly to p.1 the particular cases of the problem can be considered by using for each plates the modified integral representations automatically satisfying the boundary conditions on the straight-line edge and elliptic hole contour as well as some improvements of the problem model can be introduced: taking into account the bending in the case of two-layer plate containing a crack in one of the layer, the elasto-plastic deformation of the adhesive and mechanical attachment, the symmetry of the problem. It is noted that solution of the problem is naturally generalized for arbitrary number of the plates. The obtained numerical results illustrate the contact force behaviour in the adhesive layer and SIF in the crack tips. A comparison with the known results obtained by using FEM is given (Fig. 7).

The presented results are confirmed by the experimental investigations of the fatigue crack growth duration in the adhesively bonded panels under cyclic tension. The specimens of D16AT aluminium alloy had the stress concentrator (the centre hole of the diameter 5 mm) with initiated cracks. The crack stoppers of the same material and titanium wide patch were bonded by the cold-setting adhesive VK-9 according to the standard technology. The calculated curves obtained using Paris formula with empirical factors estimated on the basis of testing of the reference specimens as well as the experimental values are presented in Fig.8. A good agreement between the calculated and experimental data is noticed. The investigations have shown high efficiency of the adhesively bonded stiffener use for the fatigue crack retardation. The endurance was raised in a comparison with the reference specimens for the panels with two stoppers to 2.2 times, with three stoppers to 3.5 times, with wide patch to 2.4 times.

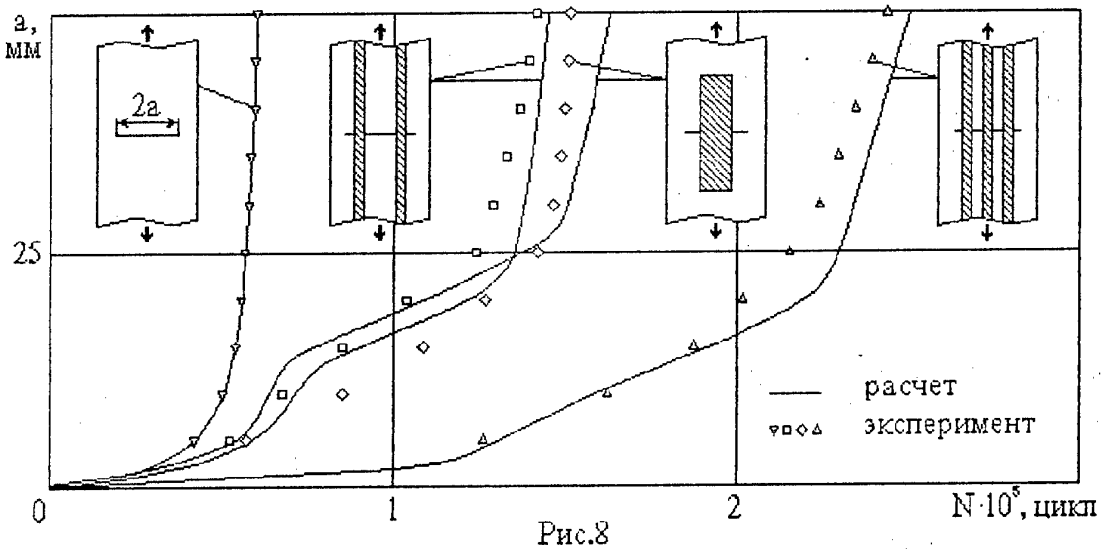

Рис.8

REFERENCES

1. Maksimenko V.N., Pavshok V.N. Effect of adhesively bonded stiffening ribs on residual strength of anisotropic and isotropic panels // Uchyonye zapiski TsAGI.-1987.-V.18,№2.-pp.84-92.

2. Maksimenko V.N., Pavshok V.N., Khan Yu.N., Tsendrovsky A.V. Effect of reinforced patches on crack growth near hole in finite anisotropic plate // Proc. of XIV All-union Conference on plate and shell theory. - Tbilisi, Publishing House of Tbilisi University, 1987.-V.2.-pp.175-180.

3. Maksimenko V.N., Pavshok V.N. Analysis of stiffened cracked plate in the case of non-linear work of patches and adhesive layer. // Prochnost i aerouprugost aviatsionnyh construktsiy.- Kazan: KAI, 1988.-pp.27-33.

4. Pavshok V.N. Residual strength of a panel with adhesively bonded patches.- Novosibirsk, 1989.-9p.- Deposited in VIMI 17.10.1989, №D08161.

5. Krasnov L.A., Maksimenko V.N., Pavshok V.N., Tyrin V.P. Determination of SIF for cracks in panels stiffened by adhesively bonded patches // Problemy prochnosti.-1989.-№5.-pp.73-76.

6. Maksimenko V.N., Pavshok V.N. Influence of adhesively bonded patches on crack tip intensity stress in anisotropic plate // Prikladnaya mehanika.-1989.-V.25, №5.-pp.69-75.

7. Maksimenko V.N., Pavshok V.N., Tyrin V.P. SIF-determination for cracks in panels stiffened by wide patches // Voprosy aviatsionnoy nauki i tehniki. Ser. Aerodinamika i prochnost letatelnyh apparatov.- 1991.-Issue 1.-pp.90-99.

8. Maksimenko V.N., Pavshok V.N. Towards analysis of anisotropic cracked plate reinforced by adhesive-riveted ribs // Prikladnaya mehanika i tehnicheskaya fizika.- 1992.- , №1.-pp.133-140.

AIRCRAFT ENGINES MADE OF COMPOSITE MATERIALS OF NONUNINFORM STRUCTURE

Karimbaev T.D., Zav'yalov A.N., and Luppov A.A.
TsIAM, Moscow

Origion and development of discontinuities is a local phenomenon and must be taken into account in designing constructions of materials with nonuniform structure. Unfortunately, the models for homogeneous anisotripic deformable continuous medim used for rating parts made of modern composite materials cannot cover these phenomena to a full extent. To improve the situation, we have developed a mathematical model for a linear deformation of a two-component medium, which was successful in estimating carrying ability of separate parts of aircraft engines made of composite materials. Some of these applications are discussed below. In terms of the models for a uniform and a two-component media, natural frequencies and oscillation form were found on the basis of the bar theory of bending oscillations of beams. The limit amplitudes of bending oscillations at the sinusoidal excitement of beams were established. The number of cycles before failure at resonance vibrations of beams was assessed, and the calculated results are comparable with experimental data obtained in fatigue testing of B-Al beams. The calulated and experimental results are in agreement in a wide range of angles of composite material armoring.

One of the vital units of working vanes are fasteners. On the basis of the abovementioned models, finite-element approaches are developed to assessment of stress state and carrying ability of a tail made of layered composite materials.

Calculations revealed behavior of stresses as a function of engine rotations, origination of a destruction center in the form of layering in the matrix material, successive growth of a crack as the load increases, and, finally, the beginning of a catastrophic failure when the tail its carrying ability. The calculated results are comparable with experimental data. These data are in agreement both qualitatively and quantitatively.

LOADING AND FATIGUE CHARACTERISTICS OF AIRLINER WING MECHANICS

V.A.Bespalov, M.I.Ryabinov, N.E.Fenyuk
Sib RIA , Novosibirsk

1. Introduction

The type construction element of wing mechanics is rails of specificprofile by means of which a motion of deflecting aerodynamic surfaces is provided along a given trajectory. Heavy conditions under which the rails work bending, contact loads from directing rolls, wearing of the surface dictate strong demands for their strength. The rails are made of high-strength doped steels with finishing of work surfaces. Dimensions of cross sections are determined from two calculated cases: total bending of a rail according to the scheme of double-seat beam and shelf bending from a concentrated force according to the scheme of cantilever plate. However, in testing of wing mechanics (flaps, slats) of the TU-154 airliner a number of rail destructions were obtained, having sufficient reserves of strength as regards loads of indicated calculated cases. In order to clear up causes of low fatigue durability, the stress state of the rails was examined in detail on a bench for mechanics lifetime tests.

Fatigue cracks appeared near the shelf edge and developed normal to it toward the rail wall (Fig. 1).

2. Laboratory experiments

In order to clear up causes of relatively early appearance of fatigue damages of rails, the TU-154M airliner wing mechanics was subjected to laboratory experiments on a bench of lifetime tests.

Strain gauges were glued onto the slat rails in a zone of crack origination on the lower surface of the shelf. Data from these gauges were taken with an interval of 1 sec in the process of bench testing of program loading block. The lower pair of fore rolls was removed from the shelf, since with a slat out, it would damage the strain gauges, and negative loads creating reactions on these rolls were excluded from the loading program (Fig. 1.2). As a roll passes above a strain gauge, distinct peaks of stresses are observed on the sweep of indications of strain gauges in time (Fig. 3) against the background of comparatively small (15...20 kg/mm^2) stresses from a general bending of the rail. These peaks are connected with a local downwarping under the effect of the concentrated contact load from the roll, not taken into account in design calculations. The peak value exceeds the stress of total bending by a factor of 3 - 4 and is the cause of small lifetime of rails.

Attention is engaged by the place of origin of a fatigue crack: it is located about 20 mm from the extreme position of rolls on the rail (with the slat out), where the loads are maximal. This is due to the fact that there is one peak of stresses at the extreme section, and two peaks are in intermediate sections (Fig. 4). One appears with the slat in, and another with the slat out. With the roll displaces from the extreme position the value of maximums decreases, but the spread of an additional cycle increases, so that at some distance the fatigue damage becomes small.

A similar pattern of stresses is on the flap rails. The only difference is that the great thickness of the shelf gave relatively smaller peaks of stresses, and a crack appeared in the extreme section.

3. Identification calculations of stress-strain state of rails

To refine the stressed state of shelf and to study the effect the constructive parameters exert on it, stresses were assessed. The calculated model was a linearly loaded cantilever-fixed plate (Fig. 5). The stresses were calculated by the finite element method, and one-dimension finite elements with a cross-section area of 0.001 mm^2 modelled strain gauges. To identify the finite element models, distribution of relative strains

$$\sigma^0_x = \sigma^{max}_x / \sigma_x$$

were compared where strain gauges are glued (Fig. 5). For a group of strain gauges №. 1-4 and 5-8 we have $\sigma^0_x = \sigma_x - \sigma^1_x / \sigma^4_x - \sigma^1_x$;

$\sigma^0_x = \sigma_x - \sigma^5_x / \sigma^8_x - \sigma^5_x$;

A quite satisfactory correspondence of the calculated model is obtained for a real construction (see Fig. 7).

By means of the finite element model we analyze possible ways to reduce a stress in shelf:

a) an increase in area of shelf-roll contact
- at the cost of increased length of the contact line (roll width);
- at the cost of increased diameter of the roll;

b) an offset of the control platform from shelf edge to rail symmetry plane;

c) an increase in shelf thickness.

An increase in contact line length was modelled with a load spread over four nodes instead of two in the initial version. The effect of roll diameter was estimated by the load spread over four nodes in the longitudinal direction. The contact platform offset was modelled by load movement over nodes in the transverse direction. The efficiency of versions was estimated by the coefficient

$$K_\sigma = \sigma^{max} / \sigma^{max}_u \ ,$$

where σ^{max}, σ^{max}_u are the maximum stresses of the current and initial versions, respectively.

As the length of the contact line increases by a factor of two, we have $K_\sigma \approx 1$, and as the contact area increases by a factor of two, we obtain $K_\sigma \approx 0.94$; thus, a change in width and diameter of the roll very weakly affects the shelf stress state. The change in shelf thickness and offset of contact load appeared to be more efficient:

- a 1-mm increase in thickness decreases K_σ to 0.75;
- a 5-mm offset of contact point from the shelf edge gives $K_\sigma = 0.6$.

Thus, a local bend of the shelf under the effect of the leading roll appears to be crucial for the durability of the wing rails. The greatest effect is exerted by the shelf thickness and distance from roll contact point to rail wall.

4. Flight-strength experiment

In connection with the above-said, loads on slat elements were measured in flight tests. Loads onto fore rolls of carriages 1-6 of the slat were measured by strain bridges, whose active gauges were glued along the upper shelves of the carriages. To obtain dependences of the strain bridge responses from the loads on the fore rolls on bench and during flight, identical calibrations
were carried out with the slats off by means of model rails providing loading of the required carriage (the calibration results obtained by the standard technique seemed to be unacceptable because of transmission of a considerable part of the applied load onto the neighboring nodes of the shed through the slat construction).

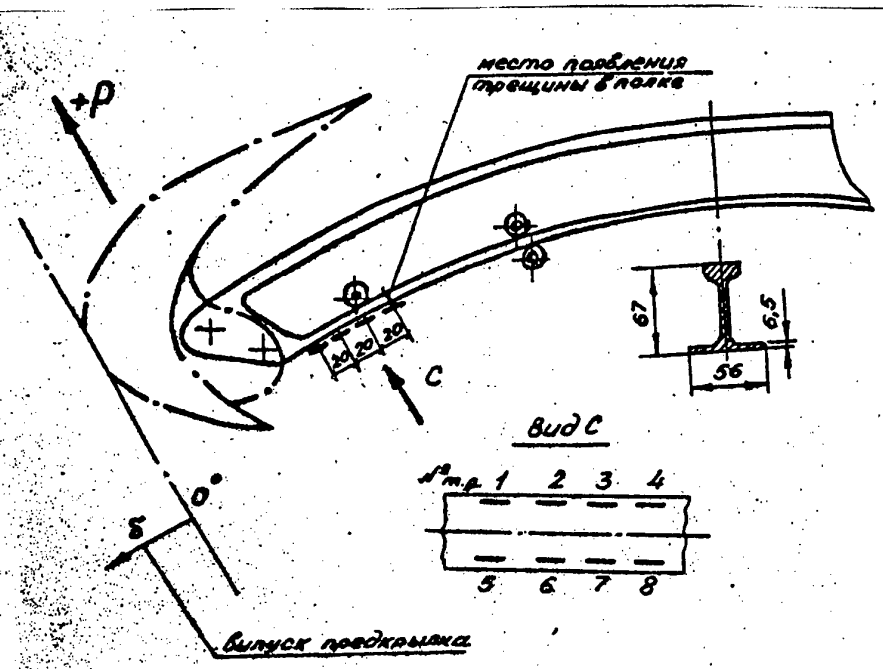

Fig.1 Схема наклейки тензорезисторов на рельсе. (Предкрылок в убранном положении).

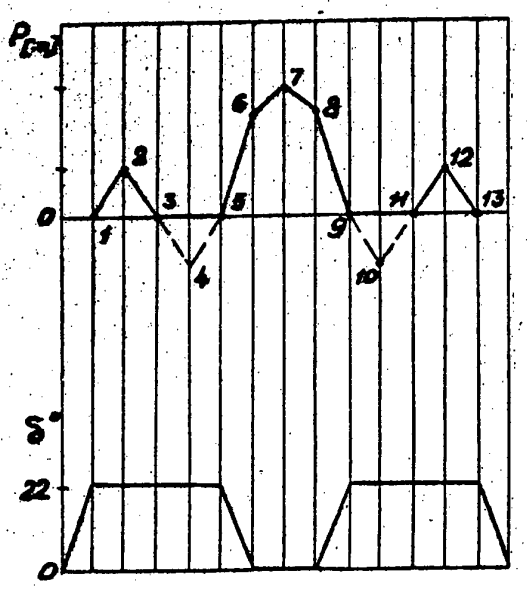

Fig.2 Программный блок.

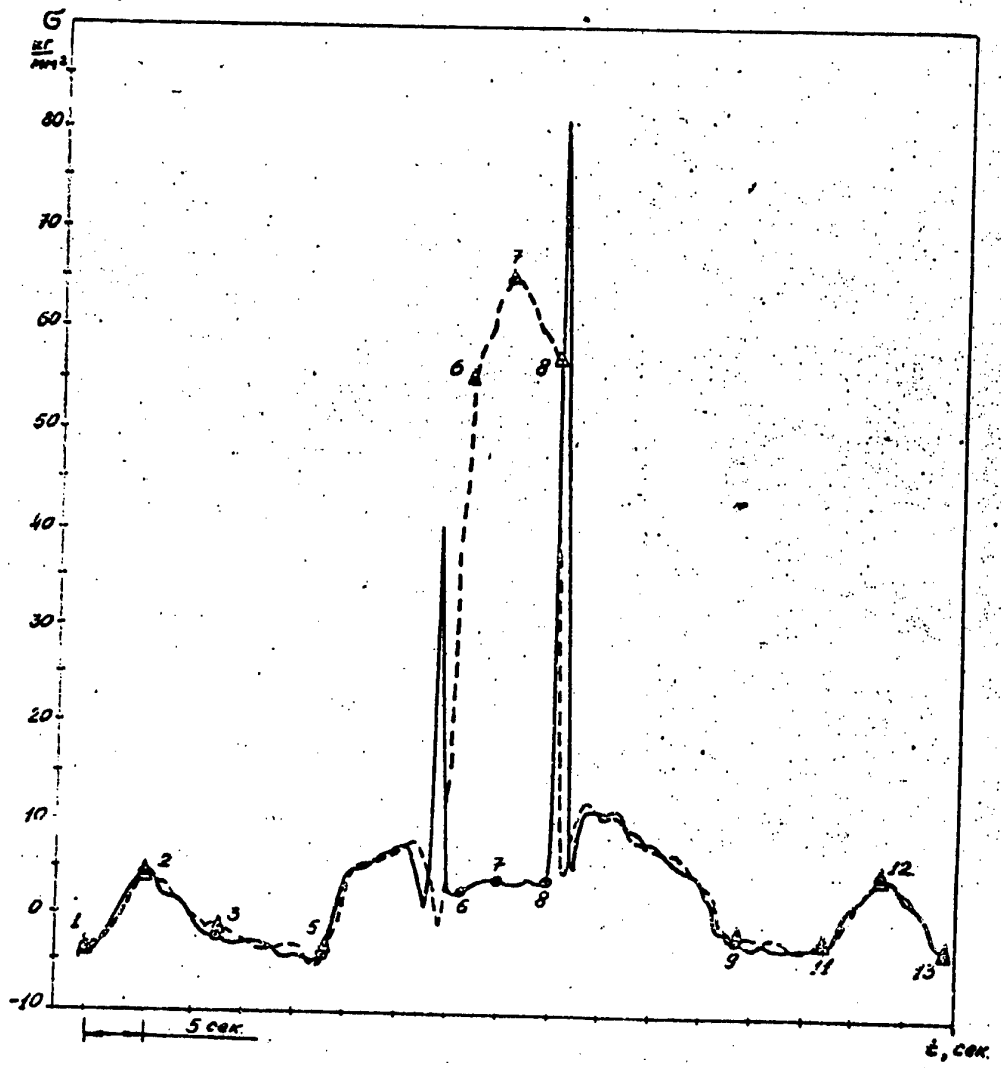

Fig.3

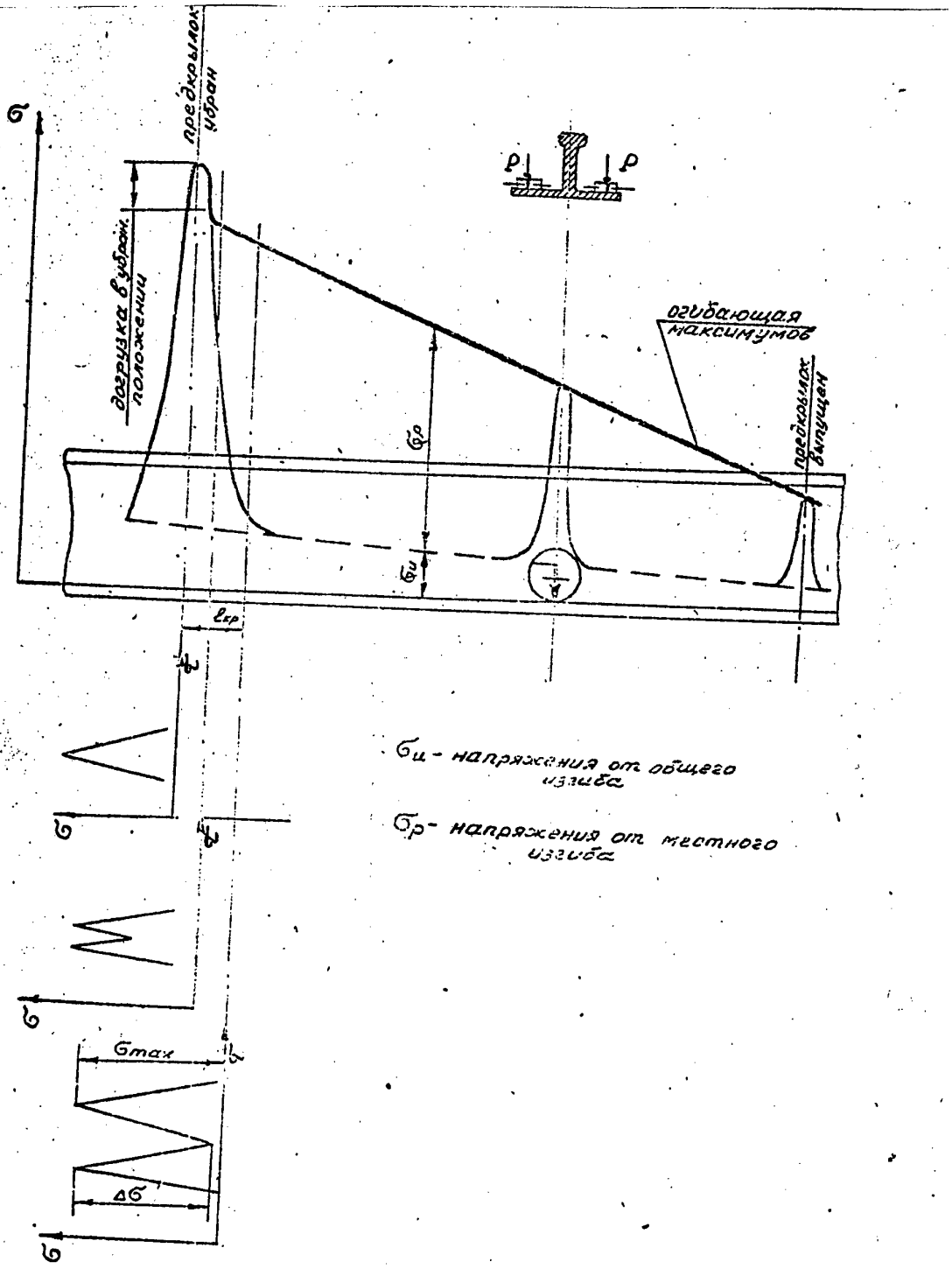

Fig.4 Качественная картина напряженного состояния полки при уборке-выпуске предкрылка.

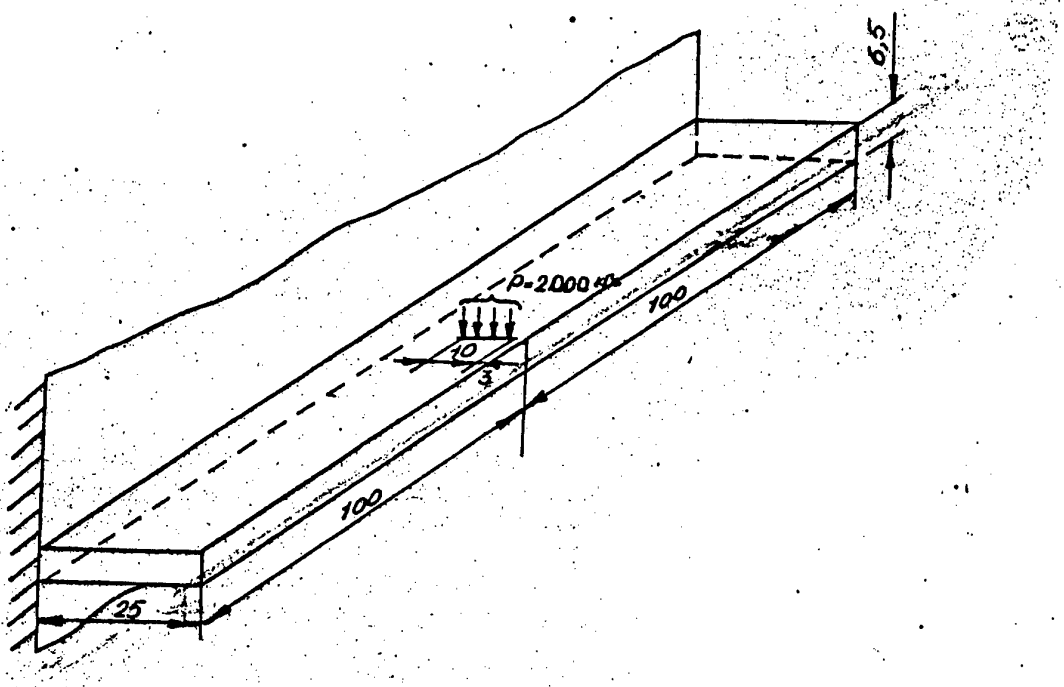

Fig.5 Расчётная схема задачи.

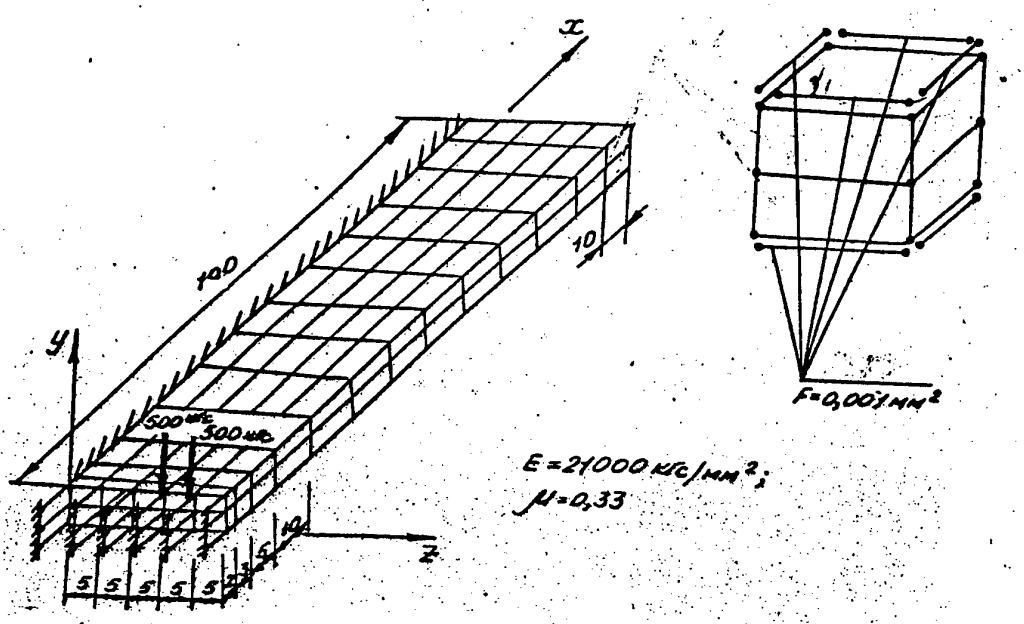

Fig.6 Конечно-элементная модель полки.

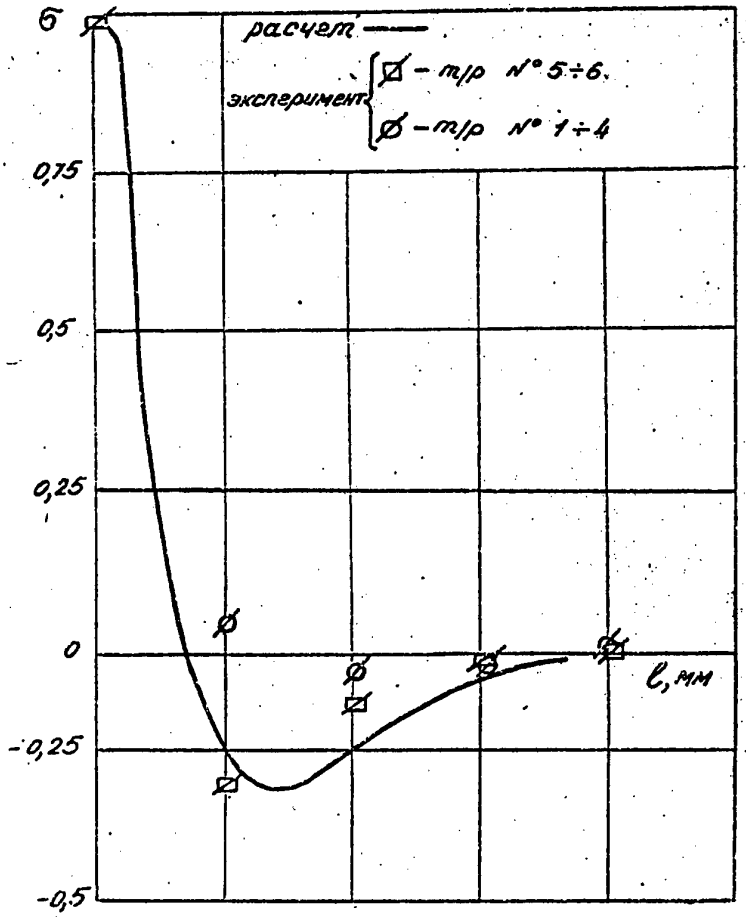

Распределение напряжений от сосредоточенной силы.

Fig.7

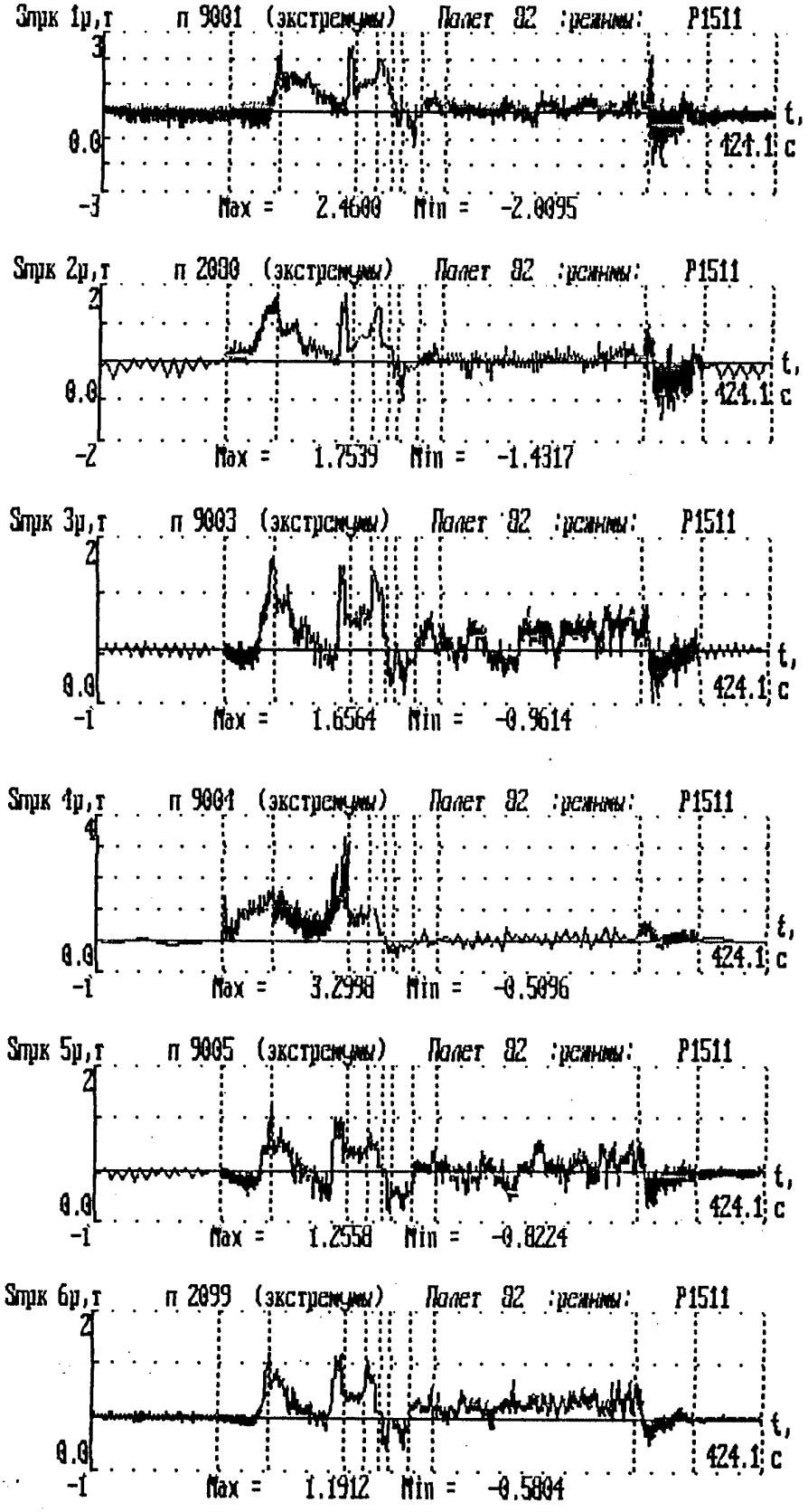

Fig.8 Нагрузки на передние ролики кареток предкрылка Ту-154м б/н 85607 в полете.

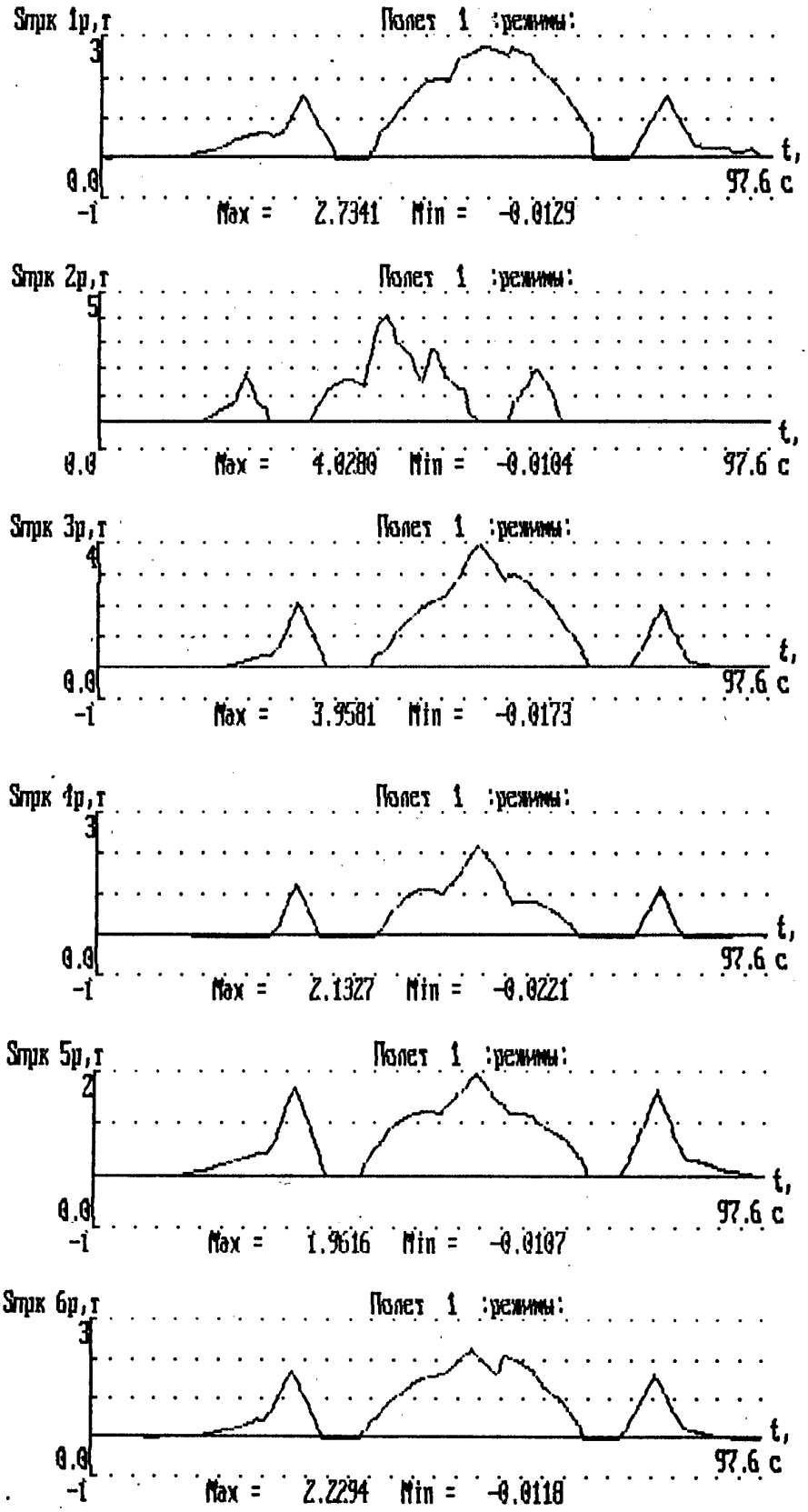

Fig.9 . Нагрузки на передние ролики кареток предкрылка Ту-154м на стенде (программные блоки 1-20450).

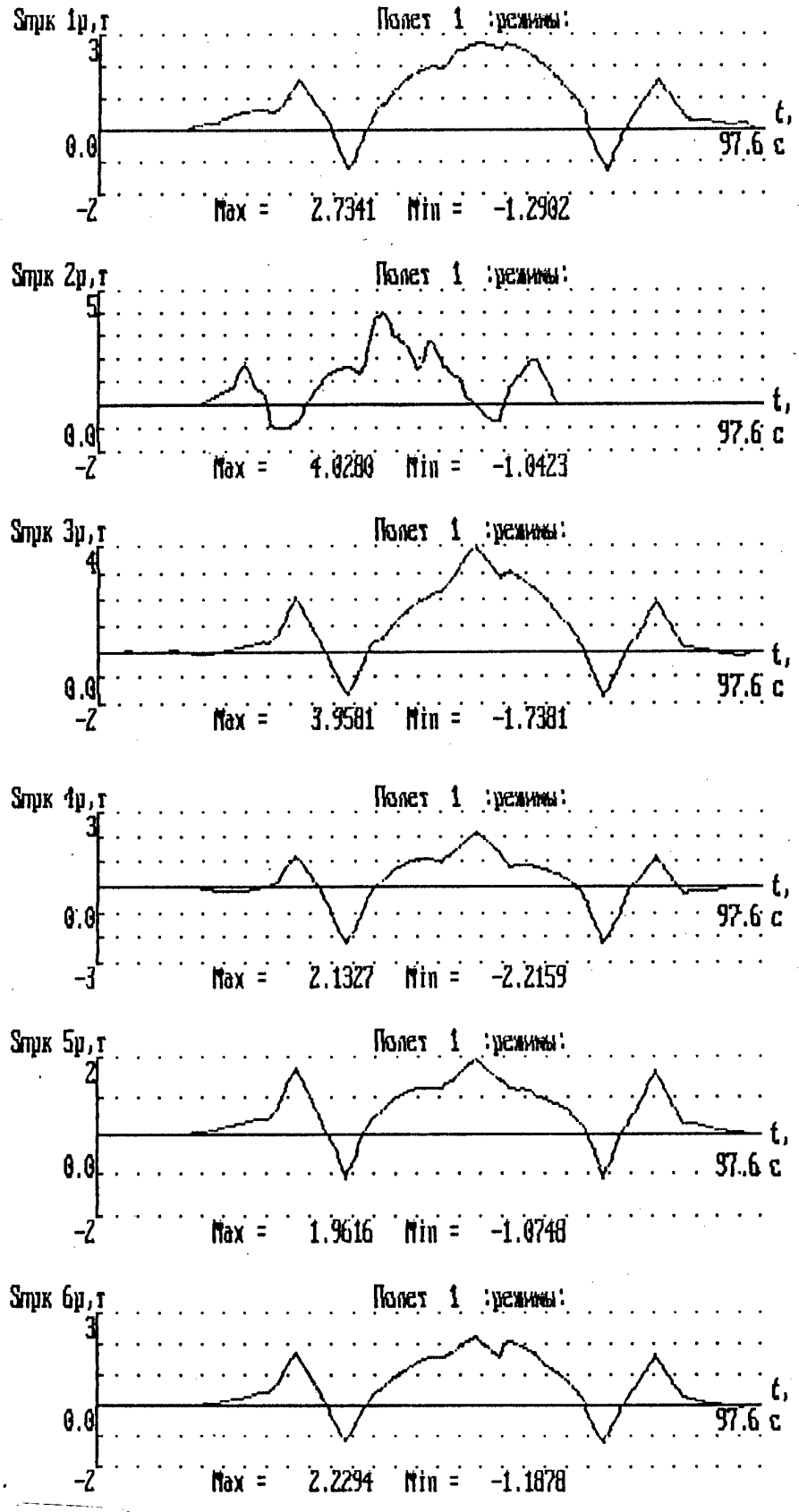

Fig.10 Нагрузки на передние ролики кареток предкрылка Ту-154м на стенде (программные блоки 20451-74392).

Table

№ пар	Название	Наработка на стенде Блок0 (I этап) Блок (II этап) Всего	Эквивалент (m=4)		Наработка в типовых полетах*	
			+N1	-N1	+N1	-N1
9001	Sпрк 1р	20450 53942 74392 Разрушений нет	0.07 0.15	0 0.21	9523	11327
2080	Sпрк 2р	20450 53942 74392 Разрушений нет	1.88 2.93	0 2.50	196496	134855
9003	Sпрк 3р	20450 41720 62170 Разрушение верхних полок	2.72 5.66	0 11.75	291760	490210
9004	Sпрк 4р	20450 53942 74392 Разрушений нет	0.19 0.87	0 15.18	50815	818840
9005	Sпрк 5р	20450 53942 74392 Разрушений нет	1.03 2.18	0 2.31	138660	124600
2099	Sпрк 6р	20450 53942 74392 Разрушений нет	1.50 3.26	0 12.11	206525	653240

* - без учета коэффициента надежности

+N - повреждаемость (наработка) для нижних полок кареток;
- N - повреждаемость (наработка) для верхних полок кареток.

To estimate the effect of secondary loading factors (rail bending), the calibration loads on the slat carriages were reproduced by rail loadings by efforts P_{cal} up and down (normal to the line passing through the axes of fore and back rolls) at two different distances from the fore roll of the carriage.

The calibration results have shown that for the chosen measuring scheme of the strain bridge responses versus loads on the fore rolls of the slat carriages are of linear character and are different for positive and negative loads. The effect of the bending moment in the rail is insignificant. The calibration coefficients for loads of different signs were calculated analytically by the least squares method.

5. Calculation of fatigue vulnerability of rails and equivalents of "program block - flight"

According to measurements in flight and on bench, block-flight equivalents are calculated, and the calculation of construction vulnerability from loads on bench is carried out using a complete record of the slat loading block.

Calculation of construction vulnerability for flight is carried out from records of loads in flight of type profile:

- taxiing out (with the mechanics extracted);
- flight (until take off the runway);
- ascent (until retraction of wing mechanics);
- platform with V_{st} = 540-550 km/hour, mechanics is retracted;
- approach (from beginning of mechanics extraction to landing);
- landing (until turn off the runway);
- taxiing in (with the mechanics retracted);
- flights were carried out according to the Rules of Flight Exploitation of TU-154M.

In calculating, the loads with the slats extracted in the absence of external (or applied) loads were taken to be equal to zero.

Load vulnerability during bumpiness, with the mechanics retracted, was not included into the flight total, because its share corresponding to the mean- statistical repeatability of overloads for a flight did not exceed 3% of vulnerability in take off-landing modes.

The load records on carriages 1-6 of the TU-154M 85607 slat in flight and on bench during testing according to various programs are given in Figs. 8-10, respectively.

On the basis of equivalents and data of durability test records, the running time of slat carriages was calculated for tests on bemch and in flight and tabulated.

6. Conclusions

As a result of the studies carried out on power elements of the wing of airliner, it has been shown that the factor crucial for the rail fatigue resistance is the local bending of shelves from the contact load of the directional roll. The main ways are determined to increase fatigue characteristics of rails. The equivalents of the program of lifetime testing were essentially improved with respect to flight loads.

ANALYSIS AND IMPROVEMENT OF LIFETIME CHARACTERISTICS OF CONSTRUCTIONS OF MANEUVER AIRCRAFTS IN THE PROCESS OF LABORATORY TESTING

V.A.Bespalov, M.I.Ryabinov
SibRIA, Novosibirsk

In the process of laboratory lifetime testing of constructions it is quite important and interesting to establish causes of fatigue failure and to make an a priori forecast of longevity of potentially hazardous zones of construction. These factors are crucial for providing a required level of endurance of a weak assembly and force to take further actions: to change construction parameters and to develop trouble-shooting documentation for the aircrafts under exploitation and control schedules under testing and exploitation.

Methodological scheme of investigations

The many-year practice of lifetime improvement tests of aircraft constructions led the SibRIA to a certain methodological scheme (Fig. 1) of analysis and improvement of lifetime characteristics of maneuver aircraft constructions in the process of laboratory tests.

1. A zone (assembly) of the airframe with a fatigue damage or a potentially hazardous zone of the construction is recognized.

2. A force scheme of the zone under study is compiled on the basis of a preliminary analysis of its functioning in the airframe aggregate system and construction drafts. The force scheme must take into account all the principal factors which may determine loading and fatigue resistance of the zone under study.

3. Based on the force scheme, a mathematical finite-element model (FEM) is developed for the zone with its sufficient discretization. The boundary conditions are determined from the results of tensometry of a full-scale construction with the system of tensometers topologically tied up with the FEM boundaries.

4. Simultaneously with tensometering of FEM boundaries, tensometry is carried out at control points corresponding to the inner region of FEM with problems of model identification taken into account. If the failure to be studied is great and can introduce errors into measurements, the tensometers are placed on the symmetrical intact half of the construction.

5. Using FEM, a local stress-strain state (LSSS) is calculated and difficult-to-measure force factors are estimated more exactly. These factors are: distribution of forces over fastening holes, level of stresses at the edges of loaded holes, etc. as well as a contribution of separate components of boundary conditions into the loading of the critical site of the construction.

6. The force scheme and FEM are identified and refined, resulting in a model adequate to a real construction and full-scale experiment, with an LSSS determined from this model.

7. Using the base fatigue curves and FEM-improved local stresses, the calculated longevity of the destroyed element of the construction is found. If it is close to the experimental value, the failure is determined by the construction parameters and loads specified on designing. If the difference is significant, a further analysis must be carried out to reveal possible mounting stresses, residual technical stresses, defects, etc.

8. Analysis is given to construction-technological factors determining the fatigue resistance of the zone under study. Recommendations are developed to increase the endurance of the weak assembly. The base is an adequate FEM, which permits, on the basis of the calculator's experience, to search for various versions of repair and improvements in the interactive mode of solution.

This scheme was used to analyze and improve lifetime characteristics of design irregularities of the maneuver aircrafts subjected to testing in the Strength Laboratory of SibRIA.

Analysis and improvement of attack plane construction

In the aircraft under consideration one of the lifetime-critical construction element was the back wall of the center section where it is connected with rib 20. The source of fatigue failure was the radial transition of a stiffness rib (Fig. 2). The construction site under study (Fig. 3) was subjected to detailed tensometry on the intact (right) half of the construction. As a result, high stresses (up to 350 MPa) where revealed at the origin of crack. In this case, it is quite evident that for the material AK-4-1chT, of which the wall is made, this level of stresses under exploitation loads is not admissibly high, and the construction is required to be improved. Possible versions are sought through FEM. The calculation scheme of the problem (Fig. 4) is constructed in assumption that the cutting force Q_y is received only by the center section wall and is transmitted to it from the beam of the detachable part of wing (DPW) uniformly at each 5th joint bolt, while the bending moment M_x is also transmitted through bolts with height-linear variation of efforts. The form of FEM in a zone of stress concentration is shown in Fig. 5. Comparison of calculated and experimental stresses for radial transition (Fig. 6) has shown that the model constructed is quite satisfactory to reproduce the stressed state of the construction at the origin of crack. Consideration and analysis of the calculated LSSS permitted us to state that the high concentration of stresses in the radial transition is determined by a combination of the following factors:

- shear strain of the wall and angle opening between ribs under the effect of cutting force Q_y;
- extension of the lower belt under the effect of the bending momentum M_x through the lower joint bolt;
- out-of-center extension of the vertical rib.

Separate calculation of LSSS from Q_y and M_x showed that 75% of the stress concentration in the radial transition is determined by the cutting force; the scheme of strains in Fig. 7 illustrates this fact. The calculations provided a way to improve the construction. The most reasonable way is to decrease the concentration of stresses by increasing the wall thickness, because it is the wall that receives the cutting force. In the admitted version of improvement (Fig. 8), not only the wall thickness is increased but also vertical rib thickness and radial transition. As a result, the stress concentration was decreased by 29% as compared with the initial one.

Another critical zone was the joint comb of the lower board of the DPW (Fig. 9). The fatigue crack on the surface in the main focus of fatigue failure was 210 mm long; in

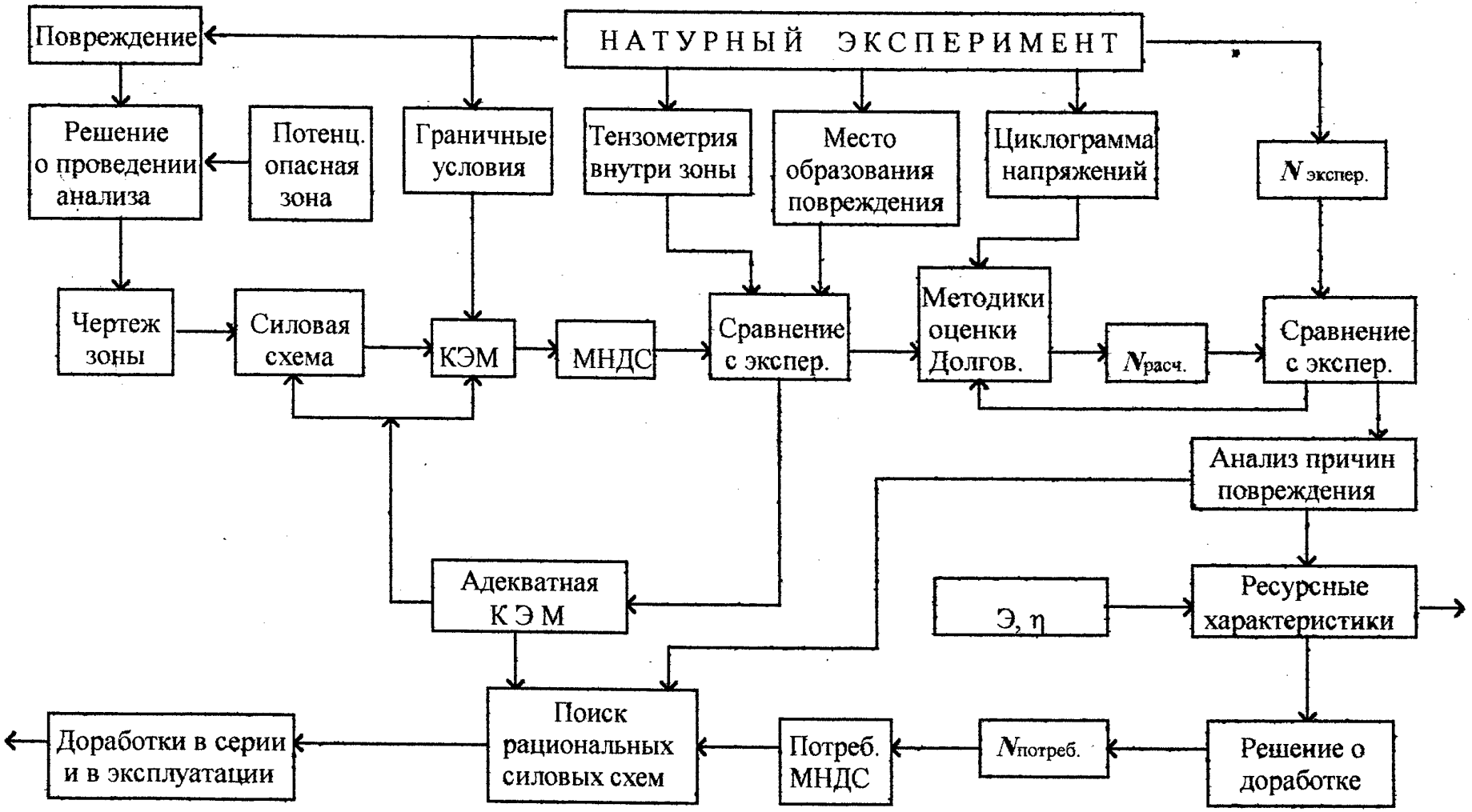

Fig.1 Схема исследований по анализу и доводке ресурсных характеристик испытываемых авиаконструкций.

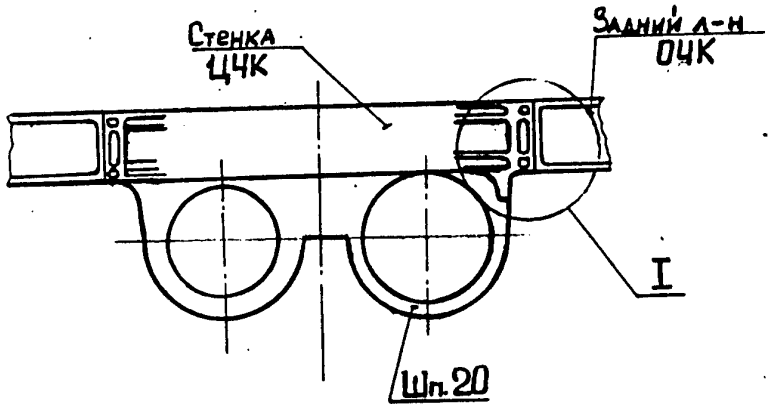

I

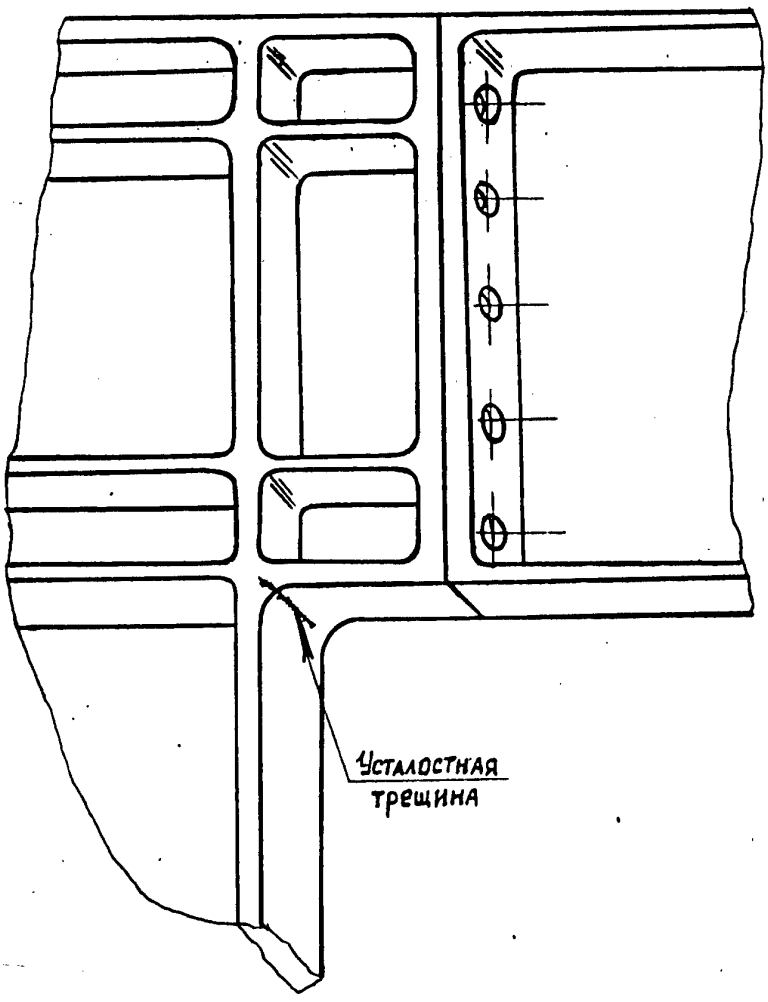

Fig.2

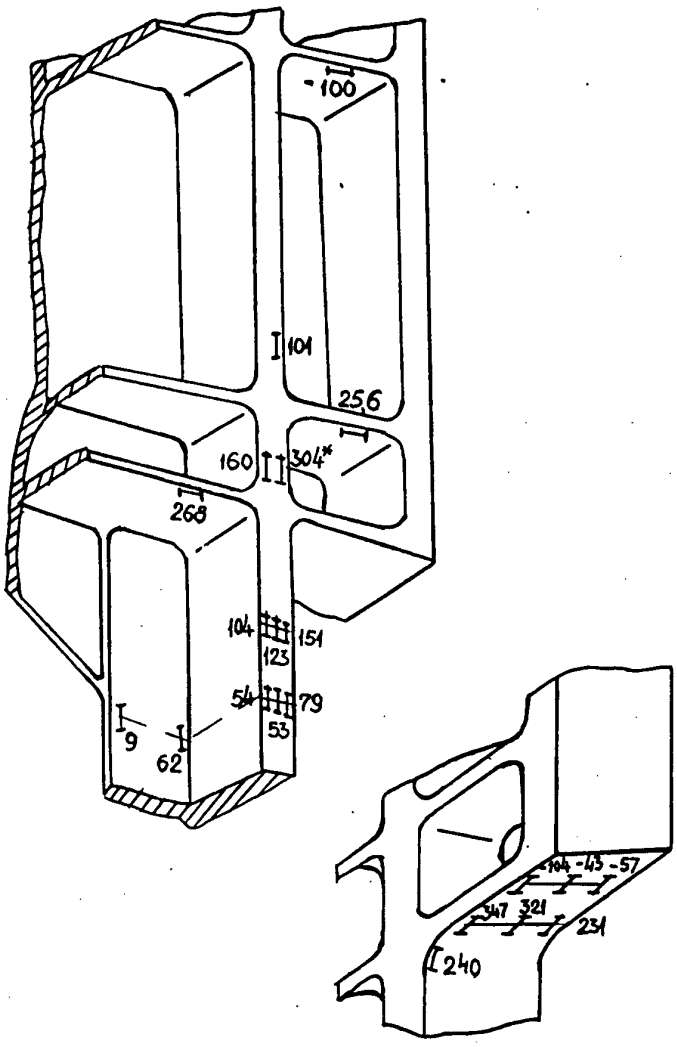
100
101
256
160
304*
268
104
123
151
54
79
53
9
62
104
45
57
347
321
231
240

Fig.3

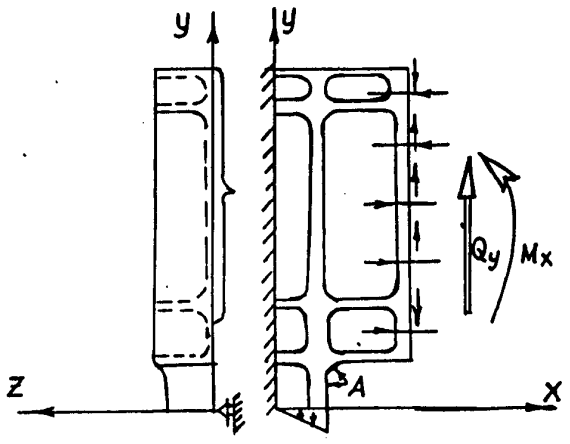
y
y
Qy
Mx
z
A
x

Fig.4

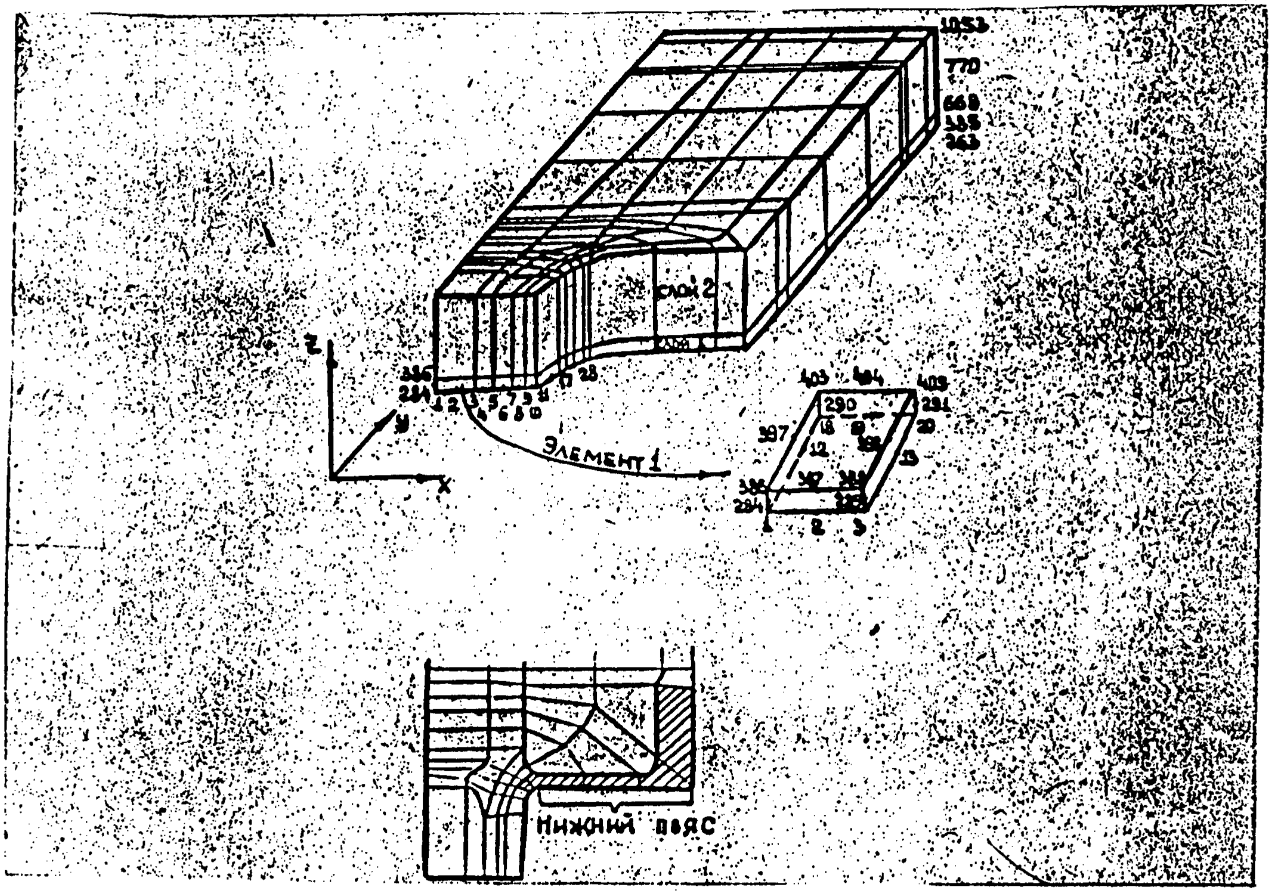

Fig.5

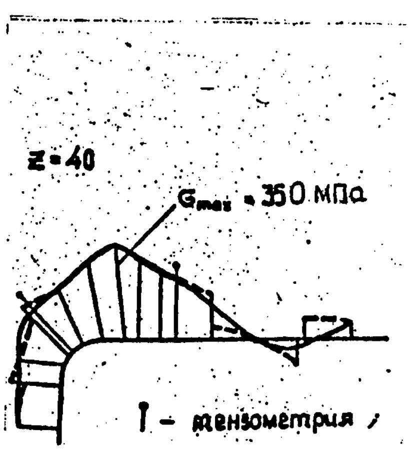

Fig.6

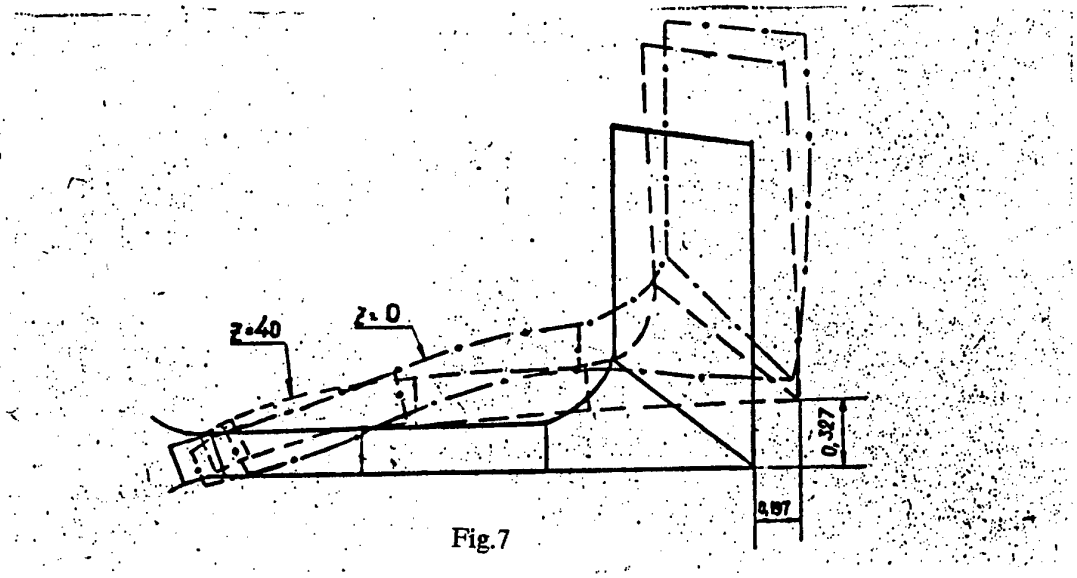

Fig.7

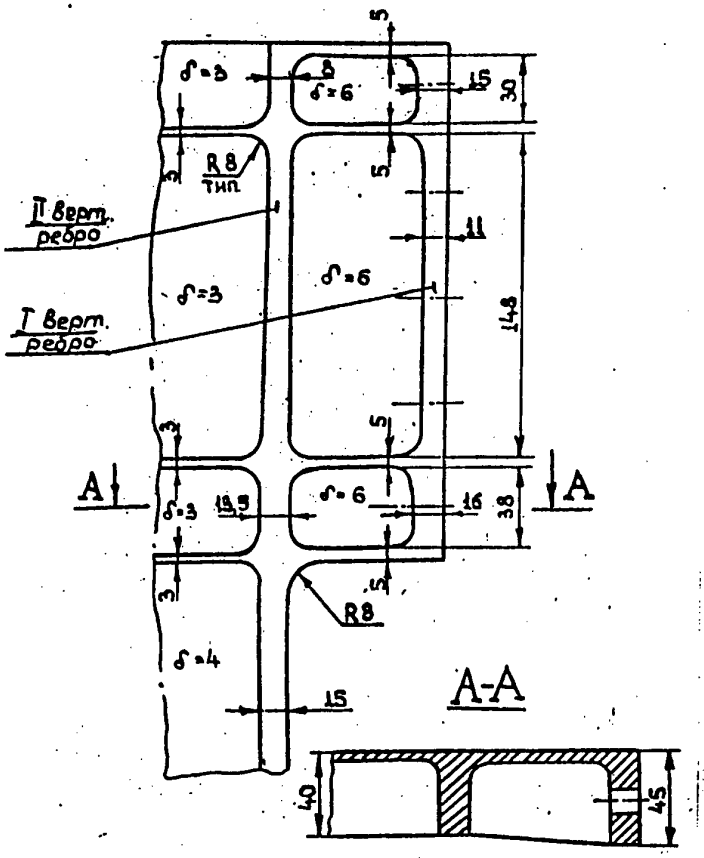

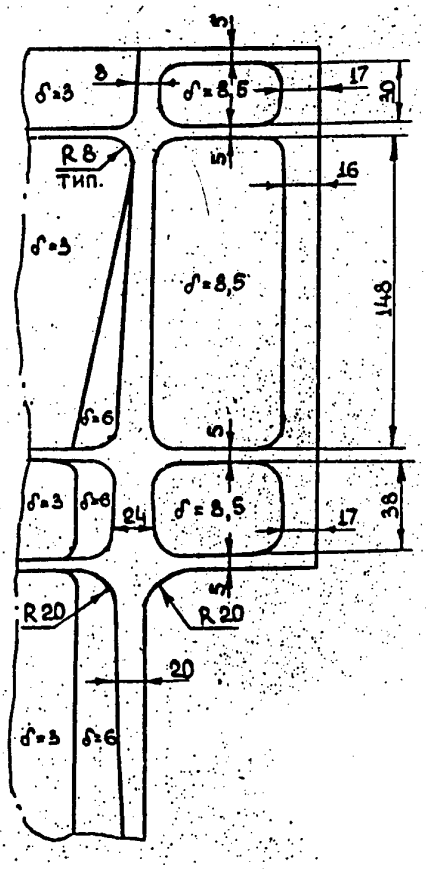

Исходная конструкция.

Доработка

Fig.8

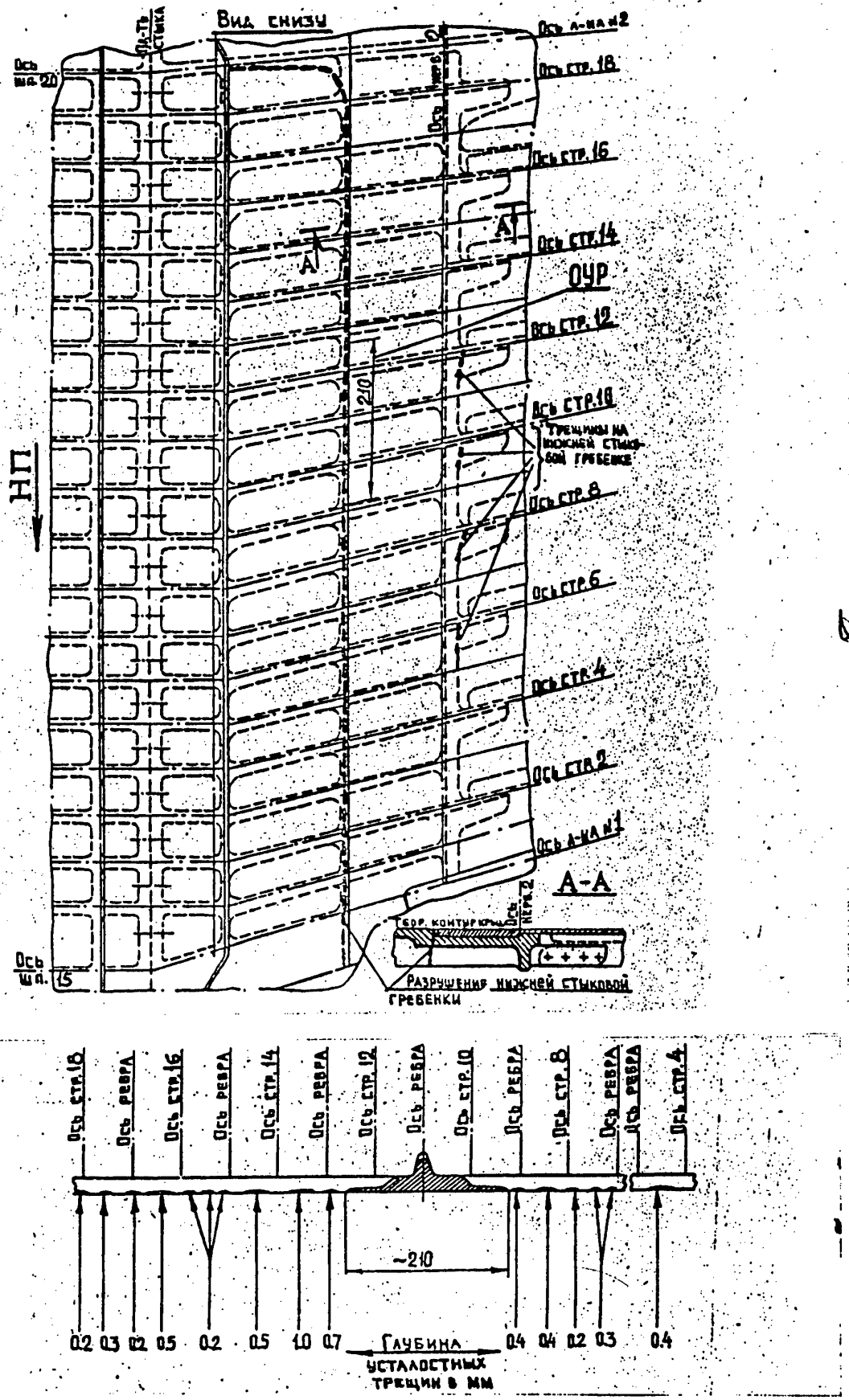
Вид снизу
Ось ш.20
Ось ш.15
Ось стр.18
Ось стр.16
Ось стр.14
Ось стр.12
Ось стр.10
Ось стр.8
Ось стр.6
Ось стр.4
Ось стр.2
Ось А-КА №2
Ось А-КА №1
ОЧР
НП
210
А-А
Трещины на нижней стыковой гребенке
Разрушения нижней стыковой гребенки
Ось ребра
~210
0.2 0.3 0.2 0.5 0.2 0.5 1.0 0.7
0.4 0.4 0.2 0.3 0.4
Глубина усталостных трещин в мм

Fig.9

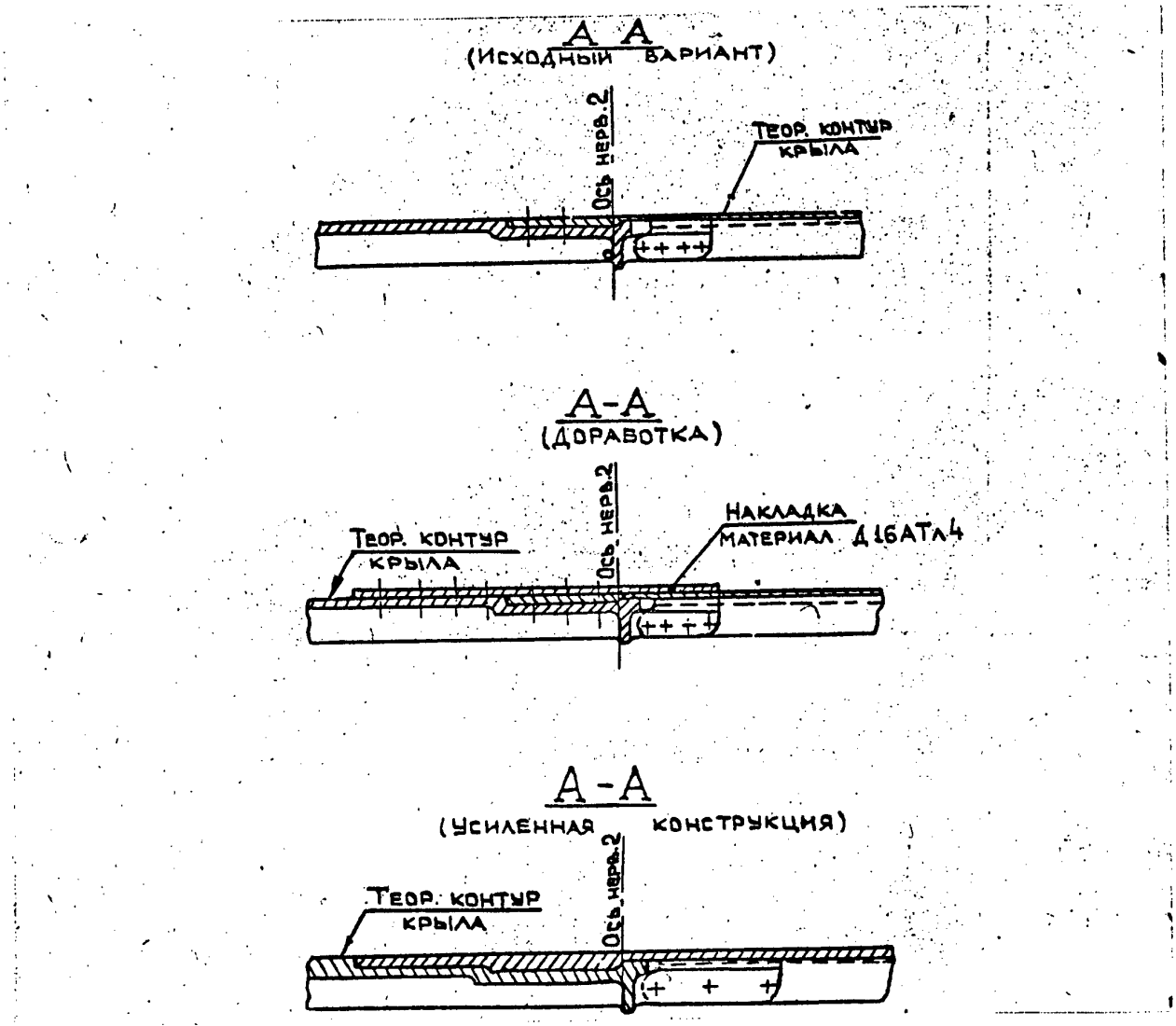
А А
(Исходный вариант)
Ось нерв.2
Теор. контур крыла
А-А
(Доработка)
Ось нерв.2
Теор. контур крыла
Накладка
Материал Д16АТ∧4
А-А
(Усиленная конструкция)
Ось нерв.2
Теор. контур крыла

Fig.10

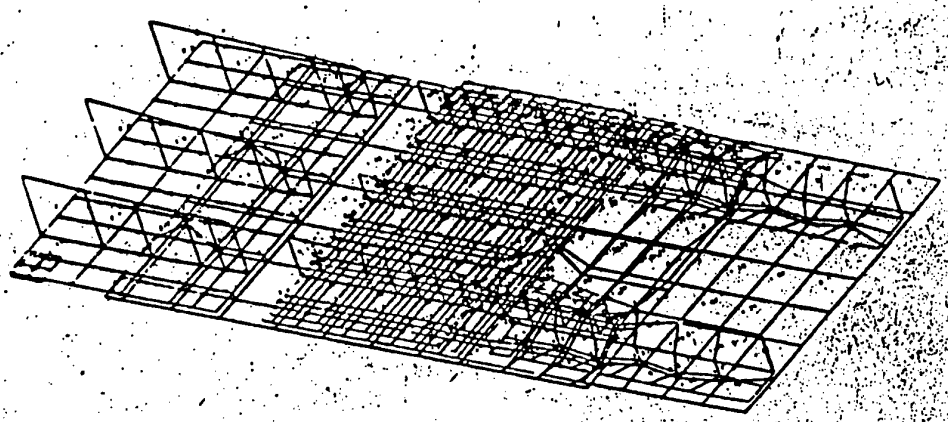

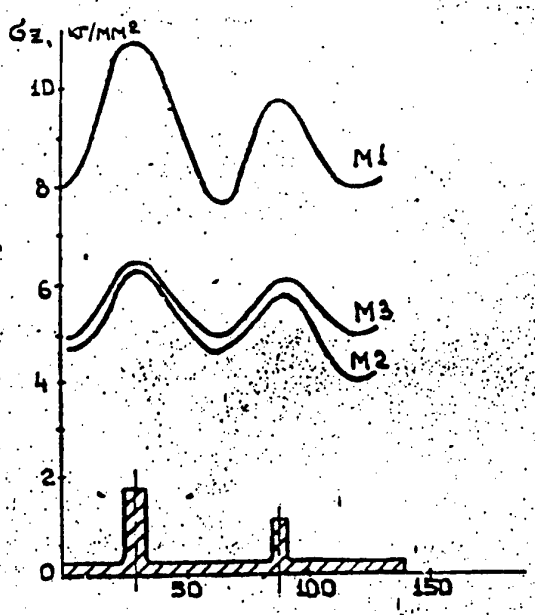
σz, кг/мм²
10
8
6
4
2
0
M1
M3
M2
50
100
150

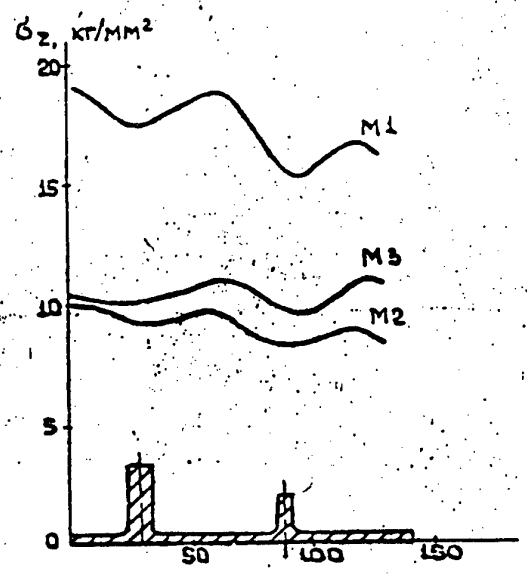
σz, кг/мм²
20
15
10
5
0
M1
M3
M2
50
100
150

Fig.11

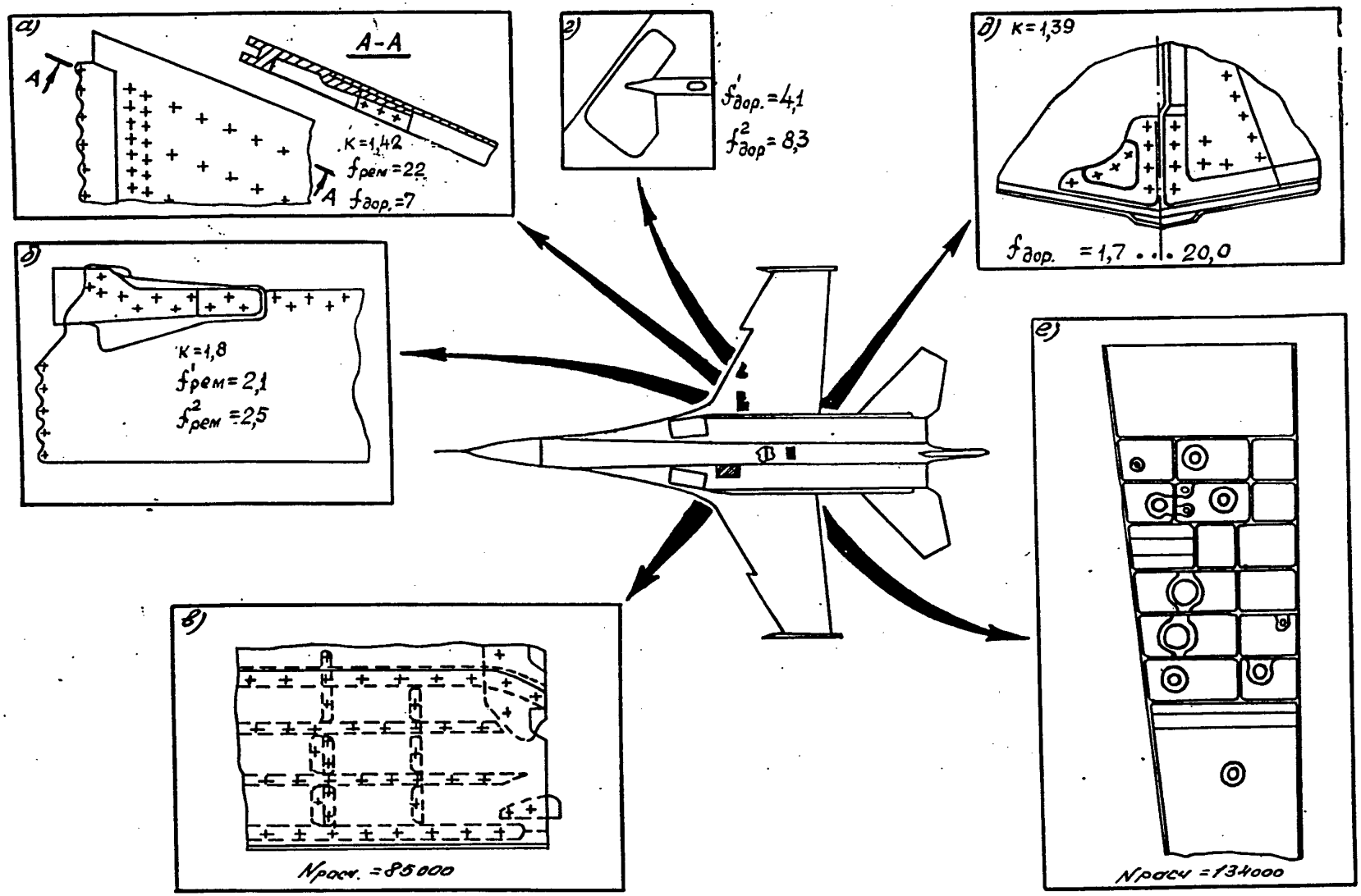
а)
А-А
А
А
К=1,42
$f_{рем}$=22
$f_{доп.}$=7
г)
$f'_{доп.}$=4,1
$f^2_{доп}$=8,3
д) К=1,39
$f_{доп.}$ =1,7 . . . 20,0
б)
К=1,8
$f'_{рем}$=2,1
$f^2_{рем}$=2,5
в)
$N_{расч.}$=85000
е)
$N_{расч}$=134000

Fig.12

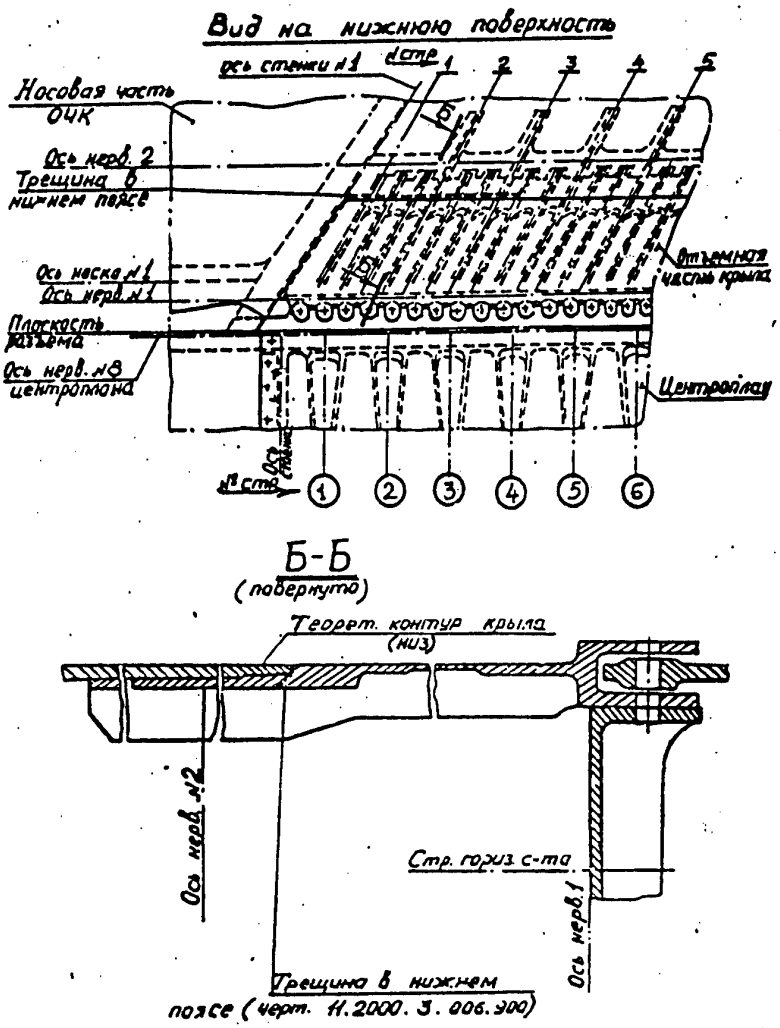
Вид на нижнюю поверхность
ось стенки №1
Носовая часть ОЧК
Ось нерв. 2
Трещина в нижнем поясе
Ось носка №1
Ось нерв. №1
Плоскость разъема
Ось нерв. №8 центроплана
Отъемная часть крыла
Центроплан
Б-Б
(повернуто)
Теорет. контур крыла (низ)
Ось нерв. №2
Стр. гориз. с-та
Ось нерв. 1
Трещина в нижнем поясе (черт. М.2000. 3. 006.900)

Fig.13

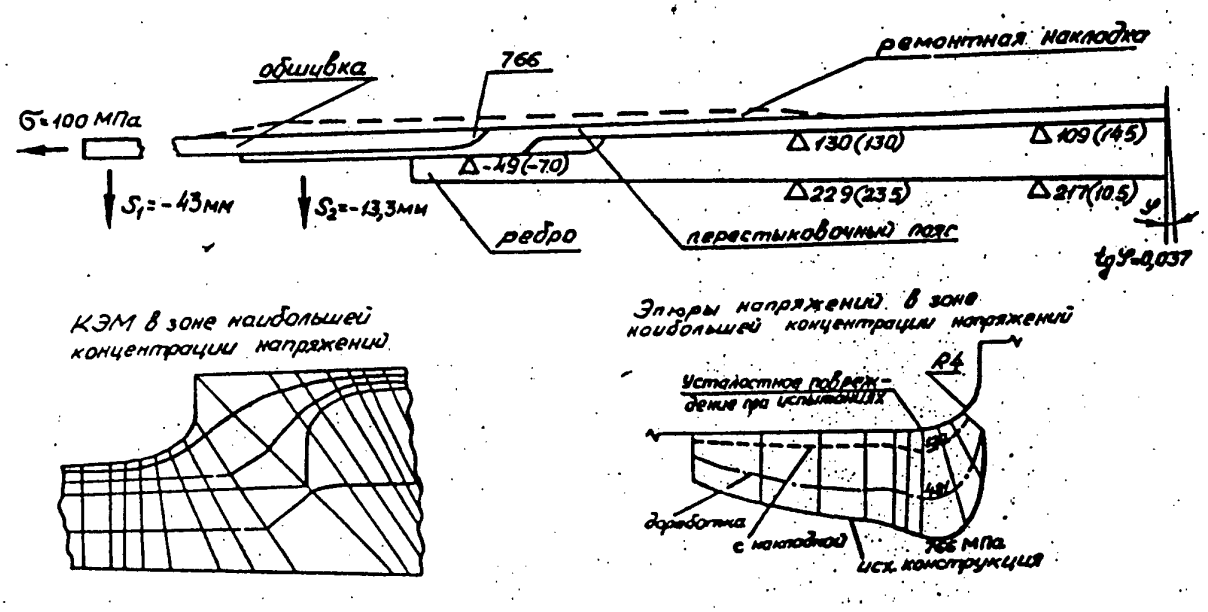
обшивка
766
ремонтная накладка
σ=100 МПа
Δ130(130)
Δ109(145)
Δ-49(-70)
Δ229(235)
Δ211(105)
S1=-43мм
S2=-13,3мм
ребро
перестыковочный пояс
tgγ=0,037
КЭМ в зоне наибольшей концентрации напряжений
Эпюры напряжений в зоне наибольшей концентрации напряжений
R4
Усталостное повреждение при испытаниях
59
48
доработка
с накладкой
766 МПа
исх. конструкция

Fig.14

Зона	Без накл. σ, МПа	
	Расч.	тенз.
1	220	244
2	182	165
3	203	180
4	213	157
5	180	137

Зона	Короткая накл. σ, МПа		
	расч.	лев.б.	пр.б.
8	69	110	19
9	66	67	62
11	78	127	96
12	74	156	115

Зона	Длинная накл. σ, МПа		
	расч.	лев.б.	пр.б
6	220	280	323
7	186	310	84
8	375	410	161
9	310	62	140
10	127	159	104
11	119	160	64
12	116	191	103
13	155	163	131

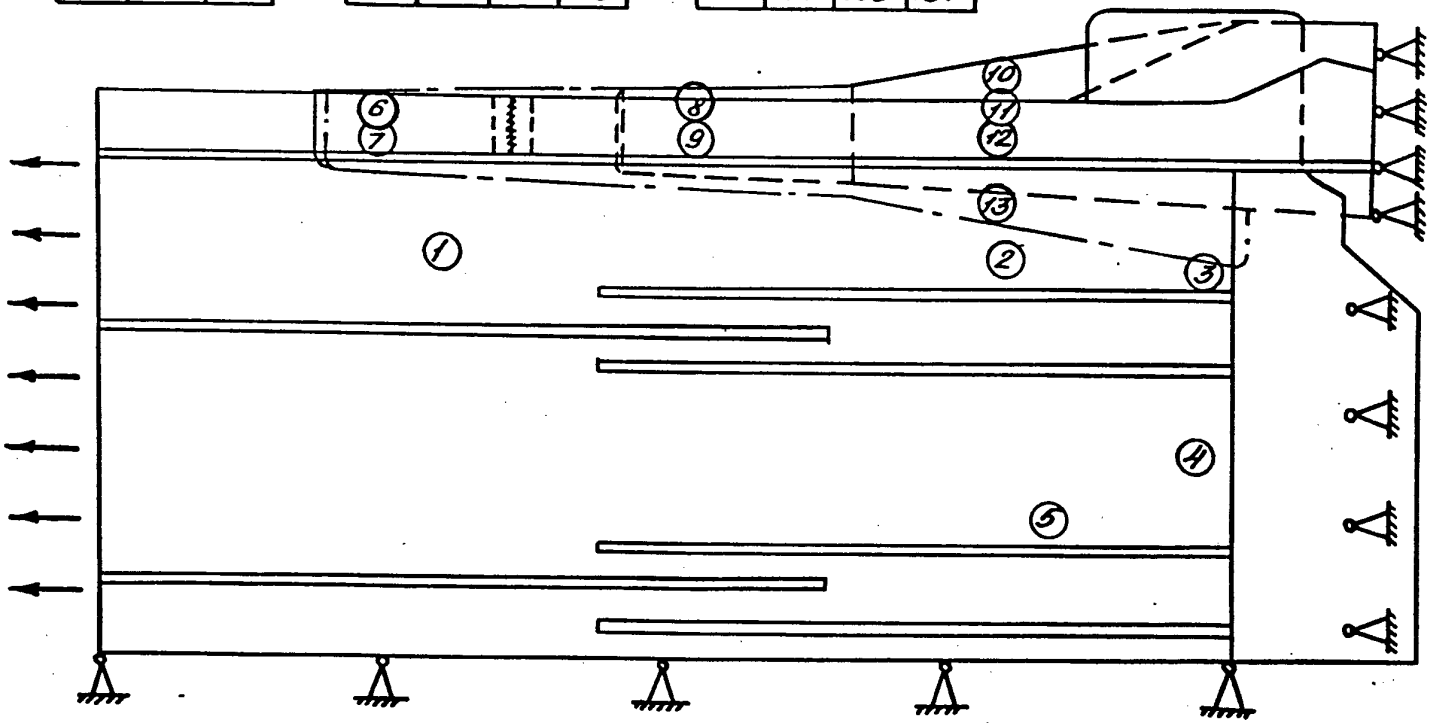

Fig.15

addition, a number of discontinuous cracks 0.2 ÷1.0 nm deep were revealed by fractography.

The comb is a milled construction of variable thickness of the material AK4-T1 with stiffness ribs.

Three versions of constructions were investigated(Fig.10):

- initial (M1);
- improved version for the aircrafts in exploitation with a preventive outer patch (M2);
- increased series version (M3) with an altered zone where stringers join with comb ribs and with increased thickness of skin and comb in the zone of joining.

Figure 11 shows the FEM of the initial construction where the comb joins with the skin and stringers. It was basic for obtaining modified FEM's of the improved versions.

The calculation results for the three versions in two sections of the comb are given in the same figure.

The repaired version decreases the stress level in the most dangerous zone by a factor of 1.9 as compared with the initial construction (the longevity is increased by a factor of about ≈ 13); the version of series improvement decreases the stress level by a factor of 1.7, thus increasing the longevity by a factor of eight.

Analysis and improvement of airframe constructions to dominate in the air

A great deal of works on improvement of lifetime characteristics were performed with the airframe of pre-series aircrafts to gain predominance in the air. Figure 12 shows zones of investigations and the results obtained. Here $k = N_{calc}/N_{exp}$ is the ratio of the calculated longevity of the zone to the experimental result, i.e. the coefficient of calculation-to-experiment correspondence; $f_{rep} = N_{rep}/N_{init}$ and $f_{imp} = N_{imp}/N_{init}$ are coefficients of the efficiency of repairs and improvements, respectively; N is calculated values.

A quite serious fatigue failure was obtained when testing an airframe of the first series: the crack originated in the lower DPW contact belt made of Ti alloy where it is cut beneath its connection with the riveted board (Fig. 13). The failure hazard is caused by the fact that potential defects of these constructions were expressed here: a high velocity of crack growth in Ti alloys plus tendency to discontinuous cracks and hindered visual control.

Versions of improvement and estimation of a local SSS at the contact were sought by means of a two-dimensional FEM (Fig. 14). A 40-mm-wide band along the wing was considered, which contained a rib and a related stringer. The kinematic boundary conditions were determined from the general calculated SSS of the wing obtained in the process of designing, while the force boundary conditions were determined from tensometry of the right (intact) console.

The SSS calculations show that the critical factor for failure is a local bending of the belt resulting from the force transmission eccentricity. In the interactive mode by means of FEM dimensions and thicknesses of stiffness ribs were selected, as well as band thicknesses in the cutting zone, permitting the zone longevity to be increased by a factor of seven. For the aircrafts available the contacts are proposed to be preventively repaired by overlapping of a 6-mm-thick patch of Al alloy, thus hindering the appearance of cracks in the belt.

In the course of testing of a preproduction aircraft, fatigue cracks were observed in the lower board of the center section, which develop from the bolt hole for fixing the board skin to the wall shelf. The early origination of damages is caused by a joint effect of

three stress concentrators of the loaded hole situated in the zone of welded suture, the welded suture itself, and submilling.

The calculation of LSSS (a scheme in Fig. 15) has shown that the setting of a short steel patch on the board in the zone of contact of center section with the DPW leads to accelerated appearance of damages. In this connection a version was considered with enlarged patch overlapping the welded suture. This increases the longevity by a factor of 2.1, and when the fitting is out of the zone of welded suture the longevity is increased by a factor of 2.5.

One of the construction elements with the lowest characteristics of fatigue resistance is a junction of center section boards (Fig. 18) on the plane of aircraft symmetry. During tests a fatigue crack formed in the shelf of wall 3 of center section from the bolt hole of the lower board fitting. Figures 19a and 20 show a sketch and a calculated scheme of the initial junction construction, respectively. The digits stand for:

1. - rib shelf (material V95T)
2. - junction band (V95T)
3. - patch (VT-20)
4. - center section board (OT-4)
5. - wall 3 (V95pchT2).

Figure 19 shows a change of extending stresses and crumpling forces in the shelf of wall 3 (curves 1). The coefficient is k = 1.39. Because the longevity obtained during tests is much less than the technical requirements to the airframe lifetime, the aircrafts under exploitation were improved: the wall was reinforced with two fittings 6 and 7 (Fig. 17b). The stress level in the shelf of the wall is somewhat decreased, but crumpling forces increase -- curves 2 in Fig. 21. An increase in calculated longevity is $f_{imp} = 1.7$.

In the construction of newly produced aircrafts (series version) the wall thicknesses were increased: from 4 mm to 8..10 mm in the shelf, from 1.8 mm to 3..4 mm in the cloth; the board thickness above the wall shelf is increased from 3.5 mm to 6 mm. In addition, the frame of manhole 8 (Fig. 17c) in the non-power skin of the central section of the fuselage rejoins projecting edges of the lower boards of the center section. Values of stresses and crumpling forces decreased very much -- curves 1 in Fig. 20, $f_{imp} = 7.8$.

In the version of increased junction for the aircrafts under exploitation the longevity may be increased by a factor of 12.5 with patch 9 (Fig. 7d) binding not only patches 1 on two sides but also boards of the center section. The stresses and crumpling efforts in the shelf are given in Fig. 19 (curve 3). The longevity appears still higher (f_{imp} = 20), with no fitting 6. The LSSS components for this case are shown by curves 4 in Fig. 21.

For the series version of junction improvement the wall loading may be decreased by emplacing a thicker patch made of Ti alloy instead of the duraluminum frame of the fuselage manhole. Curves 2 in Fig. 20 reflect the LSSS of the wall shelf, $f_{imp} = 11.4$. A further increase in f_{imp} up to 20 may be reached by increasing the wall thickness near the fitting hole, the first to the aircraft symmetry plane, from 10 mm to 14 mm, and near the second hole from 10 mm to 12 mm (curves 3 in Fig. 20).

Calculation of potentially hazardous zones

From the point of view of endurability a junction of the upper board of the fuel tank with the center section board seem to be potentially hazardous (Fig. 12c). Its work is distinguished by the presence of considerable forces of crumpling, P_{cr}, under the board

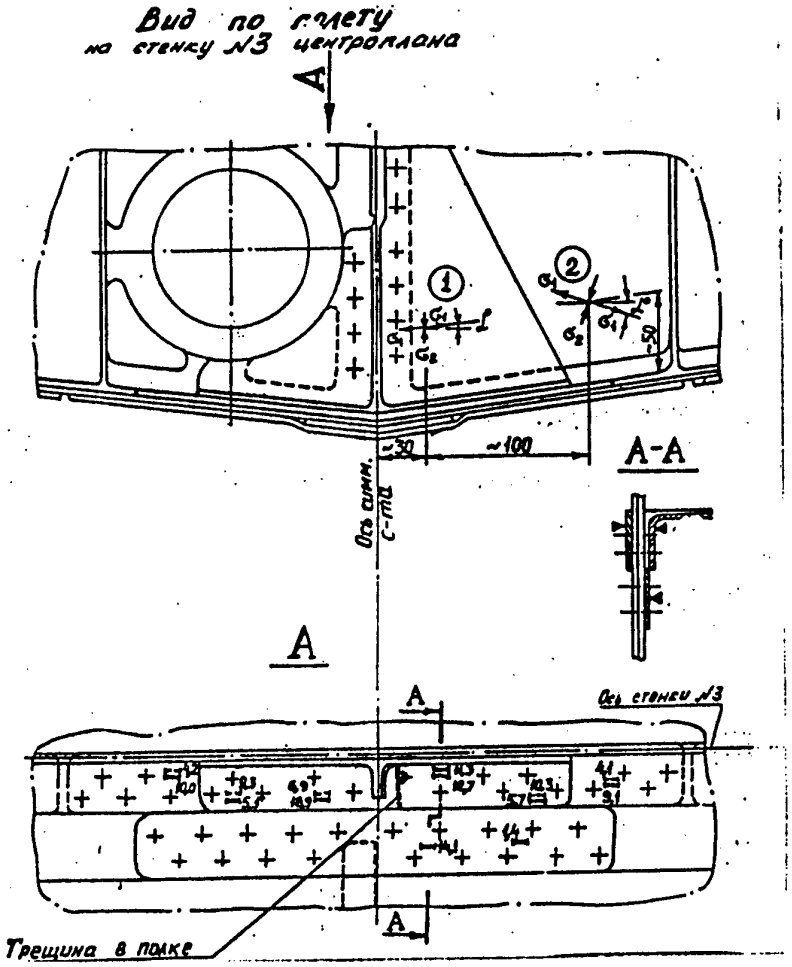

№ площ.	σ_1	σ_2	τ_{max}	α°	σ_x	σ_y	τ_{xy}
1	38	-34	36	3,2°	38	-33	4
2	120	-20	70	-17,1°	107	-8	-39

Fig.16

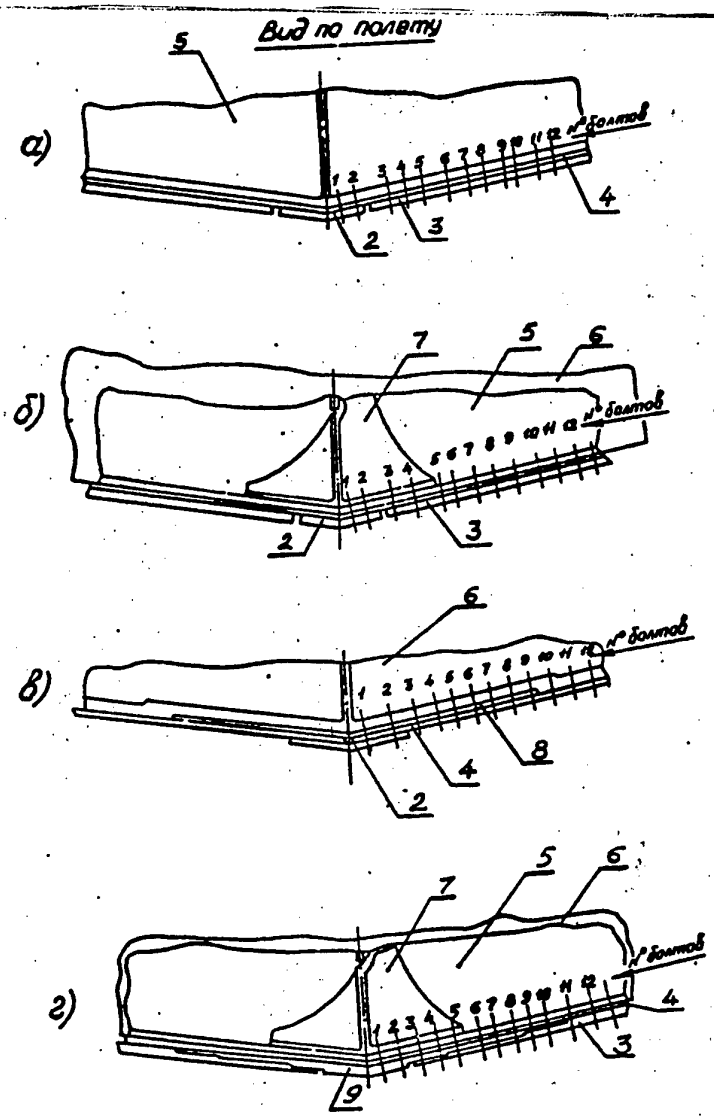

Fig.17

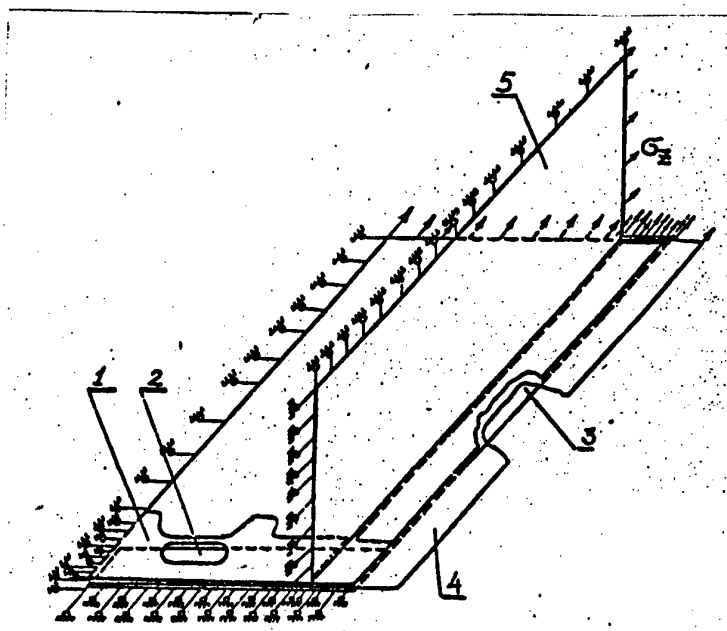
5
σ_z
1
2
3
4

Fig.18

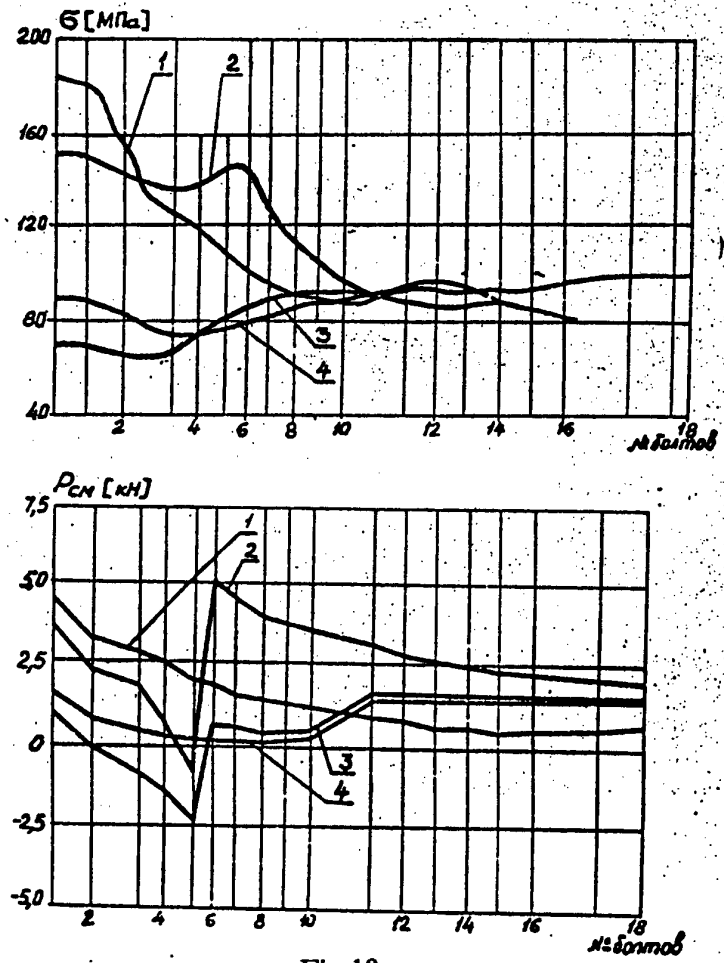
σ [МПа]
200
160
120
80
40
1
2
3
4
2
4
6
8
10
12
14
16
18
№ болтов
$P_{СН}$ [кН]
7,5
5,0
2,5
0
-2,5
-5,0
1
2
3
4
2
4
6
8
10
12
14
16
18
№ болтов

Fig.19

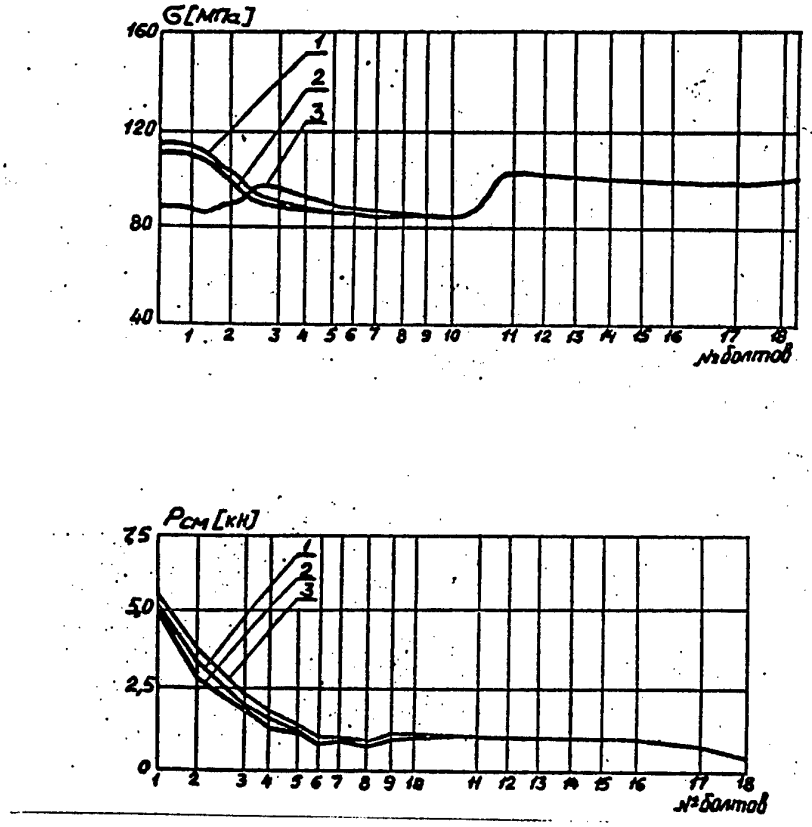
σ[МПа]
160
120
80
40
1
2
3
1 2 3 4 5 6 7 8 9 10 11 12 13 14 15 16 17 18
№болтов
Рсм[кН]
75
50
2,5
0
1
2
3
1 2 3 4 5 6 7 8 9 10 11 12 13 14 15 16 17 18
№болтов

Fig.20

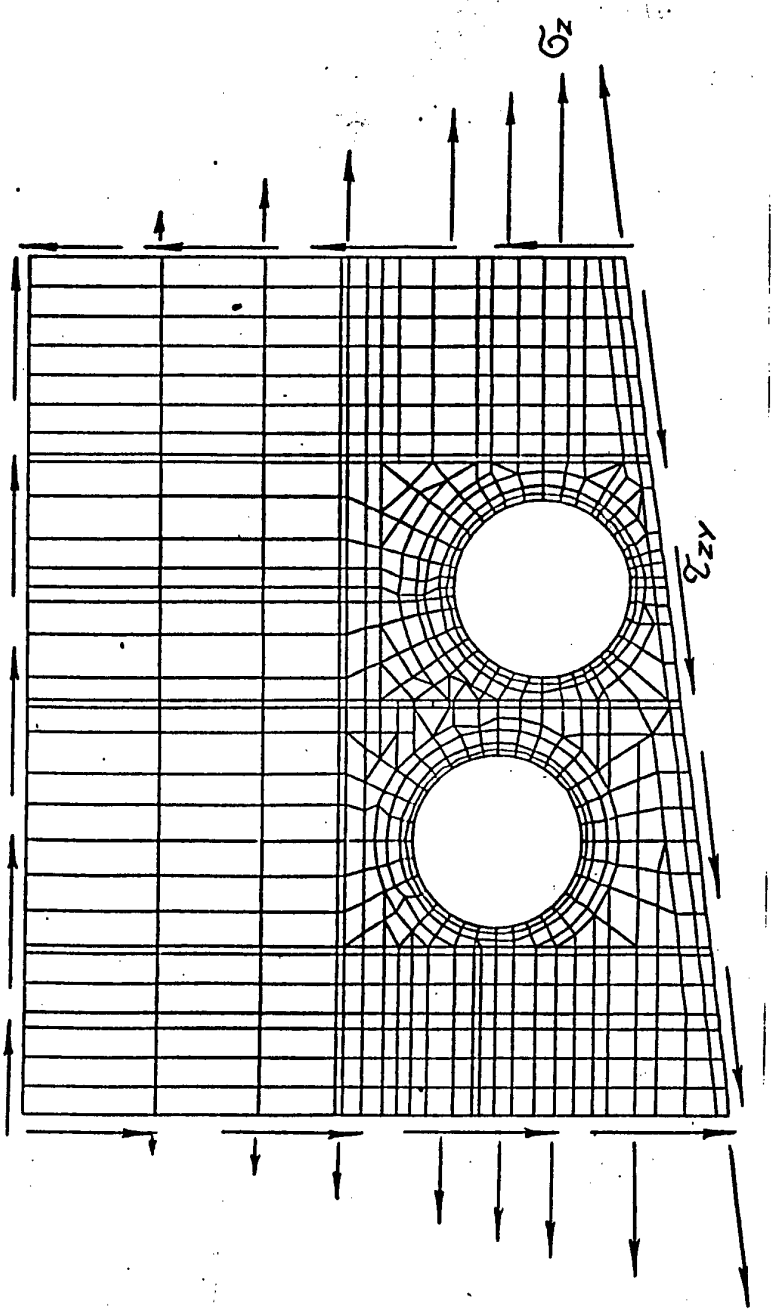

Fig.21

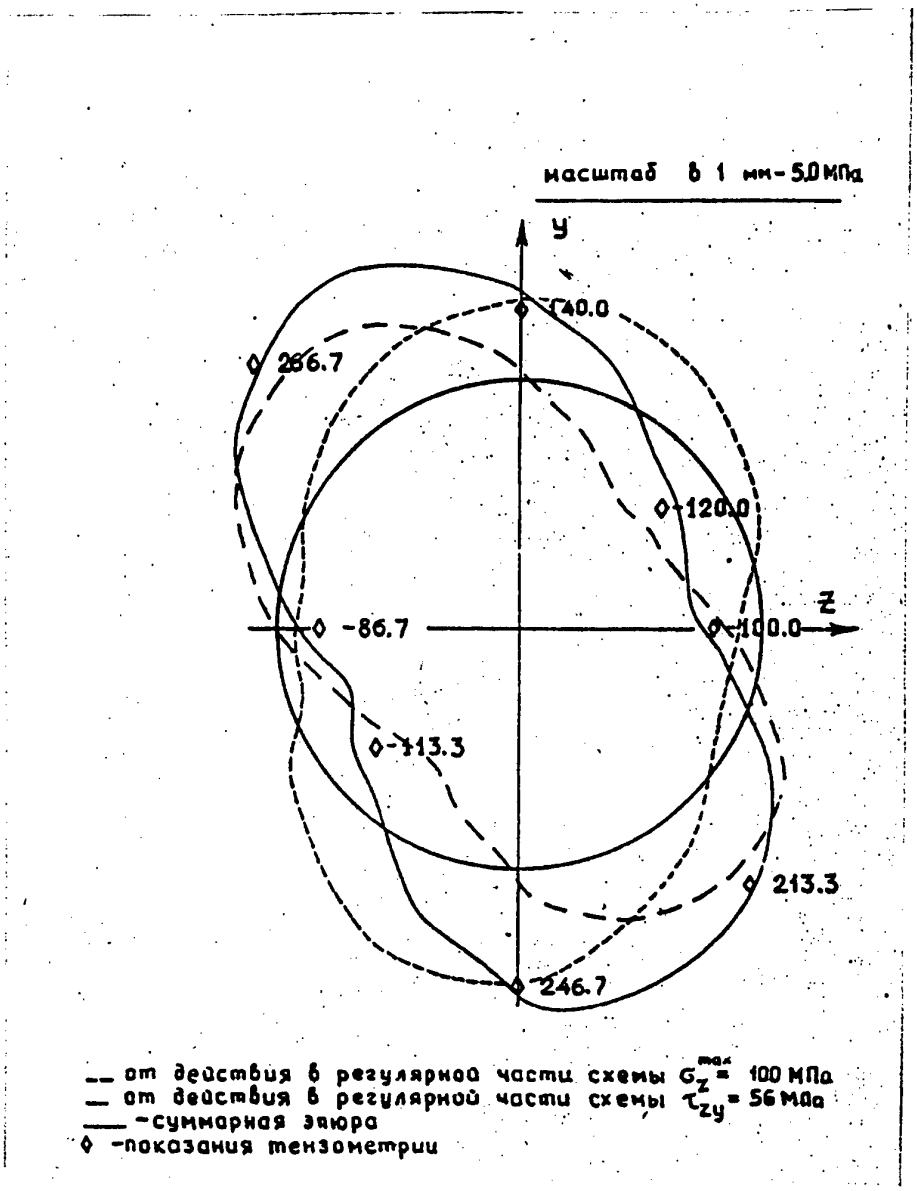
масштаб в 1 мм - 5,0 МПа
y
z
140.0
266.7
120.0
-86.7
-100.0
-113.3
213.3
246.7
— от действия в регулярной части схемы σ_z^{max} = 100 МПа
— от действия в регулярной части схемы τ_{zy} = 56 МПа
—— - суммарная эпюра
◊ - показания тензометрии

Fig.22

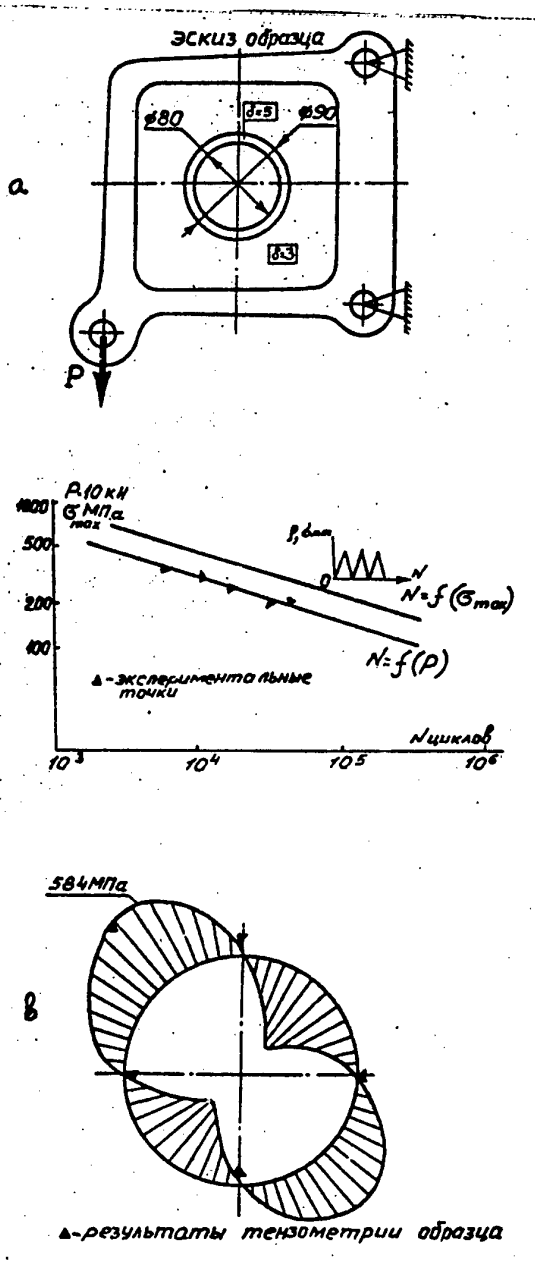
Эскиз образца
а
ф80
ф90
P
P,10кН
σ МПа max
1000
500
200
100
σ
P, 6мм
N
0
N=f(σmax)
N=f(P)
▲-экспериментальные точки
N циклов
10³
10⁴
10⁵
10⁶
584МПа
в
▲-результаты тензометрии образца

Fig.23

compression strain. The calculated LSSS showed that for the extremely loaded fitting hole P_{cr} = 6.2 KH (σ_z = -200 MPa, τ_{zx} = 70 MPA).

The estimation of longevity according to a technique taking into account the two-dimensionality of the stress field in the vicinity of stress concentrator gave

$$N_{calc} = 85{,}000 \text{ program blocks.}$$

The stamped wall 2 of the center section (Fig. 12f) with circular cuts was chosen for study because there is a relatively high level of stresses on the hole outlines and also because it is difficult to inspect the walls inside the center section. The wall is hot-stamped of material V95PCh.

Figure 21 shows part of the wall FEM. It ignored the skin stiffness and small holes in the wall cloth because of their insignificant effect on the general SSS pattern.

The power boundary conditions in the problem were determined on the basis of construction tensometry during tests. The calculation was made separately from the bending and shear strain of the wall cloth. Figure 22 shows results of calculated tangential stresses on the hole outlines: from separate components of boundary conditions, total, as well as results of tensometry.

The fatigue resistance of cuts in the wall was estimated from results of fatigue tests of specimens (Fig. 23a,b) modelling cuts made at the design bureau that developed the aircraft.

To immediately estimate the wall longevity, the LSSS of the specimen was calculated from FEM with the cut zone approximation identical to the wall FEM approximation. Figure 23c shows the calculated epure of stresses on the specimen outlines as compared with results of its tensometry. The data obtained permitted the relation coefficient $q = \sigma_{max} / P$ to be determined and a curve of endurance $N = f(\sigma_{max})$ to be plotted (Fig. 25b).

On the basis of the calculated LSSS of the specimen wall and results of its tests, it was found in the most loaded zone of the wall

$$N_{calc} = 134{,}000 \text{ program blocks.}$$

Similar reasons made us to study a zone of cuts beneath the manhole in the lower board of the DPW (Fig. 12d), where the calculated estimate of longevity appeared to be a relatively low value. The supposed version of repair by reinforcement of the joint between the cut and edge of the board increases the zone longevity by a factor of 4.1, while the version of series improvement chosen on the basis of machine design increases the longevity by a factor of 8.3.

Conclusions

The complex of studies carried out permitted a correspondence to be established between the damages caused in tests and construction parameters of damaged zones specified in design, a forecast of longevity to be made, as well as repairs and series improvements essentially increasing the resource construction characteristics to be justified.

NEW APPROACHES TO ASSESSMENT OF LIFETIME OF AN AIRCRAFT GTE AND ITS GOVERNING IN THE PROCESS EXPLOITATION

Dulnev R.A., Kuevda V.K., Nozhnitskii Yu.A.
TsIAM, Moscow

Until recently, the procedure adopted in the CIS countries for establishing and lengthening the lifetime of aircraft gas turbine engines was much different from the procedure used in the USA and West Europe. The procedure was based on special bench tests of an engine and and its basic details to assess the lifetime with regulated resources according to the number of testing cycles.

Under the new economical conditions dictating shorter terms for attaining the specified lifetime of engine and because the power supply rises in price, this money-consuming mechanism cannot be used. Hence, new approaches to establishing and lengthening the lifetime are developed, with the recent achievements in providing strength reliability and improved exploitation taken into account.

The new procedure is involved with transition to engine exploitation according to its technical state without repair until the specified lifetime is achieved and with estalishment of lifetime of principal details according to calculated thermal stress state and durability, using high-performance calculation models and experimentally defensible database on construction strength of materials.

Requirements are developed, which are to be fulfilled in the transition to a new procedure. Also, techniques are proposed, which combine the former and the new approaches to specification of lifetime for the transient period until the requirements claimed are completely fulfilled and necessary data are accumulated to support the calculation and experimental methods.

DIAGNOSING OF COMMULATIVE FATIQUE DAMAGE GAGES DURING OPERATING SERVICE OF FV

I.M.Daskovsky
State Research Institute of Civil Aviation, Moscow,

During executing of work on investigation and study of methods for diagnosing of commulative fatique damage gages (CFDG) operating servise a flying vehicle (FV), was found, that the most perspective method is evaluation of reliability of the registered data using addition fixed sertificate sample with initial fatique crack, with help quantitative fractogaphy methods, realized after dismounting of the sertificate sample. The value of service loading, acting on CFDG during certain period of work, is estimated using sertificated sample.

The separate section presents the instruction on choice sertificated sample.
The method of evaluation of reliability CFDG is described. Estimation of economic efficiency of use CFDG under operating service conditions is given for passenger planes.

THE CUMULATIVE FATIGUE DAMAGE GAGES

Troenkin D.A.
State Research Institute of Civil Aviation, Moscow

Report on the results of investigation, performed with the goal of the definition of the possibility of the use of transducers Solid Heterogeneous Structures (HTS) for the monitoring of the accumulation of fatigue damage metal and the use, as of alternative method, method Acoustic Emission (AE), reflecting dynamics of fatigue damage metal on substructure level.

The results of investigations and their analysis let establish that exists correlation between signals of transducers HTS and AE.

The regressive analysis let assume about availability statistical dependence for definite parameters HTS and AE. Hence, it is may be quantitative prediction one of them as to registered results another, what testifies about that HTS reflects the dynamics of accumulation fatigue in checked up material.

The form observed signals HTS shown, that they, at the arranging of additional investigations can be used up for the estimation of the real condition of substructures checked up element. One reflect degree fatigue damage, and hence his residual resource as far as the moment of fatigue crack appearance, as at continuous so and at periodical control.

In conclusion the investigations are given recommendations about the arranging of additional investigations, for the solution of the series of problems necessary for use transducers HTS in practice.

COMPLEX TRIBODIAGNOSTIC SYSTEM FOR TURBOMACHINE LUBRICATED FRICTION PARTS

V.A.Stepanov, I.V.Touloupov, P.A.Kadjarduzov
TsIAM, Moscow

The gas turbine service experience shows that wearing of lubricated friction parts is one of the most frequent causes of their failure (up to 27% of the total number of failures, according to Rolls-Royce information).

Of fundamental importance in this connection are developments and putting into service of special tribodiagnistic system (diagnostics based on debris of pairs material present in lubricating oil) which ensures warning of hazardous wear of friction pairs, records and makes it possible to analyze technical condition of the lubricated and oil-cooled friction parts.

A complex tribodiagnostic system is developed for early detection of signs of the commenced failure of a specific lubricated friction part as well as for prevention of this failure. The system is intended for the qualitative-quantitative evaluation of technical condition of lubricated friction parts which is realized by means of comprehensive investigations of critical characteristics of debris present in lubricating oil with help of set of hardware and software means.

The implementation of the stated system permits the upgrading of quality of diagnostics of the machine and mechanism technical condition and finally the enhancement of their operation reliability.

The solution of the reliability enhancement problem is of prime importance as applied to an aircraft engine, the most complicated and costly unit of aviation complex. This being so, such matters as provision of failure-free engine operation, enhancement of engine life and decrease in expenses associated with engine service, are very currently central.

- Development of the hardware and technique devices for complex diagnostic system of technical condition of lubricated friction parts have been realized primarily for aircraft engines being in service. The initial experience on checking the system under laboratory conditions showed its practical utility and prospects for using as applied for different mechanisms whose structure involves rolling bearings, gear meshings and other rotating lubricated friction parts.

The elaborated complex tribodiagnostic system involves:

- laboratory tribodiagnostic engine lubricated friction part system (LTELFPS);
- automatic engine lubricated friction parts hazardous wear warning system (AELFPHWWS).

LTELFPS allows the failure to be localized by the spectral analysis and ferrography methods, it makes possible to determe the cause of the failure and make a justified solution on overhaul or replacement of assemblies without engine teardown. However, LTELFPS application calls for systematic engine stoppage for sampling and investigating the oil that washes the lubricated friction parts.

The laboratory tribodiagnostic lubricated friction parts system involves an analytical ferrograph and any spectral system available at an enterprise being in service (BARS-3, MFS, Spectroscan).

The operation of analytical ferrograph is based on of magnetic deposition of metallic debris from the lubricating oil samples taken from the oil system of a functioning machine for further analysis with the use of optical or electron scanning microscope. The intent of this analysis is to determine the wearing types (normal wear, microcutting, scoring, fatigue spalling, etc.), the friction and lubrication modes to diagnose technical

condition of the machine and mechanism lubricated friction parts. The wear type depends on the form and the relationship between the sizes of individual wear particles.

The analytical ferrography method is widely used abroad to diagnose technical condition of lubricated friction parts, especially in the field of aviation.

The analytical ferrograph involves:

- device for deposition of debris from lubricating oil samples in a strong magnetic field on glass plate surface, that is, for plotting a ferrogram;
- optical biochromatic microscope to investigate debris on a ferrogram;
- counter of ferrogram wear particles coating density, thanks to which it is possible to evaluate the lubricated friction parts wearing intensity index equal to the difference in the squared relative densities of ferrogram coating with wear particles in the points of deposition of large (more than 5mkm in size) and small (more than 2 mkm in size) wear particles.

For purposes of tribodiagnostics of gas turbine engines is a spectral analysis of oil samples performed with the use of automic-emissive spectrometers of MFS type and BARS-3 X-ray-fluorescent analyzers. While making a spectral analysis, the technical condition of gas-turbine lubricated friction parts is determined by the size and the rate of metal-in-oil concentration increase. In doing so, for every engine type there are values of maximum concentration, upon reaching which an engine must be checked, and also the maximum allowable concentration (MAC) at which an engine must be removed from service experimentally determined. The chief drawbacks of spectral analysis are insensitivity to the particles more than 5 mkm in size (except for BARS analyzer) and impossibility to identify debris types that are realized in lubricated friction parts.

The most important and crucially new constituent part of the complex tribodiagnostic system is an automatic hazardous wear warning system (AHWWS).

Experience shows that among the existing methods used for diagnosing a technical condition of gas turbine lubricated friction parts, the continual automated monitoring of quantity and sizes of wear particles washed by oil out of zone of contacting of rubbing surfaces of friction parts is the least labour consuming and economically profitable one.

For a long period of time the technology for monitoring the gas-turbine engine oil debris headed in the direction of using Magnetic Chip Detectors (MCD) whose operation is highly effective for detection of failures at early stages of their development.

Following the dramatic gains reached by "Tedeco" company with the development of new technology for Quantitative Debris Monitoring (QDW) involving a magnetic-inductive sensor, an interest in MCD's application for the new automatic oil debris monitoring system designs is sharply decreased.

Thus, several evolution trends have emerged in the process of development of continual automated debris monitoring . The analysis of advantages and drawbacks of QDM and MCD made it possible to initiate the design of a new automated system to monitor the debris coming with oil from lubricated friction parts into the oil engine system. The developed new automated debris monitoring system was named "Hazardous wear warning system" (HWWS).

Designing HWWS, was based on the principles of operation of USA-developed particles separator and the procedures of interaction of the QDM system and the engine oil system, as well as, on the principle of operation of a sensor which makes up a demagnetizing self-cleaning chip detector (Figure 1).

The developed hazardous wear warning system is installed in the oil scavenging line behind scavenge pump and consists of:

- separator of cyclone type in which a sensor is installed;
- debris sensor-detector;

DESIGN OF HAZARDOUS WEAR PREVENTION SYSTEM (HWPS)

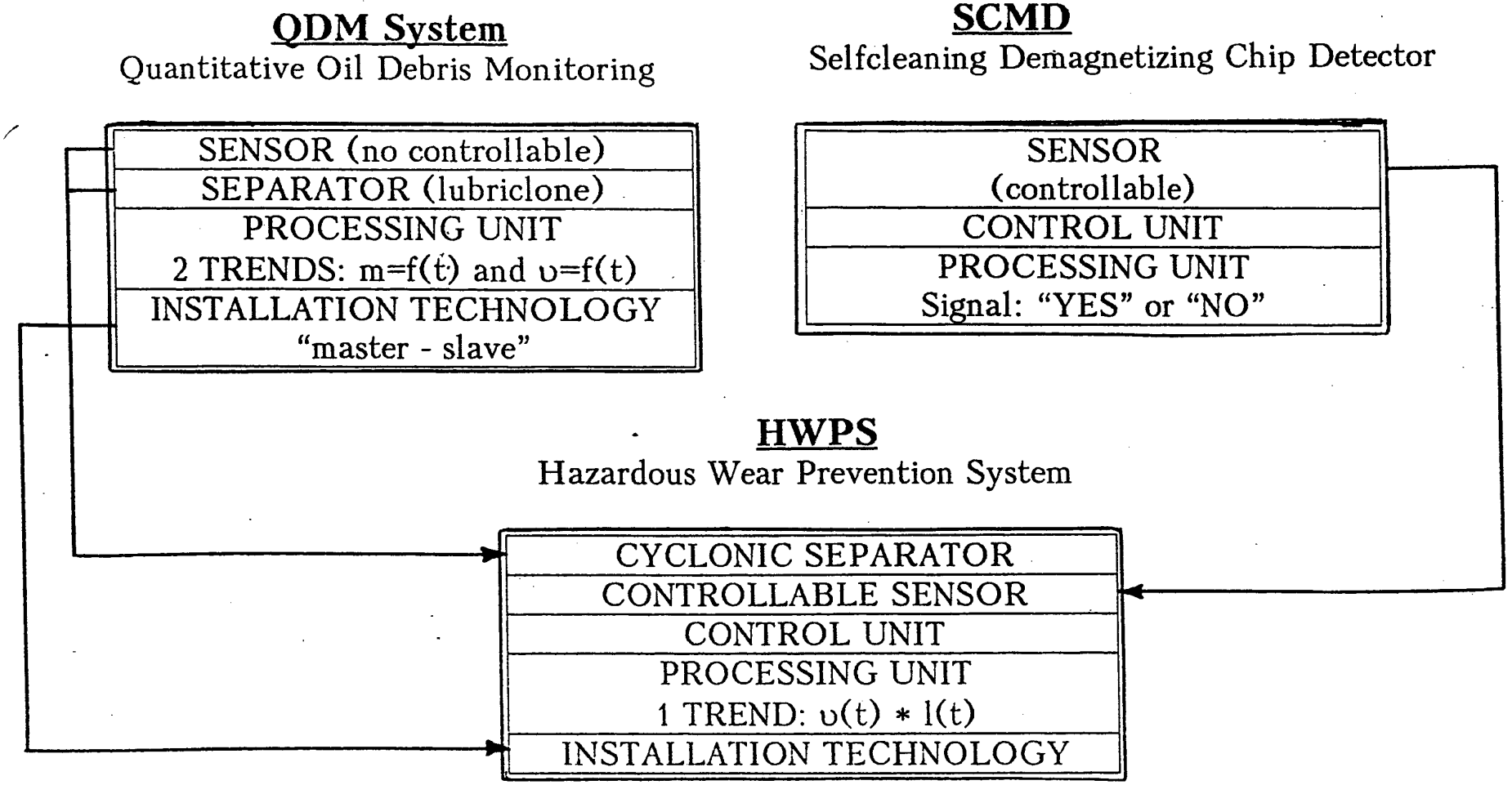

Fig.1

CHART OF THE HAZARDOUS WEAR PREVENTION SYSTEM

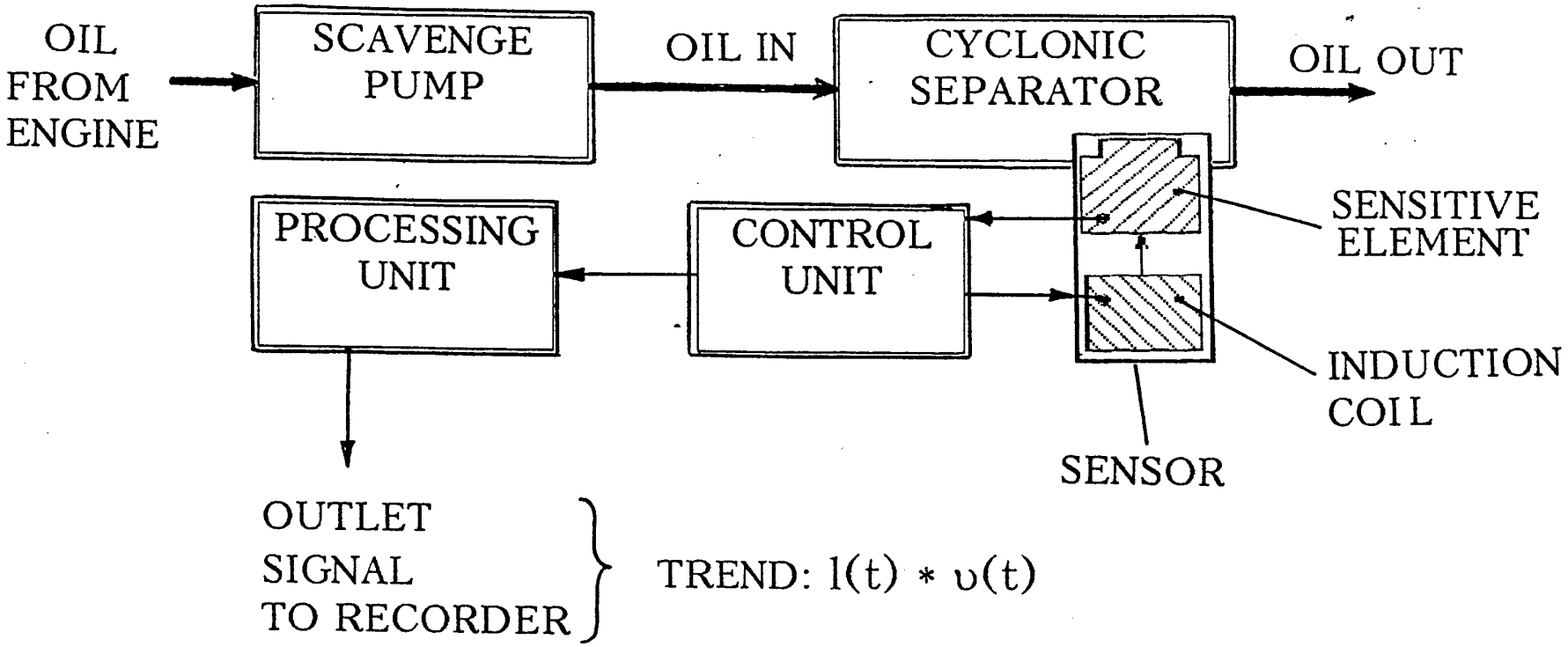

Fig.2

PRELIMINARY TESTING OF THE HWPS

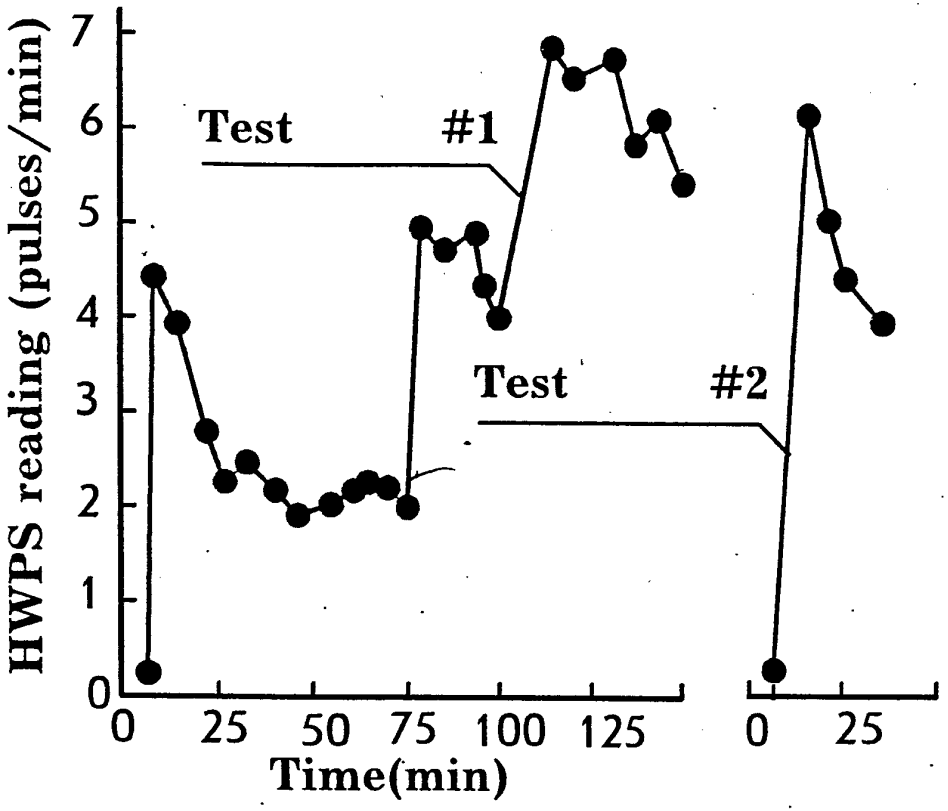

Fig.3

A COMPARISON OF HWPS AND QDMS CHARACTERISTICS

System / Characteristics	HWPS	QDMS
DEBRIS PARTICLES WEIGHT/SIZE CATEGORIES	0,2 µg - 0,8 mg 50 µm - 1 mm	5 µg - 0,8 mg 250 µm - 1 mm
TRENDS MODE	$\upsilon(t) * l(t)$	$m(t)$ and $\upsilon(t)$
DYNAMIC RATE	WIDE	NARROW
SESIBILITY	MODERATE	HIGH
SENSOR MAINTENANCE REQUIREMENTS	SELFCLEANING	PERIODICAL CLEANING

Fig.4

- electronic sensor operation control unit;
- electronic unit for processing the values of measured parameters.

It is necessary to stress that each element of the hazardous wear warning system has been specially developed and is of its own ingenious design.

The cyclone separator is designed in such a way that a swirled oil washes the surface of sensing element providing the maximum of possible ingress of debris on its surface, as well as, free removal of the, sensor-processed debris into the oil flow.

The controlled self-cleaning sensor consists of two main components: the sensing element of contact type and the controlled magnetic field source. Magnetic field in the working sensor clearance is generated by permanent magnet of low coercive force, resulting in its remagnetization with the use of small pulse current-powered inductance coil.

The magnet-controlled sensing element of contact operates as a relay with normally separated contacts. Most time the sensor operates in the particles' accumulation regime, therefore, the application of permanent magnet instead of electromagnet significantly decreases the average system power consumption. During the sensor demagnetizing-magnetizing cycle of about 2.5 seconds in duration, the hazardous wear warning system consumes an average power of about 3 W.

The sensor signals come into the control unit and in the measured information processing unit which isolates the trend of criterion for intensity of lubricated friction parts wearing and keeps track of its changes. The developed system in case of stationary mode of the process being under control ensures functioning of the sensor with constant average frequency that is proportional to the established wear intensity level.

The system realizing such way of sensor controlling and measuring the average frequency of its functioning, tracks the linear trends of the form $v(t)$, $l(t)$, where v and l are respectively the average occurrence frequency and the average length of particles coming to the sensor location from the nodal point under control in real time (t).

The operation of HAWS has been checked in the laboratory conditions.

The main purpose of the experiment was to evaluate comparative sensitivity of the system to fine (less than 0.2 microgram in mass) and medium (up to 2.5 micrograms in mass) ferromagnetic particles. As fine particles, there have been used the steel chip debris of 20 ... 50 mom in size. The medium particles represented the steel chip debris of 100 ... 150 mom in size and about 15 mom in thickness.

The experiment was broken down into two cycles. During the first cycle the system operated with fine chip and during the second cycle the system operated with medium chip. While going from cycle to cycle the oil has not been replaced. Before the beginning of each cycle, the oil was cleaned with the use of removable filter and detachable magnetic trap. The oil capacity in the oil system was equal to 25 litres, and the oil consumption was 28 l / min. The separator pressure drop was equal to 0.3 kg/cm^2.

Chips were thrown into oil tank by the prepacked portions each of 300 milligrams. During the first test cycle three portions of fine chips have been thrown in: the first portion - at the tenth minute, the second portion - at the seventy fifth minute, the third portion - at the cycle minute of a cycle. During the second cycle one portion of medium chips has been thrown in at the tenth minute.

Figure 3 illustrates the test results, where the points , by which the curves were plotted, correspond to the mean by time number of signals recorded on successive 5-minute sections of record tape.

The conducted tests have revealed that the hazardous wear warning system can operate with finer particles (0.2 microgram and 50 micrometers) as compared with the USA-developed QDM system that is capable to record particles having masses more than 5 micrograms and sizes more than 250 micrometers. Additional important indicators of

the developed system will be received during further investigations and development of the system in the engine.

Figure 4 shows the compares of some characteristics of two systems: the developed hazardous wear warning system and the QDM system.

Of course, comparison of the given characteristics of two systems requires the refinement and the performance of direct comparison during tests to be made.

Figure 5 shows the installation point for HWWS applicable for the transmission assemblies in the gas turbine engine oil system.

Combination of self-demagnetizing controlled contact sensor with cyclone separator and two electronic units made it possible to develop a new oil debris monitoring system intended for the gas-turbine engine.

The results of preliminary tests give a hope that the new system will respond to any kinds of wear of the lubricated friction parts under control, accompanied by an accelerating creation of ferromagnetic wear particles greater than 20÷50 micrometers.

Application of AELFPHWWS (the automatic engine lubricated friction parts hazardous wear warning system) makes it possible regular scheduled maintenance and requires the engine to be stopped and the LTELFPS (laboratory tribodiagnostic engine lubricated friction parts system) methods to be used only in case of real hazard of impermissibly intensive wear of lubricated friction parts

The complex tribodiagnostic system can be used when operating any rotary machines and mechanisms resulting in an their increased reliability life, and lowering of maintenance costs.

INCORPORATION HWPS WITH ENGINE OIL SYSTEM

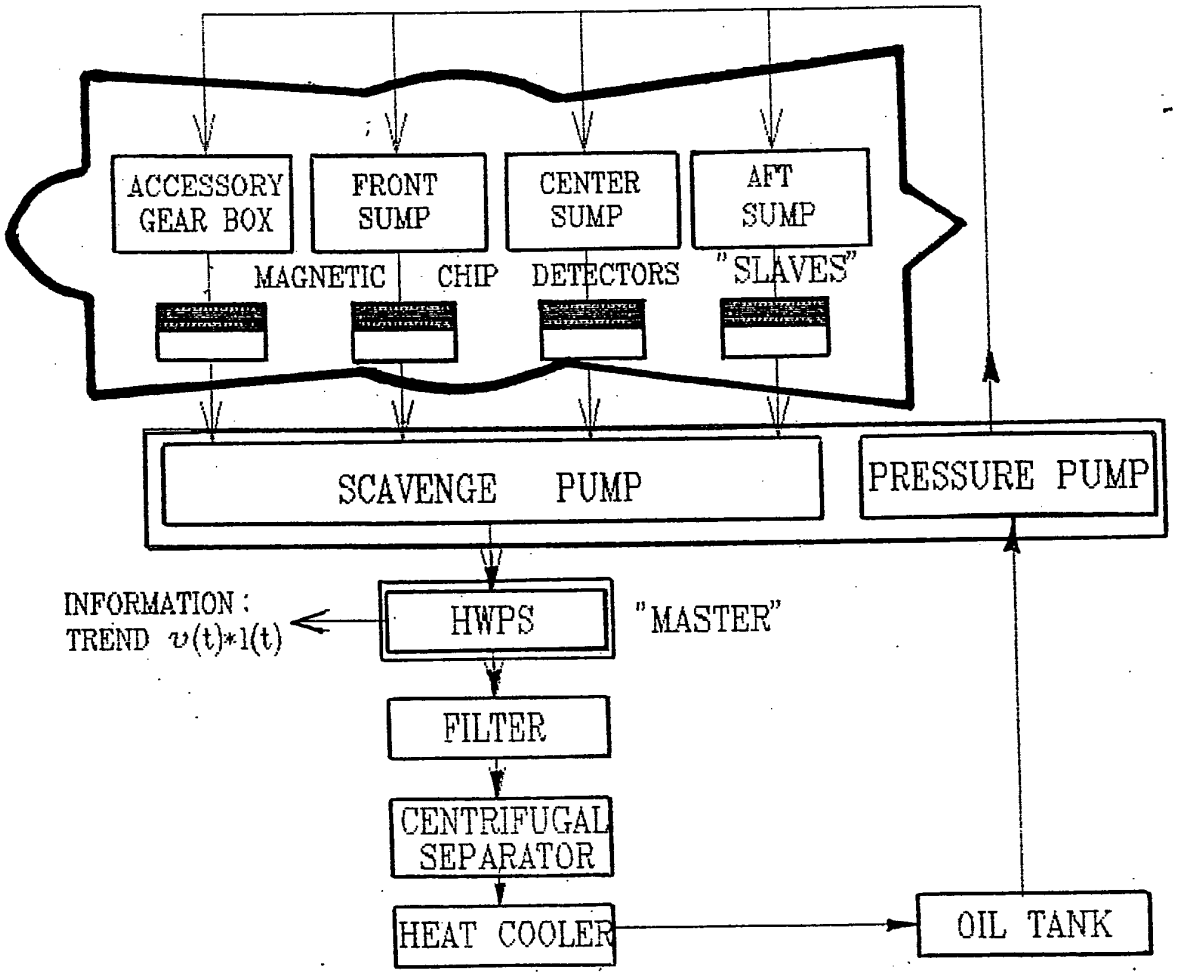

Fig.5

MODERN METHODS FULL-SCALE AIRCRAFT FATIGUE TESTS

Shcherban' K.S.

TsAGI, Zhukovsky, Russia

Currently, one can see the ever-growing significance of airframe for fatigue in order to improve the airframes, in both Russian and international aviation. The amount of structural analyses and component testing at the design stage is growing, but the full-size airframe tests are the only measure to improve elements whose service life is governed by:

- the structure manufacture/assembly process and/or;
- redistribution of forces in neighboring elements under the cyclic load.

The primary objective of the full-size airframe fatigue tests is to insure safe operation; testing is major requirement in aviation regulations in both Russia and abroad.

The other important objective of the full-size tests is to prepare the inspection schedule and the in-service maintenance procedures.

In the airframe resistance improvement program the major point is to test the airframe in a unit. Such tests make it possible, first, to better reproduce the typical in-service loads and, second, to avoid development of special adapters that would represent the stiffness of the removed portion of the structure.

The development of the airframe loading program for lab tests relies on two postulates:

1) the external loads corresponding to the actual operations should be reproduced to a maximum possible accuracy and
2) the abilities of the test facilities/equipment must be exceeded.

These requirements are completely met by programs such as "flight-by-flight" concept with:

- random sequence of flight with various load levels and
- random alteration of in-flight variable loads.

The development of such program proceeds from the spectrum of variable loads expected in flight and round conditions (Fig.1). To derive a lab test spectrum, the whole of the load factor range significant in terms of fatigue accumulation is subdivided into 5 levels. These 5 levels are included into 5 flight types: **A, B, C, D,** and **E.**

In so doing, the "least severe flight", **E,** includes only the minimum loads, whereas the "most severe flight", **A,** includes all the five levels; these are changed in a random fashion. These five flight types are the basis for a block of flights; the flights in a block are mixed at random. The total number of flights in a block is 0.1 of airframe service life. Further, the loading program derivation procedure (Fig.2) includes:

- the development of the program layout,
- the development of a logic of the multichannel load generation/application system, and
- computation of concentrated loads to be generated by the channels.

As a rule, the program layout reflects all phases of a typical flight and incorporates all loads to occur in ground-handling and flight conditions. When developing the logic of the multichannel load- generation/application system, the task is to found a compromise between the desire to minimize the total number of channels and the necessity to reproduce:

- aerodynamic and inertia loads acting on the wing, fuselage, tail, wing high-lift devices and
- loads applied to such units as the landing gear and engines.

For example, testing the IL-96 airplane required 120 channels.

The concentrated loads for each channel during each segment re defined by minimizing the root-mean-square deviation of load parameter, subject to equilibrium conditions and load limitations, The forces are determined from the condition of minimum functional:

$$F = (Klab - Koper)^2$$

where "K" is the load parameter that can be:

a) concentrated forces P,
b) shear force "Q", bending moment "Mbend", torsion moment "Mtors" or combinations threof,
c) normal stresses σ, or tangential stresses τ,
d) equivalent stresses σ^*, being a combination of normal tangential stresses.

The minimum functional is evaluated under condition of equilibrium of the airframe as a whole:

$$\sum X = 0, \sum mom\ X = 0;$$
$$\sum Y = 0, \sum mom\ Y = 0;$$
$$\sum Z = 0, \sum mom\ Z = 0.$$

and under the restriction of the concentrated loads:

$$Pi < [P]i, \quad 1 < i < n,$$

where "n" is the total number of the channels.

The sequence of concentrated loads derived in this manner are generated cyclically in lab conditions by using the automated complex (Fig.3) that provides:

- programmed cyclic loading through 200 channels,
- vibration loading at frequencies up to 50 Hz,
- real-time monitoring of loads at 1000 channels,
- permanent inspection of test structure integrity, and
- 16000 channel strain-gauging.

Monitoring of loads and airframe displacements relies on

- force monitoring for each channel,
- measurement of extreme displacements of airframe as whole, and
- permanent determination of equivalence of the actual loading to the reference loading (Fig.4).

The force monitoring is conducted by multichannel system. It ensures reproduction of the prescribed force-time function (a sine represented by 25 point per a half-period) for each of the channels. If extreme forces turn out to exceed limits then the system unloads the structure by using a special subroutine. In addition, the system envisages emergency unloading if some parameters become unacceptable. Between the extremes of each segment the overshoot (or undershoot) of forces causes the system to either retard or accelerate loading. Also, emergency unloading is made if an airframe violates limits with respect to angles of pitch , roll and/or yaw.

There is another supervision option, the real-time stress/strain monitoring system. It measures forces at extreme points and the displacements (by means of calibrated strain-gauge bridges mounted at characteristic points of the structure). These data are the basis

STRUCTURE LOADING SPECTRUM FOR FATIQUE TEST

- "FLIGHT-BY-FLGHT" TEST CONCEPT
- 5 TYPES OF FLIGHTS FOR DIFFERENT SERVICE CONDITIONS; FLIGHTS ARE MIXED AT RANDOM IN A BLOCK OF 1200 FLIGHTS

Flight type	Number of flights in a block
A (severest loads)	1
B	9
C	65
D	435
E (lowest loads)	690

- 5 LEVERS OF VARIABLE LOADS MIXED AT RANDOM IN EACH FLIGHT

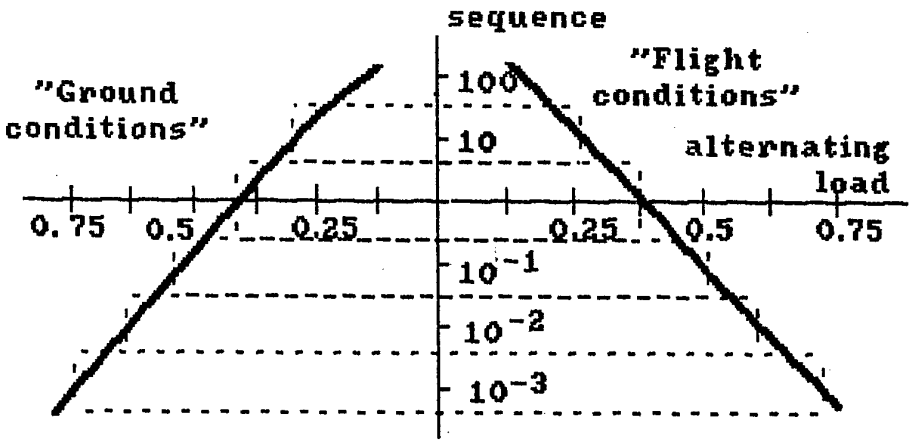

FIG.1

COMPOSING A LOADING PROGRAMME

- PROGRAMME COMPOSITION REFLECTS TYPICAL FLIGHT STAGES, INCLUDING:
  -GROUND LOADS;
  -FLIGHT LOADS.

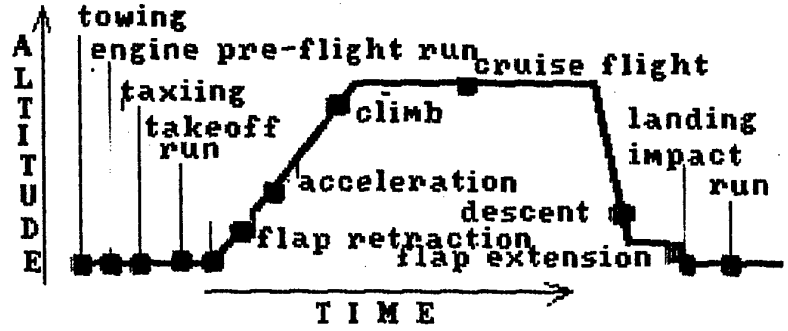

- THE LOADING SISTEM APPLIES CONCENTRATED LOADS TO ALL AIRFRAME UNITS IN THREE DIRECTIONS

- CONCENTRATED LOADS FOR EACH FLIGHT SEGMENT ARE DETERMINED TO MINIMIZE ROOT-MEAN-SQUARE DEVIATION OF LOAD PARAMETER, SUBJECT TO EQUILIBRIUM CONDITIONS AND LOAD GENERATION LIMITATIONS

$$F = (K_{test} - K_{oper.})^2 \rightarrow \min$$

$$K = \| S^*, Q, M_{bend.}, M_{tortion} \|$$

NORMAL AND SHEAR STRESSES

$$\Sigma X = 0 \qquad \Sigma mom_x = 0$$
$$\Sigma Y = 0 \qquad \Sigma mom_y = 0$$
$$\Sigma Z = 0 \qquad \Sigma mom_z = 0$$

$$P_i < [P]_i$$

FIG.2

AUTOMATED TEST COMPLEX FOR FULL-SCALE AIRFRAME FATIQUE TESTS

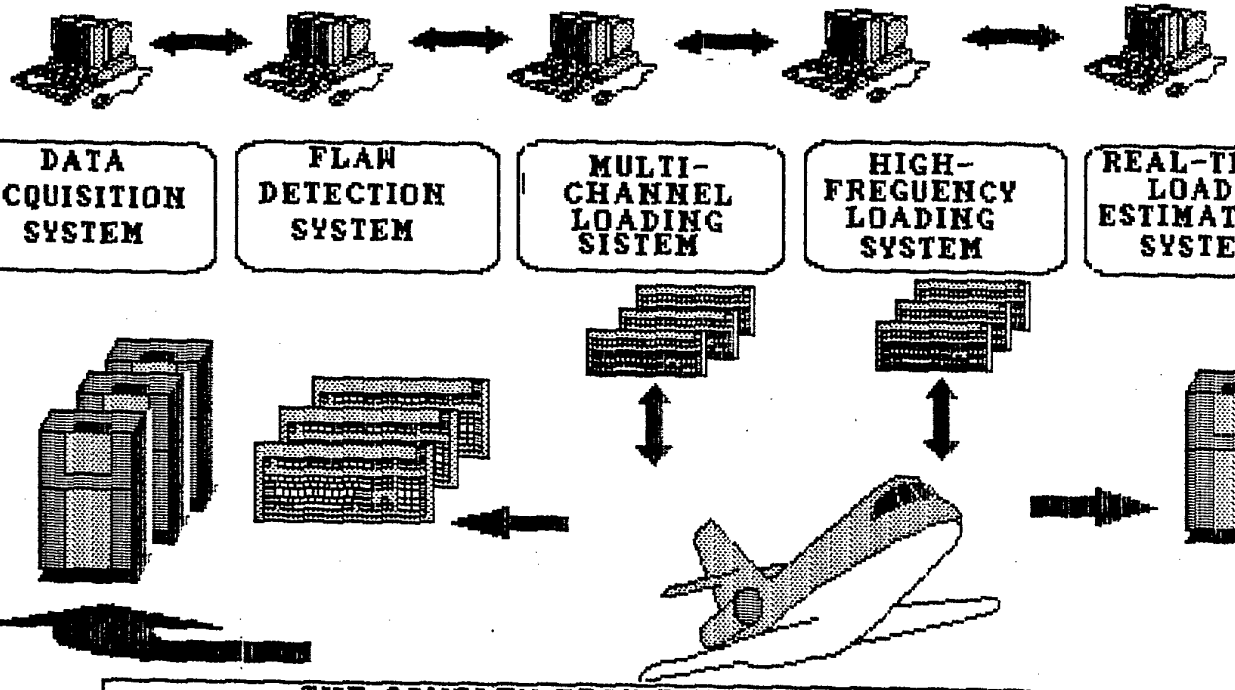

THE COMPLEX PROVIDES:

- -programmed cyclic loading through 200 channels
- -vibration loading at frequencies up to 50 Hz
- -real-time monitoring of loads at 1000 channels
- -16 000 channels strain-gauging
- -permanent inspection of test structure integrity

FIG.3

AIRFRAME LOAD/DISPLASEMENT MONITORING

- FORSE MONITORING FOR EACH CHANNEL OF AUTOMATIC LOADING CONTROL SISTEM

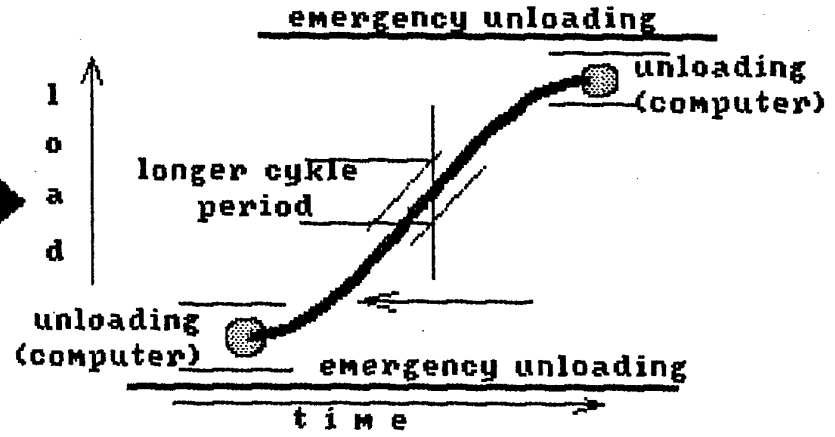

- MEASUREMENT OF EXTREME AIRFRAME DISPLACEMENTS IN ROLL, YAW AND PITCH

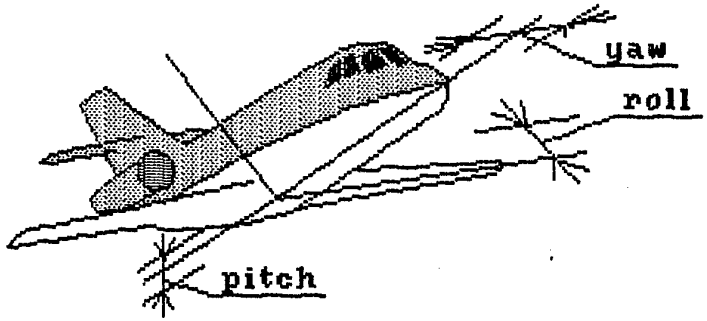

- PERMANENT DETERMINATION OF EQUIVALENCE OF THE ACTUAL LOADING TO THE REFERENCE LOADING

$$E = \frac{N(K_{test})}{N(K_{oper})}, K = \left\| \begin{matrix} P \\ Q, M_b, M_t \\ \text{STRESSES} \\ S^* \end{matrix} \right\|$$

FIG.4

UNLOADING OF DAMAGED AIRFRAME STRUCTURAL ZONES

- REPAIRS TAKE UP TO 75% OF CALENDAR TIME, INCLUDING 40% FOR PREPARATION

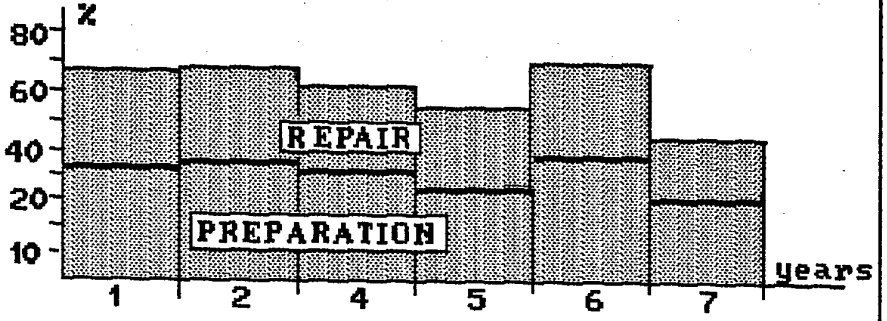

- MODIFIED PROGRAMME INCLUDING THE DAMAGED AREA UNLOADING

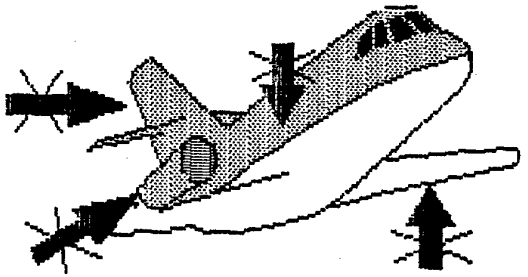

- TESTS WITH PARTIAL UNLOADING ARE CONTINUED UNTIL REPLACEMENT PARTS ARE SUPPLIED

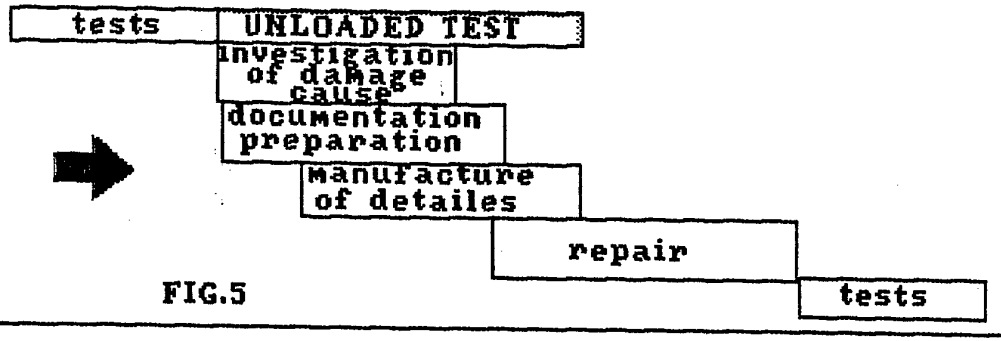

FIG.5

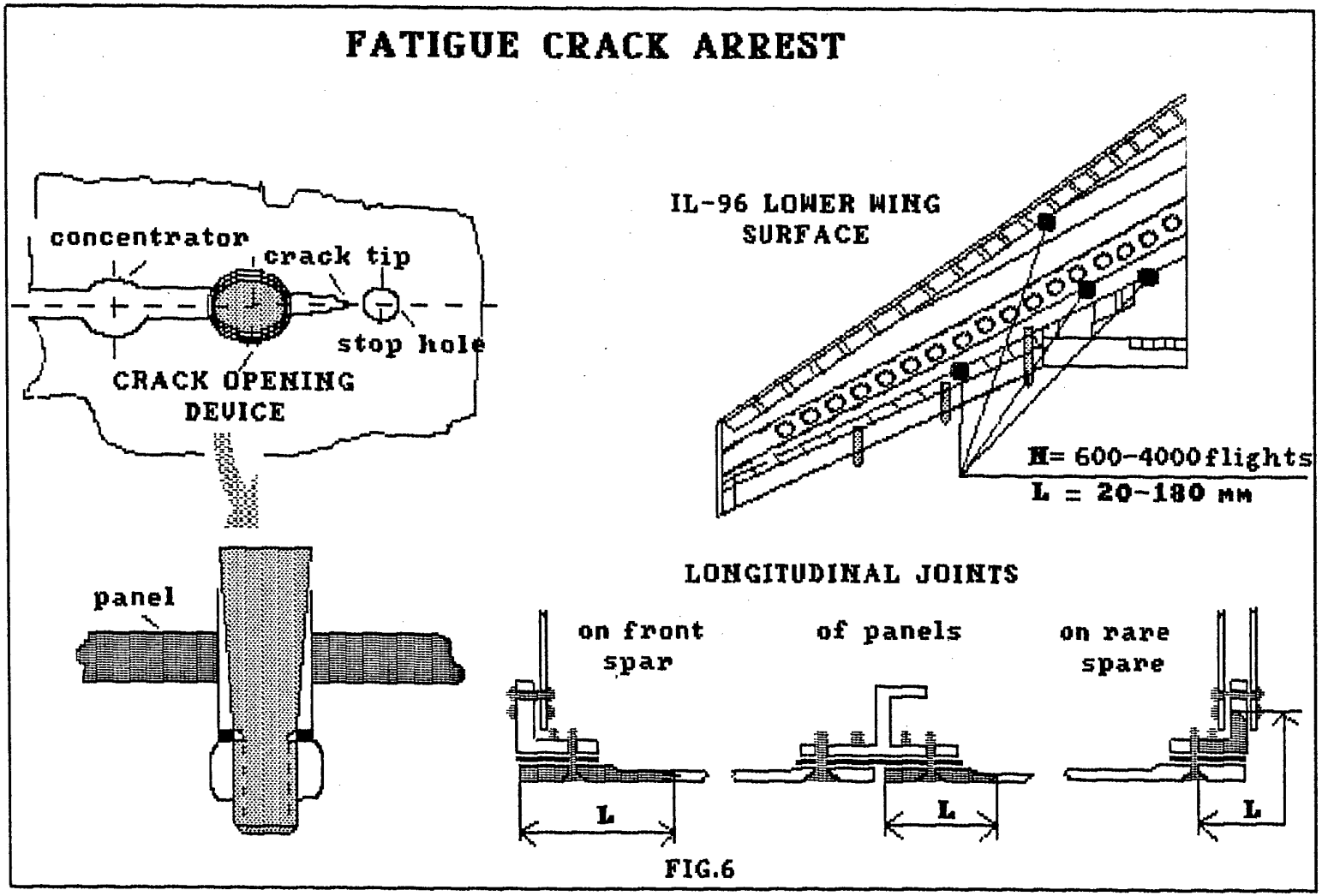
FATIGUE CRACK ARREST
concentrator
crack tip
stop hole
CRACK OPENING DEVICE
panel
IL-96 LOWER WING SURFACE
N= 600-4000flights
L = 20-180 мм
LONGITUDINAL JOINTS
on front spar
of panels
on rare spare
L
L
L

FIG.6

RESIDUAL STRENGTH EVALUATION WITH STRUCTURE FAILURE PREVENTION

- RESIDUAL STRENGTH OF A WING WITH STANDARDIZED DAMAGE IN 8 ZONES WAS CHECKED

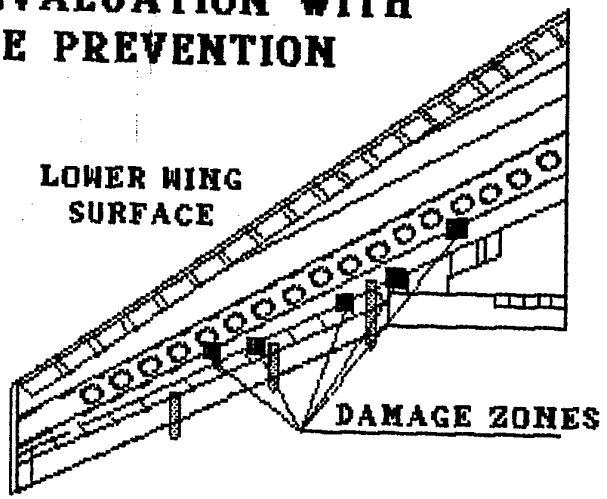

- STEP-BY-STEP LOADING IN STABLE CRACK GROWTH AREA

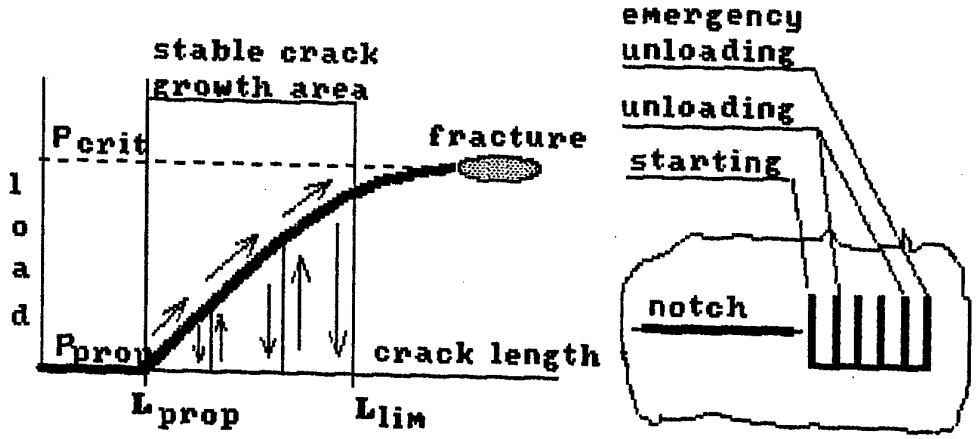

FIG.7

UNSTABLE CRACK ARREST

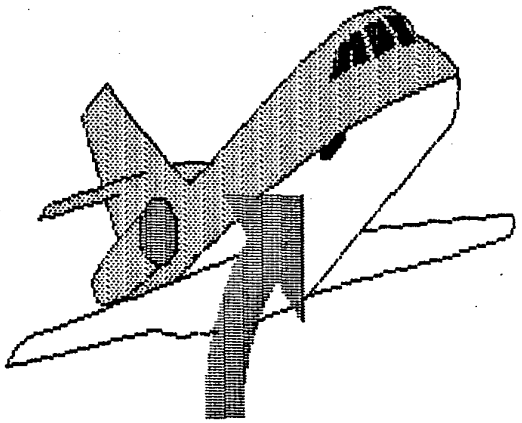

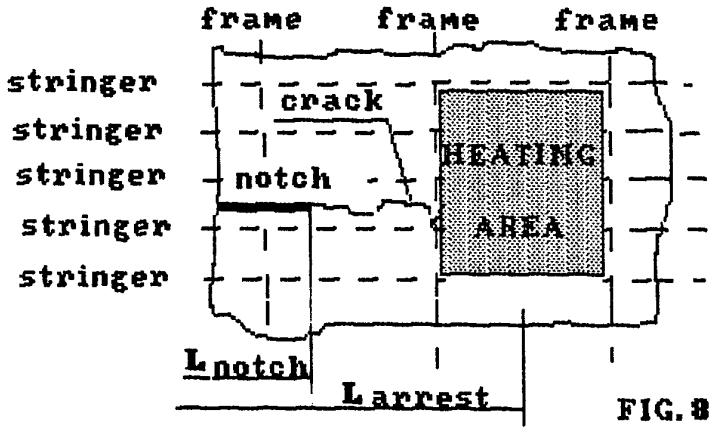

FIG. 8

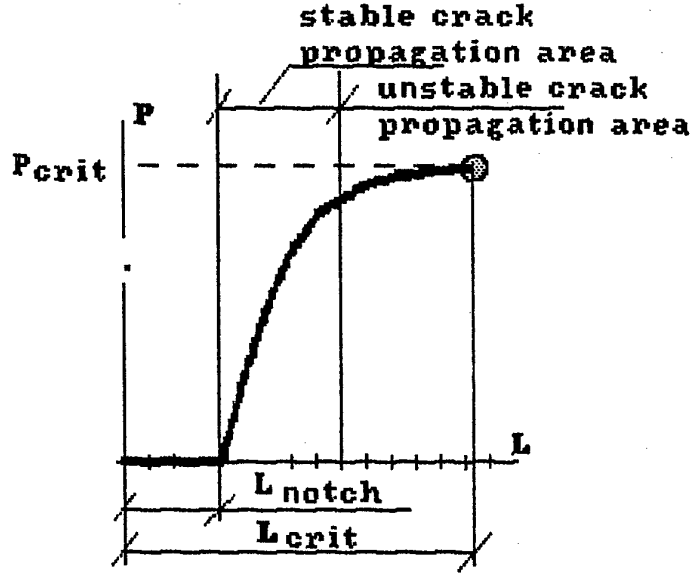

METHOD ENABLE

- precluding explosive decompression of fuselage under damage tolerance tests
- establishing limit load
- determining critical crack length for several zones of one structure

DISASSEMBLING THE IL-86 WING AND INSPECTING THE PERMANENT JOINTS

- DISASSEMBLING THE LONGITUDINAL JOINTS OF LOWER AND UPPER PANELS FROM THE WING ROOT TO RIB # 32

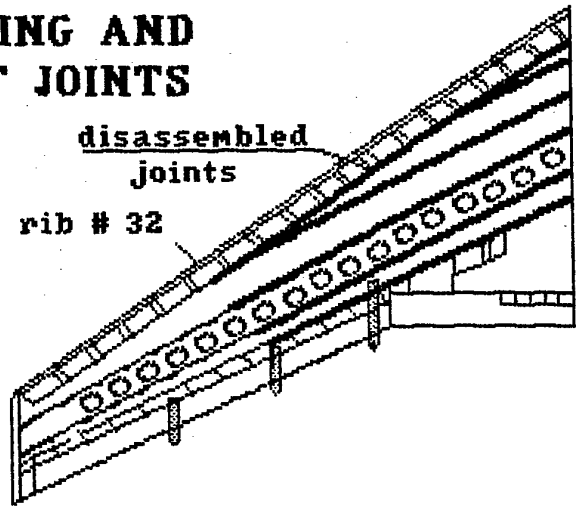

- EDDY-CURRENT INSPECTION OF 101 000 HOLES; 650 CRACKS DETECTED

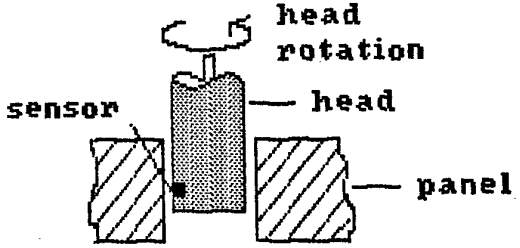

- FRACTOGRAPHY OF 27 CRACKS FROM LOWER SURFACE AND 54 CRACKS FROM UPPER SURFACE

FIG.9

for computing integral (resulting) factors and a fatigue amount accumulated during a complete flight. Thereafter, an equivalent is determines the ratio of fatigue for an actual complete flight to the fatigue amount for a reference flight. Deviation of the equivalent from the unity allows to estimate an error in load reproduction.

The experience in full airframe fatigue testing shows that over 75% of calendar time are spent for structure repair after fatigue damages. To reduce the idle time for repairs, use is made of "damaged structure zone release" method (Fig.5). With a fatigue damage revealed, the system forms a new vector of concentrated loads that cause a lower stress around the crack (so as not to develop the crack), whereas the rest of the structure is loaded with an acceptable deviation. Test is continued, and simultaneously the causes of the damage are investigated, documentation is prepared, and relevant structural parts are manufactured. The tests are only ceased when the structure itself is being recovered. After the repair the tests are continued obeying the original program.

In the case of detecting a fatigue crack the affective method for arresting the cracks is employed, as shown in Fig.6. The method is based on the drilling of a stop hole at the crack tip in addition to which a special device that keeps the crack opened during the cyclic loading is mounted on the crack. This option makes it possible to stop the 20 -180 mm long cracks in various wing components for period of 600 up to 400 lab flights.

After the structure is tested for as long as 2 or 3 design service life, the residual strength is evaluated. The major objective of tests is to show compliance with requirements to residual strength of the structure with natural or artificial cracks. The challenge is that a single structure should be utilized to evaluate the structure damaged at a number of points. There exists danger of a complete failure before the limit load is attained for all zones. The task is solved managed by employing the method protecting the airframe against complete failure (Fig.7). The essence is to load the airframe stage-by-stage and monitor the crack in the stable growth area. This method allows to cease the loading before the crack becomes critical. As for pressurized bodies, there exists a possibility to arrest a crack at unstable growth stage (Fig.8): a structural area near the crack tip should be heated so as to generate compressive thermal stresses; the unstable crack stops propagating if its tip approaches this area.

With the test work package fulfilled, the permanent joints are disassembled to detect damage in the zones difficult to access. Figure 9 demonstrates the procedure of such studies for an IL-86 wing. These studies revealed 650 cracks in longitudinal joints; the crack growth data were summarized to adjust the in-service inspection schedule.

TECHNIQUE OF ESTIMATION FOR AIRCRAFT CONS-TRUCTION AT THE STAGE OF DESIGN

Kovalevskii A.K., SlashchevV.A., and Stelmukhov I.A.
Yakovlev's Design Bureau, Moscow

The construction durability problems are vital in designing modern aircrafts, especially in designing airliners . To estimate the lifetime of a construction, it must be subjected to repeated loads. This test, however, is not possible at early stages of designing so that a low level of permissible stressesis specified for taking into account the lifetime requirements. As a result, the construction to be desiggned has an extra weight. Therefore, it seems to be very importamt to rapidly estimate durability of the construction under design in its separate zones.

The present work is an attempt to solve this problem on the basis of a series of calculations for a finite-element model for the aircraft under design. Given the cyclic loads affecting separate installations are not in equilibrium at each moment of time, and the problem is solvedfor the airframe as a whole, the calculation model for the aircraft must be brought in equilibrium. In addition to solving the main problem, this permits data to be obtained for testing with repeated loads.

Estimation of durability of airframe consructive elements is based first of all on a justifiedmchoice of a number of parameters characterizing cyclic loading and vulnerability to damage, introduced into a onstruction in a type flight of aircraft.

Having determined the strain-stressed state of the construction for each loading cycle, one can obtain equivalent stresses in a given zone and thus, on the basis of known durability curve, to estimate the design longevity.

On the basis of the technique developed, a program complex, RENK, was devised, permitting the following kinds of works:

- calculation of loading and durability of the construction under design;
- development of a program for loading constructive installations for realization of durability stand tests;
- development of cyclic and equivalent stresses in constructive elements for the cases of equilibrium amd nonequilibrium loading.

Using the program complex RENK, a full cycle of calculations of cyclic loading of constructive elements of an administrative airplane Yak-112

THE PROGRAM COMPLEX "RENK": CALCULATION OF CYCLIC LOADING OF CONSTRUCTIVE ELEMENTS

SlashchevV.A ,Kovalevskii A.K., and Stelmukhov I.A.
Yakovlev's Design Bureau, Moscow

The Renk is a program complex permitting an efficient use of your personal IBM PC/AT or compatible computer for estimating cyclic loading of a tree-dimensional engineering design.

The RENK permits integral force factors to be determined in any element of the design: equivalent stresses, forces, bending and torsional momentums obtained onthe basis of a linear theory of vulnerabilities to damage. The stress-strained state of the design is determined by means of FEM. For given parameters of endurance curve, it is possible to determine durability of some elements under determined loading of the design in bench testing.

The RANK is a system permitting to quickly and precisely estimate the design strength at all stages of design and at lifetime testing in aircraft industry, in rocket engineering, and in power mechanical engineering.

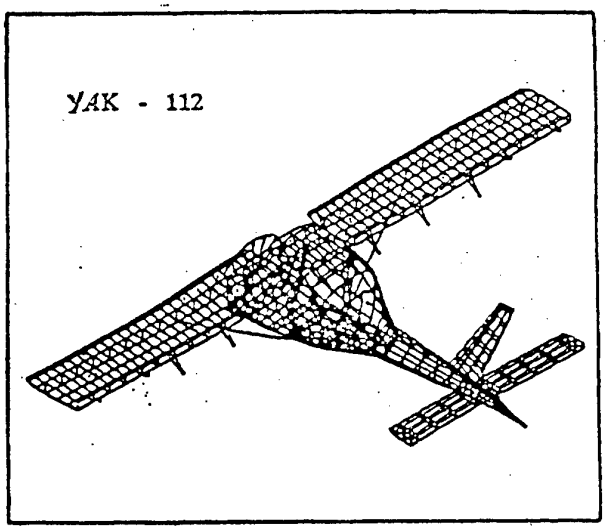

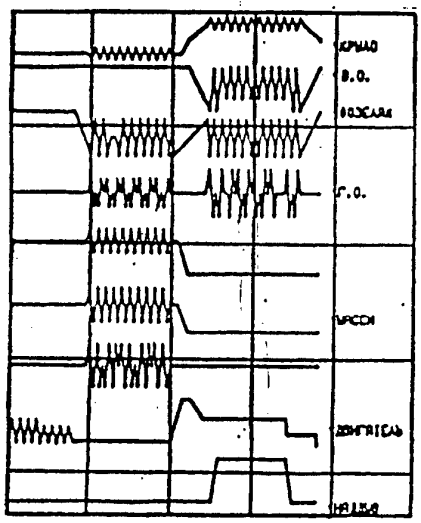

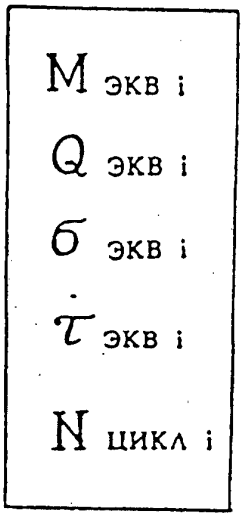

AUTOMATION OF TECHNOLOGICAL PROCESS OF FILM GAGES PRODUCING.

S.Kh.Shamirzaev, E.D.Muhamediev, G.E.Yudin, G.I.Vainerman, V.Y.Smirnov

PTI of SA "Physics-Sun" AS of RU, Tashkent

The sensitive elements (SE) of commulative fatique damage gage (CFDG) represent a heterogeneous material. They are produced by thermovacuum evaporation of initial mixture on poliamide substrate. The initial mixture consists of various pure disperse components. For example, mix granular of bismuth and antimony tellurides with cadmium. The electronic structure of a sensitive element of a film gage changes due to imposing of irreversible cyclic deformation. It causes the changes of effective electrical resistance R_{eff} SE CFDG, rigidly installed on a construction element. This changes have "autonomous" character, caused by principle of minimal joule losses. Each initial structure has its own "autonomy". The history of reorganization process of its electronic subsystem is unique. The structures, possessing identical "autonomy", are reproduced in a narrow technological interval. Therefore a high level of automation technological process is used for films production.

The system is created to automatize the process producing of semiconductor film gauges SE CFDG by a method of thermovacuum evaporation of a mix granular materials. The control of the process parameters and management of all units of the installation is executed by IBM/PC-compatible computer according to a technological card prepared beforehand. During the process it is possible to change its modes.

The installation allows one to precipitate up to three various mixes in one technological cycle. It is possible to precipitate only two of them simultaneously. The third mix is precipitated separately, after the second mix. To evaporate mixes 3 separate evaporators are used. During precipitation process the necessary temperature mode is set in each evaporator. The thermocouples supervise temperature of evaporation of a mix.

One of the major parameters of precipitation process is substrates temperature. The substrates are fixed on rotated dish located above evaporators. The halogen lamp supports their necessary temperature. The thermoresistor, which is placed beside a substrates, provides control of temperature of substrates.

For stability of the characteristics of the gages produced, it is necessary to supply a certain speed of rotation dish above evaporators. This condition permits one to expect the reproduction of a gage structure. The system provides continuous speed measurement and regulation of dish rotation according to a given law.

Two special detectors (witnesses), auxiliary and main, provide the control of the process of gages producing. The auxiliary witness is located on technological damper. The measurement of the auxiliary witness resistance permits starting of precipitate process.

After the achievement of given resistance of the auxiliary witness technological damper is opened and precipitate process on substrates begins. The precipitation process is finished till the achievement of given resistance of the main witness.

All controllable parameters are recorded into a file for a subsequent analysis and repeated reproduction, that permits one to receive gages with the maximally close characteristics in various consignments.

The structure of the system is presented in a Fig 1. The main part of a system is IBM compatible computer 1 with built - in adapter 2. The adapter 2 executes the exchange of the information and units control in measure-managing unit 3. All signals from the technological installation detectors and managing signals for its units are connected with measure-managing unit 3.

The exception is two signals, arriving from the witnesses. It is due to the fact that the resistance of the witnesses changes in a very wide range (from $1,2 \cdot 10^6$ up to 50 Om) and can be measured only by a digital voltmeter 4 with automatic choice of a range. The information on the resistance witnesses value arrives as digital code on input 24-digit register on unit 3 together with signal of the end transformation from voltmeter 4 with 0,8 sec period. At the same moment the unit 3 forms interruption for a computer. Computer reads information from the input register. Thus each 0,8 sec. the data on the resistance values of the witness are updated.

As in precipitation process the measurement of resistance of the auxiliary and then the main witnesses resistance take place the system provides an opportunity of switching inputs of a voltmeter 4 through a remote switch. Management of switch and control of its rule are made by computer program through a separate line of 8-digit input/output registers of unit 3.

The main witness is installed on the rotated dish and its contacts incorporate with an input switchboard through current collector ring contacts on a dish shaft. Such connection, especially under vacuum conditions, can considerably deteriorate the accuracy of measurement of resistance of the witness. Besides it is necessary to take into account the influence of temperature on the resistance of the connecting wires and change of resistance of demountable connections. These factors can cause the occurrence of a large error of measurement, especially at low values of the witness resistance. To minimize the influence of the above factors, all connections with voltmeter are made over 4-wire connections.

To measure the dish rotation speed the disk with the cuts was mounted on its shaft. Infra-red radiation was passed throughout these cuts from light-emitting diode to a photodiode. The measure converter 6 forms pulses, appropriate to each cut on a disk. The frequency of pulses is proportional to dish shaft rotation speed.

The pulses from gage 6 arrive on divider of frequency of unit 3. The output of the divider of frequency is connected with the circuit of interrupt formation, on which the computer 1 makes time marks and calculates rotation speed of dish shaft. The measured value of speed is compared by computer program with given value and in case of their discrepancy in DAC of unit 3, intended for management of speed dish rotation, new value of a code is placed. This code will be transformed in a analog voltage, which arrives on a control unit of engine 7.

The control unit of engine 7 consists of power amplifier with analog optoelectronics isolation of input and output. Its output is connected with rotor winding of electric engine 8 with independent excitation.

Thus, if the speed of dish rotation corresponds to a given one, the voltage on an engine is maintained at a previous level. If a deviation from given speed for any reason takes place, the voltage on a engine varies and compensates this deviation.

The temperature of substrates is supported by halogen lamp, which is placed above a dish. To control the temperature of substrates thermoresistor, which through current collector rings over 4-wire connection circuit is connected with measure unit of unit 3 is used. Through thermoresistor a stable current is passed. Measure unit amplifies voltage

from the thermoresistor and 8-digit ADC transforms the signal in digital code. At the same time the signal from the thermoresistor is compared on comparator to a signal from ADC, in which certain value substrate temperature is recorded.

The computer reads code from ADC and determines current temperature of substrates. Output condition of comparator is simultaneously read out.

If it is necessary to adjust temperature of substrates, through the output register of unit 3, the signal from output of comparator is broadcasted by computer program on the input of management thyristor of unit 9, which switches on or switches off halogen lamp 10.

If it is not required to adjust temperature, the input of unit 9 is in switched off position, but thus the measurement of substrate temperature and the work of a comparator do not cease.

The use of program compilation of a signal from output of comparator on input power unit 9, makes convenient the process thermoresistor calibration and regulation process of substrate temperature, since the substrates heating can be executed purely by software.

The realisation of technological process of the temperature regulation is executed by hardware.

For evaporation of the components mix three evaporators 12 and three power thyristor units 11 are used, by means of which power is adjusted. The power circuits of units 11 are connected directly to heating elements of evaporators 12, and the switching is executed by computer program on a signal input of units 11 with the help of a remote switch in a structure of a unit of synchronization and switching 5. The same switch switches thermocouples on an input ADC in unit 3, which are used for the temperature measurement in a chosen evaporator.

Thus in unit 3 it is enough to have 2 identical channels, which are used for the control of temperature in evaporators and management of heaters through thyristor units 11. One of these channels on input and output is switched on the second evaporator. The second channel is constantly connected with main evaporator.

In each channel there is a rationing amplifier of thermocouple signal, ADC, power regulator of heater in evaporator and DAC.

ADC transforms a signal from rationing amplifier into a binary code. This code is read out in a computer 1 and over calibrated tables is transformed into a temperature. DAC transforms a code, appropriate to required temperature in a heater, in an analog voltage. This voltage moves on regulator of power as setting point and is compared to a voltage on an output of a rationing amplifier. As a result of comparison a signal of management for power regulators 11 is formed.

As it is known, thyristor power regulators, working by phase management method, produce significant noises. If in the system there are weak signals, such as the signals from thermocouples, these noises are inadmissible. To significant decrease of a noise level we chose such way of management thyristor, when the switching of power in a load is executed at transition of a feeding voltage through 0, and thyristor is maintained open during the whole period of feeding voltage. For realization of this method of management in the system synchronizer 5, which executes temporary binding of an asynchronous signal from an output power regulator in unit 3 to frequency of a feeding electrical net is stipulated. Obviously, the evaporator heating is in this case executed on quantum a time, and the size of quantum is equal to one period of a feeding electrical

network. Accuracy of regulation in this case is a little worse, than at a phase method of regulation. However, taking into account, that the thermal processes in evaporators are inertial, and heat capacity of an evaporator design and material in it are provided with "integration" of separate quantum's power, the choice has been made just for this method.

As a result of the test heating and cooling curves were received in a whole interval of working temperatures with given accuracy acceptable for technological process (about ±10° C).

Notice, that a problem of compensation temperature cold junctions of thermocouples has been resolved. In our case the complexity of the problem is in the fact that the thermocouples are in a chamber of the technological installation at pressure about 10^{-5} mm.Hg. The output of the signals from thermocouples outside is carried out through a special tight plug. Outside contacts of a plug the wires are connected of the same materials, thermocouple is made, that permits one to compensate thermo-emf on transitions wire - contact of a plug. Towards outputs of all three thermocouples, connected this way three additional thermocouples are connected. They are placed inside Dewier vessel, filled with water and ice. All other connections with unit 3 are provided by usual assembly wire.

There is an automatic control of technological damper in a system, located above the evaporator. The management of dumper rule is executed through a regular control dumper unit. For this purpose in unit 3 a special relay is built - in, which is operated through the output register. Through the input register of unit 3 the control of a dumper rule is executed.

Structurally all system consists of a separate unit 3, which is connected with other parts of a system through plugs. The unit 3 is fed from electrical network 220V 50Hz.

The measure unit of rotation speed 6 is mounted beside an electric engine 8. The unit of synchronization 5 is executed in a kind of separate unit and mounted inside unit rack of technological installation.

The units 7, 9 and 11 are placed inside appropriate power units, included in structures of technological installation. Their circuits and connections are maded so, that switching-off from unit 3 doesn't interfere the work of regular systems of technological installation.

The whole technological process is supervised by the computer program. This program is written in the language C ++ and Assembler and is optimized for fulfillment on a computer AT-286. Working slide of the program is indicated in Fig. 2. The screen is separated in some windows:

- Menus.
- Control Bar.
- Display window of evaporators data and lamp.
- Display window of the witness resistance, dish velocity and dumper position.
- A window of ruler time.
- Status Bar, mouse cursor coordinates and timer.
- A information window, displaying current condition of process.
- A window of the event tasks of the main and auxiliary witnesses.

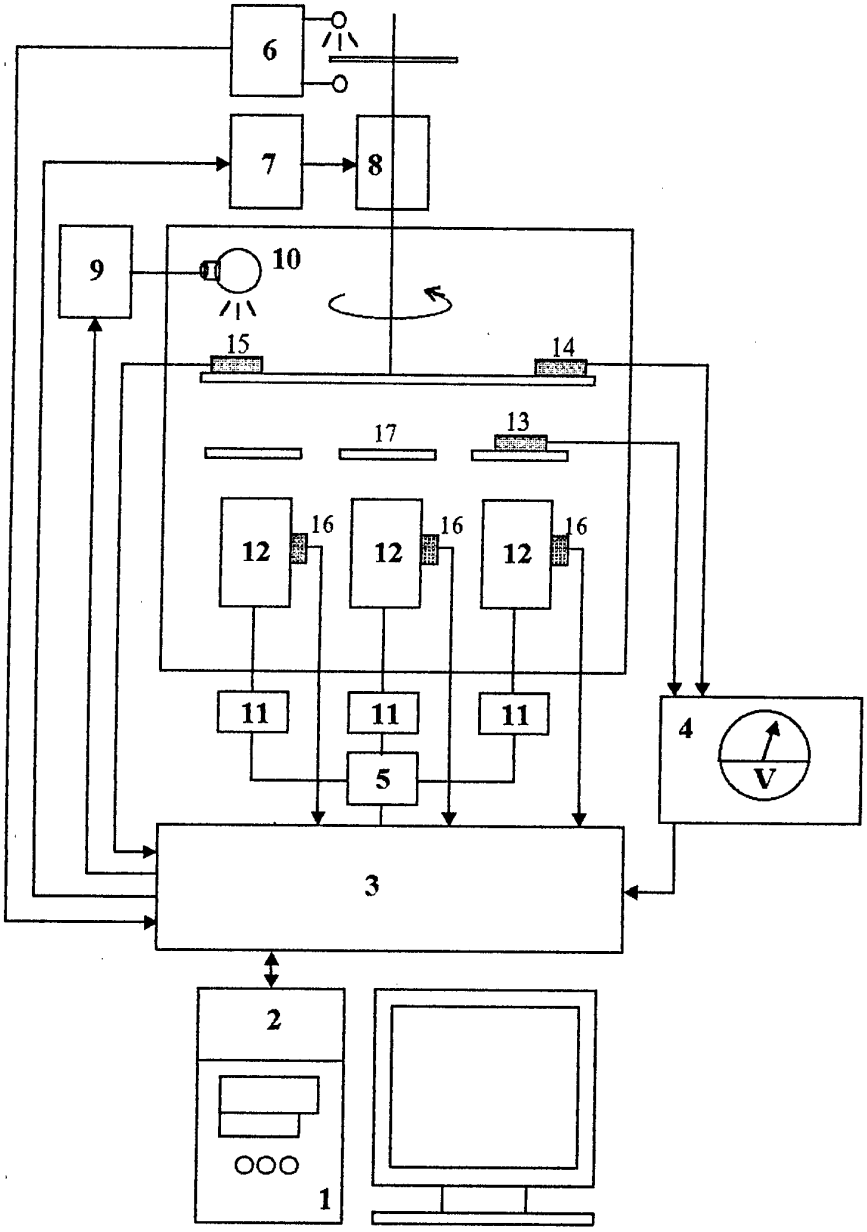

Fig.1

1 - computer, 2 - adapter, 3 - measure- managing unit, 4 - voltmeter, 5 - synchronization unit, 6 - measurement of dish velocity, 7 - electrical engine control unit, 8 - electrical engine, 9 - halogen lamp control unit, 10 - halogen lamp, 11 - thyristor unit, 12 - heater, 13 - auxiliary witness, 14 - main witness, 15 - thermoresistor, 16 - thermocouples 17 - technological dumper.

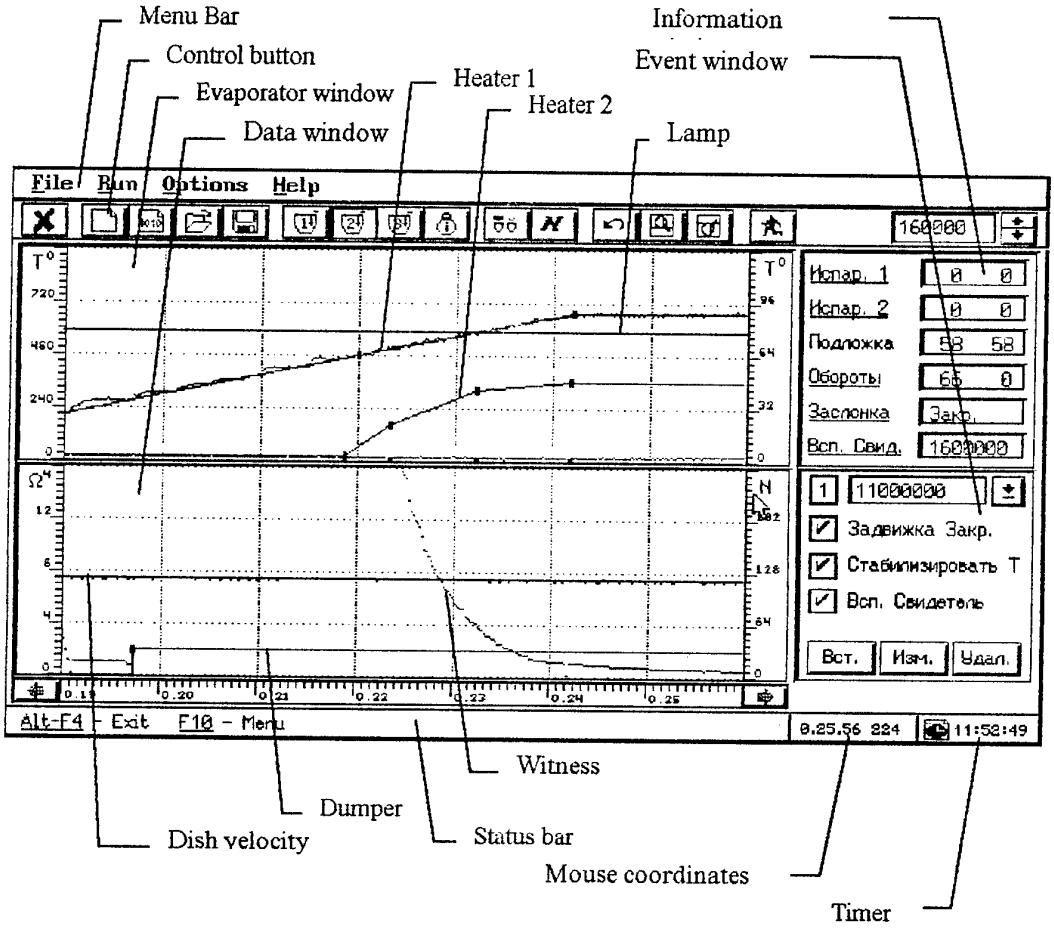

Fig.2
Arrangement of elements of management in window of the control program.

Before starting of the technological process, it is necessary to enter the data for the Protocol of work. To setup the values of evaporator temperature and the lamp it is necessary to press a button with the image of necessary evaporator and with the help of the mouse to note a point in evaporator window. Setup of the rotation speed of dish and dumper position is executed in the bottom window.

Moving in a data window the status window displays coordinates of mouse cursor in a format (Seconds Code/Temperature). The value rotation speed of dish is set and displayed in units - $Minutes^{-1}$.

The system can control simultaneously only the two evaporators. The evaporator 1 can work all time. Evaporators 2 and 3 are switched, therefore to setup the points for evaporator 2 zero values are automatically entered for evaporator 3 and conversely. Therefore, for example, if some points for evaporator 2 were entered, and then the point for evaporator 3, zero value for evaporator 2 are automatically entered. Thus whole control for evaporator 2 will be lost.

The top data window displays 1, 2, 3 evaporators condition and heating substrate lamp. The left-hand ruler scale of temperature data window correlates with evaporator 1, 2, 3. Right scale - for a lamp.

The bottom data window displays resistance value of the main or auxiliary witness, speed of dish rotation and dumper position. The left-hand ruler scale is expressed in Om. The right - $Minutes^{-1}$. It is possible to change a scale of resistance with the help of a control button "Scale R" with a step the divisible Degree 10.

The dumper position is displayed like a step: 0 - dumper is closed, 1 - dumper is open.

The operator can zoom data windows in whole screen with the help of the control buttons "Zoom evaporator window" and "Zoom witnesses window". It enables to set up data values with maximum accuracy. The accuracy of the setups for all data lies in a range of codes 0 - 255.

The information window displays a condition of current process, namely:

- Codes value of appropriate measured evaporator temperature and substrates in a given moment of a time and setup code values.
- Speed of dish rotation and setup code values.
- Dumper position.
- Resistance values of the main or auxiliary witness.

While switching the evaporator 2 on evaporator 3 and switching of the auxiliary witness on the main one titles in appropriate windows are automatically changed.

During the work process it is necessary to change the protocol of work depending on the value of the auxiliary and main witnesses. For this purpose in event window it is necessary to set appropriate value of resistance and to establish a condition of buttons, namely:

- Open/Close dumper.
- Stable temperature.
- Switch Maim/Auxiliary witness.

In operating time the System will begin to fulfil the given code values and display corresponding measured values. When achieving a right border of a window the program automatically «list» the data window on one screen ahead. The measured

values are displayed as points of appropriate color in data windows and in information window.

It is possible to edit setup values in the Protocol during the process, however the program does not permit one to correct those points, which were already fulfilled during the work.

The events are fulfilled by the program in a the special way. If the resistance of the active witness has become less than that given in the event, the program automatically switches dumper and/or witness. A point of a dumper position is entered in the protocol and all subsequent dumper positions are changed on inverse states. If the event contains stabilization of temperature, the program stops the changes of evaporator temperature 1. Two subsequent points for evaporator 1 are changed. The following point is lowered up to current value of temperature and up to a current moment of time is shifted. The point following to it is lowered up to current value of temperature too.

During the process the program stores all measured values. The information is recorded each second. Maximum time which the program can store - 4.5 hours. After this the program does not fix any values, but will fulfill all managing control.

The typed protocol of the process can be saved in a file on a disk. All measured data are automatically saved in special file too.

REACTION SE CFDG AND FACTOR OF NONLINEAR INTERNAL FRICTION OF A ELEMENT AIRCRAFT DESIGN.

S.Kh.Shamirzaev, E.D.Muhamediev, G.E.Yudin,

G.I.Vainerman, A.A.Yakimov

PTI of SA "Physics-Sun" AS of RU, Tashkent

The present work is concerned with a technique of measurement of a factor of nonlinear internal friction (FNIF) of a console beam, subjected bend fluctuations with different factors of asymmetry. Description of measuring instrument is given. On a beam sensitive elements (SE) commulative fatique damage gage (CFDG) are rigidly installed. The installation works under the control of the personal computer IBM/PC connected to the peripheral equipment through crate CAMAC. For measurement of variation of the resistance R_{var} SE gauges is used 4-channel bipolar 10-digit ADC. The tenzoresistor is used for a control of zero position and deformation of a console beam during a loading. There is the special system of automatic compensation of constant part of resistance to pick out variation of the resistance R_{var} during process of imposing of cyclic deformation. For measurement of residual resistance R of SE gauges is used standard noiseproof 32-channel 14-digit ADC. The SE gauges are connected to inputs ADC over 3-wire circuit. The gauge of number of revolutions is used for a control of number of cycles of deformations and synchronization of measurement variation of electrical resistance SE gauge.

The process of measurement of signals from SE gauge and wire tenzoresistor begins at the moment when a pulse from a gauge of number of revolutions is arrived on a input of the L- quiry standard DAC and is finished at the moment of occurrence of a next pulse.The start and stop of a electric motor is executed with the help of the output register through a terristor block under program control.

Description of installation.

The installation works under the control of the personal computer IBM/PC connected to the peripheral equipment through crate CAMAC. The block diagram of installation is indicated on Fig. 1. Gauges SE and wire tenzoresistor are installed rigidly on console beam fixed with one end. The tenzoresistor is used for a control of zero position and deformation of a console beam during a loading. Other end of a console beam is mechanically connected through a cam gear with a shaft of electrical engine. The value of enclosed cyclic deformation is adjusted with the help of various fastening of gear on a shaft of a electric motor. The gauge of number of revolutions is used for a control of number of cycles of deformations and synchronization of measurement variation of electrical resistance SE gauge.

The process of measurement of signals from SE gauge and wire tenzoresistor begins at the moment when a pulse from a gauge of number of revolutions is arrived on a input of the L-query standard DAC and is finished at the moment of occurrence of a next pulse.The start and stop of a electric motor is executed with the help of the output register through a terristor block.

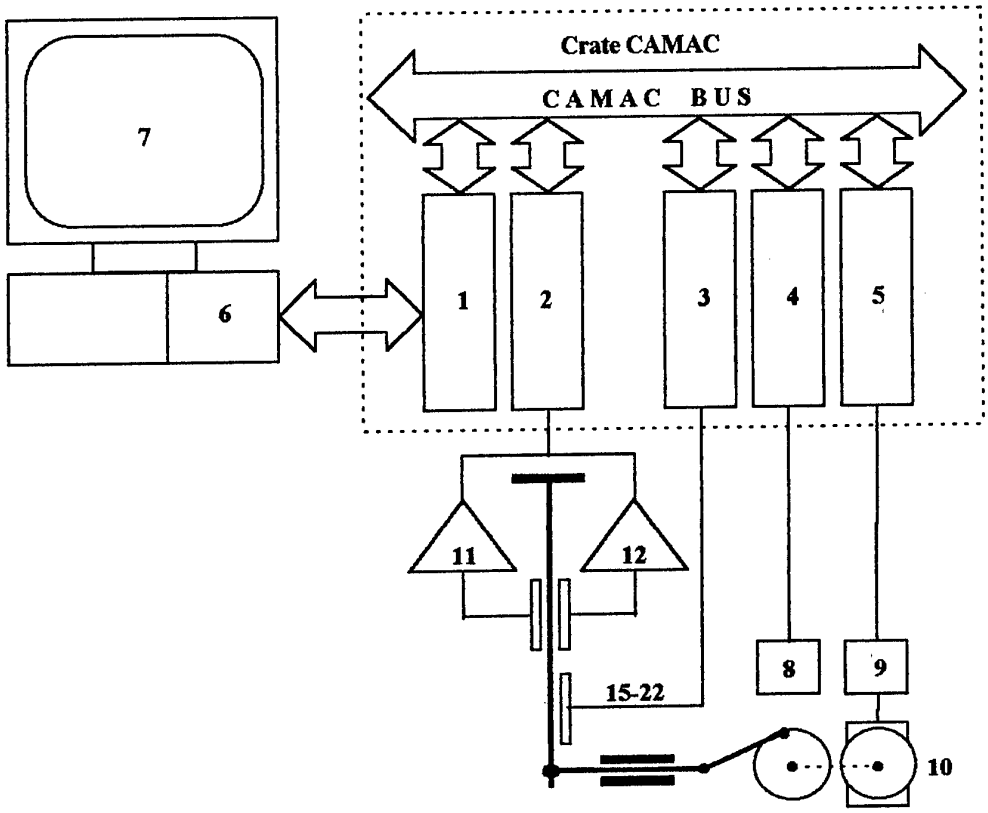

Fig. 1. The block diagram of installation.

1 - Crate Controller CAMAC, 2 - Module 4ADC10, 3 - Module 32ADC14, 4 - DAC, 5 - Output register, 6 - Adapter CAMAC for IBM/PC, 7- Computer IBM/PC, 8 - Gauge of number of revolutions, 9 - Control block of engine, 10 - Electrical engine, 11- 12 - Amplifiers, 13 - SE Gauge, 14 - Wire tenzoresistor, 15-22 - SE Gauges.

The process of measurement consists of following stages:

- Before the beginning of imposing of cyclic deformation the console beam is placed in zero (non-loaded) position. Zero levels of signals for SE gauges and wire tenzoresistor amplifiers are set up. After installation of zero levels the residual resistance R of SE gauges and wire tenzoresistor R_0 are measured for the control of a zero position of a console beam.
- Electric motor is started.

The gauge of number of revolutions counts certain quantity of cycles N after which it isnecessary to measure variation of the resistance R_{var} from one of SE gauge and wire tenzoresistor during one period of a cycle of deformation.

- When $N+1$ pulse from a gauge of revolutions is arrived a cyclic reading from a SE gauge and wire tenzoresistor are produced until a next pulse from a gauge of number of revolutions is arrived.
- The engine stays.

- Time delay is made. It is necessary that the console beam has stayed and SE gauges are relaxed.
- After a cycle of imposing of deformation residual resistance R from SE gauges is measured.
- Resistance R_0 wire tenzoresistor is measured for the control of a zero position of a console beam.

For measurement of variation of the resistance R_{var} SE gauges is used 4-channel bipolar 10-digit ADC (4ADC10) possessing following characteristics:

- A level of source signals ±10 V. Inputs have protection from excess voltage.
- Source impedance on inputs not less than 100 Kom.
- Frequency of a sine wave source signal by amplitude 10 V - not more than 300 Hz.
- Speed of increase of a source signal: not more than 20 mV/mks.
- Accuracy of transformation: not worse of 0.1 %.

The module 4ADC10 reads out data on size of input voltage from each channel in any moment of a time, i.e. each channel 4ADC10 tracks an input signal and continuously produces a code, appropriate to input voltage. There is a opportunity to record and to measure instant significance of a input voltage in all four channels. The start-up command transfers of all channels 4 ADC10 in a continuous tracking mode. The cycle of measurement lasts not more than 1 ms.

There is the special system of automatic compensation of constant part of resistance to pick out variation of the resistance R_{var} during process of imposing of cyclic deformation. The principle of work of this device was described in [1]. The function chart of a system of automatic compensation is indicated on fig. 2.

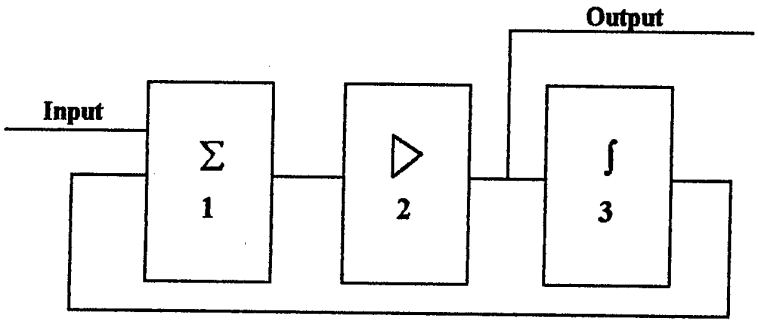

Fig.2. System of automatic compensation

1 - Adder, 2 - Amplifier, 3 - Integrator.

Signal from a SE gauge passes through a adder 1 and amplifier 2 and causes occurrence of a signal on a output of a device and input of a integrator 3. The signal on a output of a integrator 3 has opposite polarity, that causes gradual reduction of a signal on a output of a adder 1 and on a output of a device and input of a integrator 3. Over a certain time the signal from a output of a integrator 3 completely compensates a signal from a SE gauge and on a output of a device the signal will be equal for a zero. At imposing of cyclic deformation in a signal from a SE gauge occurs variable part, which passes through adder 1 and amplifier 2 and arrives on inputs

4ADC10 and integrator 3. On a output of integrator 3 signal will not change, because integral from variable part is equal zero and the device behaves as a usual amplifier.

The signal with wire tenzoresistor through a usual amplifier arrives on another channel 4ADC10.

For measurement of residual resistance R of SE gauges is used standard noiseproof 32-channel 14-digit ADC (32ADC14). The SE gauges are connected to inputs 32ADC14 over 3-wire circuit. Such connection permits to measure electrical resistance in 16 channels simultaneously. The module 32ADC14 provides measurement of electrical resistance in a range from 0 up to 5 kOm. There is 3 fixed subranges with ceilings 50, 500 and 5000 Om with accuracy of transformation 0.01, 0.1 and 1 Om accordingly.

The transformed result code has 13 digit. The main indicated error of transformation concerning the top significance for subranges 50, 500 and 5000 are equal accordingly ±0.5%, ±0.3% and ±0.2%. Active input resistance not less than 100 mOm. An input leakage current not more than 30 mkA. The current from a internal generator of a current through conected resistance is within the limits of 1 ± 0.001 mA. Time of transformation not more than 100 ms.

All modules are assembled and located in standard crate CAMAC. For communication with a computer a special 8-digit controller CAMAC and an adapter for IBM/PC-compatible computer was developed, which is set up in free slot of expansion of a system bus.

For management of experiment is developed a specially graphic Windows-like environment. It realized on the language C ++ and Assembler. The program, written with help of this tools, permits:

- To set quantity of cycles of deformations and to set a time of relax after removal of a load fig.3.
- To measure a variation of the resistance R_{var} from one of SE gauges and resistance wire tenzoresistor during imposing of deformation.
- To calculate the first 5 factors of Furies-decomposition of the law of change of variation of the resistance R_{var} of a SE gauge during imposing of deformation.
- To overlook the graphic of the law of change of variation of the resistance R_{var} on a display for various cycles of imposing of deformation fig. 4.
- To measure residual resistance SE gauges till 8-channels.
- To write and to read experimental data in a file.
- To set up a zero level for amplifiers for signals from SE gauges and wire tenzoresistor.
- To supervise zero (non-loaded) position of a console beam.

For realization of automatic repeated imposing of cycles of deformation in the program there is an opportunity to set up the quantity of a series of measurements, consisting from identical cycles of deformations. The program automatically measures variation of resistance SE gauge and wire tenzoresistor, makes time delay, measures residual resistance SE gauges, calculates factors of Furies-decomposition and records all data in a file.

This instalation permits one to measure the factor of nonlinear internal friction of a element aircraft design.

Factor of nonlinear internal friction of a construction beam (tg γ)

For beam is imposed by simple cycle loading one have :

$$\sigma(t) = \sigma_0 \sin(\omega t) \qquad (1)$$

The correspond deformation $\varepsilon(t)$ is defined by tenzoresistor is :

$$\varepsilon(t) = \Sigma_\nu^{\infty} [\, a_\nu \cos(\nu\, \omega\, t) + b_\nu \sin(\nu\, \omega\, t)\,] \; ; (\, \nu = 1,2,3,...) \tag{2}$$

$$a_\nu = (2/N)\; \Sigma_i^N \varepsilon(t_i) \cos(\, 2\, \pi\, \nu\, i/\, N\,) \; ; \; b_\nu = (2/N)\; \Sigma_i^N \varepsilon(t_i) \sin(\, 2\, \pi\, \nu\, i/\, N\,) \tag{3}$$

The energy losses (ΔW) for one cycle is

$$\Delta W = \int_t^{T+t} \sigma(t)\, d\, \varepsilon(t) = \pi\, \sigma_0\, a_1 \tag{4}$$

Namely ΔW is defined only by first harmonic a_1 So for the $tg\,\gamma$ one have :

$$\varepsilon(t) = a_1 \cos(\omega\, t) + b_1 \sin(\omega\, t) = (a_1^2 + b_1^2)^{0.5} \cos(\omega\, t - \gamma); \tag{5}$$

$$\cos\gamma = a_1 / (a_1^2 + b_1^2)^{0.5} \; ; \quad \sin\gamma = b_1 / (a_1^2 + b_1^2)^{0.5} \; ; \tag{6}$$

$$tg\,\gamma = b_1 / a_1 \, . \tag{7}$$

REFERENCES

1. S.Kh.Shamirzaev, V.M.Sviridov, I.V.Khamrakulov (1992) The conductivity of heterogeneous materials at being superimposed a random irreversible deformation.Preprint № 172-92-ФПП, PhTI of AS Uzbekistan, Tashkent, 1992.

HIGH-TEMPERATURE NONDESTRUCTIVE CONTROL SENSORS OF EMERGENCY SITUATIONS IN AERO-ENGINES

L.A.Reznitchenko, A.N.Klevtsov, A.I.Trubnikov and V.A.Chernyshkov
Institute of Physics, Rostov State University, Rostov-on-Don

During recent years considerable successes have been achieved by the workers of our Institute of Physics in developing the high-temperature piezoelectric ceramic materials operating in different temperature ranges. These materials distinguish by high values of the Curie point and operating temperatures. They may be effectively used in such devices as ultrasonic defectoscopes and thickness gauges for nondestructive control of heated bodies, flow meters and level indicators of liquid and gases in heated pipelines and tanks, sensors for controlling the processes proceeding in different industrial power plants. These devices are used in many fields of technique - atomic power energetics, space technology, automobile and aircraft construction, shipbuilding, metallurgy and geology (acoustic logging in exploring the minerals and exploiting the superdeep holes). Table summarizes the main parameters of the developed materials.

Table
The parameters of high-temperature piezoelectric ceramic materials

Materials	T, C	Toper, C	/	Kp	Kt	d, pC/N	d, pC/N	g, mVm/N	Qm
PCR-26	400	300	455	0.32	-	35	90	22,5	200
PCR-45	420	350	380	0,26	0,46	30	100	30,0	3000
PCR-40	440	350	180	0,07	0,44	5	52	33,0	2000
PCR-50	670	500	150	0,04	0,32	3	25	19,0	4000
PCR-61	1200	950	48	0,015	0,29	0,5	12	28,5	100

A special attention must be given to the PCR-61 material. There is no information in literature on similar materials. This material has the highest operating temperature (to 950^0 C). The reversible changes of the piezoelectric modulus d taking place upon heating from room temperature to 800^0 C are in the (5 - 20) % range. This material may be used as a base for high-precision piezoelectric generator-type pickups of rapidly varying pressures in the systems of controlling the object undergoing the extreme external influences (T 930^0 C, P 200 Mpa). The reversible changes of the piezoelectric d in the case of application of the pressure to 250 Mpa at 800^0 C are about 5%. Also, this material possesses a high anisotropy of piezoelectric parameters.

The experimental models of noncooled pressure pickups were based on the PCR-61 material. Their comparison with the cooled pressure pickups ("Kistler", Switzerland, and "Autronics", Norway) showed the complete identity map of operating processes proceeding in the cylinders of internal combustion engines which was fixed by the pickups for different power settings in the temperature range under study and the possibility to exploit the developed pickups at the higher temperatures (to 900^0 C).

The pressure pickups developed constitute the basis for the small-sized digital measuring instrument MIP-3 intended for diagnostics, assessment and measurement of

The pressure pickups developed constitute the basis for the small-sized digital measuring instrument MIP-3 intended for diagnostics, assessment and measurement of the gas pressure in cylinders of internal combustion engines of ships and boats and the portable diagnostic complex of internal combustion engines DIKOM-1 intended for controlling the technical state of a diesel engine.

The MIP-3 instrument allow one to measure:

1. - the instantaneous value of a number of revolutions of the engine shaft;
   - the arithmetic mean of a number of revolutions;
   - the maximum value of a number of revolutions;
   - the minimum value of a number of revolutions;
   - the instantaneous value of the maximum gas pressure in a cylinder;
   - the arithmetic mean of pressure;
   - the maximum gas pressure value;
   - the minimum gas pressure value;
2. Maximum, mean and minimum values of pressure and a number of shaft revolutions are measured for twenty successive cycles of the working piston stroke.

The MIP-3 Instrument (Specifications)

- range of measurement of the frequency of engine shaft revolutions 60 - 1200 rev/min;
- measurement error 0,5-2 rev.;
- range of measurement of gas pressure in the engine cylinder 10,0 - 120 atm.;
- measurement error 2%;
- supply
  from the voltaic cell 2 - 9 V;
  from the external power source of
  a) the direct-current voltage 12 - 30 V;
  b) the alternating voltage 10 - 25 V;
- operating temperature 20 - 800^0 C;
- mass 500 g.

The Portable Diagnostic Complex DICOM-1 (Specifications)

- range of the measured gas pressure in a cylinder - 0 - 120 atm.;
- discreteness of pressure reading - 0,1 atm.;
- pressure measurement error - 2 %;
- measurement (averaging) time - 5 sec;
- range of measured fuel pressure - 0 - 1000 atm.;
- discreteness of fuel pressure reading - 1 atm.;
- error of measurement of the fuel pressure - 2 %;
- range of measured angular intervals - 0 - 180 pKV;
- discreteness of angle reading - 1 pKV;
- error of angle reading - 0,5 pKV;
- range of the measured indicator pressure - 0 - 2 atm.;
- discreteness ofindicator pressure reading - 0,01 atm.;
- error of measurement of indicator pressure - 2%;
- range of measured revolutions - 30 - 1000 rev/min;
- error of measurement of revolutions - 2 rev/min;

- discreteness of revolution reading	- 1 rev/min;
- electronic block: overall dimensions, mm	- 400 x 340 x 90;
mass	- 6,0 Kg;
- supply from the side mains, direct current	- 24 V;
- consumed current	- 0,6 A.

The Institute of Physics at Rostov State University has the scientific, material and technical, and production base at its disposal that one needs for developing the high-temperature sensors for specific purposes and their mass production.

STUDY OF AIRCRAFTWING DEFORMATIONS BY FILMING

Pukhov A.L., Kazakova T.A., and Kulikov I.K.
Tupolev ASEC, Moscow

Appearance of new types of aircrafts; requirement for a long lifetime; flights at speeds, considerably exceeding the sonic velocity, fore more than six thousand kilometers <197> all demand improved experimental methods for investigation of aerodynamic characteristics of an aircraft to improve its flight-engineering properties.

For the supersonic liner TU-144, with a triangular wing of small extension, calculations and experiments gave a necessary distribution according to scatter of twisting and curvature and optimal profiles. But as the wing is not rigid, the flight from depends on application of aerodynamic and weight loads. Calculation of the fixing shape is, however, difficult and labor-consumimg. Therefore, it must be experimentally checked and improved.

The filming method for deformation diagnostics is essentialyy unique for solving this problem.

The main advantages of this method include:

- no direct contact with the target under study;
- possibility for obtaining spatial coordinates of visible points of the target at a certain time;
- negative material may be kept as long as possible.

The measurement of flight deformations by filmimg the rules situates normal to the wing surface was combined with subsequent mold lofting over the whole surface of the console. With a comparatively small number of sampling points, this approach provides the whole deformed surface and permits the distribution of torsion and curvature over the wing spread to be determined with a great accuracy.

The flight tests with application of the filming method permitted improvement of the calculation of flight deformations of the wing and optimization of the supersonic aircraft wing for the cruising made of flight. This was reached as a result of tracking the wing shape at all stages of evolution.

Besides the TU-144 aircraft, the wing deformation was investigated on the heavy supersonic aircraft TU-160 with the swept-variable wing.

An active element of the dynamic strain sensor based on the piezoelectric film

A.A. Bakirov, V.P. Dudkevich, I.M. Sem, E.V. Sviridov, and V.M. Mukhortov

Institute of Physics, Rostov State University, 194 Stachki Ave.,
Rostov-on-Don, 344090 Russia

Introduction

For the registration of vibrations, rates, accelerations and acoustic emission signals in the industrial strength experiment the use is made of the various mechanoelectrical sensors based on the poled ferroelectric ceramics (more frequently, PZT with modificators). The problem of controlling the construction safety makes the demands which may not be always met by using the ferroelectric ceramics as piezoelectric elements. The use of ferroelectric piezoactive films for making the transducers allows one to ensure such qualities as inertialessness, elasticity and small sizes, a wide frequency range of the recorded signals and also a large operating life at high levels of deformation.

The present paper describes the characteristics of sensors based on the polycrystalline PZT films deposited on the stainless steel foil substrates by rf cathode sputtering. After the deposition of the upper electrode and the polarization under the direct electric field the films obtained had the specific capacity $C \sim 1000$ pF/mm^2 and resistivity $r \sim 10^9$ Ohm/mm^2 and possessed the piezoelectric activity $d_{33} = 50 - 60$ pC/N

Film dynamic strain sensors with a circular directivity diagram

Fig. 1 shows schematically the sensor construction. The sensor is of no more than 0,05 g in mass, $3 \times 3 \times 0.05$ mm^3 in dimension, and its capacity ranges from 400 to 1000 pF (depending on the contraelectrode diameter). The sensor may be attached on the surface of the object under tests with epoxy or another glues, or it may be welded over the perimeter by means of the spot welding.

It is obvious that in the case of the absence of the substantial acceleration of the object surface in the direction of the normal to it the piezoelectric signal must be proportional to the sum of main components of the plane strain tensor.

For the definition of the sensor characteristics the use was made of the standard procedure of low-frequency tests on the fish-bellied beam [1]. Fig.2 shows the piezoelectric signal of the sensor based on the $Pb(Zr_{0.53}Ti_{0.45}W_{0.01}Cd_{0.01})O_3$ film as a function of the sum of main components of the strain tensor ε. As can be seen, this dependence is linear in a wide range of deformation (from 10^{-9} to 6×10^{-4}). The lower limit of the recorded strains $\varepsilon_{min} \sim 10^{-9}$ is due to the influence of acoustic disturbances leading to the uncontrollable deformation of the beam surface layer of 10^{-10}. the upper limit of $6 \times 10^{-4}$is due to the threshold of plastic deformation of the beam material. The sensor sensitivity $\gamma = 1050$ V (the piezoelectric voltage-to-deformation ratio). For the fabrication of sensors the use was made of the films with a high microdeformation and a low piezoelectric modules ($d_{33} = 50 - 60$ pC/N) to decrease the temperature dependence of the piezoelectric signal.

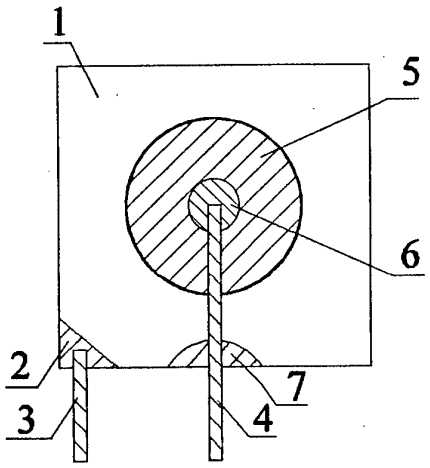

Fig. 1 The dynamic strain sensor: the film surface (1); the area of the metal substrate or the buffer layer (2); the current wires (3,4); the Al electrode (5); the drop of Ag paste or the trace of spot welding (6); the isolation of the current wire from the possible contact with a substrate (7).

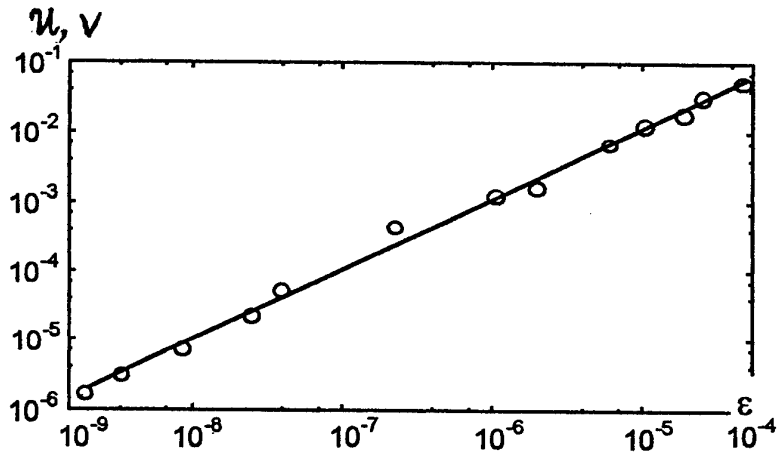

Fig. 2 The piezoelectric signal of the sensors as a function of the sum of main components of the strain tensor ε for the tests on the fish-bellied beam.

The qualitative temperature tests could not be conducted because of the absence of the right glue. So, when the glue EDP, BF-2 and OS-B2-O2 were used the piezoelectric signal began to decrease markedly at T > 100 °C (bellow this temperature the decrease was no more than 10 %). This effect was not consistent with the data on the temperature dependence of the piezoelectric modules and was related to the change of mechanical properties of the glue layer (the strain transfer coefficient). If the sensors were welded to the beam by means of spot welding the temperature of the beginning of the drop in sensitivity increased to 200 - 220 °C.

The sensors were tested under laboratory conditions and on the stands of the Rostov Helicopter Association (RHA).

At the laboratory conditions, the repeated (to 25×10^6 cycles) deformation at the level of 6×10^{-5} at room temperature and the repeated heating to the temperature of 70 °C (about 7000 cycles) were performed on the fish-bellied beam. The results are summarized in Table.

Table 1.

The results of testing the sensors based on the $Pb(Zr_{0.53}Ti_{0.45}W_{0.01}Cd_{0.01})O_3$ films

Number of deform. cycles $\varepsilon = \pm 6 \times 10^{-5}$	Number of therm. cycles $20 \leftrightarrow 70$ °C	Sensitivity, V
0	0	1050
28.8×10^3	-	1052
57.6×10^4	-	1050
23.0×10^5	-	1045
3.3×10^6	200	1045
7.7×10^6	1350	1044
11.5×10^6	2340	1057
28.7×10^6	6680	1059

To determine the operating life of sensors at high levels of deformation and to compare them with the standard tensoresistive sensors the industrial strength experiment was conducted on the vibrostand of RHA on the initiative of the Chief Designer V.A. Dolgov. The object for testing was the helicopter longeron. The tensoresistive sensors (36 pieces) and the above described sensors (3 pieces) were placed on it. The cyclic loading was performed in three regimes corresponding to the sign-variable strains $\varepsilon_1 = 24 \times 10^{-5}$ (31×10^6 cycles), then, $\varepsilon_2 = 39 \times 10^{-5}$ (20×10^6 cycles) and, at last, $\varepsilon_3 = 47 \times 10^{-5}$ (3.1×10^6 cycles). After that, the longeron destructed. The film sensors functioned during whole experiment. The tensoresistive sensors went out of operation in every $(5\text{-}6) \times 10^6$ cycles of deformation and were replaced by the new ones. The sine-wave form of the signal of tensoresistive sensors did not change during the whole experiment. The film sensor signal was of the more complicated form at the expense of the higher sensitivity and wide frequency band and its form remained unchanged up to 39×10^6 cycles of deformation.

Then, this signal began to change in form, probably, reflecting the vibrations of banks of developed cracks.

Conclusion

The models of dynamic strain sensors based on ferroelectric films were constructed. The authors express their thanks to the Russian Foundation of Basic Research supported the present work (Project # 95 - 2 - 06099a).

References

1. Short Physicotechnical Reference Book, v.2. Edit. by K.P.Yakovlev.-Moscow, State Publishing House of Physical and Mathematical Literature.-1960.-216 p.

PHOTOSENSITIVE STRUCTURE TO CONTROL DEFORMATIONS OF METAL CONSTRUCTIONS AND TO TRACE A LIGHT SOURCE

Sh.A.Mirsagatov, B.U.Aitbaev
Physical Technical Institute Uzbek Academy of Sciences, Tashkent,

The deformation of metal constructions is usually controlled in the regime of real time or with some delay from the real time, where the controllable process occurs. In the delay regime a very high precision is provided by optical systems of control with the use of a hologram of the object under control. The essence of the control method is to make a holographic image of the object before and after deformation. The deformation degree is estimated from interference lines
obtained by rotating two holographic images of the object relative to each other.

This system provides an accurate control of construction deformation at the level 0.5λ where λ is the radiation wavelength. When a He-Ne laser with $\lambda = 0.63$ mkm is used, the control accuracy reaches ~ 0.3 mkm. These systems do not operate, however, in real time and are suitable for the use under stationary conditions [1].

The device for controlling the device deformation in real time can be based on photosensitive gauges. This device includes a source of radiation, photosensitive gauge, optical system, and a device for processing information. As the construction deformation is motion of its separate parts relative to one another, the deformation degree may be measured by the photographic response level, caused by motion of the falling light radiation over the light-sensitive surface of the gauge in the process of deformation.

Traditional light-sensitive gauges are little sensitive to these motions within their openings. Therefore in some cases the photosensitive gauges are manufactured in the many-window version sensitive to coordinate motions of a ray beam, or outer diaphragming is applied to them. They do not provide, however, a sufficient accuracy of control for the motion of a light beam travelling over the light-sensitive surface.

The present work reports results of investigation of a photoreceiver based on a polycrystalline film with columnar structure of grains. Each of the grains is a microscopic photoreceiver grown on a common support. Because of high photosensitivity of sites situated at highs relative to sites near the base, a quite drastical contrast of photosensitivity appears as the light beam moves from top to bottom of the microphotoreceiver. To study potentialities of this gauge aimed at using it in devices controlling the construction deformations, in particular, aircrafts, the relief of the photosensitivity relief of the gauge surface is investigated.

To study the surface relief of polycrystalline semiconductor materials in the regime of current induced by light or electronic beam, it is necessary to create, on the basis of these materials, photosensitive structures of the type of Shottki barrier or small p-n transition. On the basis of polycrystalline Cd telluride, we have created a small p-n transition with an upper optical window by spraying Cd in an O-bearing medium on the surface of p-CdTe films by a magnetron method.

Basic p-CdTe polycrystalline films were synthesized by the gas transport method in hydrogen flow. The p-CdTe films had a resistivity in the range $\rho = 10^2 \div 10^6$ om.cm depending on parameters of the technological regime. It has been established by X-ray analysis that these films are of columnar structure, the grains being of 100-150 mkm in size and penetrating throughout the film thickness. On scanning in the regime of light or electron beam-induced current, the electron-hole pairs are generated and recorded simultaneously (Fig. 1). Thus, the perfection of a local probed point of the surface of the material under study may be inferred from the magnitude of photocurrent. The

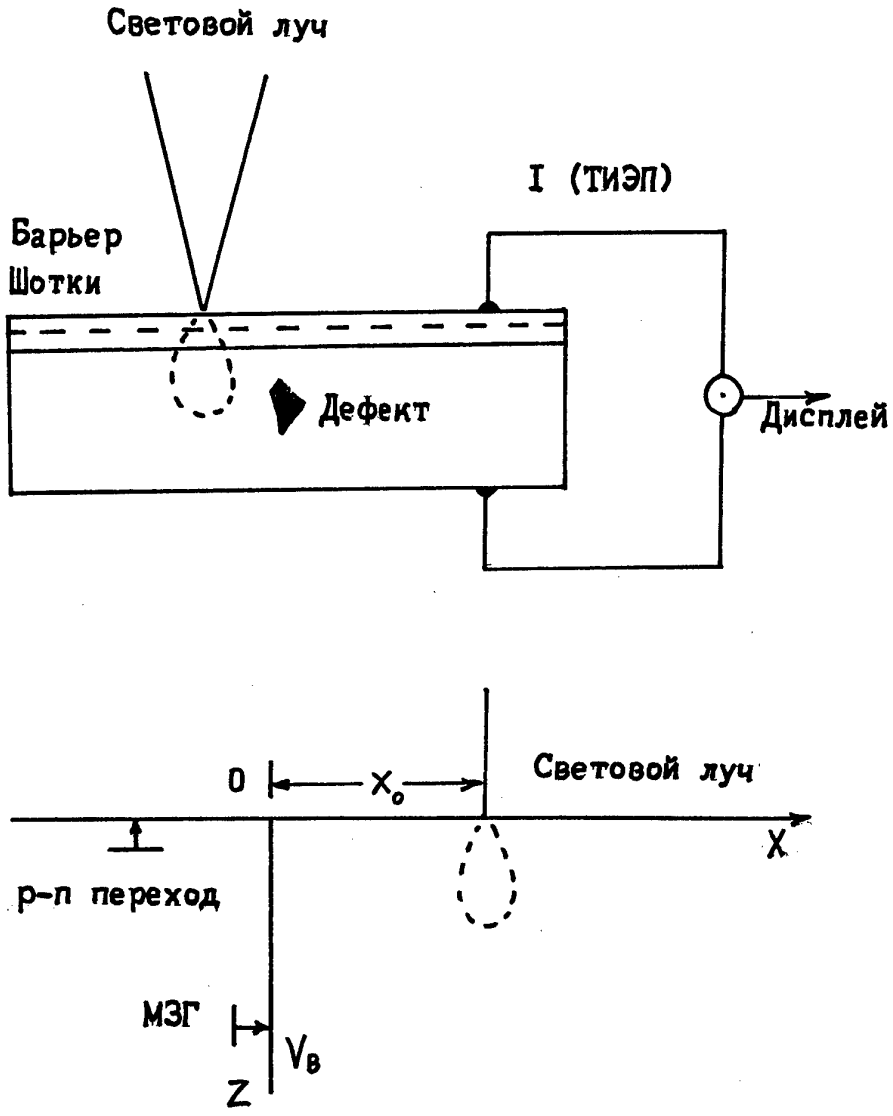
Световой луч
I (ТИЭП)
Барьер
Шотки
Дефект
Дисплей
0
X_o
Световой луч
X
p–n переход
МЗГ
$V_в$
Z

Fig. 1

photocurrent at the probed point depends on the amount of generated electron-hole pairs as well as on the material surface perfectness and velocity of surface recombination at the constant diameter of a light or electron beam.

To scan the surface of p-CdTe polycrystalline films, the regime of light-induced current was used. The light source was a He-Ne laser with $\lambda = 0.63$ mkm , with radiation power of 25 mW, and with a light beam diameter of 5 mkm. Figure 2a shows the photocurrent microrelief, which reflects the state of microsites of the surface of polycrystalline films with $\rho = 10^3$ om.cm on light scanning. An additional study under the microscope has shown that the surface is of intricate relief; as a rule, it
is hummocky, the "hummocks" being close to the truncated cone with linear dimensions of 7-10 mkm in cross section. The distance between the cones averages to 100-150mkm. Study has shown that the height of "hummocks" is different, the number of high truncated cones becoming less as the resistivity increases; at the same time the photosensitivity contrast increases. For example, the contrast of photosensitivity near the vertical axis of symmetry and at a distance of 40 mkm in films with $\rho = 10^3$ om.cm and $\rho = 10^6$ om.cm is 10 - 12 % / mkm, 1% / mkm ($\rho = 10^3$ om.cm), 20 - 25 % / mkm, and 2 - 3% / mkm respectively.

These experimental data suggest that by changing the regime of synthesis of CdTe polycrystalline films it is possible to govern not only the grain geometry as distance between their tops but also the slope of generating "cones"; as a result, it becomes possible to govern microparameters of crystallites: the velocity of surface recombination and time of life of secondary carriers.

The estimates of microparameters -- diffusion length of secondary carriers (L_n) and rates of surface recombination (S) for a film crystallite with $\rho = 10^3$ om.cm indicate that at the top of this crystallite $L_n = 200$ mkm and $S = 10^3$ cm / c, while near the bottom of the "cone" $L_n = 10$ mkm, $S \geq 10^6$ cm / c. To assess L_n and S, we have used: contrast profile (Fig. 2a) and contrast profile dependence on dispersion of depth- normalized light absorption (Fig. 2b), which were calculated as in [2]. At the bottom of "cones" crystallites (grains) are closely packed and, most likely, this massif is the basic surface of the films under study. As shown above, the growth in the p-CdTe film resistivity leads to an increase in photosensitivity and photo-e.m.f. The evidence is the 3-fold increase in diffusion length of secondary current carriers (L_n) and the 4-fold decrease in rate of surface recombination (S), respectively, on the surface of the truncated "cone" of a microcrystallite in a film with $\rho = 10^6$ om. cm as compared with similar microparameters of a microcrystallite with $\rho = 10^3$ om. cm. For example, $L_n = 10^2$ mkm, $S \sim 10^3$ cm / c. ($\rho = 10^3$ om. cm), $L_n = 5.10^2$ mkm, $S \sim 4.10^2$ cm / c ($\rho = 10^6$ om.cm). Correspondingly, these microparameters also vary near the "cone" sole, i.e. on the basic massif of the surface. This surface in p-CdTe films with becomes smoother, the distance between separate cone tops reaching The results obtained permit the following conclusions:

1. The surface of p-CdTe polycrystalline films synthesized according to the proposed technology [3] is very sensitive to parameters of technology, especially, to support parameters (T_s), cooling rates, as well as flow rates of transporting gas, in this case, hydrogen.
2. Geometrical dimensions of crystallites highs, their number, and distance between them also vary. As T_s grows, the distance between highs of crystallites becomes greater, and the slopes become steeper.
3. As T_s grows, the rate of surface recombination (S) considerably decreases, while the diffusion length of neon current carriers (L_n) increases. As a result, the photosensitivity contrast increases, which permits photoreceivers with a high resolution to be created.

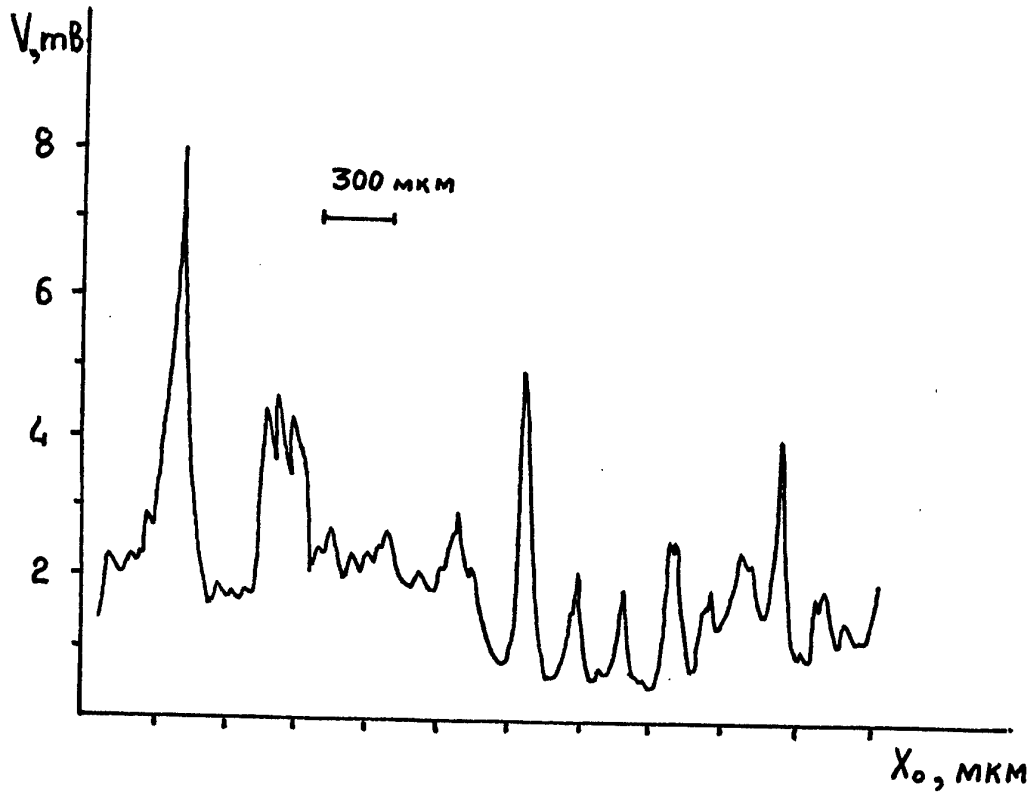

Fig.2

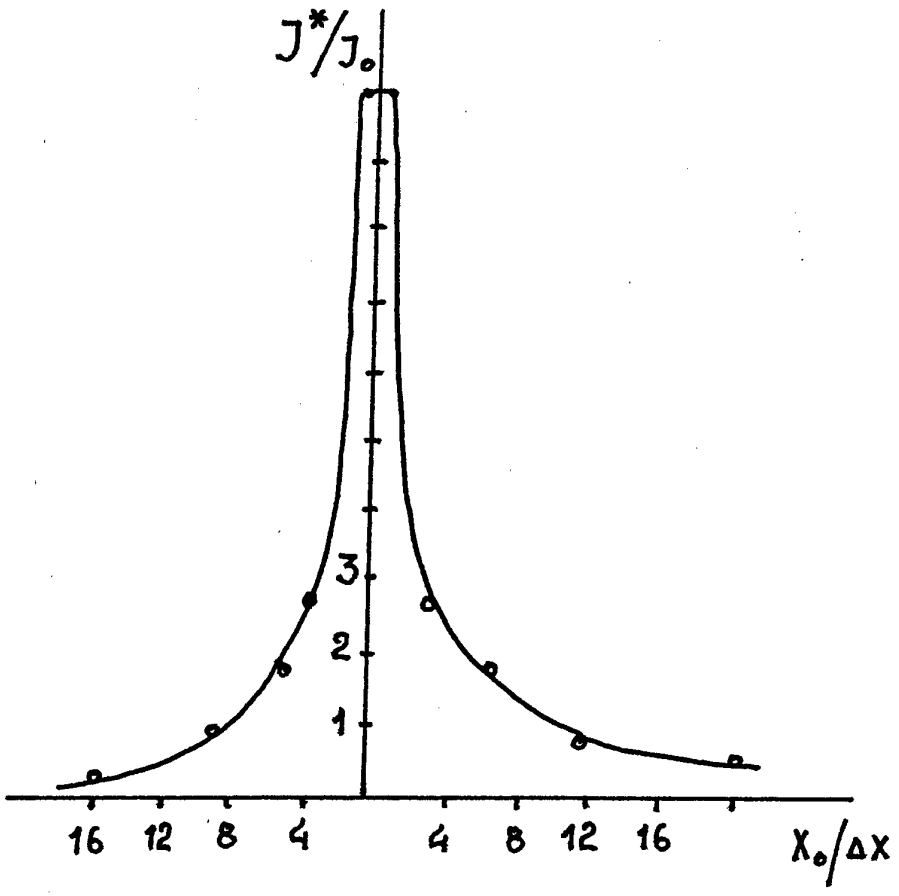

Fig.3a

In the process of studies the diameter of the light probe is 1-5 mkm, which is essentially less than the size of a typical crystallite. Therefore, the spatial resolubility of the deformation control device is limited only by the probe size and may be of a micrometer order, which is sufficient for any practical aims, including the control of aircraft deformation.

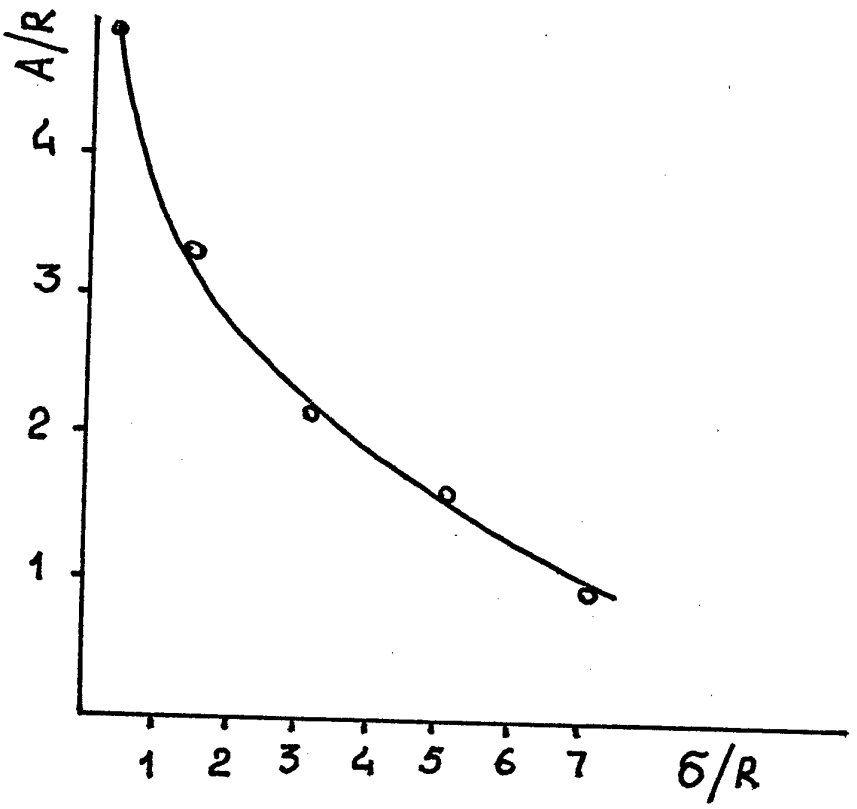

Fig.3 *б*

REFERENCES

1. D.Keisesent (ed.), Optical processing of information (translated from English), Moscow, Mir, 1980.
2. K.Donoloto, Study of polycrystalline semiconductors by the method of electron beam-induced current, in: Polycrystalline semiconductors (translated from English), Moscow, Mir, 1989.
3. Sh.A.Mirsagatov, P.I.Knigin, and M.A.Makhmudov, Geliotekhnika, no. 1, 1991.

STUDY OF DEFORMATION BY FILM THERMOELEMENTS

M.K.Korabaev, E.S.Sagatov, E.A.Abdullaev, S.Otazhonov
FSU, Fergana

When a construction is subjected to a cyclic load, its surface suffers from compression and extension, i.e. intra-atomic friction occurs to cause emanation of energy in the form of heat. It is supposed that the greatest amount of heat gives off where the constructions suffers the greatest deformations (loads). To record temperature distribution under cyclic loads along the specimen to be studied, we have developed a construction of semiconductor film thermopile. The thermopile is an alternating series of p-n-type semiconductor thermoelectric material connected successively by junctions with resistance contacts. Their solid solutions with different coefficients of temperature extension of energetic zones were used as sensitive semiconductor material in order to reduce the temperature dependence of thermo-electromotive force coefficient. The film thermopile was obtained by thermal spray-coating onto a dielectric elastic support; then terminals were solded, and together with the thermopile the support was rolled to form a cylinder averaging to 5 - 7 mm in diameter and 5 - 10 mm in height. The sensor junctions were situated at the very edge of the cylinder base and protected them from the effect of the external medium and by-passing at the contact with metal and dielectric interlayer.

To carry out investigations, we have made beams 5 cm wide, 5 mm thick, and about 30 cm long of duraluminum alloys, with a priori known sites where the beam will suffer the greatest deformation (Fig. 1a); this is a segment with the least width of the beam (segment h). One side of the beam was fixed firmly; then it was normally subjected to cyclic symmetrical loads at its unfixed end with a different frequency of 5 - 12 Hz and amplitude. Then the film pile was scanned along the beam.

It is visible from Fig. 1B that at the beam narrowing, where it suffers the greatest deformation, the thermo-electromotive force, E, grows most significantly, which is due to a temperature increase, ΔT, at the site h. These experiments were carried out many times, and the results obtained were unambiguous. The output signal may be increased by increasing the number of thermopiles per thermopiles.

Thus, by means of a film thermo-electrical pile the increase in thermal EMF E $\sim\Delta T$ indicates the site where a construction suffers the greatest deformation, i.e. the greatest load.

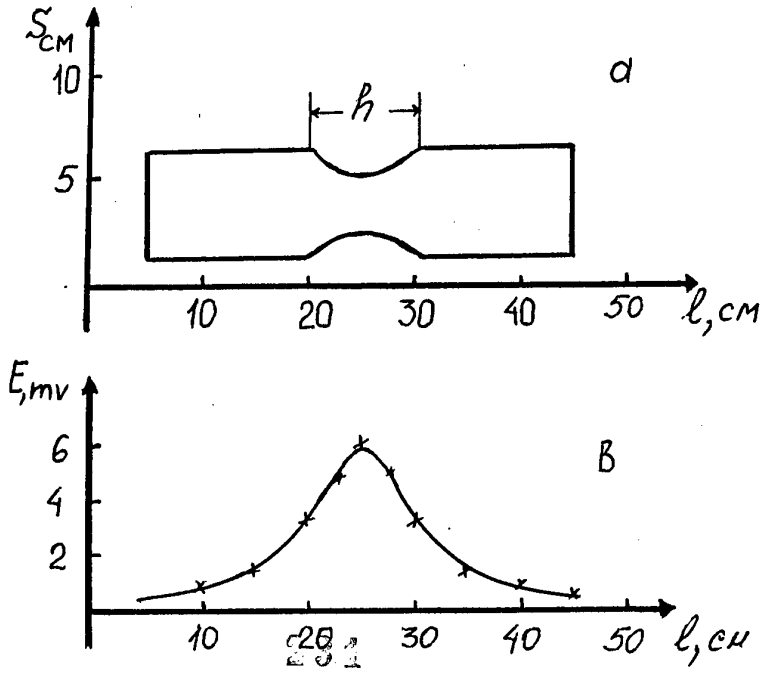

ELECTRONIC PROCESSES IN POLYCRYSTALLINE PbSe FILMS WITH FRAGMENTARY STRUCTURE

E.A. Abdullaev, A.Mirzakulov , I.V. Khamrakulov *)
FSU, Fergana ; *) TSAI, Tashkent

This work deals with the effect of condensation temperature and In-, Bi-, and Se-doping of the charge on the PbSe films. These studies were aimed at searching optimal technological regimes of producing PbSe films with expressed tensoresistive properties.

The thermovacuum preparation of PbSe condensates was carried out by the method of open evaporation. The supports were polyamide varieties PM-1. In producing PbSe films, the initial material was a lead selenide of quasistoichiometric composition. It was doped with In, Se, and Bi of high purity.

Electron microscopy and X-ray analysis of the structure of the PbSe films obtained by thermovacuum evaporation on polyamide band supports revealed the following features:

- the films are of polycrystalline structure where the majority of crystals are oriented by the plane (200) parallel to the support plane;
- lattice constants of the film and PbSe crystallites coincide within an experiment error;
- In-, Bi, and Se-admixtures introduced into the initial charge within the solubility of these substances in PbSe exert a doping effect of the films to form no compounds with PbSe components.

A joint study of how electric conductivity and tensosensitivity coefficient, TSC, of the films depend on condensation temperature and their surface macrostructure revealed a network of microfractures (fragmentary structure), this phenomenon being observed in the films obtained from the charge of quasistoichiometric composition as well as from In-, Bi-, and Se-doped charges.

Figure 1 shows a relative variation of electric conductivity, S/S_0 (S_0 is the electric conductivity at the starting temperature of condensation). According to these data at $T_0 \leq 370$ K, the films have conductivities of p-type. The electric conductivity of films continuously grows with Tc. At $T_0 \approx 370$ K the type of conductivity changes; with a further increase in T_0 the electric conductivity of films decreases quite significantly. Analysis of experimental data over a great number of specimens showed that in the range of condensation temperatures under consideration a sharp peak was observed at $T_0 \approx 360$-370 K with S/S_0 versus T_0. At the same T_0 tensoresistive properties are best expressed in the films.

Figure 2 shows the TSC of PbSe films versus condensation temperature. Also we have studied the effect of a doping admixture of In, Bi, and Se on the tensoproperties of PbSe films. With an excess of In and Se introduced into PbSe films their TSC decreases, while with an excess of Bi it increases.

The type of conductivity and electric conductivity of polycrystalline films under the thermovacuum way of their production is determined by their structure and composition and corresponding electron potential barrier. It is known that while precipitating on weakly heated supports the PbSe condensates become richer in chalcogen, and at $T_0 > 420$ K they are Se-enriched [1].

As regards a drastically nonmonotonous dependence $S/S0 = f(T_0)$, the following explanations may be considered. The vacuum PbSe condensates on strange supports tend to disintegration [2, 3] because of differences in thermal coefficients of expansion of the film and

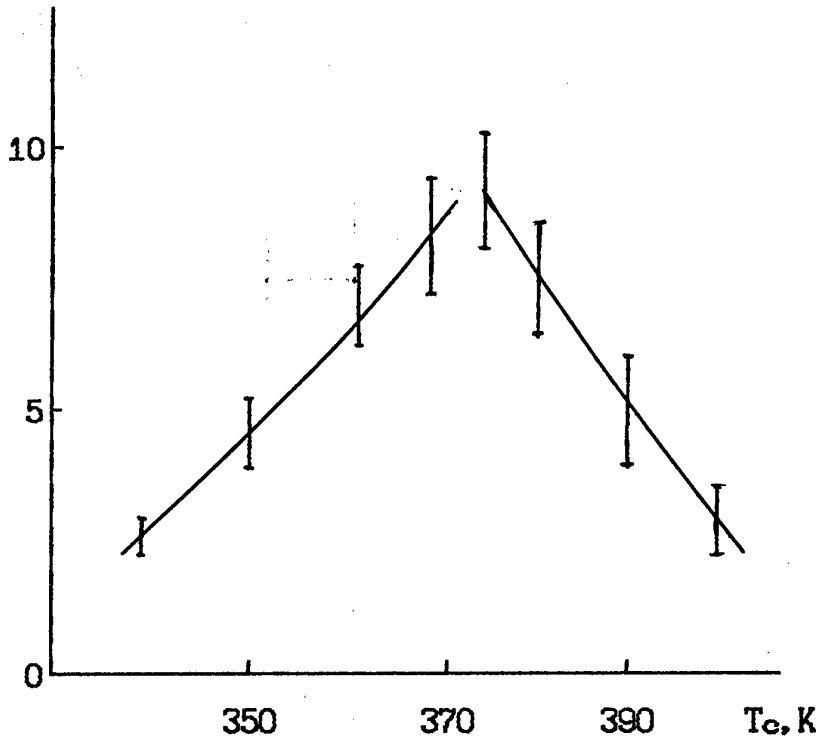

Fig.1

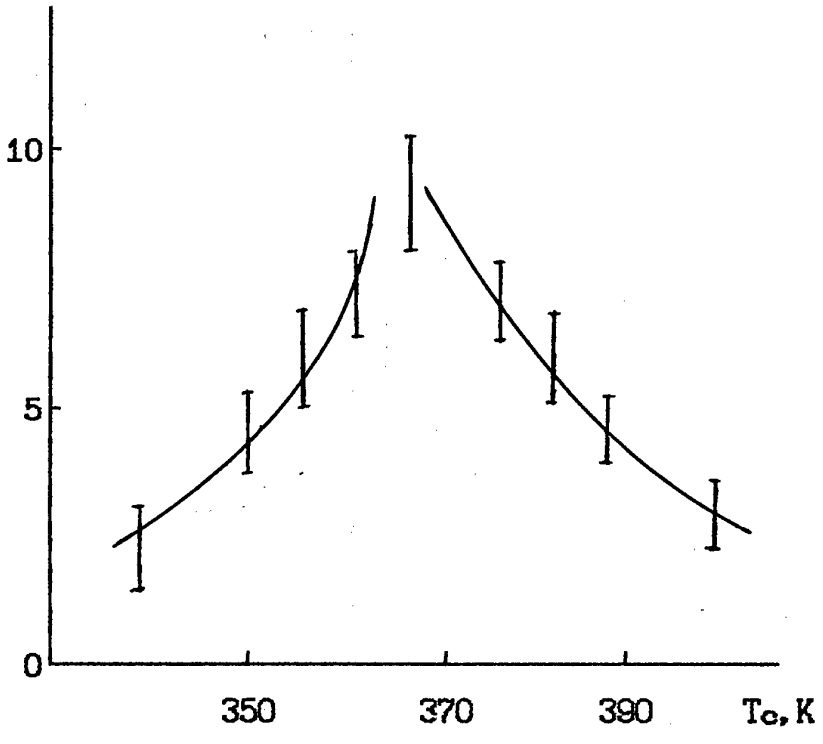

Fig.2

support materials. We believe that after the technological process has finished and the condensates have cooled, a mechanical stress appears in the film-support system. In the films obtained at T_0 > 360-370 K, the mechanical stress is sufficient for the film rupture and its continuum disturbance. A network of microfractures forms in the film, and it acquires the so-called fragmentary structure [4]. The degree of the development of the microfracture network increases with condensation temperature, because in this case mechanical stresses increase in the system.

At T_0 << 360-370 K, the inner mechanical stresses that appear in the film-support system are not sufficient for the films to be torn. The increase in electric conductivity of films with T_0 in the range under consideration is due to improved microstructure of the films. The condensation temperatures 360-370 K are sufficient for a fragmentary structure to form in the condensates. In terms of [2] at $T_0 \approx$ 360-370 K an infinite conducting cluster forms, where the conductivity occurs through "isthmuses" between fractures (through film sites with undisturbed continuity), because the network of microfractures is not simply connected at the initial stage of the formation of fragmentary structure. At T_0 > 360-370 K the infinite cluster begins to break at the cost of microfractures and decreased number and sizes of the isthmuses; the electric conductivity begins to fall.

The experimentally determined dielectric permeability in PbSe films, in the UHF range, condensed at $T_0 \approx$ 360 K, providing the highest tensosensitivity in the films appeared at 300 K to be equal $(3 \div 6)^* 10^4$, which is three orders of magnitude higher than the dielectric permeability of the same films measured in the optical range. The reason of the significant difference in dielectric properties of films measured in the optical and UHF ranges is connected with heterogeneity of the specimens under study. To consider the phenomenon nature in more detail, we have studied the dielectrical permeability of the above-mentioned PbSe films as a function of temperature and level of a one-axial deformation of extension.

Figure 3 shows the dielectric permeability of films as a function of inverse temperature at various levels of one-axial deformations of extension. It is visible that the dielectric permeability actively grows with temperature up to T $\approx$ 360 K, then it passes over the maximum and decreases. The dielectric permeability decreases as the deformation level increases, but the character of the temperature dependence of dielectrical permeability does not change, the maximum corresponding to 360 K in the deformed state as well.

To explain this interesting effect we remember that the highest tensosensitivity in the PbSe films corresponds to the threshold of the formation of fragmentary structure with the appearance of an infinite conducting cluster. In the tensosensitive film condensed at $T_0 \approx$ 360 K, a multiply connected network exists at room temperature. In the process of temperature growth to T = T_0 the film and support extend to different degrees, and at T = T_0 the microfractures collapse: a structural phase transition of 2nd kind occurs, i.e. the fragmentary structure becomes continuous. It is in the phase transition that the maximum is observed with the dielectric permeability as a function of temperature.

Thus, the anomalies of dielectric properties of tensosensitive PbSe films are connected with the specific nature of their microfracture structure.

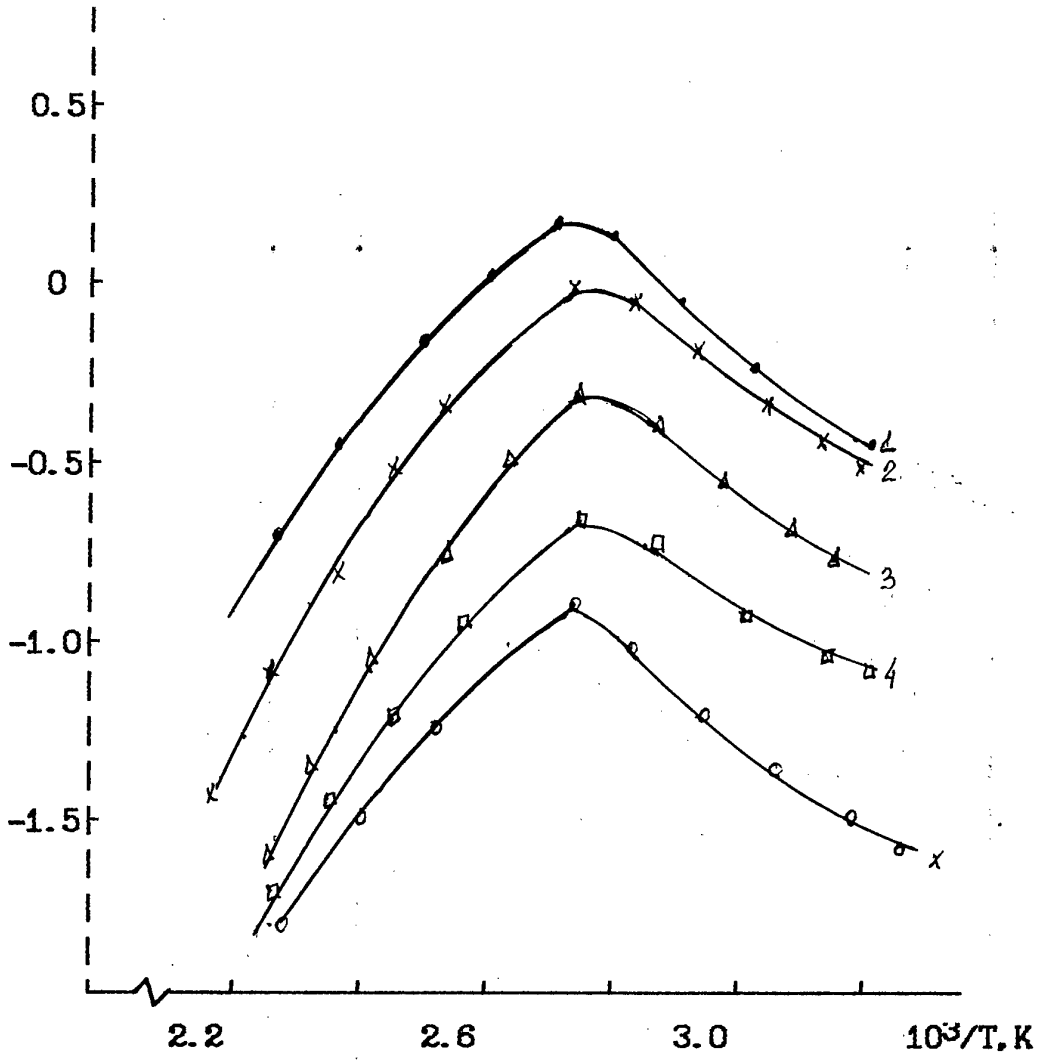

Fig. 3 . æ * 10^3 : 0 (1); 1.4 (2); 2.8 (3); 4.2 (4); 5.6 (5).

REFERENCES

1. L.S.Palatnik and V.K.Sorokin, Thin levels of semiconductor compounds // Izv. AN SSSR. Neorganicheskie Materialy, 1969, vol. 5.
2. S.P.Varfolomeev, V.G.Karpov, N.V.Kolesnikov, et al. Current flow in polycrystalline film with disturbed continuum // FTP, 1984, vol. 18, issue 9, pp. 1698-1700.
3. V.A.Zykov, S.A.Kazmin, and V.I.Kaidanov. Determination of the mobility of current carriers in semiconductor films with macrodefects // PTE, 1982, no. 5, pp. 190-192.
4. Yu.A.Tkhorik and L.S.Khazan. Plastic deformation and disagreement dislocations in heteroepitaxial systems. Kiev: Naukova Dumka, 1983, 304 p.

TEMPERATURE AND FREQUENCY DEPENDENCES OF KINETIC COEFFICIENTS OF STRAIN-SENSITIVE Bi2-xSbxTe3 FILMS

M.M.Akhmedov, K.E.Onarkulov, A.M.Khudoiberdiev
Fergana StateUniversity, Fergana

To make efficiency film tensoresistant structures, knowledge of features of physical processes in films under various environments and recognition of their mechanisms are necessary. The knowledge of regularities of current transfer in $Bi_{2-x}Sb_xTe_3$ films may be a means in identification of nature of tensoresistive effect.

Methods of investigation of processes of electron transfer in $Bi_{2-x}Sb_xTe_3$ films are studies of temperature and frequency dependences of their kinetic coefficients.

Figure 1 shows temperature dependences of electric conductance, coefficient of strain sensitivity (CSS), Hall coefficient and thermal e.m.f. of $Bi_{2-x}Sb_xTe_3$ films condensed on oxidized duraluminum at T_c = 360 K. Figure 1 shows that electric conductance σ weakly depends on temperature, and electric conductance of films condensed at T_c = 420 K decreases as temperature grows like the situation observed in the massive $Bi_{2-x}Sb_xTe_3$ crystals. The dependence σ in films is, however, weaker than in crystals. This character of temperature dependences of electric conductance is related to the structure of the indicated films. The results of electron microscopic investigations have shown that the films obtained at T_s = 360 K and T_s = 420 K have fragmentary and massive structure, respectively. In the films of fragmentary structure, the microcracks existing in the films give rise to energy barriers, and the charge carriers overcome them by tunneling. The height of these barriers may be commensurate with the work of output from Bi_2-xSb_xTe_3 or somewhat less at the cost of forces of mirror image between charged planes forming cracks. Since the current transfer in films is limited by the possibility for holes to pass through the barriers, which does not depend on temperature, the electric conductance does not depend on temperature either or depends very weakly at the cost of temperature dependence of the efficient mass of holes. In the second case the change is explained by the fact that in the massive specimens σ depends on acoustic phonons and in some cases by dissipation on neutral defects [1].

Thus, the difference in dependences σ (T) in the films obtained at T_c = 360 K and T^c = 420 K is related to differences in their microstructure.

A frequency dependence of electric conductance of polycrystalline $Bi_{2-x}Sb_xTe_3$ films was studied at a variable signal within frequencies of 0 to 20 MHz. Figure 2 shows a relative change of film conductance versus frequency of a variable signal for three films obtained at different temperatures of condensation. It is seen that the character of dependences σ (ω) / σ (0) for various films is qualitatively similar. However, the ratio of changes in electric conductance considerably depends on temperature of their condensation. The ratio of changes of electric conductance at a variable signal, the greatest in the films condensed at T_c = 360 K, i.e. at the condensation temperature providing the greatest strain sensitivity in condensates. Data of Fig. 2 show that the parameter σ (ω) / σ (0) is structure-sensitive. It decreases as the condensation temperature grows, which improves with increasing condensation temperature, thus improving the film structure.

REFERENCES

1. A.I.Anselman, Introduction to the theory of semiconductors, Moscow, 616 p.
2. T.S.Gudkin, I.N.Drabkin, V.I.Kaidanov, et al. FTP, 1974, vol.8, issue 11,
3. Sh.B.Atakulov, U.A.Gafurov, and S.A.Kazmin, FTP, 1988, vol.22, issue 3, p.567.

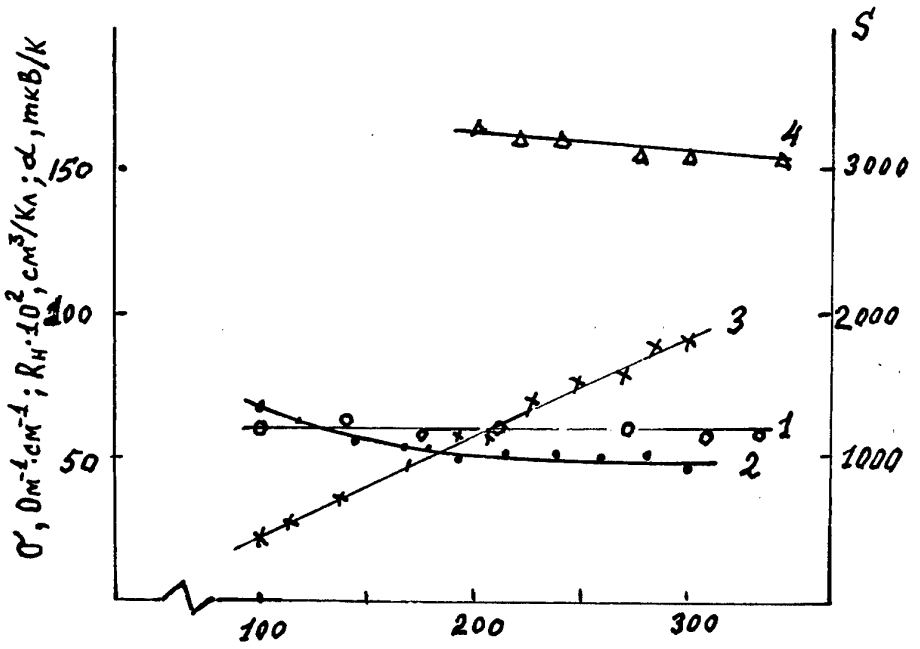

Fig. 1 . The temperature dependences of conductivity (1) ; deformation's coefficient (2); Holl coefficient (3) and thermo e.m.f. (4) of $Bi_{2-x}Sb_xTe_3$ films condensed at 360 K

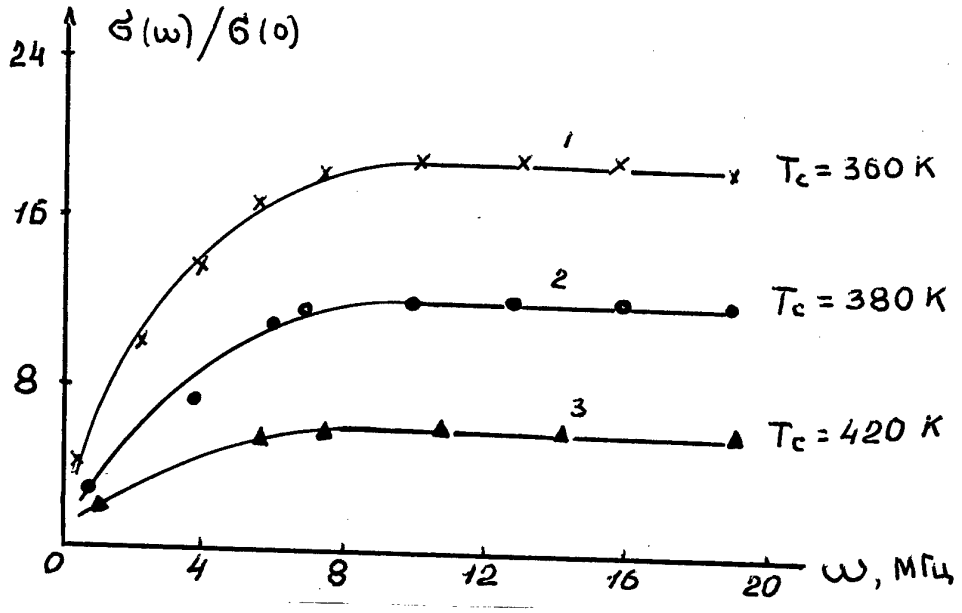

Fig. 2. The frequency dependences of relative conductivity of $Bi_{2-x}Sb_xTe_3$ films.

SURFACE TENSION AND LOCAL ELECTRIC FIELDS IN STRAIN-SENSITIVE FILMS

E.A.Abdullaev, M.I.Ubaidullaev, and A.Shakhanov
FSU, Fergana

A spontaneous bend is observed in single-crystal semiconductor plates made of InSb and GaSb. This is a result of etching and mechanical polishing of plates in the air [1]. The bend magnitude measured under the microscope and calculation of mechanical stresses show that given this phenomenon is due to differences in surface tension at the opposite faces of the plate, the difference in surface tensions would be 10^3 to 10^5 dn/cm. Somewhat later these experiments were repeated by other investigators [1] but this time in a high vacuum with cleaning the surface by ionic bombardment and using a laser interferometer to record a sag.

The measurements were carried out on specimens made of the same materials. The sensitivity threshold at both faces was decreased to 800 dn/cm. It was shown that the plate bend under observation was the result of the action of inner stresses appearing at mechanical polishing of the specimen. With the surface level removed by ionic bombardment, the flat form of the plate restored, and the surface tension did not manifest itself.

The film formation on the support was shown [2-6] to be followed by diverse imperfections of crystal structure (dislocations, vacancies, interstices, impurity atoms, grain boundaries, etc.). They lead to structural inner mechanical stresses. On the other hand, these imperfections create local electrical fields resulting in potential barriers. In the scientific and practical context, it is interesting to determine, first, the connection between surface tension and inner mechanical stress; second, the connection between inner mechanical stresses and intensity of local electrical field; third, the height of micropotential barriers. Kinetic phenomena in these structures may be studied on this basis.

It is known from laws of thermodynamics that the elementary thermodynamical work is

$$dA = \gamma d\Sigma \qquad (1)$$

where Y is the coefficient of surface tension of the film; Σ is the change of surface area of the film. On the other hand, this work may be equated to a change of free energy (2) >

$$dA = -dF \qquad (2)$$

From (1) and (2) we have (3)

$$\gamma(\Sigma_2 - \Sigma_1) = F_1 - F_2 \qquad (3)$$

Taking into account the Gibbs-Helmgoltz for free energy into two states we can write:

$$F_1 = U_1 + T\left(\frac{\delta F_1}{\delta T}\right)_v \qquad (4)$$

$$F_2 = U_2 + T\left(\frac{\delta F_2}{\delta T}\right)_v$$

Using the generalized Hook law for the coefficient of surface tension we will have

$$\gamma = -\frac{Ed}{V \ln T_2/T_1}\left[\frac{U_2 - U_1}{\sigma_x - \mu\sigma_y}\right] \qquad (5)$$

where E is the Young modulus;
μ is the Poisson coefficient;
d is the film thickness;
σ_x and σ_y are the inner stresses;
V is the film volume;
U_2 and U_1 are changes in inner energy;
T_2 is temperature of film melting;
T_1 is room temperature.

The surface tension does exist in thin films, and it is determined by:
1) inner energy;
2) Young module and Poisson coefficient;
3) volume and thickness of the film;
4) inner stress and temperature of the film.

Now we will find the connection between inner mechanical stresses and intensity of the local electrical field. The problem will be considered under the following assumptions. We consider that the defects in a strain-sensitive film create around themselves spherical electrical fields with outer and inner radii R1 and R2.

Suppose that the shell thickness is:

$$h = R_2 - R_1 > L_D \qquad (6)$$

where L_D is the Debye length of screening.

On the other hand, an additional sphere caused by near defects may appear around this sphere. Designate distances between outer sphere surfaces by R (Fig. 1). A community of these near charged defects create charged dislocation walls. It is quite established that local electrical fields and potential barriers appear between these spherical defects (Fig. 1). For the sake of more convenient calculation, we suppose that between spheres I and II a ball-like cavity was situated; its radius was

$$h = R_2 - R_1 < d + \frac{h}{2} = \frac{L}{2} = r \qquad (7)$$

where L is the distance between centers of sphere shells I and II (Fig. 1). The ball-like cavity is subjected to uniform confining compression. The appearing deformation ε^* is [7]:

$$\varepsilon^* = \frac{P^*(d + \frac{h}{2})^2(1-\nu)}{2Eh^2} \qquad (8)$$

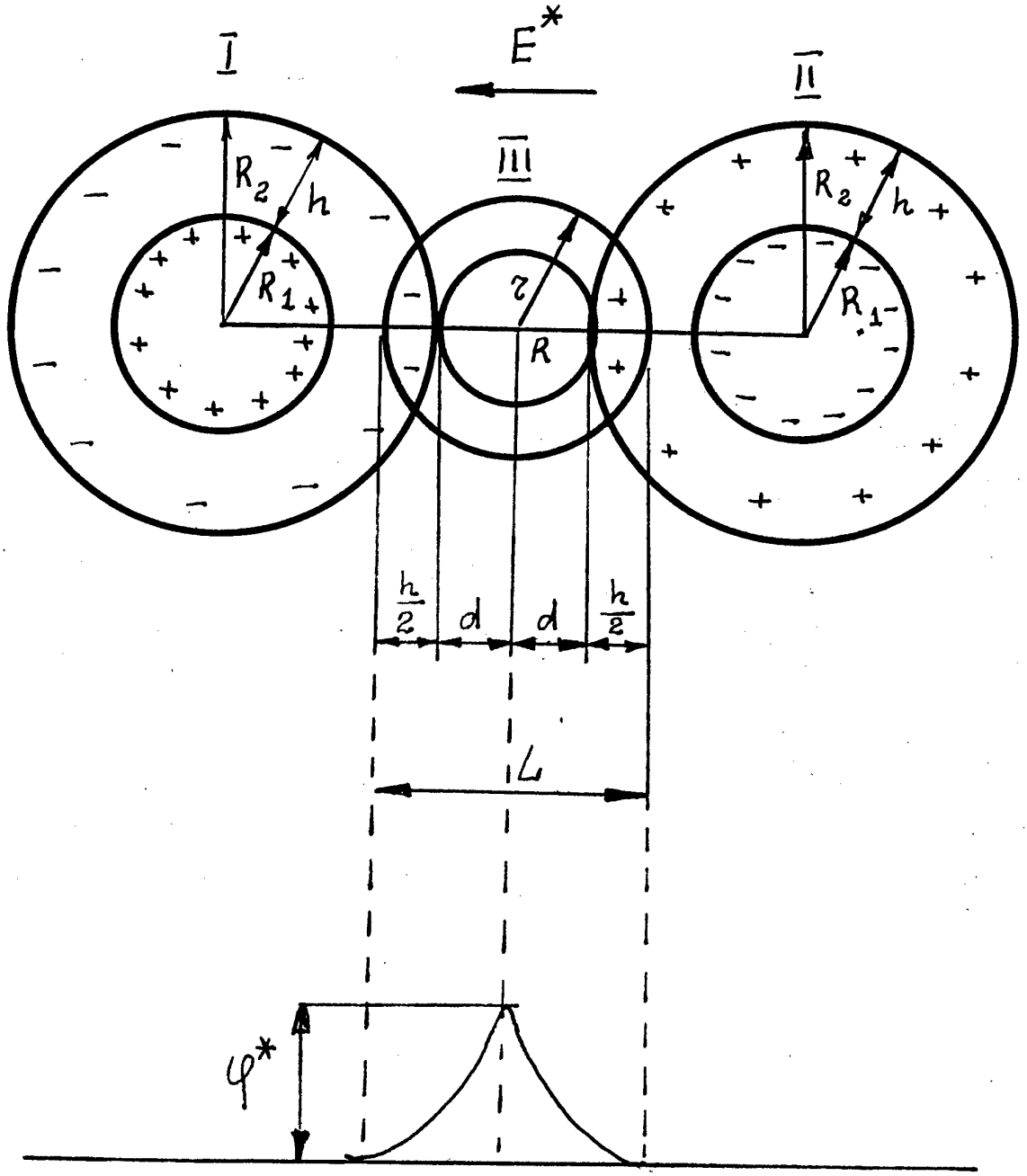

Fig.1. The model of internal tensity and local electric fields in DC films

where P* is the inner pressure defined in the form

$$P^* = \frac{F^*}{S} \qquad (9)$$

where F' is the force of interaction between defects;

S is the surface of ball cavity III.

To find F*, we suppose that within the range of distances h/2 charges q_1 and q_2 are concentrated in spheres I and II. The energy of interaction is [8]:

$$U(R) = \frac{q_1 q_2}{\varepsilon R}\left(1-\frac{R}{L_D}\right)\cdot\exp\left(-\frac{R}{L_D}\right) \qquad (10)$$

Taking into account (8), (9), (10), and Hooke's law, we have for the field intensity:

$$E^* = \frac{8\pi h^2\sigma^*}{q_2\left\{1+\frac{R}{L_D}-\left(\frac{R}{L_D}\right)^2\right\}(1-\nu)}\cdot\exp\left(\frac{R}{L_D}\right) \qquad (11)$$

Analysis of (11) showed that R and h may acquire the following values:

$$R = 1{,}5\,L_D \qquad (12)$$

$$h = 5L_D$$

With (12) taken into account, we have

$$E^* = \frac{3600\cdot\pi\cdot\sigma^*\cdot L_D^2}{q_2(1-\nu)} \qquad (13)$$

Using (13) we can find the height of potential barrier created by defects I and II:

$$\varphi^* = \frac{3600\cdot\pi\cdot\sigma^*\cdot L_D^2}{q_2(1-\nu)}\cdot L \qquad (14)$$

where $L = 6{,}5L_D$ (15)

The calculations were made for films φ' with the inner stress
$\varphi' = 10^8\,n/m^2$ and $L_D = 10^8$ m; $\varphi' = 0{,}0669$ eV ≈ 0.07eV
These values of stresses and Debye lengths are characteristic of $(BiSb)_2Te_3$ films.

The electric conductivity of strain-sensitive films is known to be determined by the barrier mechanism (9). The results obtained show that as barriers appear, a certain contribution comes from the defects that appear in the strain-sensitive films in the process

of growth. A change in quantity and character of defects leads to barriers of various forms and heights, which in turn results in a change of kinetic phenomena in them. For the films made of different materials an optimal concentration of defects seem to exist, thus leading to film tensoresistors with high deformation coefficient (DC). The theoretical results obtained are in agreement with experimental observations for multicomponent semiconductor materials. Now, using (5) we calculate the surface tension on the surface of sensitive films. For the sake of convenience in calculation of the surface tension coefficient in (5), we suppose:

$$\sigma_x = 0, \quad \sigma_Y = \sigma_{tot}$$

$$dU = \lambda dm, \quad m = \rho v,$$

$$\gamma = \frac{E \cdot d \cdot \lambda \cdot \rho}{\mu \cdot \sigma_{tot} \ln \cdot \frac{T_2}{T_1}}$$

where λ is the specific heat of melting of film material;
ρ is the film density.

With the following data typical of semiconductor materials such as CdTe, Sb2Te3, Bi2Te3 and some others:

$\mu = 0.1 + 0.5$
$E = 6 \cdot 10^5$ n /m^2
$d = 6 \cdot 10^{-6}$ m
$\rho = 7.8 \cdot 10^3$ kg/m^3
$\sigma_{tot} = 10^8$ n/m^2
$\lambda = 125.51$ kDj /kg
ln300 = 5.7

we will have $\gamma = 0.8 \cdot 10^8$ dn/cm.

This result is comparable with experimental observations.

The authors are grateful to Drs. I.E.Bilyalov and B.A.Volkov for discussion and valuable advice.

REFERENCES

1. 1.A.Ya.Gokhshtein, Surface tension of solids and adsorption, Nauka, Moscow, p.399
2. B.A.Atakulov et al., Deformation effects in inhomogeneous semiconductors, Fan, UzSSR, 1978, 275 p.
3. G.Matare, Electronics of defects in semiconductors, Mir, Moscow, 1974, 463 p.
4. Technology of thin films. Handbook, Moscow, Sovetskoe Radio, vol. 2, 1977, 768
5. T.Azimov, E.I.Bilyalov, and M.I.Ubaidullaev, On surface tensions in thin films. Abstracts of the VI Republic School of Young Physicists. Tashkent, 1981.
6. M.G.Milvidskii, Physicochemical principles for obtaining heterostructures on

the basis of multicomponent solid solutions of semiconductor compounds of type $A^{iii}B^{vii}$: Proceedings of the IX Winter School on Semiconductor Physics, Leningrad, 1979, pp. 127-160.
7. 7.L.D.Landau and E.M.Lifshits, Theory of elasticity, vol. VII, Nauka, Moscow, p. 203..
8. V.G.Karpov, The screened interaction of charged defects in a semiconductor, FTP, 1977, vol. II, issue 8, p. 1602.
9. B.A.Atakulov, E.I.Bilyalov, and A.Ya.Afuzov, Electromechanical properties of inhomogeneous semiconductors. Fan, UzSSR, Tashkent, 1977, 84 p.

STUDY OF ELECTROPHYSICAL PROPERTIES OF CdTe FILMS WITH ANOMALOUS PHOTOVOLTAGE IN A COORDINATE-SENSITIVE AUTONOMOUS RECEIVER OF OPTICAL EMISSION

T.M.Mirzamakhmudov, N.R.Rakhimov
Fergana State University

A deformations may be recorded by means of a source of monochromatic emission (emitting diode) and coordinate-sensitive receiver of optical emission. It is known [1, 2] that coordinate-sensitive autonomous receivers of optical emissions (C-SAROE) are designed for determination of coordinates of the source of light emission. The input signal contains information on direction and magnitude of displacement of the emitting object.

A distinctive feature of the C-SAROE is that its light-sensitive element is films with anomalous photovoltage (APV) providing some hundreds of volts in illumination.

The APV films are a functional converter transforming a light flow into an anomalously high photovoltage. In this connection, study of external effects on properties of the films plays an important role in its use in different media.

This work deals with the effect of a gas discharge and thermal processing on electrophysical properties of CdTe films with APV. Changes in V_{apv} , R and J_{shc} were studied during bombardment. Temperature dependences of V_{apv} ,R and J_{shc} were investigated in films.

The APV CdTe films were obtained by spraying CdTe powder in a vacuum of 10^{-4} mm Hg onto a glass support. The support temperature varied from 100 ^{0} to 300 ^{0} C. The film thicknesses were within 0.8-1.5 mkm.

Some of the main parameters of AFV films are given in Table 1. The results obtained show that V_{apv} ,R and J_{shc} strongly depend on the bombardment duration (Fig. 1). Figure 1 shows that V_{apv} ,R reach their maximum after a 10-min bombardment, and since the 11-min bombardment values of V_{apv} ,R decrease. The short-circuit current (J_{shc}) does not virtually depend on the bombardment duration. This dependence of V_{apv} , R and J_{shc} on the bombardment duration was shown in [1], where effects of electronic and ionic bombardments on electrophysical properties of Si and Ge films were studied.

In the process of study the optimal regime for increasing photovoltage was established. The results obtained indicate that under the effect of gas discharge on the film the main film characteristics change. This seems to be related to absorption and desorption of oxygen atoms and action of cathode ions on the film properties.

To clear up the behavior of AFV films in the process of thermal treatment, we investigated the temperature dependences of the generated photovoltage V_{apv} of short-circuit current J_{shc} and resistance R of CdTe films.

The films were treated in vacuum and in air for one hour in a stove whose construction permits us to measure temperature in volume up to ~400 ^{0} C. All papers [2, 3] dealing with the APV effect report that as temperature falls, the photovoltage and resistance of films increase. In the films treated in the air the photovoltage first grew (Fig. 2, curve 1) and then monotonically dropped. The short-circuit current decreased as the temperature

increased to 200 ^{0} C (Fig.2, curve 2); film resistance at 50-100 ^{0} C increased (Fig. 2, curve 3). In the films treated in a vacuum at 50-200 ^{0} C, photovoltage and resistance increased (Fig. 3, curve 1 and 2), short-circuit current decreased (Fig. 3, curve 3). A further increase in temperature led to decrease in V_{apv} ,R while the short-circuit current remained unchanged.

APV Films Specifications

Sensitivity, V/mm*mW..... 1-3
Fast response, sec 0.8-1.0
Emission spectrum, mkm 0.3-1.2
Sensitive area, mm 3*10
Overall dimensions, mm 20*20*25
Weight, kg, no more than 0.06

In the process of thermal treatment the film polarity remained constant, and illumination in all measurements was also constant (1 = 5*10^4 Lx).

It is shown in [4-7] that the dependence of . V_{apv} ,R and J_{shc} of CdTe films at 20-180 ^{0} C is of intricate character, for example, it decreased in some specimens and increased in the others. The change in APV parameters of CdTe films as a function of temperature seems to be due to their oxidation, i.e. partings appeared during thermal treatment, and at a certain temperature saturation occurred. As a result, in the films treated in the air resistance and photovoltage decreased monotonically. The increase in volumes of V_{apv} ,R during their treatment in a vacuum may be explained by oxygen desorption in the specimens investigated.

№	Spraying time (min)	T^{0}C Temperature sub.	V_{apv} (V)
24	15	200	350
60	60	200	900
77	20	200	60
89	30	225	350
90	80	225	500

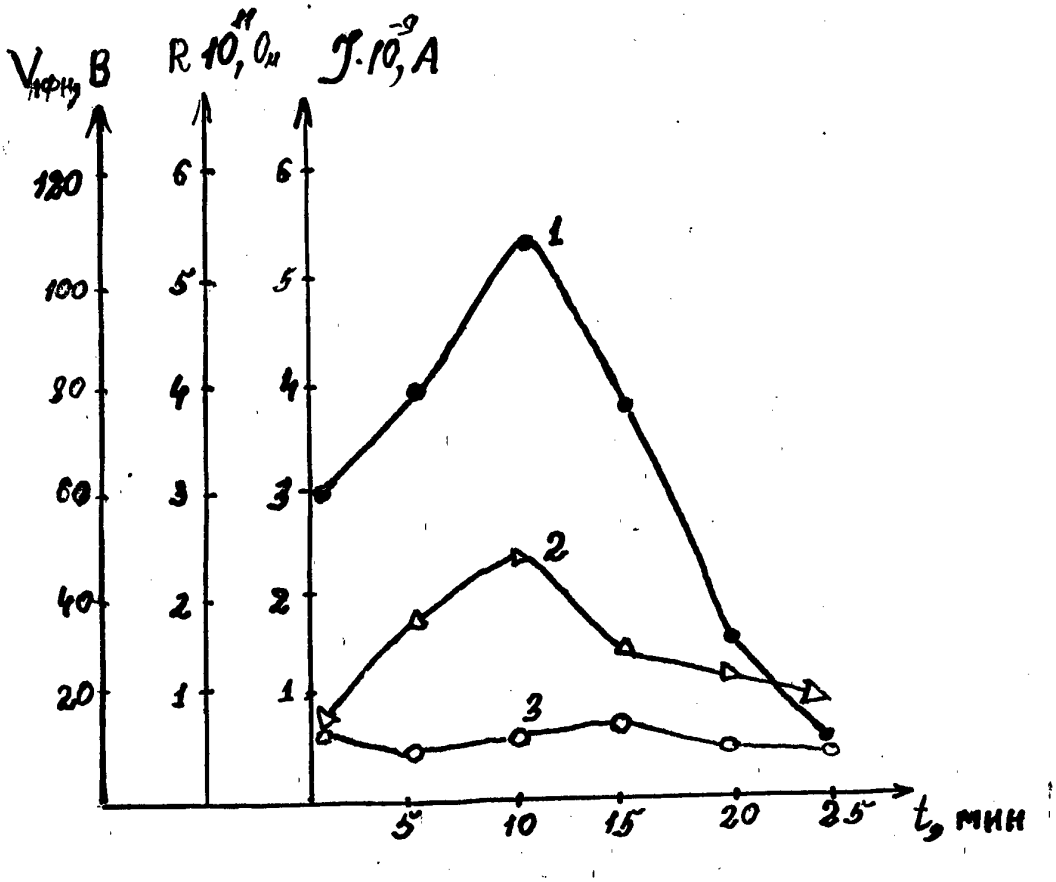

Fig. 1. Parameters V_{apv} ,R and J_{shc} as a function of bombardment duration.

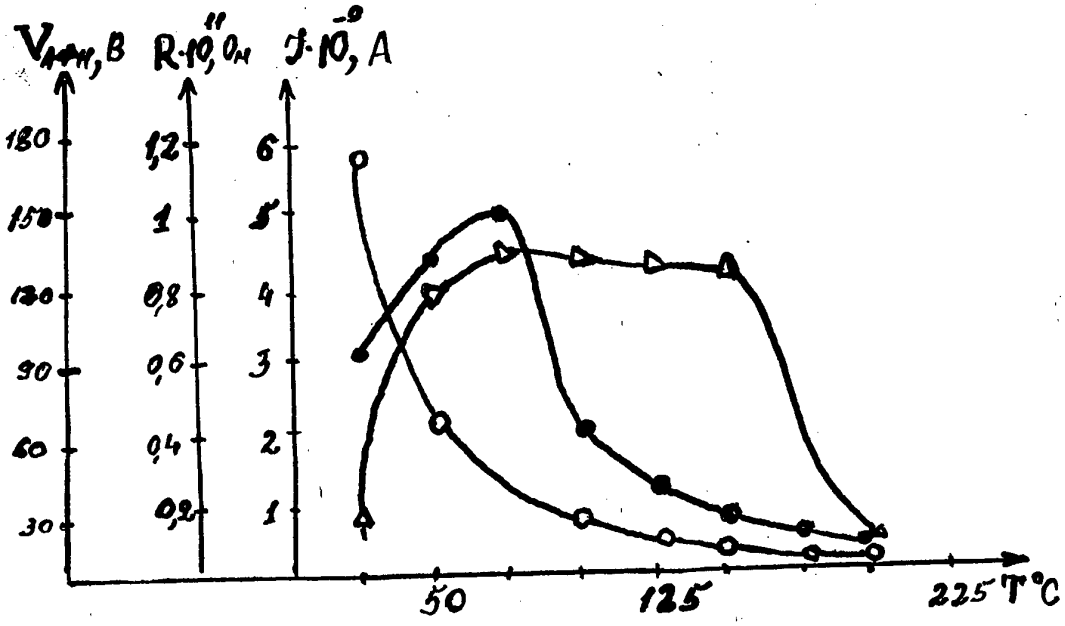

Fig. 2. Parameters V_{apv} ,R and J_{shc} versus T: a) in air.
No. Spraying time (min) T<198>C Temperature sub.

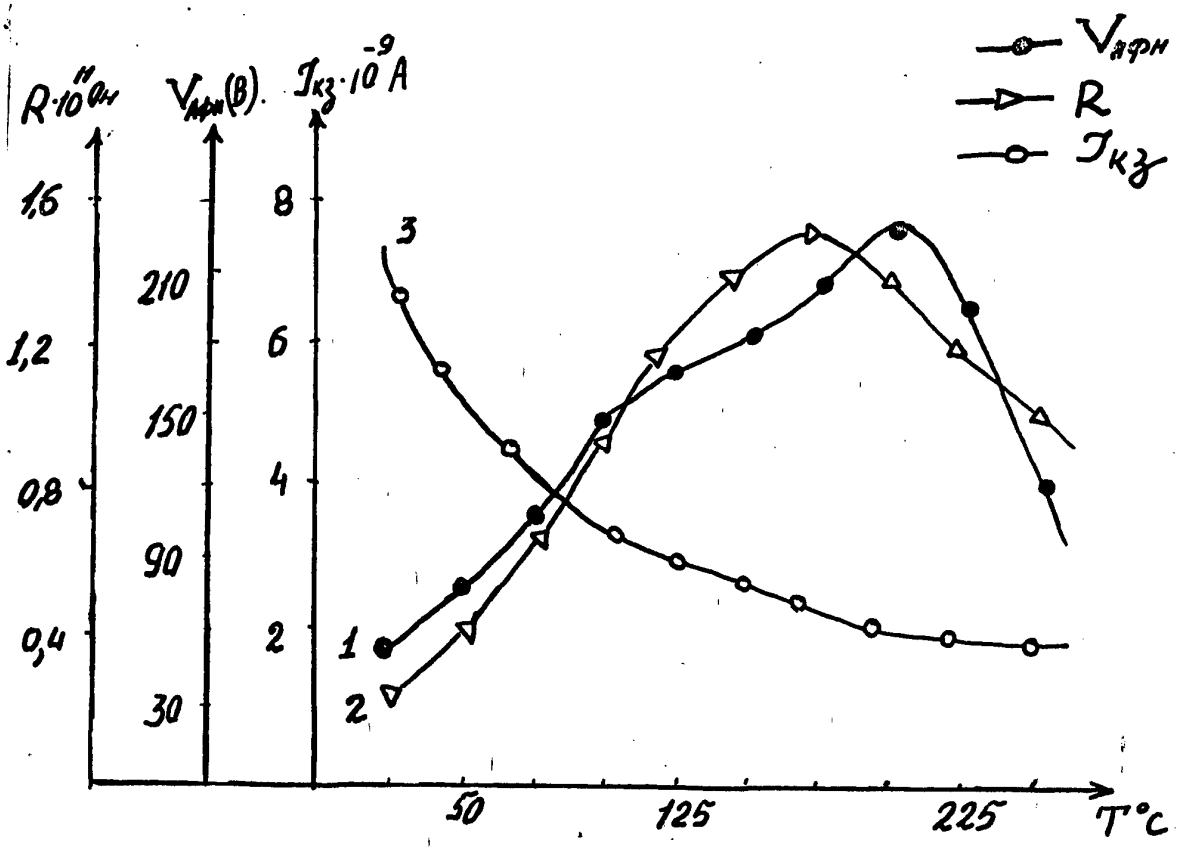

Fig. 2. Parameters V_{apv} ,R and J_{shc} versus T: b) in vacuum.
No. Spraying time (min) T<198>C Temperature sub.

REFERENCES

1. T.M.Mirzamakhmudov, N.R.Rakhimov, U.A.Gafurov, Independent receiver of optical emission AF-4M, Vneshtorgizdat, 1990.
2. T.M.Mirzamakhmudov, N.R.Rakhimov, U.A.Gafurov, Coordinate-sensitive independent receiver of optical emission K4P-1M, Vneshtorgizdat, 1991.
3. N.Abdullaev, PhD thesis, Tashkent, 1972.
4. L.Pensak, B.Goldstein, High-voltage Photovoltaic Effect, J.Appl.Phys., 1959,vol.30, pp.155-157.
5. Yu.M.Yuabov, Semiconductor films with anomalously great photovoltage. PhDthesis, Tashkent, 1965.
6. M.I.Korsunskii, S.S.Kiseleva, Effect of thermal treatment of APV CdTe filmsn various media on their properties. Izv. AN KazSSR, ser. fiz.mat. nauk, 1967,no. 4, pp. 13-16.
7. T.M.Mirzamakhmudov, B.Kh.Karimov, Effect of thermal treatment on the APV effect in CdTe films. Izv. AN UzSSR, ser. fiz.mat.nauk, 1978, no. 5, pp. 75-76.

DIFFRACTION OF A SYSTEM OF SHOCK WAVES ON A CYLINDRICAL BODY

R.A.Sadykov ,B.Sh.Usmonov
TSAI, ASF, Tashkent

Under consideration is a plane problem on diffraction of a system of shock waves o an absolutely rigid cylinder of radius r_0 sold in a continuous medium with specifie properties. In particular, study is given to interaction of two shock waves situated at a arbitrary angle relative to one the other (Fig. 1).

To obtain a numerical solution, the method of "particles" is used [1, 2]. The movemen of "particles" is described by a system of ordinary differential equations, derived fron Lagrangian equations of second kind. Movement of p-particle is described in stress an strain tensor invariants as follows:

$$\Delta m_p \frac{d^2 U_p^{(k)}}{d\tau^2} = -\sum_{j=1} \left\{ \frac{d\sigma}{d\varepsilon} \frac{d\varepsilon}{dU_p}^{(k)} + \frac{d\sigma_i}{d\varepsilon_i} \frac{d\varepsilon_i}{dU_p}^{(k)} \right\}_j \Delta V_j$$

where $k = 1,2$; $p = 1,2,...,N$;
$U_p^{(k)} = U_k (r_p , \varphi_p, t)$ is a constituent of displacement vector of a p-th particle;
$\Delta m_p = \rho \Delta V_p$ is the particle mass with density ρ and volume V_p;

$$\left.\begin{array}{l} \sigma = \sigma(\varepsilon) \\ \sigma_i = \sigma_i(\varepsilon_i) \end{array}\right\} \text{ experimental equations of the medium state.}$$

Equations of linear motion of a cylinder and boundary conditions on a body ar added to the equations of motion of inner "particles". The resulting system of ordinar differential equations of second kind is integrated with regard to time under startin conditions corresponding to an initially stationary body and a given position of the system o shock waves specified by the normal vector to a flat front and by intensity.

Interaction of a system of two mutually perpendicular plane shock waves with a stationary body and a movable one is considered. The calculation results are given for th grid (Fig. 2):

$$0.2. \le r \le 1 \;; \qquad \Delta r = 0.01,$$
$$0 \le \varphi \le 2\pi; \qquad \Delta \varphi = 5 .$$

Diffraction of shock waves on a cylinder goes through several subsequent stages (Fig 3). The forms of reflected shock waves change from circle to parabola and then tend to hyperbola. The point where two shock waves intersect is the source of additiona perturbations making the diffraction pattern irregular.

Figures 4 and 5 show what effect is exerted by the body movability on the radia constituent of the stress tensor. The body movability does not only change stresses on th surface but also introduce qualitative changes into the shock-wave pattern. When the cylinde is movable, at the initial times (t =0.05) the cylinder is surrounded by shock waves to an

equal degree. Then the zone of stressed state enlarges; "wings" and "tail" appear, which are stretched along the diagonal and back to assume the shape of "butterfly", completely surrounding the body (t=0.2). Since then restructuring of the stressed state of the body surface has begun to form a ring with the displaced center relative to the body center toward the point where the shock-wave fronts intersect.

To conclude, we note that the results given in this work are obtained with the help of an automatic system oriented toward solution of continuum mechanics problems. The software developed makes it possible to follow the problem from the step of its formulation to solution and graphical representation of the results obtained. The system permits us:

- to consider elastic, nonlinearly-elastic, and viscoelastic laws of deformation;
- to establish randomly-oriented plane-shock fronts of various intensity at the initial moment and to trace their development and interaction;
- to carry out graphical treatment of the results by plotting time curves and using space coordinates; to construct isometrical images and isolines in space-time sections.

REFERENCES

1. Sadykov R.A., "Propagation of waves of volume strain in physically nonlinear continuous media", in: Proceedings of the Conference on Nonlinear Strain Waves, Tallin, 1978, 1978, p. 5.
2. Sadykov R.A. and Yuldashev M.E., "Interaction of a plane stepwise wave with a deformable cylinder with masses", in: Mathematical modeling and computation experiment in dynamics and stability of deformable systems", Tashkent, TashGAI, 1995.

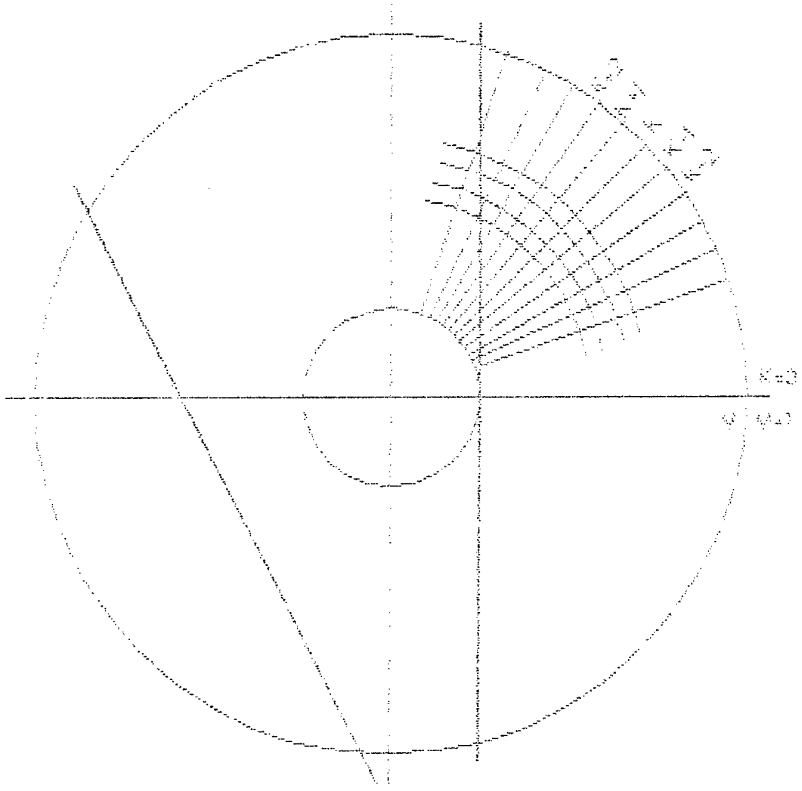

Рис.1 Постановка задачи.

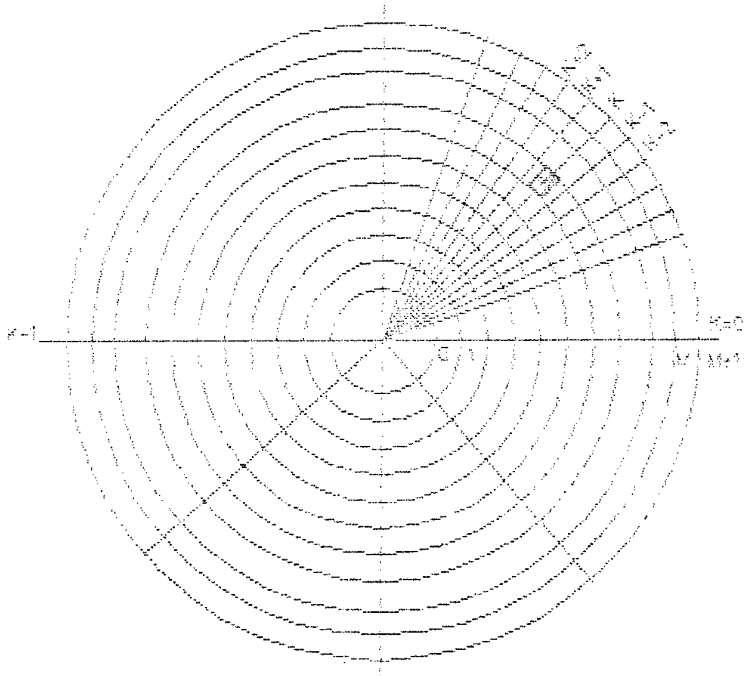

Рис. 2 Расчетная сетка задачи

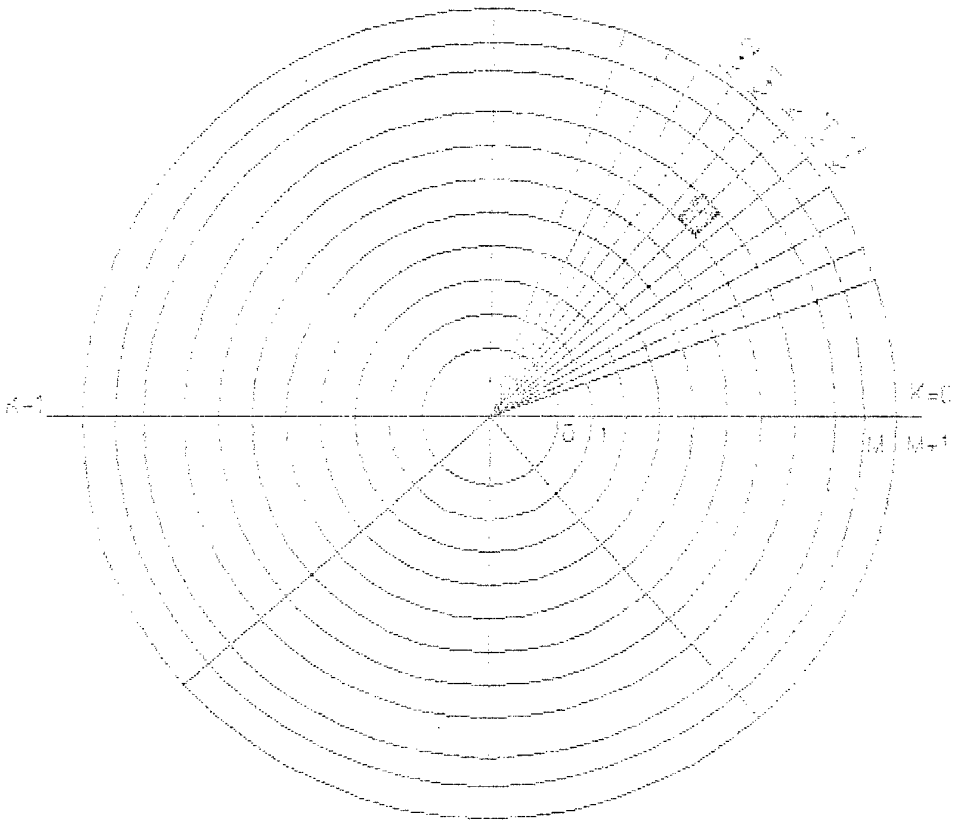

Fig. 1. Accounts grid of a problem.

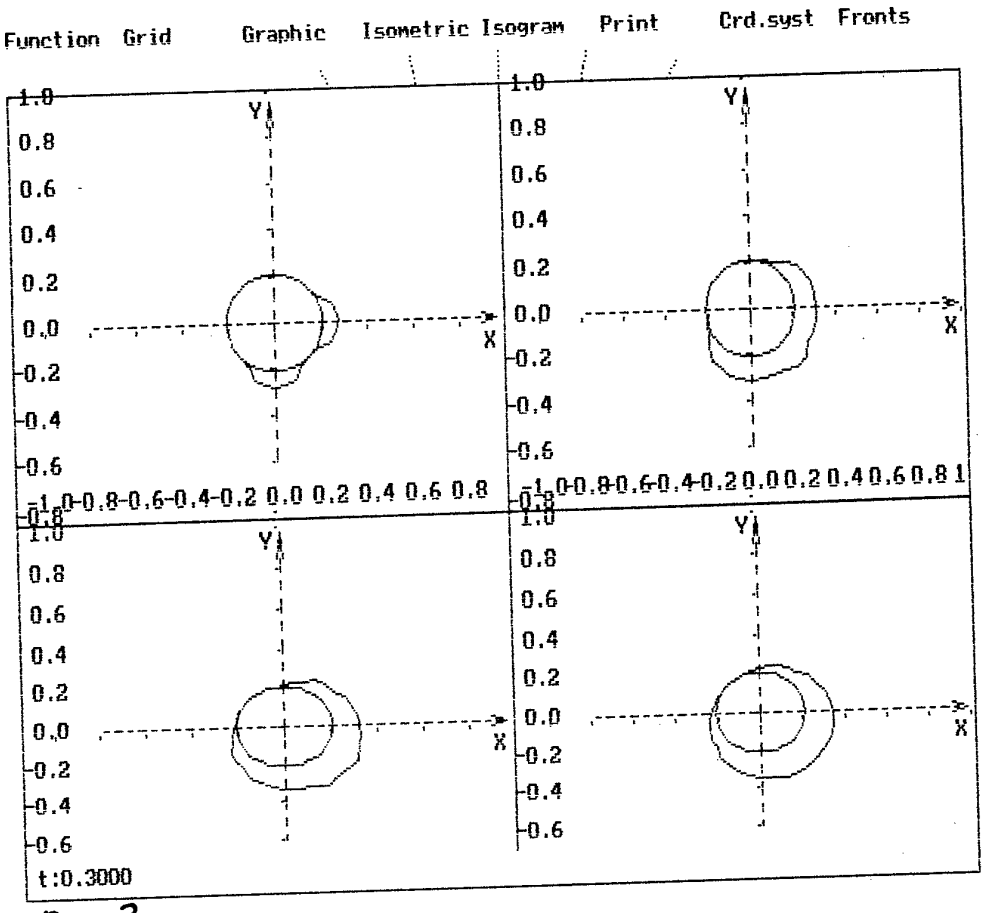
Function Grid Graphic Isometric Isogram Print Crd.syst Fronts
Y
X
1.0
0.8
0.6
0.4
0.2
0.0
-0.2
-0.4
-0.6
-1.0-0.8-0.6-0.4-0.2 0.0 0.2 0.4 0.6 0.8
-0.8
t:0.3000

Fig. 3.

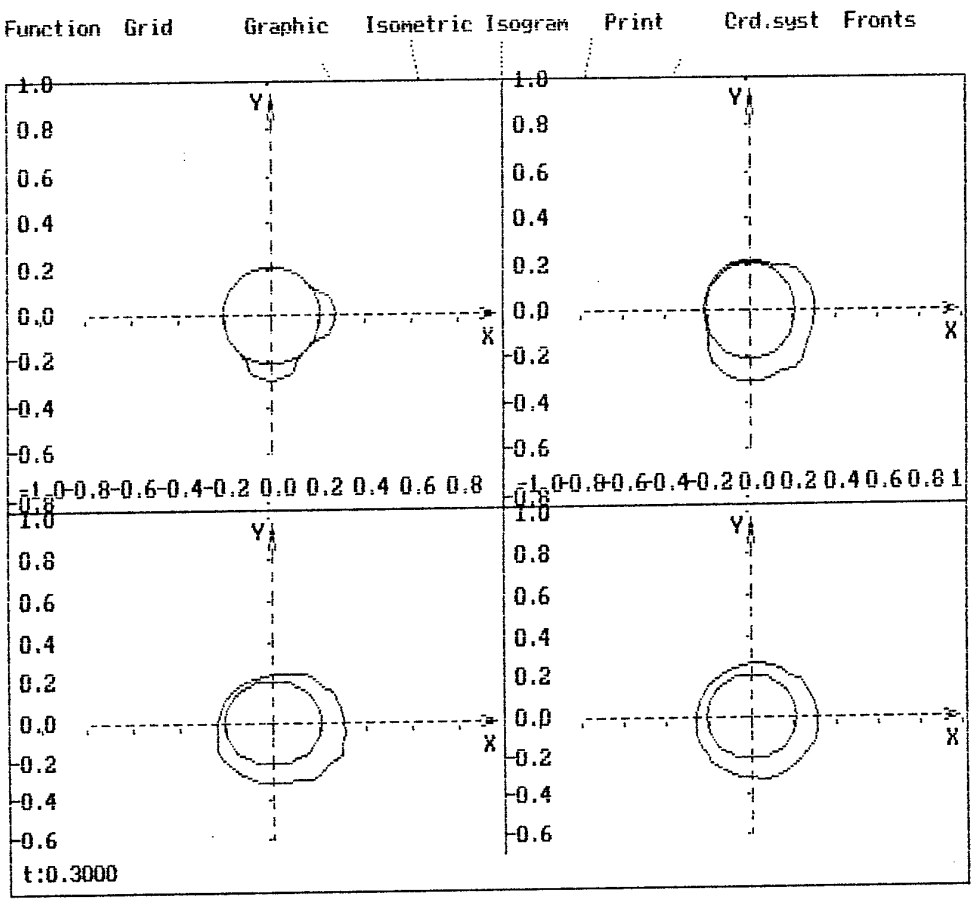
Function Grid Graphic Isometric Isogram Print Crd.syst Fronts
Y
X
1.0
0.8
0.6
0.4
0.2
0.0
-0.2
-0.4
-0.6
-1.0-0.8-0.6-0.4-0.2 0.0 0.2 0.4 0.6 0.8
-1.0-0.8-0.6-0.4-0.2 0.0 0.2 0.4 0.6 0.8 1
t:0.3000

Fig. 4.

DIFRACTION OF A SYSTEM OF SHOCK WAVES ON HARD CYLINDER

B.Sh.Usmonov
TSAI , Tashkent

One of the most important exploitation-technical characteristic of a flying vehicle (FV) is survivability, whose element in turn is an index permitting estimation of vulneribility of the aircraft or its elements. In connection with the vulnerability factor a problem arises, concerning interaction of sub- or supersonic FV with a shock wave as a killing means. When estimating the force action on various bodies, in particular, in strength assessment or in solving problems of stability and controllability, it is necessary to know nonstationary gas dynamic characteristics of FV elements, with the shock wave effect taken into account. Estimation of the force effect of the wave on bodies is however not always possible, for there are such situations of interaction which require special means of simulation.

Multiple effects are among hard-toreproduce situations with shock wave-body interaction. It is this problem that is considered in this report.

MULTIPLE EFFECTS OF A SHOCK WAVE ON IMMOBILEBODIES

Consider the effect of several shock waves (SW) arriving at various times arrangements on immobile bodies.
The initial parameters are:

- number of arriving shock waves, n;
- intensity of shock wave front and duration, t_1, when the wave approaches the immobile body;
- travel time, t_2 of the front of each shock wave to body and its propagation direction characterized by angle φ.

STATEMENT OF THE PROBLEM

Let a system of shock waves fall at a constant velocity, V, on a cylinder-shaped body with outer radius, r, and a time t_1 it encounters a cylindric barrier stationary at the initial moment of time. The effect is considered in the Cartesian system of coordinates (x, y) tied with the body, and the velocity vector is always directed normally to the cylinder surface. The material of cylindric ring is generally subjected to the law

$$\sigma = E(\varepsilon(x,t) - q\int_0^t R(t-\tau)\varepsilon(x,\tau)d\tau);$$

On solving the problem we believe that before the SW system arrives the body to be deformed is at rest, and the SW system encounters it at velocity V. We obtain differential equations of movement of a discrete problem model:

$$\Delta m_{ij} \ddot{U}_{ij} = -\sum_{pq} \left\{ \delta_{11}^{pq} \frac{d\varepsilon_{11}^{pq}}{dU_{ij}} + \delta_{22} \frac{d\varepsilon_{22}^{pq}}{dU_{ij}} + \delta_{12} \frac{d\varepsilon_{12}^{pq}}{dU_{ij}} \right\} \Delta V_{pq}$$

$$\Delta m_{ij} \ddot{V}_{ij} = -\sum_{pq} \left\{ \delta_{11}^{pq} \frac{d\varepsilon_{11}^{pq}}{dV_{ij}} + \delta_{22} \frac{d\varepsilon_{22}^{pq}}{dV_{ij}} + \delta_{12} \frac{d\varepsilon_{12}^{pq}}{dV_{ij}} \right\} \Delta V_{pq}$$

We introduce a polar system of coordinates (r, φ). The calculated domain is subdivided r up to R by a step Δr, $\Delta\varphi$.

$$r_0 \le r \lesssim R$$
$$0 \le \varphi \lesssim 2\pi$$

The position of material particles surrounding the body in the polar system of the coordinates is determined by radial and tangential components of the transfer vector.

It is assumed that during motion there is an intimate sticking contact between the surface and medium particles:

1) complete sticking.

An equation of body movement

$$M\ddot{U} = \int_0^{2\pi} (\sigma_\pi \cos(\varphi) + \sigma_r \sin(\varphi))\, r_0 d\varphi$$

and symmetry conditions, provided the symmetrical problem is under consideration, are added to the system of equations.

$$i = 0,\ 0 \le j \le n$$

$$d^2 U_{0j} / d^2 t = \dot{u}'(t) \cos(\varphi_j) + \dot{v}'(t) \sin(\varphi_j);$$

$$d^2 V_{0j} / d^2 t = -\dot{v}'(t) \sin(\varphi_j) + \dot{u}'(t) \cos(\varphi_j);$$

An equation for nodes of outer boundaries is written:

$$0 \le j \ge n;\quad u = 0;\ \dot{u}_{ij} = 0;\quad v = 0;\ \dot{v}_{ij} = 0$$

Initial conditions at t = 0:

1) $u_{ij} = v_{ij} = u_{ij} = v_{ij} = 0$ - conditions at the ring surface;

2) $r_o = z(0)$ $V(t) = - V_0$ - at the front of shock waves;

$$\dot{U}_{ij} = V(t) \cos(\varphi_j) + V(t) \sin(\varphi_j);$$

$$\dot{V}_{ij} = - V(t) \sin(\varphi_j) + V(t) \cos(\varphi_j);$$

$$U = (r \cdot \cos \varphi_j - r_0 / a)^* V$$
$$u_{ij} = (r_i \cos \varphi_j - r_0)^* V / a \cos \varphi_j$$
$$v_{ij} = (r_i \cos \varphi_j - r_0) ^* V / a \sin \varphi_j$$

3) $r < z(0)$ - the medium at rest;

$$u_{ij} = v_{ij} = \dot{u}_{ij} = \dot{v}_{ij} = 0$$

A stress-strained state of the cylinder is required to be estimated with the waves reflected from he body taken into account. The cases are considered when the cylinder is made of:

a) elastic material:
b) viscous material.

We have developed a mathematical model for the process of multiple action of shock waves with an immovable cylinder and with a movable one. The mathematical model is based on ideology of methods of particles. The front of shock waves is not specially recognized, i.e. the method of through calculation is applied.

Consider some shock waves - cylinder interaction:

1. Single shock waves (SW) - body interaction.
2. The SW fronts move toward one another and touch the body at the same moment of time, t_0 (symmetrical interaction).
3. The SW fronts move toward one another and touch the body at different moments of time, t_0 and t_1 (nonsymmetrical interaction).
4. The SW fronts move toward one another at the angle of 90^0 and touch the body at the same moment of time.

First of all, these interactions are characterized by the fact that the shock waves interact before they reach the immovable cylinder. Figure 1 shows that the interaction of two shock waves with the immovable cylinder results in reflected Sw_{r1} and Sw_{r2}, which, in turn, mutually interacting form an intricate configuration. It is interesting, for example, to trace the double effect on the SW shape varying as the process develops.

To quantitatively estimate how the processes considered develop in time, we have measured time characteristics: variation of the field of stresses and strains on the body surface, and variation of the medium reaction with time. These variations are recorded and illustrated by slides.

ANALYSIS OF CALCULATION RESULTS

The calculated systems of motion equations in the problems were integrated by numerical methods on a computer with corresponding initial conditions. In this case fields of movements U_{rmk} , $U_{\varphi mk}$, and velocities are determined for discrete moments of time. Stress and strain components are found from the known movement values for any

"particle" of the calculated domain. Given the normal and tangent components of stresses in "particles" on the cylinder surface, we may assess the medium resistance to an immobile or arbitrarily moving cylinder.
The problems under consideration, A, B, C, and D, have solutions obtained by the method of through calculation (see Table 1).

Table 1

	A	B	C	D
grid interaction type calculation time the particle size in corner the particle size in radius degree of cylinder mobility boundary condition	72 x 80 symmetric. T = 0.4 $\Delta\psi = 2.5^0$ $\Delta r = 0.01$ immobile adhesion	72 x 100 under < 90 t= 0.5 $\Delta\psi = 2.5^0$ $\Delta r = 0.008$ immobile adhesion	36 x 80 non- symmetric t = 0.4 $\Delta\psi = 5^0$ $\Delta r = 0.01$ mobile adhesion	36 x 80 arbitrary t = 0.2 $\psi = 5^0$ $\Delta r = 0.01$ immobile adhesion

The calculations carried out with the use of various sizes of "particles", time steps, and comparison of the solutions obtained with the known solutions provide information on the stability and convergence of the proposed difference method. To reveal the effect of "particle" sizes on solution behavior, calculations with various values of $\Delta\varphi$, Δr were carried out.
Now we will show qualitative patterns of the shock-wave structure of the SW system--body interaction.

REFERENCES

1. .A. R Sadikov. Distribution waves of volumetric deformation in phisically nonlinear continuous environments. Materials of a symposium "Nonlinear waves of deformations", Tallinn, p.5, 1978.
2. .A. R Sadikov, M.E. Yuldashev. Interaction of a flat stop wave of compression computing experiment in dynamics and stability of deforable systems. TashSAI, Tashkent, 1995.

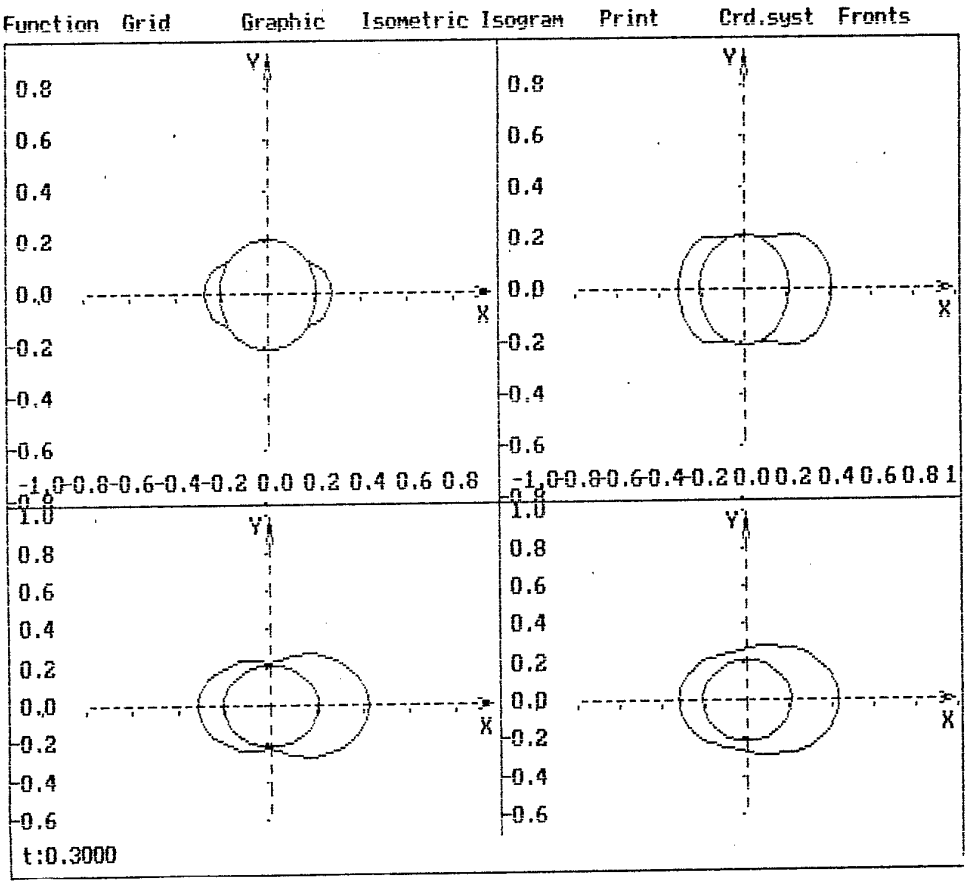

Problem A
Figure 1 shows a moment of shock wave incidence and field of stress isolines.

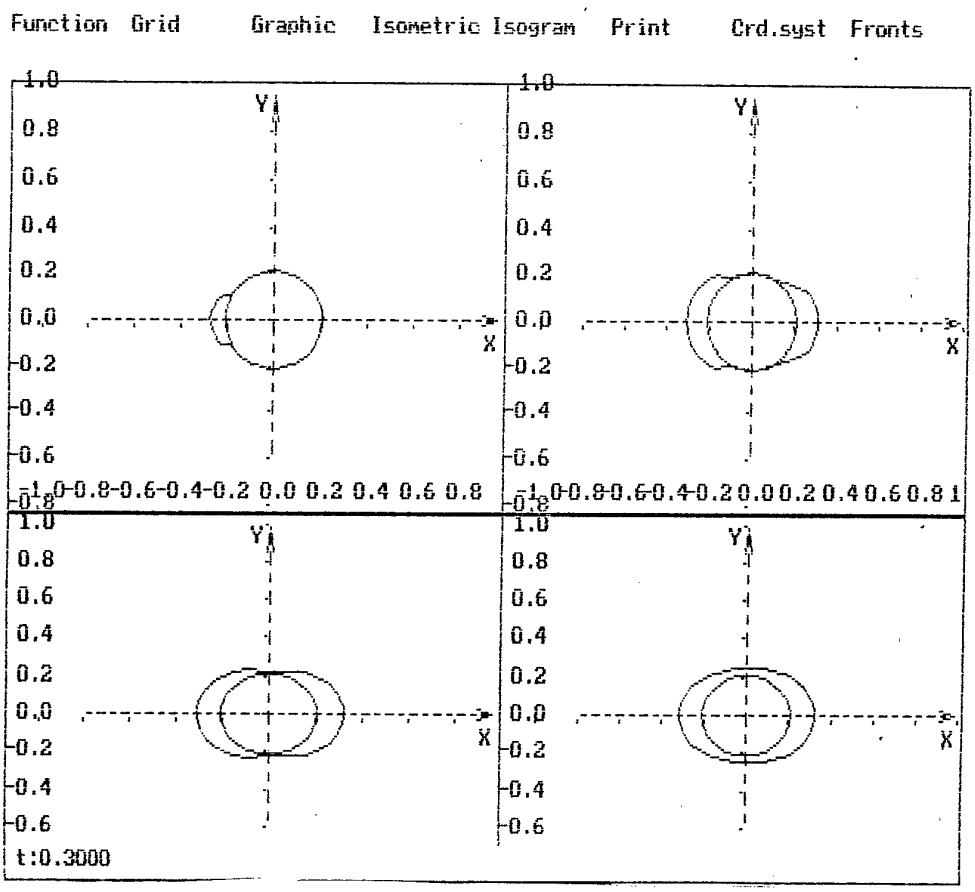

Problem C

Figure 1 gives a field of stress and strain field on the body surface with the shock wave diffraction taken into account.

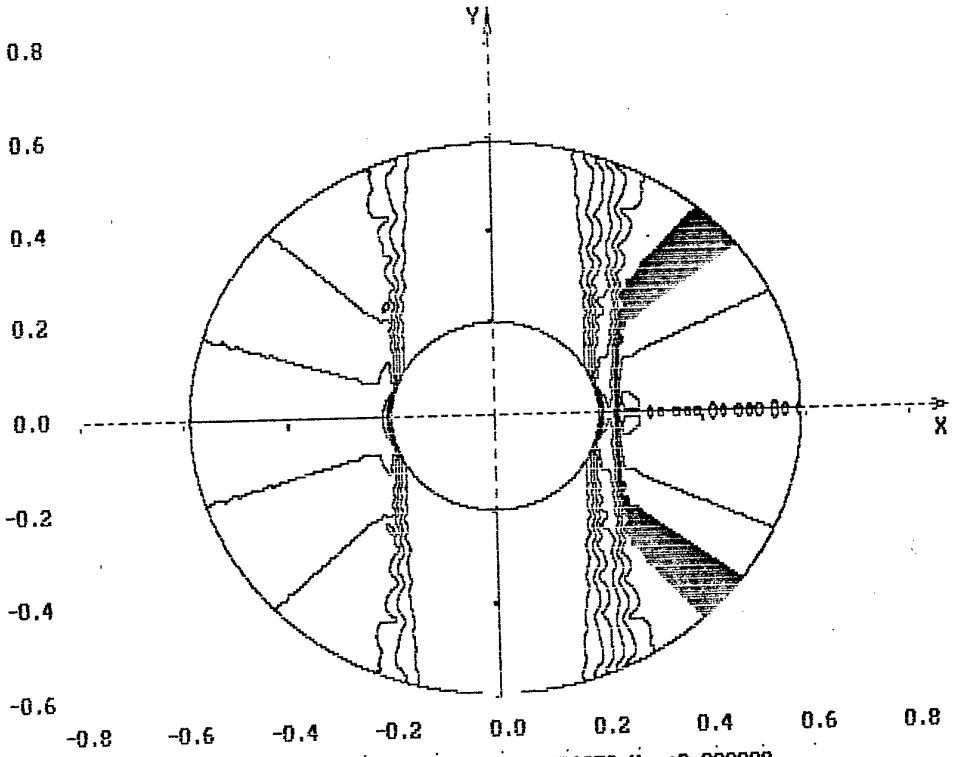

t:0.0100 функция: H11 кол.уровней:14 Min:-0.021072 Max:0.000000

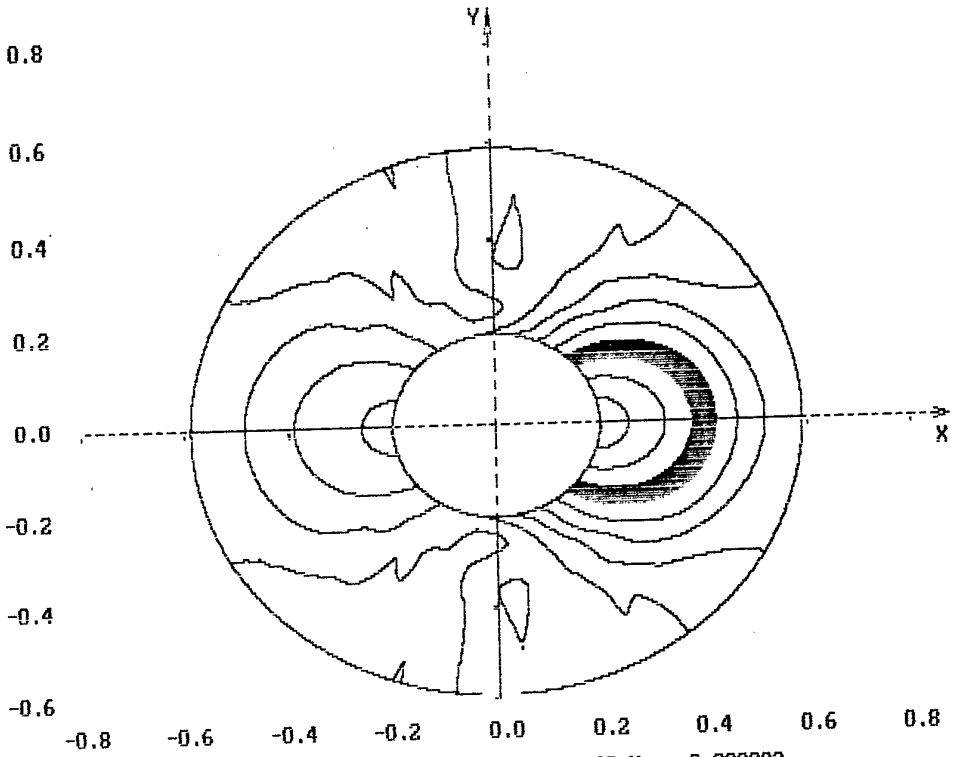

t:0.3000 функция: H11 кол.уровней:14 Min:-0.045043 Max:-0.002283

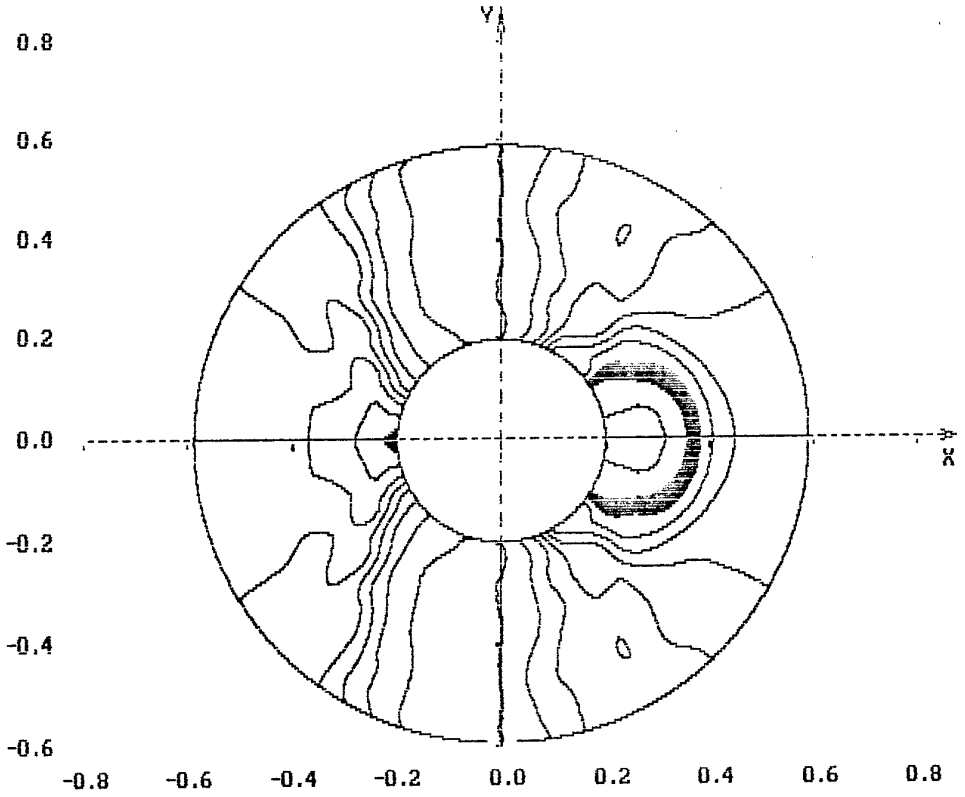

t:0.2000 функция: Hil кол.уровней:14 Min:-0.018187 Max:-0.000699

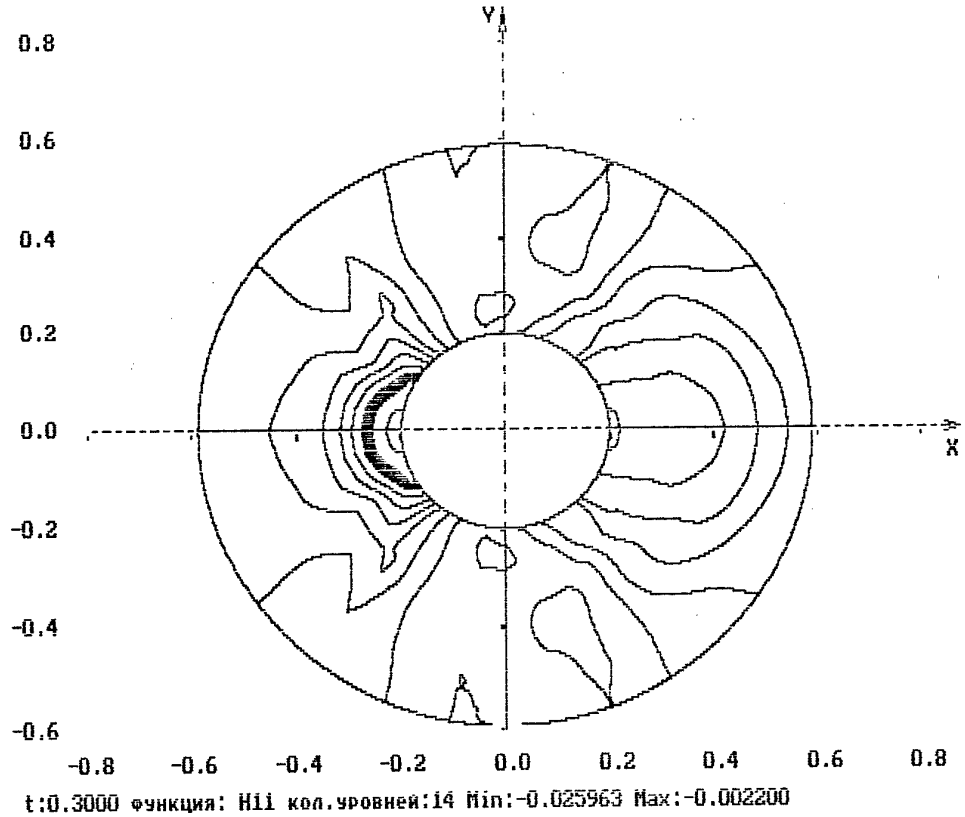

t:0.3000 функция: Hil кол.уровней:14 Min:-0.025963 Max:-0.002200

Функция Сетка Графика Изометрия Изолинии Вывод Крд.сист Фронты

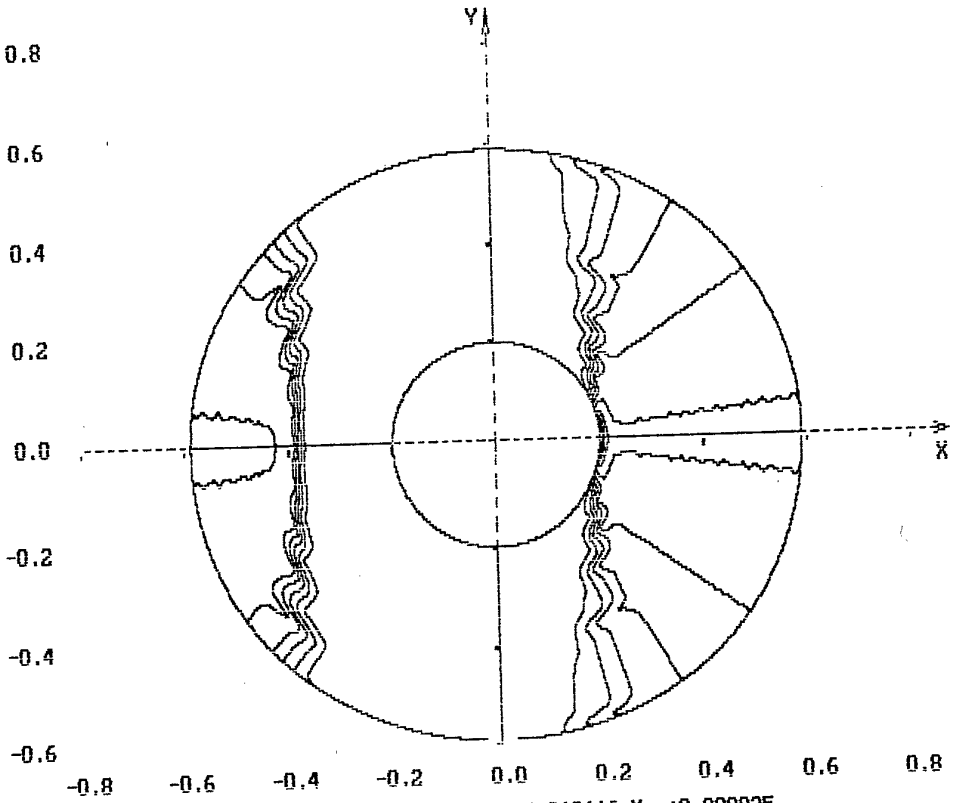

t:0.0100 функция: H11 кол.уровней:14 Min:-0.018116 Max:0.000035

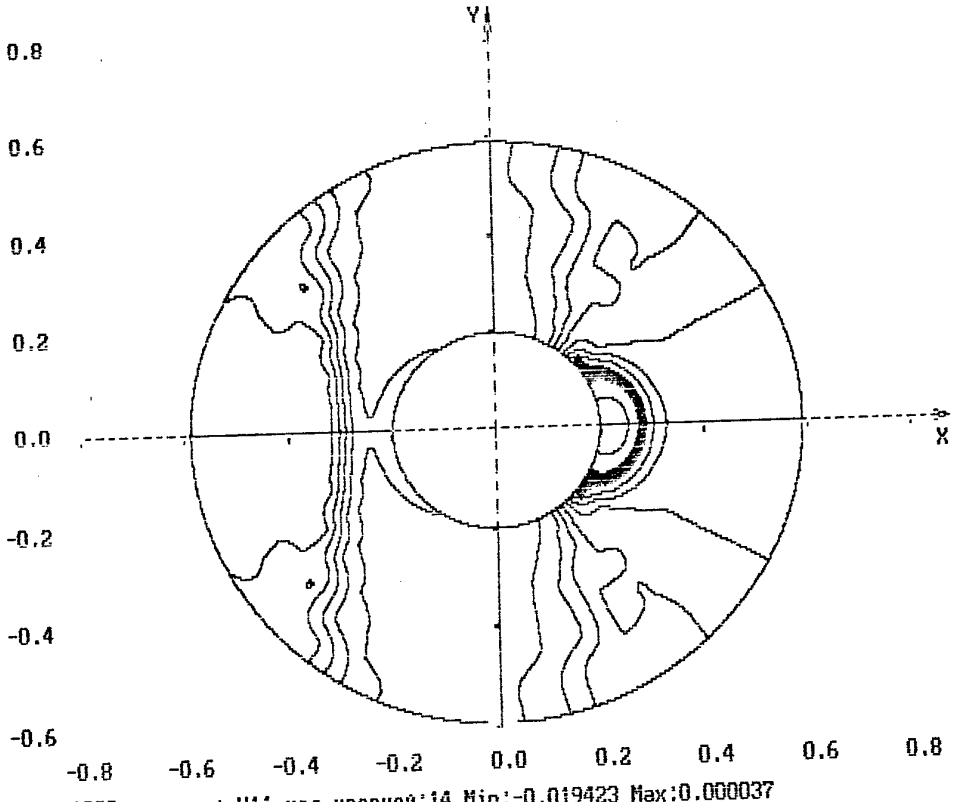

t:0.1000 функция: H11 кол.уровней:14 Min:-0.019423 Max:0.000037

HORIZONS OF THE CHKALOV AVIATION INDUSTRIAL ASSOCIATION OF TASHKENT UNDER MARKET CONDITIONS

V.Kucherov, I..Polovnikov
ChAIAT SSA ,RU, Tashkent

The Chkalov Aviation Industrial Association of Tashkent is the greatest aircraft construction plant in the CIS and in Asia.

The necessary actions preparatory to passing the Aviation Association into the corporate ownership were pioneered by the cabinet of minister of the Uzbek Republic and by President I.A.Karimov on May 17, 1996. The constituent assembly with the participation of Prime Minister U.T.Sultanov has transformed the Tashkent Aviation Industrial Plant into the state stock company Chkalov Aviation Association of Tashkent (SSC ChAIAT).

The SSC ChAIAT comprises:

- Tashkent leading plant;
- Assembly plant in Tashkent (carriages, aggregates of pneumatic fuel systems, standards foundry-forge complex);
- Machine plant in Andizhan (land equipment, hydroaggregates);
- Machine plant in Fergana (wings, mechanics, empennage, aviacontainers and trays).

The SSC ChAIAT is a multiple-discipline aviaconstruction plant. It has a powerful industrial potential, specialized works equipped with unique devices and programmers, computer networks and up-date technologies. High-skilled personnel and specialists much experienced in management of new aviation equipment are engaged in this company.

Combination of these factors permits the company to construct largest and complicated haul and passenger airlines and their modifications, as well as special-purpose airplanes for civil aviation and air forces.

The association history begins since 1932, when an aircraft-maintenance plant was built in Khimki, a village near Moscow. Before the war the plant produced the aircraft LI-2 (bought by the USA license as the aircraft DC-3). In the beginning of the Great Patriotic War, in the autumn of 1941, the plant was evacuated to Tashkent, where in January 1942 it began to produce aircrafts LI-2 as haul planes.

After the war until 1954 the Tashkent Aviation Plant produced passenger and haul airliners LI-2. In 1954 it began to produce a new passenger airliner, IL-14. Later, this aircraft was also produced as a haul plane.

Since 1972 the Tashkent Aviation Plant, reorganized into the Aviation Industrial Association in Tashkent, has been considerably developed by producing new heavy haul airliners - AN-8, AN-12, AN-22, and IL-76. Association turn into a large aviation plant of the former Soviet Union, producing the up-to-date aircrafts.

On the basis of the aircrafts AN-12 and IL-76, the Association manufactured tens of various civil and military modifications. The largest ones are: IL-76MD (with increased take off weight), IL-76K and IL-76MDKP (laboratory aircraft for astronautics), IL-78 and IL-78M (fuel supplier), A-50 (Soviet AWACS), IL-76TD "Lancet" (flying hospital), IL-76MD "SKIP" (command and measurement station), IL-76MD-324 (retranslator).

Under new conditions of market economics it most seriously affects the large machine-constructing industry, including aviation industry, which produces expensive unique machines - airplanes and helicopters, purchasers of which may be large profitable aviation-exploiting companies or air forces of the CIS and far foreign countries. But because the market economics deeply affects exploiters as well, the "powerful" Aeroflot of

the FSU appeared to be fragmented into many hundreds of dwarf plants, which were not able to purchase such expensive aircrafts as, say, IL-76TD.

As regards air forces of Russia and CIS, the "holey" budgets of these countries do not permit allotment of money to order new airplanes. It is clear that without new aircrafts neither air forces nor civil aviation companies cannot live for a long time, because the airplanes under exploitation exhaust their lifetimes and are requires to be replaced. But now the fact is that the plants producing aircrafts do not find purchasers and are subjected to a serious material-financial crisis. Approximately 80 - 85 % of the aviation plants are found to be in this situation.

These complicate conditions require nonordinary actions as well as active and reasonable enterprise for finding optimal versions for the use of powerful industrial potential, for producing such aircrafts, which would inevitably find their purchasers in spite of the long-term stagnation of aviation market. Like many other plants, the Tashkent Aviation Association suffers for the last 3 - 4 years a heavy stagnation in purchasing its main production - series-produced aircrafts IL-76TD, IL-76MD - for the above-mentioned reasons. Another reason is also that the main purchasers of these airplanes - Russian and Ukrainian air forces and civil aviation companies - have saturated their fleets.

Despite the aircrafts IL-76TD and IL-76MD have high exploitation characteristics (none of the countries in the world produces aircrafts of this kind), their large-scale production and realization are not promising). Nearly all developing countries, having civil and military aviation, have acquired transport airplanes IL-76TD and IL-76MD. The Tashkent Association has sold more than a hundred of the IL-76 aircrafts to many countries such as: China, Syria, Algeria, Egypt, Korea, Cuba, etc.

The question of devising new competitive aviation machines is high on the agenda. Nothing else but production of the aircrafts that are in demand not only in the CIS and developing countries but also in the western states permit the ChAIAT to be kept at an acceptable value and, moreover, to receive a new impetus. Well realizing the existing situation, the SSA ChAIAT together with Ilyushin Aviation Company, the General Designer of aircrafts, take actions to develop and produce precisely this kind of competitive machines.

In 1994 - 95 a highly updated aircraft was built. Essentially, it was a new aircraft, IL-76MF, with the fuselage extended for 6.6 m, with new engines PS-90A-76 certified by the ICAO, and with improved flight-engineering and exploitation parameters. The IL-76MF aircraft was built according to Ilyushin Co, drawing, at the cost of the ChAIAT own financial means. On the 1 st August, 1995, it was raised into the air.

The aircraft was successfully demonstrated at the aviation display MOSAEROSHOW-95 in the town of Zhukovski (near Moscow) and was highly estimated by experts. At present this aircraft is under certification test on the Ilyushin Co, ground. The aircraft Il-76MF may transport a load of up to 52 tons for a distance of up to 4500 km. The outer dimensions of the aircraft and the volume of the freight cabin are considerably enlarged, the freight cabin being capable to hold three 20-ton or nine 5-ton standard containers.

The aircraft is equipped with the engines PS-90A-76 characterized by a 20 % increase in power and 15 % decrease in specific fuel consumption as compared with new engines D30KP; also noise and emission of the engines fit the ICAO norms.

In the future the aircraft is planned to be equipped with an improved navigation system KUPOL-III instead of KUPOL-II-76 used at present.

According to experts' estimates, this aircraft is a promising haul airliner of the class for the nearest 10<196>20 years and, taking this into account, the association has put into mass production two versions of this aircraft: military IL-76MF and civil IL-76TF.

This is not the end of the IL-76 updating. Together with the Ilyushin Co., negotiations were carried out with the French company "Snecma" and American "General Electric" about the use of the engine SGM-56 of joint production of "Snecma" and "General Electric" in the IL-76TF aircraft. The Department of Commerce and banks of the USA sponsor the program of joint production of the IL-76TF with the SGM-50-5s2 engines and new avionics. The engines SGM-56-5s2 of the same power are thoroughfully during production, are distinguished by a great lifetime, and correspond to the word standards. According to the joint program, the IL-76TF aircraft with the engine SGM56-5s will enter the western aviation market so that the association will significantly improve its economical state.

At present, it is vital to quickly carry out certification of the IL-76MF aircraft. Unfortunately, the tests are hindered because of insufficient financial support.

Another direction in the activity of the ChAIAT is the series production of the new passenger airliner IL-144 and the haul airliner IL-144T developed on its basis. The 64-seat passenger airline IL-114 is aimed at using on local and mid-range avialines at a velocity of 500 km for a distance of 1000 km (with full loading). This aircraft meets all demands of the word standards for its class. It is quipped with two low-noise turbo-props TV7-117s of 2750 e.h.p., with an independent built-in system VD-100, as well as with a modern navigation complex TsPNK-114 with five displays on the control panel, permitting automatic navigation according to a given program and loading to 2nd categogy of ICAO.

The IL-114 aircraft has a modern interior made of light multilayer constructions of composite materials. The interior and aircraft systems make the stay of the passengers on board quite comfortable. The IL-114 has to replace the aircrafts AN-21 and YAK-40 on the regional lines of the CIS, because within 2 or 3 years these aircrafts will exhaust their lifetimes and be written off.

There is, however, a delay in putting the aircraft into exploitation because of no certificate for the aircraft type. The certification is planned to be finished in the IV quarter of 1996. And this is one of the priority President's programs of the Russian Federation. The General developer of the aircraft, the Ilyushin Co., is responsible for testing and receiving the certificate. The Russian aviation companies which will be forced soon to replace the old AN-24 and YAK-40 aircrafts are interested in accelerated large-scale production of aircrafts.

The enlarged series series production of the IL-114 aircrafts will provide jobs not only to ChAIT but also to more than 500 plants of the Russian Federation participating in the cooperative production of the aircrafts and in supply of materials and standard equipment. The ChAIAT contribution is two aircrafts IL-114 nos. 0105 and 0108, built and given to Ilyushin Co.

Under conditions of market economics the load, including perishable ones, are required to be transported quickly for short distances. These requirements gave rise to an idea to produce a transport version of the IL-114 aircraft.

In 1995 drawings were developed for the haul airliner IL-114T in the Ilyushin Company, and the ChAIAT built this aircraft in short terms. On 31 August, 1996, when the fifth anniversary of independence of the Uzbek Republic was celebrated, The IL-114 aircraft was given to the flight and test station for testing on the ground and in the air.

The IL-114 aircraft can carry loads of up to 7tons in weight for a distance of 1000 km. For handling loads in special containers and on trays (numbered up to 8), a large hole (3300 x 1800 mm), controlled by an electrohydraulic system, is made on the fuselage board; the freight floor is equipped with roller mechanization, permitting the containers and trays to be loaded and unloaded with the minimum expenditures of human labor.

It is important to note that despite large sizes of the hole, the freight cabin of the aircraft is sealed so that the load-accompanying personnel may be present in the cabin during flight.

Some design improvements are made on the IL-114T airplane. They include a new hawser system of control for ailerons, elevators, and rubbers with a stand-by remote system; pod construction and exhaust systems were reduced; also other design changes were made.

The new haul airliner IL-114T has no analogs of the class in the word aviation. So there is reason to believe that this aircraft will be in demand on the market. In September of this year the IL-114T aircraft will be given to Ilyushin Company for certification tests. Though there is no certification yet, the IL-114 is now in series production on the ChAIAT.

Together with the Ilyushin Company, the ChAIAT intends to invite famous foreign companies to participate in the joint production of the aircraft in order to improve it.

Thus, the more perfect stand-by power station 36-KL-150 of Island Signal Co., USA, as well as the new navigation complex ARIA-114, jointly produced by the NIIAO (Zhukovski) and Island Signal Co., USA, are planned to be used in the IL-114 aircraft. In the future, Pratt-Witney or Allison engines are supposed to be used.

To conclude, we state that despite great economical difficulties or association actively searches for ways to escape from this situation. The core of this direction is the timely and quick transition to development and production of new kinds of goods.

The aviation association is also ready to begin to produce wings for the new haul airliner AN-70 of the Antonov Company. The association has necessary equipment and fitting.

The first specimens of new competitive aircrafts IL-76MF and IL-114T produced in 1995 and 1996, correspondingly, are the first real steps to advance the frontiers of production of modern aircrafts and to receive stable orders for their supply.